

ANALYSIS AND NUMERICAL SIMULATION OF FREE SURFACE FLOWS

THÈSE N° 2893 (2003)

PRÉSENTÉE À LA FACULTÉ SCIENCES DE BASE

Institut d'analyse et de calcul scientifique

SECTION DE MATHÉMATIQUES

ÉCOLE POLYTECHNIQUE FÉDÉRALE DE LAUSANNE

POUR L'OBTENTION DU GRADE DE DOCTEUR ÈS SCIENCES

PAR

Alexandre CABOUSSAT

ingénieur mathématicien diplômé EPF
de nationalité suisse et originaire de Gland et Bursinel (VD)

acceptée sur proposition du jury:

Prof. J. Rappaz, directeur de thèse

Prof. J. He, rapporteur

Dr M. Picasso, rapporteur

Prof. O. Pironneau, rapporteur

Prof. A. Quarteroni, rapporteur

Lausanne, EPFL
2003

Version Abrégée

Nous nous intéressons à quelques aspects mathématiques et numériques liés à des problèmes de fluides à surface libre.

Dans la première partie de cette thèse, quelques problèmes mathématiques sont traités, à commencer par un problème simplifié à une dimension d'espace. Ce problème est l'équation de Burgers avec diffusion sur un intervalle en espace dont une extrémité est inconnue et dépend du temps. Une équation différentielle décrivant le déplacement de l'extrémité libre permet de fermer le problème mathématique. Nous démontrons un résultat d'existence et d'unicité locale en temps avant d'étudier une semi-discrétisation en espace. Nous discutons la stabilité et la convergence d'un schéma numérique à pas fractionnaires. La démarche adoptée est identique pour résoudre un problème à frontière libre à deux dimensions d'espace. Les équations de Navier-Stokes incompressibles avec conditions de bords de type Neumann sont résolues dans le domaine liquide. La surface libre est constituée par la totalité du bord du domaine liquide. Une équation supplémentaire permet de décrire l'évolution du domaine liquide. Nous obtenons un résultat d'existence et d'unicité locale en temps pour ce problème.

Dans la deuxième partie de cette thèse, nous proposons une méthode numérique pour la résolution d'écoulements de fluides à surface libre à deux et trois dimensions d'espace. Nous considérons un liquide se déplaçant dans une cavité remplie de gaz compressible. Les équations régissant le comportement de la vitesse et la pression dans le liquide sont les équations de Navier-Stokes évolutives incompressibles. La fonction caractéristique du domaine liquide satisfait une équation de transport. La vitesse dans le gaz est négligée et la pression à l'intérieur de chacune des bulles de gaz enfermées dans le liquide est calculée en utilisant la loi des gaz parfaits. Un algorithme permettant de numérotter les bulles de gaz est présenté. La pression dans le gaz induit une force normale sur la surface libre. Les effets de tension de surface sont également pris en compte et nous présentons une méthode pour le calcul de la courbure de l'interface entre le liquide et le gaz. Un algorithme à pas fractionnaires est utilisé pour découpler les différents phénomènes physiques. Des simulations numériques de fluides à frontière libre sont proposées dans le cadre de processus de coulée en moule ainsi que pour des problèmes dominés par les effets de tension de surface.

Abstract

Mathematical and numerical aspects of free surface flows are investigated.

On one hand, the mathematical analysis of some free surface flows is considered. A model problem in one space dimension is first investigated. The Burgers equation with diffusion has to be solved on a space interval with one free extremity. This extremity is unknown and moves in time. An ordinary differential equation for the position of the free extremity of the interval is added in order to close the mathematical problem. Local existence in time and uniqueness results are proved for the problem with given domain, then for the free surface problem. *A priori* and *a posteriori* error estimates are obtained for the semi-discretization in space. The stability and the convergence of an Eulerian time splitting scheme are investigated. The same methodology is then used to study free surface flows in two space dimensions. The incompressible unsteady Navier-Stokes equations with Neumann boundary conditions on the whole boundary are considered. The whole boundary is assumed to be the free surface. An additional equation is used to describe the moving domain. Local existence in time and uniqueness results are obtained.

On the other hand, a model for free surface flows in two and three space dimensions is investigated. The liquid is assumed to be surrounded by a compressible gas. The incompressible unsteady Navier-Stokes equations are assumed to hold in the liquid region. A volume-of-fluid method is used to describe the motion of the liquid domain. The velocity in the gas is disregarded and the pressure is computed by the ideal gas law in each gas bubble trapped by the liquid. A numbering algorithm is presented to recognize the bubbles of gas. Gas pressure is applied as a normal force on the liquid-gas interface. Surface tension effects are also taken into account for the simulation of bubbles or droplets flows. A method for the computation of the curvature is presented. Convergence and accuracy of the approximation of the curvature are discussed. A time splitting scheme is used to decouple the various physical phenomena. Numerical simulations are made in the frame of mould filling to show that the influence of gas on the free surface cannot be neglected. Curvature-driven flows are also considered.

Acknowledgements

I am very much indebted to Professor Jacques Rappaz for having accepted to be my thesis director. He introduced me to numerical analysis and has confidence in me since I have been a student. He accepted me in his group and gave me the opportunity to work on very interesting and various subjects in the fields of numerical analysis and scientific computing. I have learned a lot from his suggestions and remarks, as well in research or in teaching.

I am most grateful to Dr Marco Picasso for his scientific support and for being part of my jury. I particularly appreciate his availability and his numerous good advices and indications. It is also a pleasure to thank Dr Vincent Maronnier for his kind and frequent support.

Professors Jiwen He, Olivier Pironneau and Alfio Quarteroni who honoured me by being part of my jury and by reading this work are gratefully acknowledged. Thanks also to Professor Anthony C. Davison, president of the jury.

I thank the Swiss National Science Foundation for its financial support and the company Calcom SA, ESI Group, for graciously providing the numerical software calcoSOFT.

At this point, I also want to thank all the present and former members of the team of Numerical Analysis and Simulation. For a couple of years, we have shared many interesting discussions about mathematics or other aspects of a Ph.D. student's life. In particular, thanks for the very good atmosphere inside our group. Finally I would like to thank all my friends, inside and outside the EPFL, who contributed from far or near to making this period so rich and interesting.

Finalement, je remercie de tout coeur mes parents pour leur écoute et leur compréhension durant toutes ces années d'études et de thèse.

Enfin merci à Anouck.

Contents

Introduction	1
1 Analysis of a One-Dimensional Free Surface Problem	7
1.1 Mathematical Model	7
1.2 Moving Boundary Problem	8
1.3 Free Surface Problem	15
1.4 Semi-Discretization in Space	20
1.5 A Priori and A Posteriori Error Estimates	22
1.6 A Time Splitting Scheme	34
1.6.1 Advection Step	36
1.6.2 Diffusion Step	44
1.7 Numerical Results	45
2 A Two-Dimensional Free Surface Problem	49
2.1 Mathematical Model	49
2.2 Stokes Problem	53
2.3 Modified Stokes Problem	56
2.4 Given Boundary Problem	62
2.5 Free Surface Problem	64
3 Numerical Simulation of Free Surface Flows with Bubbles of Gas	69
3.1 Mathematical Model	69
3.1.1 Volume-of-Fluid method	69
3.1.2 Governing Equations in the Liquid	70
3.1.3 Governing Equations in the Gas	72
3.2 Time Discretization	74
3.2.1 Advection Step	74
3.2.2 Numbering of the Bubbles of Gas	75
3.2.3 Computation of the Pressure in the Gas	77
3.2.4 Diffusion Step	77
3.3 Space Discretization	78
3.4 Numerical Results	83

4 Numerical Approximation of Surface Tension Effects and Curvature	97
4.1 Modelling	97
4.2 Computation of the Curvature in two dimensions	101
4.2.1 A Geometrical Method	101
4.2.2 A Projection Method	103
4.3 Smoothing the Volume Fraction of Liquid	105
4.4 Smoothing the Curvature along the Interface	106
4.5 The Three-Dimensional case	108
4.6 Convergence and Accuracy	109
4.6.1 A Geometrical Method	109
4.6.2 A Projection Method	111
4.7 Numerical Results	117
Conclusions	127
Bibliography	129

Introduction

Numerical methods for solving free surface problems are of great importance in many engineering applications. Problems with free surfaces appear in fluid-structure interactions [31, 45], blood flows in moving arteries [95], immiscible multi-fluids problems [57, 68, 121], motion of glaciers [89], viscoelastic flows [10, 104], mould filling [66, 76, 102] and many other domains.

Free surface flows are investigated here, with particular emphasis on the process of mould filling. In foundry applications for example, the filling stage is a crucial point in the process. Complex topological shapes can be obtained and every occlusion of gas during the filling stage may lead to a manufacturing defect. It is therefore very important to have a good approximation of the position of the interface between the liquid and the gas.

A model for liquid-gas flows with a free surface is investigated here. A cavity containing a liquid and a gas is considered. In most of the numerical methods both media are generally assumed to be either incompressible, as in [9, 83, 114, 117] for instance, or compressible, see [1, 61, 105, 106]. The velocity and pressure satisfy either incompressible Navier-Stokes equations or Euler compressible equations in the whole cavity. Methods mixing an incompressible liquid and a compressible gas have also been considered. For instance, a one-dimensional model involving incompressible liquid and compressible gas with chemical reactions has been presented in [18]. In [37] the incompressible liquid satisfies the Navier-Stokes equations, while Euler's equations are satisfied in the compressible gas. However such a model is expensive from a computational point of view.

In this work, the liquid is assumed to be incompressible, viscous and Newtonian, while the gas is assumed to be compressible. Surface tension effects on the free surface between liquid and gas are taken into account. A model has been considered in [73] for the simulation of liquid free surface flows when the surrounding gas and the surface tension effects are disregarded. Our main objective is to take into account the compressibility effect of the gas without solving the Euler compressible equations in the gas domain. The Navier-Stokes equations are therefore considered only in the liquid domain and computational cost is lower, especially for three-dimensional computations.

The model is as follows. The liquid domain Ω_t , $t \in (0, T)$, is assumed to be contained in a bounded cavity Λ and is described by the volume fraction of liquid φ . Let Q_T be the space-time liquid domain. The volume fraction of liquid φ satisfies (in a weak sense):

$$\frac{\partial \varphi}{\partial t} + \mathbf{v} \cdot \nabla \varphi = 0, \text{ in } Q_T ,$$

where \mathbf{v} is the liquid velocity. The governing equations inside the liquid are the *incompressible Navier-Stokes equations*:

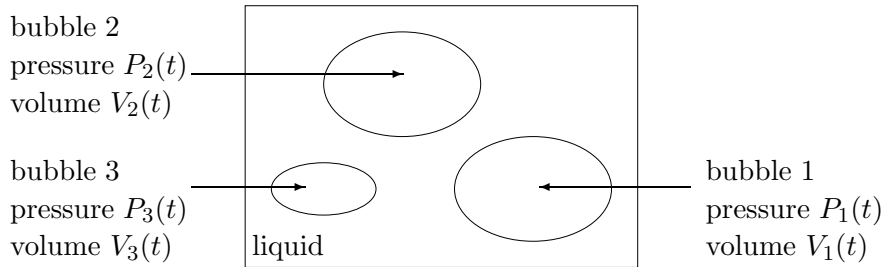
$$\begin{cases} \frac{\partial \mathbf{v}}{\partial t} - 2\operatorname{div}(\mu D(\mathbf{v})) + (\mathbf{v} \cdot \nabla) \mathbf{v} + \nabla p = \mathbf{f}, & \text{in } Q_T, \\ \operatorname{div} \mathbf{v} = 0, & \text{in } Q_T, \end{cases}$$

where $D(\mathbf{v})$ is the deformation tensor. Furthermore, a simple algebraic turbulence model is added (see [30, 112] for a general review of turbulence models) since high Reynolds numbers are considered. Neumann boundary conditions are imposed on the free surface, while slip and/or Dirichlet boundary conditions are imposed on the boundary being in contact with the walls of the cavity.

Rather than solving the Euler compressible equations in the gas domain, the velocity in the gas is disregarded and the pressure is computed from the *ideal gas law*. The pressure P is assumed to be constant in space in each bubble of gas trapped by the liquid, but varying in time. That means $P(x, t) = P_i(t)$ if x belongs to bubble number i . The pressure is then computed by using the ideal gas law

$$P_i V_i = n_i R \theta,$$

where in each bubble of gas, P_i is the pressure, V_i the volume, n_i the fraction number of molecules, R the constant of ideal gases and θ the temperature which is assumed to be constant.



For mould filling processes, the effects of surface tension can generally be neglected since the Capillary number is much smaller than the Reynolds number. If this is not the case, the behaviour of the gas bubbles trapped inside the liquid strongly depends on surface tension. In our algorithm, surface tension effects are modelled by a force on the interface. The liquid being surrounded by compressible gas and surface tension effects being taken into account, the following relation holds on the liquid-gas interface:

$$-p\mathbf{n} + 2\mu D(\mathbf{v})\mathbf{n} = -P\mathbf{n} + \sigma\kappa\mathbf{n}.$$

Here \mathbf{n} is the unit normal vector oriented towards the gas domain, P is the gas pressure and κ is the curvature of the interface. The surface tension coefficient σ depends on the physical properties of both, the liquid and the gas and is supposed to be constant.

Since the Navier-Stokes equations are solved only in the liquid domain, the size of the linear system corresponding to the generalized Stokes problem depends only on the size of

INTRODUCTION

the liquid domain, but not on the size of the cavity. CPU time and memory are spared. Thus our algorithm permits to take into account the compressibility effect of the gas at a relatively low computational cost.

This thesis consists of two different parts. In a first part, two problems related to this model are investigated from a theoretical point of view. The second part focuses on the simulation of such free surface liquid-gas flows. Many methods exist in the literature to treat free surface problems. References appearing in this work, and especially in this introduction, give only a non-exhaustive list of examples.

The first part of this thesis (chapters 1 and 2) is devoted to theoretical studies related to free surface flows.

In chapter 1, a one-dimensional model problem for the velocity u is first investigated. This model is a one-dimensional simplification of the free surface problem described before. It consists of Burgers' equation with an additional diffusion term in a space interval with one free extremity. This extremity is unknown and moves in time. Compressibility of gas and surface tension effects are not taken into account. A zero force boundary condition is thus enforced on the free extremity of the interval. This problem is an example of non-cylindrical space-time domain problems [69, 70]. Other results for the Burgers equation with a free surface can be found in [8, 36] for instance.

The one-dimensional model is as follows. Let T be a final time and α and ε two given positive parameters. The problem reads: given $f(x, t)$, $u_0(x)$ and $s_0 > 0$, find $u(x, t)$ and $s(t)$ such that:

$$\left\{ \begin{array}{ll} \frac{\partial u}{\partial t}(x, t) + \alpha u(x, t) \frac{\partial u}{\partial x}(x, t) - \varepsilon \frac{\partial^2 u}{\partial x^2}(x, t) = f(x, t) , & x \in (0, s(t)), \quad t \in (0, T) , \\ u(x, 0) = u_0(x) , & x \in (0, s_0) , \\ u(0, t) = 0 , & t \in (0, T) , \\ \frac{\partial u}{\partial x}(s(t), t) = 0 , & t \in (0, T) , \\ \dot{s}(t) = u(s(t), t) , & t \in (0, T) , \\ s(0) = s_0 . & \end{array} \right.$$

Here $\dot{s}(t)$ denotes the derivative of s with respect to t . First, existence and uniqueness of a solution are proved for a problem with a given boundary function $s(t)$ in a well-chosen function space, disregarding the equation $\dot{s}(t) = u(s(t), t)$. The Faedo-Galerkin method [29] and the Schauder fixed point theorem [42] are used. Then existence and uniqueness of a solution to the free surface problem are proved using again a fixed point theorem for the equation $\dot{s}(t) = u(s(t), t)$.

A finite element discretization in space is introduced and the existence of an approximated solution is obtained. *A priori* error estimates are derived using variational and duality arguments [19, 52]; *a posteriori* error estimates are also presented [4, 125].

A time splitting scheme is then considered. This scheme is a one-dimensional version of the scheme used in [73]. Advection and diffusion phenomena are decoupled. The advection

step (Burgers' equation without diffusion) is solved with a method of characteristics with projection. This method is proved to be equivalent, under the Courant-Friedrichs-Lewy condition, to a finite difference scheme. Furthermore it is $\mathcal{O}(\tau + h)$ -convergent under some stability conditions. Numerical experiments confirm the theoretical predictions.

In chapter 2, a two-dimensional Navier-Stokes problem with a free surface is considered. Neumann boundary conditions are imposed on the whole boundary. The free surface is assumed to be the whole boundary of the domain. Gas pressure and surface tension effects are not taken into account. In this work, existence and uniqueness of a solution are proved for small times. The methodology is the same as in chapter 1.

A similar problem is also studied in [107, 110] where the existence is proved by using Lagrange coordinates and a fixed point theorem for the velocity field. In [108, 111], existence results are obtained for the same problem, but in different function spaces. In [45], the problem with Dirichlet boundary conditions is considered and in [6] the domain is assumed to be an infinite horizontal layer domain and mixed Dirichlet-Neumann boundary conditions are enforced. Small-time existence of the Navier-Stokes problem with a free surface in other situations can be found in [2, 7] for instance.

Given the shape of the moving domain, the fluid flow problem is first considered. For each time t , the domain is mapped into a reference domain by a given mapping η which is first assumed to be known. A modified Navier-Stokes problem is obtained in the reference domain. Two successive fixed point theorems are used to obtain the existence of a solution to the fluid flow problem. Finally, the equation for the mapping η is considered,

$$\frac{\partial \eta}{\partial t}(x, t) = \mathbf{v}(\eta(x, t), t), \quad \eta(x, 0) = x \quad ,$$

where \mathbf{v} is the velocity. A fixed point theorem is used to obtain the existence and uniqueness of a solution to the free surface problem for small times.

The second part of this thesis (chapters 3 and 4) is devoted to numerical methods. The simulation of liquid-gas free surface flows in two and three space dimensions is presented.

Several numerical procedures can be used for solving free surface flows, especially to describe with accuracy the motion of the free surface. Two different methodologies can be distinguished: the *Lagrangian* methods and the *Eulerian* methods. Lagrangian methods, described for instance in [50, 51] (included front-tracking methods [43, 122]), or *Arbitrary-Lagrangian-Eulerian* (ALE) methods [54, 78, 119] are mainly used if the displacement of the liquid domain is small, for example in fluid-structure interactions. The domain of computation is stretched and re-meshed at each time step. For flows in complex topological domains, re-meshing can be difficult since the deformation of the liquid domain is large.

On the other hand, Eulerian methods introduce an additional unknown in the whole cavity in order to track the presence of liquid. A supplementary equation for this additional unknown is required in order to guarantee the well-posedness of the problem. The *pseudo-concentration* methods, see *e.g.* [28, 32, 67, 79, 120, 123], the *level set* methods, see [21, 27, 85, 84, 113], or the *volume-of-fluid* (VOF) methods, see [53, 77, 100, 129], are the most-used Eulerian methods. In the level set method, the free boundary is defined by a level line of a smooth function. This additional function generally satisfies a Hamilton-Jacobi equation [5, 44, 55]. The gradient of this smooth function can vanish into the

INTRODUCTION

neighbourhood of the free surface and the function may be rescaled, see [86] for instance. Conservation of the mass of liquid is not guaranteed. In the pseudo-concentration method, the free boundary is also defined by a level set of a smooth function. This additional function satisfies an advection equation. In the VOF methods, the fluid domain is tracked by its characteristic function. This function has value one in the liquid, zero in the gas and jumps over the interface. It satisfies an advection equation, see for instance [100]. The mass of fluid is rigorously conserved but the computation of the curvature is not easy due to the lack of regularity of the characteristic function. It is well-adapted to problems with changes in the topology of the domain, see [46], or cavity filling, see [59]. Mixing VOF and level set methods (see *e.g.* [115, 124]), conjugates the smoothness character of the level sets and the mass conservation.

Our main application is mould filling. In such situations, the geometry of the cavity is complex and the domain may present non-trivial topological changes due to the splitting or merging of the bubbles of gas trapped inside the liquid domain. As the liquid domain may take any shape in the cavity, an Eulerian method is more adapted. Moreover a VOF approach is considered.

In chapter 3, the numerical simulation of free surface flows involving an incompressible liquid and a compressible gas is presented. Surface tension effects are not taken into account. A numerical algorithm for the resolution of Navier-Stokes equations with a free surface in two and three space dimensions has been presented in [73]. This algorithm does not take into account the surrounding gas. As a consequence, the bubbles of gas trapped by the fluid are vanishing rapidly in the simulations.

Here a finite element-characteristics method on two different grids has been used together with a time splitting algorithm for the simulation of liquid-gas flows. This numerical method for the treatment of the liquid domain is the one presented in [73] when the surrounding gas was disregarded. The advection and diffusion parts of the Navier-Stokes equations are decoupled. The advection part and the transport of the volume fraction of liquid are treated on a fine grid of regular cells with the method of characteristics, see for instance [90, 91, 96]. The gas pressure is then computed at each grid node of a finite element mesh which belongs to the gas domain. A *numbering* (or *coloration*) *algorithm* is included to capture the positions of the connected components of the gas domain, as they represent the gas bubbles trapped by the liquid. This numbering algorithm consists in solving successively Poisson problems. All connected components of the gas domain are thus recognized one after the other. Once these connected components are located, the pressure inside each of them is updated by using the ideal gas law. The changes of topology of the gas domain which may appear (splitting and merging of bubbles) are taken into account in the computation of the pressure in the gas. A generalized Stokes problem is solved afterwards on the finite element unstructured mesh, by using a $\mathbb{P}_1 - \mathbb{P}_1$ finite element method with Galerkin Least Squares stabilization, as described in [38, 39].

Numerical simulations are in better agreement with experiments when taking into account the effect of gas compressibility. Gas compressibility is considered mainly in mould filling experiments in two and three space dimensions. The case of a rising bubble flow is also presented. Convergence results are obtained for the pressure in the gas. The supplementary computational cost due to bubbles treatment is relatively low.

In chapter 4, the approximation of surface tension effects is presented. Contact angles (see for instance [98]) are not taken into account. Since surface tension effects are generally not relevant for mould filling situations, curvature-driven flows are considered. For such flows, the behaviour of the bubbles of gas trapped inside the liquid strongly depends on surface tension [122, 131]. This is for example the case of crashing droplets of water [56, 57, 115], viscoelastic flows [104] or wave propagation [41]. Different methods can be used to model surface tension effects (see [12, 101] for a review). In our algorithm, surface tension effects are modelled by the *continuous surface force* (CSF), see [11, 33, 100, 128] for instance. This force is expressed by

$$\mathbf{F}_{ST} = \sigma \kappa \mathbf{n} ,$$

on the free surface. Here κ is the curvature and the surface tension coefficient σ is constant and depends on the physical properties of both, the liquid and the gas. Approximations of the curvature κ and the normal vector \mathbf{n} are thus required. The curvature can be computed by approximating the second derivatives of the volume fraction of liquid [94], or by computing the volume fraction of a sphere which lies on one side of the interface [14], or with geometric considerations as in [25, 92]. Generally computation of the curvature is carried out on a structured grid. Several methods are presented here in the two-dimensional case to compute the curvature of the interface between the liquid and the gas at each time step. Our computations are performed on an unstructured finite element mesh.

The first method is a local reconstruction of the interface, as in [80, 99] for instance. The method consists in computing one value of the curvature at each node of the interface by approximating the radius of the osculating circle of the interface. In order to remove mesh size effects, a smoothing procedure is applied on the interface [48, 87]. This method is convergent but not very accurate.

A second method is then proposed. The curvature κ is defined by the divergence of the external normal vector to the liquid domain [84, 103],

$$\kappa = \operatorname{div} \mathbf{n}, \quad \text{where} \quad \mathbf{n} = -\frac{\nabla \varphi}{|\nabla \varphi|} .$$

The L^2 -projection (with mass lumping) of this curvature on the \mathbb{P}_1 finite element space is considered. Because of its lack of regularity, the volume fraction of liquid φ is convoluted with a smooth kernel [20, 99, 128]. Thus an artificial curvature is obtained at each grid point of the unstructured mesh. Convergence results are obtained for the approximation of the curvature.

It is reported in [99, 124] for instance that the addition of the surface tension force on the interface leads to parasitic currents, namely regions of recirculation close to the interface. Numerical results show that the magnitude of these currents compares well with previous results.

Numerical simulations when taking into account the surface tension effects are presented mainly in the two-dimensional case. Bubbles and droplets flows (see for instance [65] for the case of a rising bubble) or curvature-driven flows are considered.

Chapter 1

Analysis of a One-Dimensional Free Surface Problem

A one-dimensional simplified model of a free surface problem is considered in this chapter, namely the Burgers equation with an additional diffusion. This problem is a simplification in one space dimension of the Navier-Stokes equations with a free surface encountered in [74, 75]. Local existence in time and uniqueness of a solution are proved (see also [8, 36] for instance) and space and time discretizations are investigated (see also [15, 63] for instance).

The structure of this chapter is the following: in the next section, the governing equations of the one-dimensional model problem are presented. Then, the existence and uniqueness of a solution to the problem with given but non constant boundary are proved. In Sect. 1.3, existence and uniqueness of a solution of the free surface problem are obtained. Sections 1.4 and 1.5 deal with finite element approximation in space and *a priori* and *a posteriori* error estimates. Then an Eulerian time splitting scheme is discussed in Sect. 1.6 and numerical results are presented in Sect. 1.7.

1.1 Mathematical Model

A one-dimensional free surface problem is presented, namely the Burgers equation with an additional diffusion. Let $T > 0$ be a finite time which represents the final time of the simulation. Let $s : (0, T) \rightarrow \mathbb{R}$ be a function *a priori* unknown defined on the interval of time $(0, T)$ and let the space-time domain Q_T be defined by:

$$Q_T = \{(y, t) : y \in (0, s(t)) : t \in (0, T)\} . \quad (1.1)$$

The problem we want to consider later is the following. Given $s_0 > 0$ and the functions $\bar{f} : Q_T \rightarrow \mathbb{R}$, $\bar{u}_0 : (0, s_0) \rightarrow \mathbb{R}$, find $s : (0, T) \rightarrow \mathbb{R}$ and $u : Q_T \rightarrow \mathbb{R}$ such that:

$$\left\{ \begin{array}{ll} \frac{\partial u}{\partial t}(y, t) + \alpha u(y, t) \frac{\partial u}{\partial y}(y, t) - \varepsilon \frac{\partial^2 u}{\partial y^2}(y, t) = \bar{f}(y, t) , & (y, t) \in Q_T , \quad (1.2) \\ u(y, 0) = \bar{u}_0(y) , & y \in (0, s_0) , \quad (1.3) \\ u(0, t) = 0 , & t \in (0, T) , \quad (1.4) \\ \frac{\partial u}{\partial y}(s(t), t) = 0 , & t \in (0, T) , \quad (1.5) \\ \dot{s}(t) = u(s(t), t) , & t \in (0, T) , \quad (1.6) \\ s(0) = s_0 . & \quad (1.7) \end{array} \right.$$

Here α and ε are real strictly positive numbers. Equations (1.2)-(1.5) are the Burgers equation with mixed Dirichlet-Neumann boundary conditions. Equations (1.6)-(1.7) are the coupling equations, necessary to determine the free surface $y = s(t)$ and to ensure that the mathematical problem is well-posed. Situation is illustrated in Fig. 1.1.

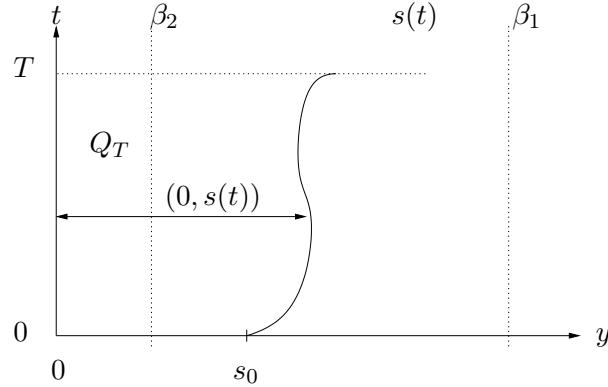


Figure 1.1: Free surface problem formulation in space-time domain.

The goal is to prove the local in time existence and uniqueness of the solution (u, s) to the problem (1.2)-(1.7). We will mainly prove that, if \bar{f}, \bar{u}_0 are sufficiently regular given functions, there exists a final time $0 < \hat{T} \leq T$ such that the problem (1.2)-(1.7) admits one unique solution (u, s) defined on $(0, \hat{T})$.

1.2 Moving Boundary Problem

Let $\beta_1 > \beta_2 > 0$ and $K > 0$ be given real numbers. The set $\mathcal{S}(T)$ of admissible functions for s is defined by:

$$\mathcal{S}(T) = \left\{ s \in W^{1,\infty}(0, T) \quad : \quad \beta_2 \leq s(t) \leq \beta_1, \quad \forall t \in [0, T], \quad s(0) = s_0 \quad (1.8) \right. \\ \left. \text{and } |\dot{s}(t)| \leq K, \quad \text{a.e. } t \in [0, T] \right\} ,$$

1.2. MOVING BOUNDARY PROBLEM

where s_0 is the initial value given by (1.7). Let the function s be fixed in $\mathcal{S}(T)$. Our first goal is to find a function $u : Q_T \rightarrow \mathbb{R}$ such that

$$\left\{ \begin{array}{ll} \frac{\partial u}{\partial t}(y, t) + \alpha u(y, t) \frac{\partial u}{\partial y}(y, t) - \varepsilon \frac{\partial^2 u}{\partial y^2}(y, t) = \bar{f}(y, t) , & (y, t) \in Q_T , \\ u(y, 0) = \bar{u}_0(y) , & y \in (0, s_0) , \\ u(0, t) = 0 , & t \in (0, T) , \\ \frac{\partial u}{\partial y}(s(t), t) = 0 , & t \in (0, T) . \end{array} \right. \quad (1.9)$$

The functions \bar{f} and \bar{u}_0 are assumed to belong respectively to $L^2(0, T, H^1(0, \beta_1))$ and $H^1(0, s_0)$ with compatibility condition $\bar{u}_0(0) = 0$.

The problem (1.9) on the moving interval $(0, s(t))$ is turned into a problem on a fixed interval, namely $(0, 1)$. The velocity on the fixed domain is denoted by $\tilde{u}(x, t) = u(s(t)x, t)$. The functions f and u_0 are defined by $f(x, t) = \bar{f}(s(t)x, t)$ and $u_0(x) = \bar{u}_0(s_0x)$, $0 < x < 1$, $0 < t < T$. In the following \tilde{u} is denoted again by u for the sake of simplicity. The problem (1.10) is obtained. Let U^T be the space-time domain:

$$U^T = \{(x, t) \in (0, 1) \times (0, T)\} .$$

The problem reads: find $u : U^T \rightarrow \mathbb{R}$ such that:

$$\left\{ \begin{array}{ll} \frac{\partial u}{\partial t}(x, t) + \frac{\alpha}{s(t)} u(x, t) \frac{\partial u}{\partial x}(x, t) \\ \quad - \frac{\varepsilon}{s(t)^2} \frac{\partial^2 u}{\partial x^2}(x, t) - \frac{\dot{s}(t)}{s(t)} x \frac{\partial u}{\partial x}(x, t) = f(x, t) , & (x, t) \in U^T , \\ u(x, 0) = u_0(x) , & x \in (0, 1) , \\ u(0, t) = 0 , & t \in (0, T) , \\ \frac{\partial u}{\partial x}(1, t) = 0 , & t \in (0, T) . \end{array} \right. \quad (1.10)$$

The problem (1.10) without the nonlinear term is considered first, namely find $u : U^T \rightarrow \mathbb{R}$ such that:

$$\left\{ \begin{array}{ll} \frac{\partial u}{\partial t}(x, t) - \frac{\varepsilon}{s(t)^2} \frac{\partial^2 u}{\partial x^2}(x, t) - \frac{\dot{s}(t)}{s(t)} x \frac{\partial u}{\partial x}(x, t) = f(x, t) , & (x, t) \in U^T , \\ u(x, 0) = u_0(x) , & x \in (0, 1) , \\ u(0, t) = 0 , & t \in (0, T) , \\ \frac{\partial u}{\partial x}(1, t) = 0 , & t \in (0, T) . \end{array} \right. \quad (1.11)$$

Let the space V be defined by $\{v \in H^1(0, 1), v(0) = 0\}$ with norm $\|v\|_V$ induced by the norm of $H^1(0, 1)$. The dual space of V is denoted by V' . The variational form associated to the problem (1.11) is to find $u : t \in (0, T) \rightarrow u(t) \in V$ such that a.e. $t \in (0, T)$:

$$\int_0^1 \frac{\partial u}{\partial t} v dx - \frac{\dot{s}(t)}{s(t)} \int_0^1 x \frac{\partial u}{\partial x} v dx + \frac{\varepsilon}{s(t)^2} \int_0^1 \frac{\partial u}{\partial x} \frac{\partial v}{\partial x} dx = \int_0^1 f v dx, \quad \forall v \in V. \quad (1.12)$$

Proposition 1.1 (Energy inequality)

Let $T > 0$ and $s \in \mathcal{S}(T)$ be given. There exists a constant C independent of s such that, if $f \in L^2(U^T)$ and $u_0 \in L^2(0, 1)$, any solution u to (1.12) satisfies the following energy inequality:

$$\|u\|_{L^\infty(0,T,L^2(0,1)) \cap L^2(0,T,V) \cap H^1(0,T,V')}^2 \leq C \left(\|f\|_{L^2(U^T)}^2 + \|u_0\|_{L^2(0,1)}^2 \right). \quad (1.13)$$

PROOF : Consider $v = u(t) \in V$ in (1.12):

$$\int_0^1 \frac{\partial u}{\partial t} u dx - \frac{\dot{s}(t)}{s(t)} \int_0^1 x \frac{\partial u}{\partial x} u dx + \frac{\varepsilon}{s(t)^2} \int_0^1 \frac{\partial u}{\partial x} \frac{\partial u}{\partial x} dx = \int_0^1 f u dx,$$

so that the following relation can be obtained:

$$\frac{1}{2} \frac{d}{dt} \|u\|_{L^2(0,1)}^2 + \frac{\varepsilon}{\beta_1^2} \left\| \frac{\partial u}{\partial x} \right\|_{L^2(0,1)}^2 \leq \|f\|_{L^2(0,1)} \|u\|_{L^2(0,1)} + \frac{K}{\beta_2} \left\| \frac{\partial u}{\partial x} \right\|_{L^2(0,1)} \|u\|_{L^2(0,1)}.$$

The Young inequality leads to:

$$\frac{1}{2} \frac{d}{dt} \|u\|_{L^2(0,1)}^2 + \frac{\varepsilon}{2\beta_1^2} \left\| \frac{\partial u}{\partial x} \right\|_{L^2(0,1)}^2 \leq C_1 \|f\|_{L^2(0,1)}^2 + C_2 \|u\|_{L^2(0,1)}^2, \quad (1.14)$$

where C_1 and C_2 are two constants depending only on β_1 , β_2 , K and ε . Gronwall's lemma (see for instance [96, page 13]) leads to:

$$\|u(t)\|_{L^2(0,1)}^2 \leq C e^{C_2 T} \left(\|f\|_{L^2(U^T)}^2 + \|u_0\|_{L^2(0,1)}^2 \right), \quad \forall t \in (0, T). \quad (1.15)$$

Furthermore, by integrating (1.14) on $(0, T)$ and by using Poincaré inequality, we obtain the estimation:

$$\|u\|_{L^2(0,T,V)}^2 \leq C_3 \|f\|_{L^2(U^T)}^2 + C_4 \|u\|_{L^\infty(0,T,L^2(0,1))}^2, \quad (1.16)$$

where C_3 and C_4 are two constants depending only on β_1 , β_2 , K and ε . The boundedness in $L^2(0, T, V)$ -norm is a direct consequence of (1.15) and (1.16). Finally, the estimation for $\frac{\partial u}{\partial t}$ is obtained from (1.12):

$$\left\| \frac{\partial u}{\partial t} \right\|_{V'} \leq \frac{K}{\beta_2} \left\| \frac{\partial u}{\partial x} \right\|_{L^2(0,1)} + \frac{\varepsilon}{\beta_2^2} \left\| \frac{\partial u}{\partial x} \right\|_{L^2(0,1)} + \|f\|_{L^2(0,1)}.$$

By squaring this relation and integrating on $(0, T)$, the conclusion holds by using (1.15) and (1.16). \square

1.2. MOVING BOUNDARY PROBLEM

Theorem 1.1 (Existence and uniqueness of the linear problem)

Let $T > 0$ and $s \in \mathcal{S}(T)$ be given. If $f \in L^2(U^T)$ and $u_0 \in L^2(0, 1)$, then problem (1.12) admits one unique solution $u \in L^2(0, T, V) \cap H^1(0, T, V')$.

PROOF : Existence is proved with the Faedo-Galerkin method, see [29, volume 8]. This method is detailed hereafter for the convenience of the reader. Consider the eigenfunctions $\Phi_j(x)$ of the laplacian operator on $(0, 1)$ associated with eigenvalues λ_j , $j = 1, \dots, N$. These functions are solutions to:

$$\begin{cases} -\frac{d^2}{dx^2}\Phi_j(x) = \lambda_j\Phi_j(x), & x \in (0, 1) , \\ \Phi_j(0) = \Phi_j'(1) = 0 . \end{cases}$$

The functions $(\Phi_j)_{j=1}^\infty$ constitute a Hilbert basis of V . In this one-dimensional case, $\Phi_j(x) = \sin\left(\left(\frac{\pi}{2} + j\pi\right)x\right)$ and $\lambda_j = \left(\frac{\pi}{2} + j\pi\right)^2$. We define the following spaces:

$$\begin{aligned} W_N &= \left\{ v \in H^1(0, T, V) : v(x, t) = \sum_{j=1}^N \alpha_j(t)\Phi_j(x), \quad \alpha_j(t) \in H^1(0, T) \right\} ; \\ V_N &= \left\{ v \in V : v(x) = \sum_{j=1}^N \alpha_j\Phi_j(x), \quad \alpha_j \in \mathbb{R} \right\} . \end{aligned}$$

The problem in finite dimension reads: find $u_N \in W_N$ such that:

$$\begin{aligned} &\int_0^1 \frac{\partial u_N}{\partial t} \Phi_j dx - \frac{\dot{s}(t)}{s(t)} \int_0^1 x \frac{\partial u_N}{\partial x} \Phi_j dx + \frac{\varepsilon}{s(t)^2} \int_0^1 \frac{\partial u_N}{\partial x} \frac{\partial \Phi_j}{\partial x} dx \\ &= \int_0^1 f \Phi_j dx, \quad j = 1, \dots, N, \text{ a.e. } t \in (0, T) , \end{aligned} \quad (1.17)$$

with initial condition $u_N(x, 0) = u_{0,N}(x)$, $x \in (0, 1)$, where $u_{0,N}$ is the L^2 -projection of u_0 on V_N .

By setting $u_N(x, t) = \sum_{j=1}^N \alpha_j(t)\Phi_j(x)$ with $\alpha_j(t) \in H^1(0, T)$ and by defining $\boldsymbol{\alpha}(t) = (\alpha_1(t), \dots, \alpha_N(t))$, (1.17) can be written as a system of linear ordinary differential equations for $\boldsymbol{\alpha}(t)$ which admits one unique global solution (see [49] for instance).

A priori estimates are obtained (see Prop. 1.1). The sequence (u_N) is then uniformly bounded in $L^\infty(0, T, L^2(0, 1)) \cap L^2(0, T, V) \cap H^1(0, T, V')$. The spaces $L^2(0, T, V)$ and $L^2(0, T, V')$ are reflexive, so that there exist subsequences, also denoted by (u_N) , which converge weakly:

$$\begin{aligned} (u_N) &\rightharpoonup u \quad \text{in } L^2(0, T, V) \quad \text{weakly} , \\ (u_N) &\rightharpoonup v \quad \text{in } L^\infty(0, T, L^2) \quad \text{weakly} * , \\ \left(\frac{\partial u_N}{\partial t}\right) &\rightharpoonup w \quad \text{in } L^2(0, T, V') \quad \text{weakly} . \end{aligned}$$

Since $L^2(0, T, H^1(0, 1)) \cap H^1(0, T, V') \xrightarrow{c} L^2(Q_T)$, $u_N \rightarrow u$ strongly in $L^2(Q_T)$. Then $u_N \rightharpoonup u$ weakly in $L^2(Q_T)$. Moreover $u_N \rightharpoonup u$ weakly in $L^2(Q_T)$ implies $u_N \rightharpoonup u$ weakly in $L^\infty(L^2)$. By uniqueness of the weak limit, we obtain $u = v$.

Furthermore $\int_0^T \int_0^1 (u_n - u)v \frac{\partial \phi}{\partial t} dx dt \rightarrow 0$, $\forall v \in V$, $\forall \phi \in C_c^\infty(]0, T[)$, the space of functions infinitely differentiable with compact support in $(0, T)$. Integrating by parts leads to $\int_0^T \left\langle \frac{\partial(u_n - u)}{\partial t}, v \right\rangle \phi dt \rightarrow 0$. Since $\int_0^T \left\langle \frac{\partial u_n}{\partial t} - w, v \right\rangle \phi dt \rightarrow 0$, we can conclude by uniqueness of the weak limit that $w = \frac{\partial u}{\partial t}$ in $L^2(V')$.

Hence the limit u belongs to $L^\infty(0, T, L^2(0, 1)) \cap L^2(0, T, V) \cap H^1(0, T, V')$ and satisfies (1.13) (see [130, page 120]). By the same technique as in [29, volume 8, page 620ff], we take the limit when $N \rightarrow \infty$ and prove that the function u is the solution to (1.12). Let φ be a function of $C_c^\infty(]0, T[)$, the space of functions infinitely differentiable with compact support in $(0, T)$. For all $v \in V$, there exists a sequence (v_N) , $v_N \in V_N$ such that $v_N \rightarrow v$ strongly in V when $N \rightarrow \infty$. Set $v_N = \sum_{j=1}^N \beta_j \Phi_j$, $\beta_j \in \mathbb{R}$, and $\psi_N(x, t) = \varphi(t)v_N(x)$, $j = 1, \dots, N$; hence $\psi_N \in L^2(0, T, V)$. Multiply (1.17) by $\beta_j \varphi(t)$, sum on $j = 1, \dots, N$ and integrate on $(0, T)$ to obtain $\forall j = 1, \dots, N$:

$$\begin{aligned} & \int_0^T \int_0^1 \frac{\partial u_N}{\partial t} \psi_N dx dt - \int_0^T \frac{\dot{s}}{s} \int_0^1 x \frac{\partial u_N}{\partial x} \psi_N dx dt \\ & + \int_0^T \frac{\varepsilon}{s^2} \int_0^1 \frac{\partial u_N}{\partial x} \frac{\partial \psi_N}{\partial x} dx dt = \int_0^T \int_0^1 f \psi_N dx dt. \end{aligned}$$

Since the sequence (u_N) converges weakly and (ψ_N) converge strongly in $L^2(0, T, V)$, we can take the limit in this relation and conclude.

A variational argument leads to uniqueness: let u_1 and u_2 be two solutions. The difference $w = u_1 - u_2$ satisfies the same problem (1.17) with homogeneous right-hand side and initial condition. The estimate (1.13) implies $u_1 = u_2$. \square

Remark 1.1 *In this particular one-dimensional case, the Faedo-Galerkin method corresponds to the Fourier method on the space interval $(0, 1)$. The boundary conditions imply that the functions φ_j of the Hilbert basis of V are sinus-type functions.*

Notice that Thm 1.1 is also true if $f \in L^2(0, T, V')$ with the same arguments. Assuming more regularity on the data, the solution to (1.12) is more regular. This result is the subject of Thm 1.2.

Theorem 1.2 (Regularity of the solution)

Let $T > 0$ and $s \in \mathcal{S}(T)$ be given and assume that $f \in L^2(U^T)$ and $u_0 \in V$. The solution to the problem (1.12) belongs to $L^2(0, T, H^2(0, 1)) \cap H^1(0, T, L^2(0, 1))$ and is also the solution to the problem (1.11). Furthermore, there exists a constant C , independent of s, f and u_0 , and which depends only on $\beta_1, \beta_2, K, \varepsilon$ and T such that:

$$\|u\|_{L^\infty(0, T, V) \cap L^2(0, T, H^2(0, 1)) \cap H^1(0, T, L^2(0, 1))}^2 \leq C \left\{ \|f\|_{L^2(U^T)}^2 + \|u_0\|_V^2 \right\}. \quad (1.18)$$

1.2. MOVING BOUNDARY PROBLEM

PROOF : Since $-\frac{\partial^2 u_N}{\partial x^2}(x, t) = \sum_{j=1}^N \alpha_j(t) \lambda_j^2 \Phi_j(x)$, (1.17) leads to:

$$-\int_0^1 \frac{\partial u_N}{\partial t} \frac{\partial^2 u_N}{\partial x^2} dx + \frac{\dot{s}(t)}{s(t)} \int_0^1 x \frac{\partial u_N}{\partial x} \frac{\partial^2 u_N}{\partial x^2} dx - \frac{\varepsilon}{s(t)^2} \int_0^1 \frac{\partial u_N}{\partial x} \frac{\partial^3 u_N}{\partial x^3} dx = -\int_0^1 f \frac{\partial^2 u_N}{\partial x^2} dx ,$$

Integrating by parts yields:

$$\frac{1}{2} \frac{d}{dt} \left\| \frac{\partial u_N}{\partial x} \right\|_{L^2}^2 + \frac{\varepsilon}{\beta_1^2} \left\| \frac{\partial^2 u_N}{\partial x^2} \right\|_{L^2}^2 \leq C \|f\|_{L^2} \left\| \frac{\partial^2 u_N}{\partial x^2} \right\|_{L^2} + \frac{K}{\beta_2} \left\| \frac{\partial u_N}{\partial x} \right\|_{L^2} \left\| \frac{\partial^2 u_N}{\partial x^2} \right\|_{L^2} ,$$

so that Young inequalities and (1.13) lead to:

$$\|u_N\|_{L^2(0,T,H^2(0,1)) \cap L^\infty(0,T,V)}^2 \leq C \left\{ \|f\|_{L^2(U^T)}^2 + \|u_0\|_V^2 \right\} ,$$

which implies $u \in L^2(0, T, H^2(0, 1)) \cap L^\infty(0, T, V)$ by uniqueness of the limit function.

Relationship (1.11) leads to $\frac{\partial u}{\partial t} = \frac{\varepsilon}{s(t)^2} \frac{\partial^2 u}{\partial x^2} + \frac{\dot{s}(t)}{s(t)} x \frac{\partial u}{\partial x} + f$ in the sense of distributions.

This implies $\frac{\partial u}{\partial t} \in L^2(0, T, L^2(0, 1))$ and $u \in H^1(0, T, L^2(0, 1))$. \square

The inverse change of variables permits to conclude to the existence and uniqueness of a solution defined on the non-cylindrical domain Q_T , as in [69].

The existence of a solution to the nonlinear problem (1.10) is proved with a fixed point argument. Let the spaces $W_1(T)$ and $W_2(T)$ be defined by

$$\begin{aligned} W_1(T) &= \{v \in L^2(0, T, H^2(0, 1)) \cap L^\infty(0, T, V) \cap H^1(0, T, L^2(0, 1))\} , \\ W_2(T) &= \{v \in L^2(0, T, V) \cap L^\infty(0, T, L^2(0, 1)) \cap H^1(0, T, V')\} . \end{aligned}$$

Theorem 1.3 (Existence and uniqueness of the solution to nonlinear problem)

Let $s \in \mathcal{S}(T)$, $f \in L^2(U^T)$ and $u_0 \in V$ be given functions. There exists $0 < \tilde{T} \leq T$ such that (1.10) admits one unique solution $u \in W_1(\tilde{T})$.

PROOF : Let the operator τ_1 be defined by:

$$\begin{aligned} \tau_1 : \quad W_1(T) &\rightarrow W_2(T) , \\ u(x, t) &\rightarrow u(x, t) \frac{\partial u}{\partial x}(x, t) = \frac{1}{2} \frac{\partial}{\partial x} u^2(x, t) . \end{aligned}$$

Since the application $v \in H^1(0, 1) \rightarrow v^2 \in H^1(0, 1)$ is continuous, the operator τ_1 is continuous and its range is included in $W_2(T)$. Moreover the embedding of $W_2(T)$ inside $L^2(U^T)$ is compact (see for instance [70]). Let τ_2 be the continuous operator defined by:

$$\begin{aligned} \tau_2 : L^2(U^T) &\rightarrow W_1(T) , \\ f(x, t) &\rightarrow \tilde{u}(x, t) , \end{aligned} \tag{1.19}$$

where $\tilde{u}(x, t)$ is the solution to (1.11) associated with right-hand side $f(x, t)$ and initial condition $u_0(x)$. Let $L > 0$ be the real positive number given by:

$$L^2 = 2C \left\{ \|f\|_{L^2(U^T)}^2 + \|u_0\|_V^2 \right\} , \quad (1.20)$$

where the constant C is defined in (1.18). We consider the set $W(T)$ defined by $W(T) = \left\{ v \in W_1(T) : \|v\|_{W_1(T)} \leq L \right\}$. The application τ is defined by:

$$\begin{aligned} \tau : W(T) \subset W_1(T) &\xrightarrow{\tau_1} W_2(T) \xrightarrow{c} L^2(U^T) \xrightarrow{\tau_2} W_1(T) , \\ u &\longrightarrow u \frac{\partial u}{\partial x} \longrightarrow f - \frac{\alpha}{s(t)} u \frac{\partial u}{\partial x} \longrightarrow \tilde{u} . \end{aligned}$$

Application τ is continuous and compact. Since $s \in \mathcal{S}(T)$ and by using (1.18), we obtain:

$$\begin{aligned} \|\tilde{u}\|_{W_1(T)}^2 &\leq C \left\{ \left\| f - \frac{\alpha}{s(t)} u \frac{\partial u}{\partial x} \right\|_{L^2(U^T)}^2 + \|u_0\|_V^2 \right\} \\ &\leq C \left\{ \|f\|_{L^2(U^T)}^2 + \|u_0\|_V^2 \right\} + C \frac{\alpha}{\beta_2} \left\| u \frac{\partial u}{\partial x} \right\|_{L^2(U^T)}^2 \\ &\leq \frac{L^2}{2} + C \frac{\alpha}{\beta_2} \left\| u \frac{\partial u}{\partial x} \right\|_{L^2(U^T)}^2 \quad \text{by using (1.20)} . \end{aligned}$$

Here C depends on T (through Gronwall's lemma) and is uniformly bounded in $(0, T)$ by a constant denoted by \bar{C} . The last term can be bounded by:

$$C \frac{\alpha}{\beta_2} \|u\|_{L^\infty(U^T)}^2 \int_0^T \left\| \frac{\partial u}{\partial x} \right\|_{L^2}^2 dt \leq \bar{C} \frac{\alpha}{\beta_2} \|u\|_{L^\infty(U^T)}^2 \|u\|_{L^\infty(V)}^2 T \leq \bar{C} \frac{\alpha}{\beta_2} L^4 T . \quad (1.21)$$

Hence there exists $0 < \tilde{T} \leq T$ such that $\bar{C} \frac{\alpha}{\beta_2} L^4 \tilde{T} \leq \frac{L^2}{2}$ and $\|\tilde{u}\|_{W_1(\tilde{T})}^2 \leq L^2$.

The Schauder fixed point theorem (see for instance [42, page 279]) is used to conclude that application $\tau : W(\tilde{T}) \rightarrow W(\tilde{T})$ allows one fixed point in $W(\tilde{T})$. This fixed point is solution to (1.10) on $(0, \tilde{T})$. Uniqueness is proved with a variational argument; let u_1 and u_2 be two solutions to (1.12) and set $w = u_1 - u_2$. The function w satisfies, $\forall v \in V$ and a.e. $t \in (0, T)$:

$$\int_0^1 \frac{\partial w}{\partial t} v dx - \frac{\dot{s}(t)}{s(t)} \int_0^1 x \frac{\partial w}{\partial x} v dx + \frac{\varepsilon}{s(t)^2} \int_0^1 \frac{\partial w}{\partial x} \frac{\partial v}{\partial x} dx = -\frac{\alpha}{s(t)} \int_0^1 \left(u_1 \frac{\partial u_1}{\partial x} - u_2 \frac{\partial u_2}{\partial x} \right) v dx ,$$

with initial condition $w(0) = 0$. With $v = w$, the following relationship is obtained:

$$\begin{aligned} \int_0^1 \frac{\partial w}{\partial t} w dx + \frac{\varepsilon}{s(t)^2} \left\| \frac{\partial w}{\partial x} \right\|_{L^2(0,1)}^2 &\leq \frac{\alpha}{s(t)} \int_0^1 \left| u_1 \frac{\partial u_1}{\partial x} - u_2 \frac{\partial u_2}{\partial x} \right| |w| dx \\ &\quad + \frac{|\dot{s}(t)|}{s(t)} \int_0^1 x \left| \frac{\partial w}{\partial x} \right| |w| dx . \end{aligned} \quad (1.22)$$

1.3. FREE SURFACE PROBLEM

We notice that:

$$\int_0^1 \left| u_1 \frac{\partial u_1}{\partial x} - u_2 \frac{\partial u_2}{\partial x} \right| |w| dx \leq \tilde{C}(t) \|w\|_{L^2(0,1)} \left\| \frac{\partial w}{\partial x} \right\|_{L^2(0,1)},$$

with $\tilde{C}(t) = C \left(\left\| \frac{\partial u_1}{\partial x} \right\|_{L^2(0,1)} + \|u_2\|_{C^0([0,1])} \right)$, where C depends only on the domain $(0, 1)$.

Thanks to the regularity of $u_i, i = 1, 2$, the function $\tilde{C}(t)$ is uniformly bounded. Finally, we use a Young inequality to show that there exists a constant C_2 such that:

$$\frac{d}{dt} \|w\|_{L^2(0,1)}^2 + \frac{\varepsilon}{2\beta_1^2} \left\| \frac{\partial w}{\partial x} \right\|_{L^2(0,1)}^2 \leq C_2 \|w\|_{L^2(0,1)}^2. \quad (1.23)$$

Gronwall's lemma allows us to conclude that $w = 0$. □

1.3 Free Surface Problem

The problem with a free boundary is now investigated. The set $\mathcal{S}(T)$ defined by (1.8) is convex and closed in the Banach space $W^{1,\infty}(0, T)$. For each $s \in \mathcal{S}(T)$ there exists $0 < \tilde{T} \leq T$ (\tilde{T} independent of s) and one unique $u \in W_1(\tilde{T})$ which is solution to (1.10). Let the function $\tilde{s} : (0, \tilde{T}) \rightarrow \mathbb{R}$ be defined by:

$$\tilde{s}(t) = s_0 + \int_0^t u(1, \tau) d\tau, \quad (1.24)$$

where u is the solution to (1.10) associated to s previously given. Theorem 1.3 implies that the application (1.24) is well-defined. The following lemma is proved first:

Lemma 1.1

Let $f \in L^2(U^T)$ and $u_0 \in V$ be given functions. We assume $s_0 \in]\beta_2, \beta_1[$, $s \in \mathcal{S}(\tilde{T})$ and $\bar{C} \|u_0\|_V^2 < K^2/2$ (where \bar{C} is the constant defined in (1.21)). Let L be the constant defined in (1.20). We denote by $0 < \tilde{T} \leq T$ and $u \in W(\tilde{T}) = \left\{ v \in W_1(\tilde{T}) : \|v\|_{W_1(\tilde{T})} \leq L \right\}$ the solution to problem (1.10) on $(0, \tilde{T})$ associated to $s \in \mathcal{S}(\tilde{T})$. Then there exists $0 < \tilde{T} \leq \tilde{T}$ independent of s such that $\tilde{s} \in \mathcal{S}(\tilde{T})$.

PROOF : Clearly $\tilde{s}(0) = s_0$. Furthermore, since $u \in W_1(\tilde{T}) \stackrel{c}{\hookrightarrow} C^0(\overline{U^{\tilde{T}}})$ (see for instance [58, theorem 3.8, page 1.88]), the function $u(1, t)$ is continuous. By definition

$$\tilde{s}(t) = s_0 + \int_0^t u(1, t) dt \leq s_0 + t \|u\|_{C^0([0,1])} \leq s_0 + \tilde{T} \|u\|_{W_1(\tilde{T})} \leq s_0 + \tilde{T} L$$

and the assumption $s_0 \in]\beta_2, \beta_1[$ implies that there exists $0 < T_1 \leq \tilde{T}$ such that $\tilde{s}(t) \in]\beta_2, \beta_1[$ for $0 \leq t \leq T_1$. As $\dot{\tilde{s}}(t) = u(1, t)$, we have, according to (1.18):

$$|\dot{s}(t)|^2 = |u(1,t)|^2 \leq \|u\|_{W_1(\tilde{T})}^2 < \frac{K^2}{2} + \bar{C} \|f\|_{L^2(U^T)}^2 ,$$

and there exists $0 < T_2 \leq \tilde{T}$ such that $|\dot{s}(t)| \leq K$ for $0 < t \leq T_2$. Conclusion is obtained by taking $\bar{T} = \min\{T_1, T_2\}$. \square

The value of \bar{T} depends on f, s_0, β_1, β_2 and K but is independent of s . In the following, the time \bar{T} is denoted again by T . The following application is considered:

$$\begin{aligned} \gamma : \mathcal{S}(T) &\rightarrow \mathcal{S}(T) ; \\ s &\rightarrow \tilde{s} \quad \text{defined by (1.24)} . \end{aligned} \tag{1.25}$$

With lemma 1.1, application (1.25) is well-defined. It suffices to prove the existence and uniqueness of a fixed point of the operator γ defined by (1.25) to conclude to the existence and uniqueness of the solution to the free surface problem.

Theorem 1.4 (Existence and uniqueness of a fixed point of γ)

Let $f \in L^2(U^T)$ and $u_0 \in V$ be given functions. We assume $\bar{C} \|u_0\|_V^2 < K^2/2$ and $s_0 \in]\beta_2, \beta_1[$. There exists $0 < \hat{T} \leq T$ such that the application $\gamma : \mathcal{S}(\hat{T}) \rightarrow \mathcal{S}(\hat{T})$ allows one unique fixed point s . If u is the solution to the problem (1.10) associated with this fixed point s (such that $\dot{s}(t) = u(1,t)$), the couple (u, s) is then the unique solution to the problem:

$$\left\{ \begin{array}{ll} \frac{\partial u}{\partial t} + \frac{\alpha}{s(t)} u \frac{\partial u}{\partial x} - \frac{\varepsilon}{s(t)^2} \frac{\partial^2 u}{\partial x^2} - \frac{\dot{s}(t)}{s(t)} x \frac{\partial u}{\partial x} = f, & (x,t) \in U^{\hat{T}} , \\ u(x,0) = u_0(x), & x \in (0,1) , \\ u(0,t) = 0, & t \in (0,\hat{T}) , \\ \frac{\partial u}{\partial x}(1,t) = 0, & t \in (0,\hat{T}) , \\ \dot{s}(t) = u(1,t) & t \in (0,\hat{T}) , \\ s(0) = s_0 . \end{array} \right. \tag{1.26}$$

PROOF : According to lemma 1.1, the range of γ is included in $\mathcal{S}(T)$. We are starting by proving that the operator γ defined by (1.25) is continuous and compact.

Consider a sequence $(s_n)_{n=0}^\infty$ strongly convergent in $\mathcal{S}(T)$ and let its limit be denoted by $s \in \mathcal{S}(T)$:

$$(s_n) \rightarrow s \text{ in } \mathcal{S}(T) \text{ strongly, according to the norm } \|\cdot\|_{W^{1,\infty}(0,T)} . \tag{1.27}$$

A function $u_n \in W_1(T)$ is associated with each term s_n of this sequence. The function u_n is solution to (1.10) with given boundary s_n . The sequence (u_n) is uniformly bounded in $W_1(T)$ by a constant which does not depend on the sequences $(u_n)_{n=0}^\infty$ and $(s_n)_{n=0}^\infty$ (see Thm 1.3). The following compact inclusions are true (see [70] and [58]):

1.3. FREE SURFACE PROBLEM

$$L^2(0, T, H^2(0, 1)) \cap H^1(0, T, L^2(0, 1)) \xrightarrow{c} L^2(0, T, V) , \quad (1.28a)$$

$$L^2(0, T, H^2(0, 1)) \cap H^1(0, T, L^2(0, 1)) \xrightarrow{c} C^0(\overline{UT}) . \quad (1.28b)$$

The space $H^1(0, T, L^2(0, 1)) \cap L^2(0, T, H^2(0, 1))$ being reflexive, there exist subsequences, also denoted by $(u_n)_{n=0}^\infty$, which are weakly convergent:

$$(u_n) \rightharpoonup u \text{ in } L^2(0, T, H^2(0, 1)) \text{ weakly} , \quad (1.29)$$

$$\left(\frac{\partial u_n}{\partial t}\right) \rightharpoonup v \text{ in } L^2(0, T, L^2(0, 1)) \text{ weakly} , \quad (1.30)$$

$$(u_n) \rightarrow w \text{ in } C^0(\overline{UT}) \text{ strongly} . \quad (1.31)$$

By using the same arguments as in Thm 1.1, $u = w$ and $v = \frac{\partial u}{\partial t}$.

Moreover, relationship (1.31) implies $(u_n(1, \cdot)) \rightarrow u(1, \cdot)$ strongly in $C^0([0, T])$. If we define $\tilde{s}_n(t) = s_0 + \int_0^t u_n(1, \tau) d\tau$ and $\tilde{s}(t) = s_0 + \int_0^t u(1, \tau) d\tau$, we necessarily have $\tilde{s}_n \rightarrow \tilde{s}$ strongly in $W^{1, \infty}(0, T)$.

Now we want to prove that u is the solution to (1.10) with $\dot{s}(t) = u(1, t)$. Our definition of u_n from s_n is leading to:

$$\begin{aligned} & \int_{UT} \frac{\partial u_n}{\partial t} v dx dt + \int_{UT} \frac{\varepsilon}{s_n(t)^2} \frac{\partial u_n}{\partial x} \frac{\partial v}{\partial x} dx dt - \int_{UT} \frac{\dot{s}_n(t)}{s_n(t)} x \frac{\partial u_n}{\partial x} v dx dt \\ & + \int_{UT} \frac{\alpha}{s_n(t)} u_n \frac{\partial u_n}{\partial x} v dx dt = \int_{UT} f v dx dt, \quad \forall v \in L^2(0, T, V) . \end{aligned}$$

By taking the limit in this last relationship and by using (1.27), (1.29)-(1.31), we obtain:

$$\begin{aligned} & \int_{UT} \frac{\partial u}{\partial t} v dx dt + \int_{UT} \frac{\varepsilon}{s(t)^2} \frac{\partial u}{\partial x} \frac{\partial v}{\partial x} dx dt - \int_{UT} \frac{\dot{s}(t)}{s(t)} x \frac{\partial u}{\partial x} v dx dt \\ & + \int_{UT} \frac{\alpha}{s(t)} u \frac{\partial u}{\partial x} v dx dt = \int_{UT} f v dx dt, \quad \forall v \in L^2(0, T, V) , \end{aligned}$$

Then u is the unique solution to (1.10) with $\dot{s}(t) = u(1, t)$ and γ is thus a continuous operator. Let $s \in \mathcal{S}(T)$ and u be the solution to (1.10) with boundary $\dot{s}(t) = u(1, t)$. Application γ can be written:

$$\begin{aligned} \mathcal{S}(T) & \rightarrow W_1(T) \xrightarrow{c} C^0(\overline{UT}) \rightarrow C^0([0, T]) \rightarrow \mathcal{S}(T) \subset W^{1, \infty}(0, T) \\ s(t) & \rightarrow u(x, t) \xrightarrow{c} u(x, t) \rightarrow u(1, t) \rightarrow \tilde{s}(t) = s_0 + \int_0^t u(1, \tau) d\tau . \end{aligned}$$

The application γ is composed by continuous applications and one compact embedding (1.28b). Hence γ is compact.

Schauder's theorem together with Lemma 1.1 permit to conclude that application γ admits one fixed point in $\mathcal{S}(T)$ which is denoted in the following by $s(t)$. Finally we want to prove that application γ is a contraction. Let s_1, s_2 be two elements of $\mathcal{S}(T)$ and u_1 (respectively u_2) the solution to (1.10) with $s = s_1$ (respectively $s = s_2$). Definition (1.24) with $u(1, t) = \int_0^1 \frac{\partial u}{\partial x}(\xi, t) d\xi$ leads to:

$$\|\tilde{s}_1 - \tilde{s}_2\|_{W^{1,\infty}(0,T)} \leq C \left\| \frac{\partial u_1}{\partial x} - \frac{\partial u_2}{\partial x} \right\|_{L^\infty(0,T,L^2(0,1))} . \quad (1.32)$$

Problem (1.10) is considered with (u_1, s_1) (respectively (u_2, s_2)). By taking the difference between these two problems, (1.33) is obtained:

$$\begin{cases} \frac{\partial(u_1 - u_2)}{\partial t}(x, t) - \frac{\dot{s}_1(t)}{s_1(t)} x \frac{\partial(u_1 - u_2)}{\partial x}(x, t) \\ \quad - \frac{\varepsilon}{s_1^2(t)} \frac{\partial^2(u_1 - u_2)}{\partial x^2}(x, t) = \hat{f}(x, t), & (x, t) \in U^T, \\ (u_1 - u_2)(x, 0) = 0, & x \in (0, 1), \\ (u_1 - u_2)(0, t) = \frac{\partial(u_1 - u_2)}{\partial x}(1, t) = 0, & t \in (0, T), \end{cases} \quad (1.33)$$

with

$$\hat{f} = x \frac{\partial u_2}{\partial x} \left(\frac{\dot{s}_2}{s_2} - \frac{\dot{s}_1}{s_1} \right) + \varepsilon \frac{\partial^2 u_2}{\partial x^2} \left(\frac{1}{s_2^2} - \frac{1}{s_1^2} \right) + \alpha u_2 \frac{\partial u_2}{\partial x} \left(\frac{1}{s_2} - \frac{1}{s_1} \right) + \frac{\alpha}{s_1} \left(u_2 \frac{\partial u_2}{\partial x} - u_1 \frac{\partial u_1}{\partial x} \right) .$$

By setting $w = u_1 - u_2$ and $s = s_1$, the left-hand side of the first equation of (1.33) is the same we have in (1.22). Estimate (1.18) permits to write:

$$\left\| \frac{\partial u_1}{\partial x} - \frac{\partial u_2}{\partial x} \right\|_{L^\infty(0,T,L^2(0,1))}^2 \leq \bar{C} \|\hat{f}\|_{L^2(U^T)}^2 .$$

Notice that $\int_0^T \int_0^1 \left(\frac{\partial u_2}{\partial x} \right)^2 dx dt \leq T \left\| \frac{\partial u_2}{\partial x} \right\|_{L^\infty(L^2)}^2$. The previous right-hand side can be bounded by:

$$\begin{aligned} \|\hat{f}\|_{L^2(U^T)}^2 &\leq CT \left\| \frac{\partial u_2}{\partial x} \right\|_{L^\infty(L^2)}^2 \|s_1 - s_2\|_{W^{1,\infty}}^2 \\ &\quad + C \int_0^T \int_0^1 \left(\frac{\partial^2 u_2}{\partial x^2} \right)^2 dx dt \|s_1 - s_2\|_{L^\infty}^2 \\ &\quad + CT \|u_2\|_{L^\infty(U^T)}^2 \left\| \frac{\partial u_2}{\partial x} \right\|_{L^\infty(L^2)}^2 \|s_1 - s_2\|_{L^\infty}^2 \\ &\quad + C \|u_2\|_{L^\infty(U^T)}^2 \int_0^T \left\| \frac{\partial(u_1 - u_2)}{\partial x} \right\|_{L^2}^2 dt \\ &\quad + C \left\| \frac{\partial u_2}{\partial x} \right\|_{L^\infty(L^2)}^2 \int_0^T \|u_1 - u_2\|_{L^2}^2 dt . \end{aligned}$$

1.3. FREE SURFACE PROBLEM

Here the last two terms of the right-hand side are bounded by

$$C \left(\|u_2\|_{L^\infty(U^T)}^2 \left\| \frac{\partial(u_1 - u_2)}{\partial x} \right\|_{L^\infty(L^2)}^2 + \left\| \frac{\partial u_2}{\partial x} \right\|_{L^\infty(L^2)}^2 C_p \left\| \frac{\partial(u_1 - u_2)}{\partial x} \right\|_{L^\infty(L^2)}^2 \right) T ,$$

where C_p is the constant introduced by using the Poincaré inequality. Thus there exist two constants C_1 and C_2 such that:

$$\|\hat{f}\|_{L^2(U^T)}^2 \leq \left(C_1 T + C \left\| \frac{\partial^2 u_2}{\partial x^2} \right\|_{L^2(U^T)}^2 \right) \|s_1 - s_2\|_{W^{1,\infty}}^2 + C_2 T \left\| \frac{\partial(u_1 - u_2)}{\partial x} \right\|_{L^\infty(L^2)}^2 . \quad (1.34)$$

Relationships (1.34) and (1.18) lead to:

$$\left\| \frac{\partial(u_1 - u_2)}{\partial x} \right\|_{L^\infty(L^2)}^2 \leq \bar{C} \left[\left(C_1 T + C \left\| \frac{\partial^2 u_2}{\partial x^2} \right\|_{L^2(U^T)}^2 \right) \|s_1 - s_2\|_{W^{1,\infty}}^2 + C_2 T \left\| \frac{\partial(u_1 - u_2)}{\partial x} \right\|_{L^\infty(L^2)}^2 \right] .$$

If T is assumed to be smaller than $T_U = \frac{1}{2\bar{C}C_2}$, this inequality becomes:

$$\frac{1}{2} \left\| \frac{\partial(u_1 - u_2)}{\partial x} \right\|_{L^\infty(L^2)}^2 \leq \bar{C} \left(C_1 T + C \left\| \frac{\partial^2 u_2}{\partial x^2} \right\|_{L^2(U^T)}^2 \right) \|s_1 - s_2\|_{W^{1,\infty}}^2 . \quad (1.35)$$

Since $u_2 \in L^2(0, T, H^2(0, 1))$, the term $\left\| \frac{\partial^2 u_2}{\partial x^2} \right\|_{L^2(U^T)}^2$ tends to zero when T tends to zero.

The combination of (1.32) and (1.35) permits to conclude that there exists a constant $E(T)$ depending on T such that:

$$\|\tilde{s}_1 - \tilde{s}_2\|_{W^{1,\infty}(0,T)} \leq E(T) \|s_1 - s_2\|_{W^{1,\infty}(0,T)} ,$$

with $E(T)$ tends to zero when T tends to zero. Then there exists $0 < \hat{T} \leq T_U$ such that γ is a contraction from $\mathcal{S}(\hat{T})$ to $\mathcal{S}(\hat{T})$ and conclusion follows. \square

This result of existence and uniqueness is independent of the value of coefficient $\alpha > 0$ (see [36] for $\alpha = 3/2$). The solution (u, s) to the free surface problem (1.26) can be transferred on the original domain $Q_{\hat{T}}$ to obtain existence and uniqueness of original problem (1.2)-(1.7). In order to conclude, we can claim that Problem (1.2)-(1.7) is well-posed at least for small times.

In the following, a semi-discretization in space will be introduced using finite elements and the existence and uniqueness of the solution to the discrete problem is proved. In a second step *a priori* error estimates will be obtained in a same way as in [52]. Finally, *a posteriori* error estimates are also presented (see [125] for instance).

1.4 Semi-Discretization in Space

A \mathbb{P}_1 finite element semi-discretization in space is introduced. Let $N \in \mathbb{N}$ be a given integer and $h = 1/(N + 1)$. The discretization points are denoted by $x_i = ih$, $i = 0, \dots, N + 1$ and the space of continuous functions on $[0, 1]$ which are vanishing into $x = 0$ and whose restrictions on $[x_i, x_{i+1}]$, $i = 0, \dots, N$ belong to \mathbb{P}_r by $X_h^r(0, 1)$. Let $V_h \subset V$ be the subspace of V defined by $X_h^1(0, 1)$.

Let $u_{0,h}$ be the interpolant of $u_0 \in V$ in V_h . For all $u_0 \in V$, the interpolant satisfies $\|u_{0,h}\|_V \leq C_0 \|u_0\|_V$. Furthermore, if $u_0 \in H^2(0, 1)$, then we have (see for instance [26, Volume 2]):

$$\|u_0 - u_{0,h}\| \leq Ch^2 \|u_0\|_{H^2(0,1)} .$$

If the right-hand side of (1.2) is denoted by \bar{f} and $s(t)$, $s_h(t)$ are two elements of $\mathcal{S}(T)$, the function $f \in L^2(U^T)$ is the image of \bar{f} by the linear application which transforms $(0, s(t))$ onto $(0, 1)$ and similarly the function $f_h \in L^2(U^T)$ is defined by the image of \bar{f} by the linear application which transforms $(0, s_h(t))$ onto $(0, 1)$. With this change of variables, $\|f_h\|_{L^2(U^T)}$ is bounded by $C_S \|\bar{f}\|_{L^2(Q_T)}$ where C_S is a constant independent of s_h and h . From now on, \bar{f} is assumed to belong to $L^2(0, T, H^1(0, \beta_1))$ in order to estimate the difference between f and f_h in the following.

The problem semi-discretized in space reads: find $u_h : (0, T) \rightarrow u_h(t) \in V_h$ and $s_h \in \mathcal{S}(T)$ such that, a.e. $t \in (0, T)$ and $\forall v_h \in V_h$:

$$\begin{aligned} \int_0^1 \frac{\partial u_h}{\partial t} v_h dx + \frac{\alpha}{s_h(t)} \int_0^1 u_h \frac{\partial u_h}{\partial x} v_h dx - \frac{\dot{s}_h(t)}{s_h(t)} \int_0^1 x \frac{\partial u_h}{\partial x} v_h dx \\ + \frac{\varepsilon}{s_h(t)^2} \int_0^1 \frac{\partial u_h}{\partial x} \frac{\partial v_h}{\partial x} dx = \int_0^1 f_h v_h dx , \end{aligned} \quad (1.36)$$

$$u_h(x, 0) = u_{0,h}(x) , \quad x \in (0, 1) , \quad (1.37)$$

$$\dot{s}_h(t) = u_h(1, t) , \quad t \in (0, T) . \quad (1.38)$$

$$s_h(0) = s_0 . \quad (1.39)$$

The existence and uniqueness of a local in time solution to (1.36)-(1.39) are proved in the following theorem.

Theorem 1.5 (Solution to Semi-Discrete Problem)

Assume that $s_0 \in]\beta_2, \beta_1[$ and $\bar{C}C_0 \|u_0\|_V^2 < K^2/2$. There exists $0 < \hat{T} \leq T$ (\hat{T} independent of $h > 0$) such that (1.36)-(1.39) admits one unique solution $(u_h, s_h) \in H^1(0, \hat{T}, V_h) \times \mathcal{S}(\hat{T})$, $\forall h > 0$. Furthermore, there exists a constant C independent of h such that:

$$\|u_h\|_{H^1(0, \hat{T}, V_h)}^2 \leq C \left\{ \|\bar{f}\|_{L^2(Q_{\hat{T}})}^2 + \|u_0\|_V^2 \right\} , \quad (1.40)$$

where \bar{f} is the right-hand side function of (1.2).

1.4. SEMI-DISCRETIZATION IN SPACE

PROOF : The steps of the proof are mainly the same as the ones used in the continuous frame. Let $h > 0$ be fixed. We want to solve (1.36)-(1.39). In order to consider first the problem with fixed boundary, we set $s_h \in \mathcal{S}(T)$. The problem without the nonlinear term is treated first: find $u_h : t \in (0, T) \rightarrow u_h(t) \in V_h$ such that, a.e. $t \in (0, T)$ and $\forall v_h \in V_h$:

$$\int_0^1 \frac{\partial u_h}{\partial t} v_h dx - \frac{\dot{s}_h(t)}{s_h(t)} \int_0^1 x \frac{\partial u_h}{\partial x} v_h dx + \frac{\varepsilon}{s_h(t)^2} \int_0^1 \frac{\partial u_h}{\partial x} \frac{\partial v_h}{\partial x} dx = \int_0^1 f_h v_h dx \quad (1.41)$$

$$u_h(0) = u_{0,h} \quad (1.42)$$

Let $\{\psi_i\}_{i=1}^{N_h}$ be the finite element basis of V_h (N_h denotes the dimension of V_h). The decomposition of u_h in this basis is:

$$u_h(x, t) = \sum_{j=1}^{N_h} \alpha_j(t) \psi_j(x), \quad \alpha_k \in H^1(0, T), \quad k = 1, \dots, N_h \quad (1.43)$$

The insertion of (1.43) into (1.41) leads to an ordinary differential equations system with initial conditions $\alpha_j^0 = u_0(x_j)$. Theory of ordinary differential equations (see [49]) permits to conclude to the existence of u_h , defined on $(0, T_h)$, $\forall h > 0$. *A priori* estimates like (1.13) permit to conclude that u_h is a global maximal solution and is defined on $(0, T)$, independently of $h > 0$. The following estimation is obtained: there exists a constant C independent of h such that:

$$\|u_h\|_{L^\infty(0, T, L^2(0, 1)) \cap L^2(0, T, V) \cap H^1(0, T, V')}^2 \leq C \left(\|f_h\|_{L^2(U^T)}^2 + \|u_{0,h}\|_{L^2(0, 1)}^2 \right) \quad .$$

The projection $u_{0,h}$ satisfies $\|u_{0,h}\|_{L^2(0, 1)} \leq C_0 \|u_0\|_V$, while the function f_h satisfies $\|f_h\|_{L^2(U^T)} \leq C_S \|\bar{f}\|_{L^2(Q^T)}$ where C_0, C_S are constants independent of h . The right-hand side of previous relation is then bounded independently of $h > 0$.

The solution u_h to the problem (1.41)-(1.42) can be expressed by (1.43); hence:

$$u_h \in H^1(0, T, V_h) \subset H^1(0, T, V) \quad .$$

Further estimations are needed. Set $v_h = \frac{\partial u_h}{\partial t}$ in (1.41). Young inequalities lead to:

$$\frac{1}{4} \left\| \frac{\partial u_h}{\partial t} \right\|_{L^2(0, 1)}^2 + \frac{\varepsilon}{2s_h(t)^2} \frac{d}{dt} \left\| \frac{\partial u_h}{\partial x} \right\|_{L^2(0, 1)}^2 \leq \frac{1}{2} \|f_h\|_{L^2(0, 1)}^2 + C \frac{K^2}{s_h(t)^2} \left\| \frac{\partial u_h}{\partial x} \right\|_{L^2(0, 1)}^2 \quad .$$

By multiplying this relation by $s_h(t)^2$, we obtain:

$$\frac{\beta_2^2}{4} \left\| \frac{\partial u_h}{\partial t} \right\|_{L^2(0, 1)}^2 + \frac{\varepsilon}{2} \frac{d}{dt} \left\| \frac{\partial u_h}{\partial x} \right\|_{L^2(0, 1)}^2 \leq \frac{\beta_2^2}{2} \|f_h\|_{L^2(0, 1)}^2 + CK^2 \left\| \frac{\partial u_h}{\partial x} \right\|_{L^2(0, 1)}^2 \quad .$$

Gronwall's lemma permits to obtain a first estimate:

$$\|u_h\|_{L^\infty(0,T,V)}^2 \leq C \left(\|f_h\|_{L^2(U^T)}^2 + \left\| \frac{\partial u_{0,h}}{\partial x} \right\|_{L^2(0,1)}^2 \right),$$

and then integration in time leads to:

$$\left\| \frac{\partial u_h}{\partial t} \right\|_{L^2(U^T)}^2 \leq C \left(\|f_h\|_{L^2(U^T)}^2 + \left\| \frac{\partial u_{0,h}}{\partial x} \right\|_{L^2(0,1)}^2 \right).$$

Both right-hand sides are bounded independently of h since $\|f_h\|_{L^2(U^T)}$ and $\|u_{0,h}\|_V$ are bounded independently of h . In conclusion, if $u_0 \in V$ and $\bar{f} \in L^2(Q_T)$, the function u_h is bounded uniformly in $h > 0$ in $L^\infty(0, T, V) \cap H^1(0, T, L^2(0, 1))$.

Uniqueness is obtained by a variational argument. The function u_h is in $L^\infty(0, T, V)$, and hence $u_h \in L^\infty(U^T)$. The second step consists in defining the application τ_1 to determine the existence of a solution to nonlinear problem:

$$\begin{aligned} \tau_1 : H^1(0, T, V_h) &\longrightarrow H^1(0, T, V_h) \xrightarrow{c} L^2(U^T) \\ u_h &\longrightarrow u_h \frac{\partial u_h}{\partial x} \longrightarrow f_h - \frac{\alpha}{s_h(t)} u_h \frac{\partial u_h}{\partial x}. \end{aligned}$$

Application τ_1 is continuous and compact. The operator τ_2 defined in (1.19) is also continuous. Then there exists $0 < \tilde{T} \leq T$ such that the application $\tau_2 \circ \tau_1$ admits a fixed point for small times and \tilde{T} is independent of h since \tilde{T} depends on the norms of f_h and u_h which are bounded independently of h . Problem (1.36)-(1.37) with given boundary $s_h(t)$ admits then a solution. Uniqueness is guaranteed with a variational argument. This solution is bounded independently of $h > 0$.

By using the same procedure as in the continuous case, the continuity and compactness of application γ given by (1.25) are proved independently of $h > 0$. To prove the existence, we need to check that there exists $0 < T_{inf} \leq T$ independent of $h > 0$ such that the range of γ is included in $\mathcal{S}(T_{inf})$. The proof of lemma 1.1 can be applied here again with similar notations. \square

Then there exists one unique solution (u_h, s_h) to the problem (1.36)-(1.39) at least for small times (independent of h). This solution is compared with the unique solution (u, s) to the continuous problem (1.2)-(1.7) in the next section, where error estimates are obtained.

1.5 A Priori and A Posteriori Error Estimates

Convergence orders for the semi-discretized approximation in space of the continuous problem are investigated in this section. *A priori* and *a posteriori* error estimates are obtained. *A priori* error estimates are proposed in the next result.

Theorem 1.6 (A priori error estimates)

Let $\bar{f} \in L^2(0, T, H^1(0, \beta_1))$ and $u_0 \in H^2(0, 1) \cap V$ be given functions. There exists $0 < \tilde{T} \leq T$ such that (1.26) and (1.36)-(1.39) admit one unique solution (u, s) , respectively (u_h, s_h) , $\forall h > 0$ on $(0, 1) \times (0, \tilde{T})$. The following error estimate is obtained:

1.5. A PRIORI AND A POSTERIORI ERROR ESTIMATES

$$\|u - u_h\|_{L^\infty(0, \tilde{T}, L^2(0,1)) \cap L^2(0, \tilde{T}, V)}^2 + \|s - s_h\|_{L^\infty(0, \tilde{T})}^2 + \|\dot{s} - \dot{s}_h\|_{L^2(0, \tilde{T})}^2 \leq C_1 h^2, \quad (1.44)$$

where the constant C_1 does not depend on h , but only on \bar{f} , u_0 , $\mathcal{S}(\tilde{T})$ and \tilde{T} . Furthermore the following error estimate is obtained:

$$\|u - u_h\|_{L^2(U\tilde{T})}^2 \leq C_2 \left\{ h^4 + \|s - s_h\|_{L^\infty(0, \tilde{T})}^2 + \|\dot{s} - \dot{s}_h\|_{L^2(0, \tilde{T})}^2 \right\}, \quad (1.45)$$

where the constant C_2 does not depend on h , but only on \bar{f} , u_0 , $\mathcal{S}(\tilde{T})$ and \tilde{T} .

Remark 1.2 Estimate (1.44) means that the error on the boundary function s satisfies $\|s - s_h\|_{H^1(0, \tilde{T})} \leq Ch$. Estimate (1.45) imply that the error on the velocity is governed by the error on the boundary function and therefore $\|u - u_h\|_{L^2(U\tilde{T})} \leq Ch$. If $s(t)$ is fixed, $s = s_h$ and classical results are obtained (i.e. $\|u - u_h\|_{L^2(U\tilde{T})} \leq Ch^2$). Our belief is that we cannot obtain better estimates in the general case.

PROOF : Recall that the weak form of the continuous problem (1.2)-(1.7) is

$$\begin{aligned} \int_0^1 \frac{\partial u}{\partial t} v dx - \frac{\dot{s}(t)}{s(t)} \int_0^1 x \frac{\partial u}{\partial x} v dx + \frac{\varepsilon}{s(t)^2} \int_0^1 \frac{\partial u}{\partial x} \frac{\partial v}{\partial x} dx \\ + \frac{\alpha}{s(t)} \int_0^1 u \frac{\partial u}{\partial x} v dx = \int_0^1 f v dx, \quad \forall v \in V, \quad \text{a.e. } t \in (0, T), \end{aligned} \quad (1.46)$$

$$u(x, 0) = u_0(x), \quad x \in (0, 1), \quad (1.47)$$

$$\dot{s}(t) = u(1, t), \quad \text{a.e. } t \in (0, T), \quad (1.48)$$

while the Galerkin approximation satisfies:

$$\begin{aligned} \int_0^1 \frac{\partial u_h}{\partial t} v_h dx - \frac{\dot{s}_h(t)}{s_h(t)} \int_0^1 x \frac{\partial u_h}{\partial x} v_h dx + \frac{\varepsilon}{s_h(t)^2} \int_0^1 \frac{\partial u_h}{\partial x} \frac{\partial v_h}{\partial x} dx \\ + \frac{\alpha}{s_h(t)} \int_0^1 u_h \frac{\partial u_h}{\partial x} v_h dx = \int_0^1 f_h v_h dx, \quad \forall v_h \in V_h, \quad \text{a.e. } t \in (0, T), \end{aligned} \quad (1.49)$$

$$u_h(x, 0) = u_{0,h}(x), \quad x \in (0, 1), \quad (1.50)$$

$$\dot{s}_h(t) = u_h(1, t), \quad \text{a.e. } t \in (0, T). \quad (1.51)$$

The function u belongs to $L^2(0, T, H^2(0, 1)) \cap H^1(0, T, L^2(0, 1))$ and is bounded by the data (see (1.13)). The function u_h belongs to $L^\infty(0, T, V) \cap H^1(0, T, L^2(0, 1))$ and is bounded independently of $h > 0$ (see Sect. 1.4). We denote again the final time \tilde{T} by T .

The applications $A : V \times V \rightarrow \mathbb{R}$ and $B : V \times V \times V \rightarrow \mathbb{R}$ are defined by:

$$\begin{aligned}
 A(e, v) &= -\frac{\dot{s}(t)}{s(t)} \int_0^1 x \frac{\partial e}{\partial x} v dx - \left(\frac{\dot{s}(t)}{s(t)} - \frac{\dot{s}_h(t)}{s_h(t)} \right) \int_0^1 x \frac{\partial u_h}{\partial x} v dx, \\
 &\quad + \frac{\varepsilon}{s_h(t)^2} \int_0^1 \frac{\partial e}{\partial x} \frac{\partial v}{\partial x} dx + \frac{\varepsilon}{s(t)^2 s_h(t)^2} (s_h(t)^2 - s(t)^2) \int_0^1 \frac{\partial u}{\partial x} \frac{\partial v}{\partial x} dx, \\
 B(u, u_h, v) &= \alpha \int_0^1 \left(\frac{u}{s(t)} \frac{\partial u}{\partial x} - \frac{u_h}{s_h(t)} \frac{\partial u_h}{\partial x} \right) v dx.
 \end{aligned}$$

The applications A and B are linear in their last argument v . The scalar product in $L^2(0, 1)$ is denoted by (\cdot, \cdot) . The difference between (1.46) and (1.49) can be expressed by:

$$\left(\frac{\partial(u - u_h)}{\partial t}, v_h \right) + A((u - u_h), v_h) + B(u, u_h, v_h) = (f - f_h, v_h), \quad \forall v_h \in V_h. \quad (1.52)$$

We define $I(v) = (v_t, v) + A(v, v)$ and we are looking for an estimation of $I(u - u_h)$. Relation (1.52) leads to:

$$\begin{aligned}
 I(u - u_h) &= \left(\frac{\partial(u - u_h)}{\partial t}, u - v_h \right) + A(u - u_h, u - v_h) \\
 &\quad + (B(u, u_h, u_h) - B(u, u_h, v_h)) + (f - f_h, v_h - u_h), \quad \forall v_h \in V_h.
 \end{aligned}$$

With these definitions of I , A and B , we obtain $I(u - u_h) \leq \left\| \frac{\partial(u - u_h)}{\partial t} \right\|_{L^2} \|u - v_h\|_{L^2} + A(u - u_h, u - v_h) + B(u, u_h, u_h - v_h) + (f - f_h, v_h - u_h)$ and explicitly:

$$\begin{aligned}
 &\frac{1}{2} \frac{d}{dt} \|u - u_h\|_{L^2(0,1)}^2 - \frac{\dot{s}(t)}{s(t)} \int_0^1 x \frac{\partial(u - u_h)}{\partial x} (u - u_h) dx \\
 &- \left(\frac{\dot{s}(t)}{s(t)} - \frac{\dot{s}_h(t)}{s_h(t)} \right) \int_0^1 x \frac{\partial u_h}{\partial x} (u - u_h) dx + \frac{\varepsilon}{s_h(t)^2} \int_0^1 \left(\frac{\partial(u - u_h)}{\partial x} \right)^2 dx \\
 &+ \frac{\varepsilon}{s(t)^2 s_h(t)^2} (s_h(t)^2 - s(t)^2) \int_0^1 \frac{\partial u}{\partial x} \frac{\partial(u - u_h)}{\partial x} dx \\
 &\leq \left\| \frac{\partial(u - u_h)}{\partial t} \right\|_{L^2(0,1)} \|u - v_h\|_{L^2(0,1)} - \frac{\dot{s}(t)}{s(t)} \int_0^1 x \frac{\partial(u - u_h)}{\partial x} (u - v_h) dx \\
 &- \left(\frac{\dot{s}(t)}{s(t)} - \frac{\dot{s}_h(t)}{s_h(t)} \right) \int_0^1 x \frac{\partial u_h}{\partial x} (u - v_h) dx + \frac{\varepsilon}{s_h(t)^2} \int_0^1 \frac{\partial(u - u_h)}{\partial x} \frac{\partial(u - v_h)}{\partial x} dx \\
 &+ \frac{\varepsilon}{s(t)^2 s_h(t)^2} (s_h(t)^2 - s(t)^2) \int_0^1 \frac{\partial u}{\partial x} \frac{\partial(u - v_h)}{\partial x} dx \\
 &+ \alpha \int_0^1 \left(\frac{u}{s(t)} \frac{\partial u}{\partial x} - \frac{u_h}{s_h(t)} \frac{\partial u_h}{\partial x} \right) (u_h - v_h) dx + (f - f_h, v_h - u_h).
 \end{aligned}$$

Let us consider $0 < t \leq T$ (where T is such that $s \in \mathcal{S}(T)$ and $s_h \in \mathcal{S}(T)$, $\forall h > 0$). Cauchy-Schwarz inequalities are then used. Hence, (1.13) (1.40) and $s, s_h \in \mathcal{S}(T)$ imply that there exist constants C_1, \dots, C_8 , independent of t and h such that:

1.5. A PRIORI AND A POSTERIORI ERROR ESTIMATES

$$\begin{aligned}
& \frac{1}{2} \frac{d}{dt} \|u - u_h\|_{L^2(0,1)}^2 + \frac{\varepsilon}{\beta_1^2} \left\| \frac{\partial(u - u_h)}{\partial x} \right\|_{L^2(0,1)}^2 \\
& \leq \left\| \frac{\partial(u - u_h)}{\partial t} \right\|_{L^2(0,1)} \|u - v_h\|_{L^2(0,1)} + C_1 \left\| \frac{\partial(u - u_h)}{\partial x} \right\|_{L^2(0,1)} \|u - v_h\|_{L^2(0,1)} \\
& + C_2 \|u - v_h\|_{L^2(0,1)} \left| \frac{\dot{s}(t)}{s(t)} - \frac{\dot{s}_h(t)}{s_h(t)} \right| + C_3 \left\| \frac{\partial(u - u_h)}{\partial x} \right\|_{L^2(0,1)} \left\| \frac{\partial(u - v_h)}{\partial x} \right\|_{L^2(0,1)} \\
& + C_4 |s(t) - s_h(t)| \left\| \frac{\partial(u - v_h)}{\partial x} \right\|_{L^2(0,1)} \tag{1.53} \\
& + C_5 \left\| \frac{u}{s(t)} \frac{\partial u}{\partial x} - \frac{u_h}{s_h(t)} \frac{\partial u_h}{\partial x} \right\|_{L^2(0,1)} \|u_h - v_h\|_{L^2(0,1)} + \|f - f_h\|_{L^2(0,1)} \|u_h - v_h\|_{L^2(0,1)} \\
& + C_6 \left\| \frac{\partial(u - u_h)}{\partial x} \right\|_{L^2(0,1)} \|u - u_h\|_{L^2(0,1)} + C_7 \|u - u_h\|_{L^2(0,1)} \left| \frac{\dot{s}(t)}{s(t)} - \frac{\dot{s}_h(t)}{s_h(t)} \right| \\
& + C_8 |s(t) - s_h(t)| \left| \int_0^1 \frac{\partial u}{\partial x} \frac{\partial(u - u_h)}{\partial x} dx \right|.
\end{aligned}$$

The following relations hold, with constants D_1 , D_2 and E which depend only on β_1 , β_2 and K :

$$\begin{aligned}
\int_0^1 \frac{\partial u}{\partial x} \frac{\partial(u - u_h)}{\partial x} dx & = - \int_0^1 \frac{\partial^2 u}{\partial x^2} (u - u_h) dx \tag{1.54a} \\
& + \underbrace{\left[\frac{\partial u}{\partial x} (u - u_h) \right]_{x=0}^{x=1}}_{=0},
\end{aligned}$$

$$\left| \frac{\dot{s}(t)}{s(t)} - \frac{\dot{s}_h(t)}{s_h(t)} \right| \leq D_1 |s(t) - s_h(t)| + D_2 |\dot{s}(t) - \dot{s}_h(t)|, \tag{1.54b}$$

$$\begin{aligned}
\left\| \frac{u}{s(t)} \frac{\partial u}{\partial x} - \frac{u_h}{s_h(t)} \frac{\partial u_h}{\partial x} \right\|_{L^2(0,1)} & \leq E \left(\|u\|_{L^2(0,1)} \left\| \frac{\partial(u - u_h)}{\partial x} \right\|_{L^2(0,1)} \tag{1.54c} \right. \\
& + \left\| \frac{\partial u_h}{\partial x} \right\|_{L^2(0,1)} \|u - u_h\|_{L^2(0,1)} \\
& \left. + |s(t) - s_h(t)| \left\| u_h \frac{\partial u_h}{\partial x} \right\|_{L^2(0,1)} \right).
\end{aligned}$$

Moreover, let $\tilde{u} \in H^1(0, 1)$ be a given function; the \mathbb{P}_1 - *Lagrange interpolant* of \tilde{u} is defined by the function $R_h \tilde{u} \in X_h^1(0, 1)$ which satisfies $R_h \tilde{u}(x_i) = \tilde{u}(x_i)$, $i = 0, \dots, N + 1$. If \tilde{u} is sufficiently regular, this function satisfies the following lemma, whose demonstration can be found in [26, volume 2] for instance.

Lemma 1.2 (Lagrange interpolant)

Let (a, b) be an interval of \mathbb{R} and $\tilde{u} \in H^2(a, b)$. The Lagrange interpolant $R_h \tilde{u}$ satisfies:

$$\begin{aligned} \|\tilde{u} - R_h \tilde{u}\|_{L^2(a,b)} &\leq \gamma_1 h^2 |\tilde{u}|_{H^2(a,b)} ; \\ \|\tilde{u} - R_h \tilde{u}\|_{H^1(a,b)} &\leq \gamma_2 h |\tilde{u}|_{H^2(a,b)} , \end{aligned}$$

where γ_1, γ_2 are constants independent of h and $|\tilde{u}|_{H^2} = \left\| \frac{\partial^2 \tilde{u}}{\partial x^2} \right\|_{L^2}$.

We consider $v_h = R_h u$ in relation (1.53). Lemma 1.2 and relations (1.54a-c) imply that there exist other constants C_1, \dots, C_{16} , depending only on $\beta_1, \beta_2, T, \varepsilon, K, \alpha, \gamma_1$ and γ_2 , such that (1.53) becomes:

$$\begin{aligned} &\frac{1}{2} \frac{d}{dt} \|u - u_h\|_{L^2}^2 + \frac{\varepsilon}{\beta_1^2} \left\| \frac{\partial(u - u_h)}{\partial x} \right\|_{L^2}^2 \leq \left\| \frac{\partial(u - u_h)}{\partial t} \right\|_{L^2} C_1 h^2 \|u\|_{H^2} \\ &+ C_2 \left\| \frac{\partial(u - u_h)}{\partial x} \right\|_{L^2} h^2 \|u\|_{H^2} + C_3 h^2 \|u\|_{H^2} (|\dot{s} - \dot{s}_h| + |s - s_h|) \\ &+ C_4 \left\| \frac{\partial(u - u_h)}{\partial x} \right\|_{L^2} h \|u\|_{H^2} + C_5 h \|u\|_{H^2} |s - s_h| + C_6 \left\| \frac{\partial(u - u_h)}{\partial x} \right\|_{L^2} \|u - u_h\|_{L^2} \\ &+ C_7 \left\| \frac{\partial(u - u_h)}{\partial x} \right\|_{L^2} h^2 \|u\|_{H^2} + C_8 \|u - u_h\|_{L^2}^2 + C_9 \|u - u_h\|_{L^2} h^2 \|u\|_{H^2} \\ &+ C_{10} |s - s_h| \|u - u_h\|_{L^2} + C_{11} |s - s_h| h^2 \|u\|_{H^2} \\ &+ \|f - f_h\|_{L^2} \|u - u_h\|_{L^2} + C_{12} \|f - f_h\|_{L^2} h^2 \|u\|_{H^2} \\ &+ C_{13} \left\| \frac{\partial(u - u_h)}{\partial x} \right\|_{L^2} \|u - u_h\|_{L^2} + C_{14} \|u - u_h\|_{L^2} |\dot{s} - \dot{s}_h| \\ &+ C_{15} \|u - u_h\|_{L^2} |s - s_h| + C_{16} \|u - u_h\|_{L^2} |s - s_h| \left\| \frac{\partial^2 u}{\partial x^2} \right\|_{L^2} , \end{aligned}$$

By ordering some terms and defining other constants C_1, \dots, C_8 , it gives:

$$\begin{aligned} &\frac{1}{2} \frac{d}{dt} \|u - u_h\|_{L^2}^2 + \frac{\varepsilon}{\beta_1^2} \left\| \frac{\partial(u - u_h)}{\partial x} \right\|_{L^2}^2 \leq \left\| \frac{\partial(u - u_h)}{\partial t} \right\|_{L^2} C_1 h^2 \|u\|_{H^2} \quad (1.55) \\ &+ C_2 \left\| \frac{\partial(u - u_h)}{\partial x} \right\|_{L^2} h \|u\|_{H^2} + C_3 h^2 \|u\|_{H^2} |\dot{s} - \dot{s}_h| + C_4 h \|u\|_{H^2} |s - s_h| \\ &+ C_5 \left\| \frac{\partial(u - u_h)}{\partial x} \right\|_{L^2} \|u - u_h\|_{L^2} + C_6 \|u - u_h\|_{L^2} h^2 \|u\|_{H^2} + \|f - f_h\|_{L^2} \|u - u_h\|_{L^2} \\ &+ C_7 \|f - f_h\|_{L^2} h^2 \|u\|_{H^2} + C_8 \|u - u_h\|_{L^2} |\dot{s} - \dot{s}_h| + C(t) \|u - u_h\|_{L^2} |s - s_h| , \end{aligned}$$

where $C(t) = C \left(1 + \|u\|_{H^2(0,1)} \right) \in L^2(0, T)$. Furthermore (1.48) and (1.51) lead to:

$$|\dot{s} - \dot{s}_h| \leq \left\| \frac{\partial(u - u_h)}{\partial x} \right\|_{L^2(0,1)} , \quad (1.56a)$$

$$\frac{d}{dt} (|s - s_h|^2) \leq \left\| \frac{\partial(u - u_h)}{\partial x} \right\|_{L^2(0,1)}^2 + |s - s_h|^2 . \quad (1.56b)$$

1.5. A PRIORI AND A POSTERIORI ERROR ESTIMATES

The functions f, f_h are defined by $f(x, t) = \bar{f}(s(t)x, t)$ and $f_h(x, t) = \bar{f}(s_h(t)x, t)$, $x \in (0, 1)$. If $\bar{f} \in L^2(0, T, H^1(0, \beta_1))$, a Taylor expansion shows that:

$$\bar{f}(s(t)x, t) = \bar{f}(s_h(t)x, t) + x(s(t) - s_h(t)) \frac{\partial \bar{f}}{\partial x}(\xi, t) ,$$

where ξ belongs to the interval with extremities $s_h(t)x$ and $s(t)x$. So we have:

$$|f(x, t) - f_h(x, t)| \leq |s(t) - s_h(t)| \left| \frac{\partial \bar{f}}{\partial x}(\xi, t) \right| . \quad (1.57)$$

Therefore $\|f - f_h\|_{L^2(0,1)}^2 \leq C_s(t) |s(t) - s_h(t)|^2$, with $C_s(t) = \|\bar{f}\|_{H^1}^2 \in L^1(0, T)$. Recall that $\left\| \frac{\partial(u - u_h)}{\partial t} \right\|_{L^2}$ is bounded. By using (1.56a) and Young inequalities, relationship (1.55) gives:

$$\begin{aligned} \frac{d}{dt} \|u - u_h\|_{L^2(0,1)}^2 + C \left\| \frac{\partial(u - u_h)}{\partial x} \right\|_{L^2(0,1)}^2 &\leq C_1 h^2 \left(\|u\|_{H^2(0,1)} + \|u\|_{H^2(0,1)}^2 \right) \\ &\quad + (C_2 + C_s(t)) |s - s_h|^2 \\ &\quad + (C_3 + C(t)^2) \|u - u_h\|_{L^2(0,1)}^2 . \end{aligned} \quad (1.58)$$

Relationship (1.56b) implies that:

$$\begin{aligned} \frac{d}{dt} \|u - u_h\|_{L^2(0,1)}^2 + C \frac{d}{dt} (|s - s_h|^2) &\leq C_1 h^2 \left(\|u\|_{H^2(0,1)} + \|u\|_{H^2(0,1)}^2 \right) \\ &\quad + (C_2 + C_s(t) + C) |s - s_h|^2 \\ &\quad + (C_3 + C(t)^2) \|u - u_h\|_{L^2(0,1)}^2 . \end{aligned}$$

Since $u_0 \in H^2(0, 1)$ and $\|u(0) - u_h(0)\|_{L^2} \leq Ch^2 \|u_0\|_{H^2}$, conclusion holds by using Gronwall's lemma (see for instance [96, page 14]) for the quantity $\|u - u_h\|_{L^2(0,1)}^2 + C |s - s_h|^2$:

$$\|u - u_h(t)\|_{L^2(0,1)}^2 + C |s(t) - s_h(t)|^2 \leq Dh^2, \quad \forall t \in (0, T) . \quad (1.59)$$

The integration of (1.58) on $(0, T)$ and (1.59) lead to the existence of another constant D such that:

$$\left\| \frac{\partial(u - u_h)}{\partial x} \right\|_{L^2(U^T)}^2 \leq Dh^2 .$$

This leads to the first estimate (1.44) since $\|\dot{s} - \dot{s}_h\|_{L^2}^2 \leq \left\| \frac{\partial(u - u_h)}{\partial x} \right\|_{L^2(U^T)}^2 \leq Dh^2$.

Let us turn now to the second estimate (1.45). The second estimation is obtained with a duality argument (see for instance [19, 52]). In order to obtain (1.45), a dual problem backward in time is introduced. Find $r(t) \in V$ such that, a.e. $t \in (0, T)$:

$$\left\{ \begin{array}{l} \int_0^1 \frac{\partial r}{\partial t} v dx - \frac{\varepsilon}{s^2(t)} \int_0^1 \frac{\partial r}{\partial x} \frac{\partial v}{\partial x} dx - \frac{\alpha}{s(t)} \int_0^1 \left(ur \frac{\partial v}{\partial x} + \frac{\partial u_h}{\partial x} r v \right) dx \\ \quad + \int_0^1 x \frac{\dot{s}(t)}{s(t)} r \frac{\partial v}{\partial x} dx = \int_0^1 (u - u_h) v dx, \\ r(x, T) = 0, \end{array} \right. \quad \forall v \in V, \quad (1.60)$$

$$x \in (0, 1) .$$

Right-hand side $u - u_h$ belongs to $L^2(U^T)$ as (u, s) is the solution to (1.46)-(1.48) and (u_h, s_h) is the solution to (1.49)-(1.51). The following existence result holds.

Lemma 1.3 (Existence, Uniqueness and Regularity of dual problem)

Let $(u, s) \in W_1(T) \times \mathcal{S}(T)$ be the solution to (1.46)-(1.48) and $(u_h, s_h) \in H^1(0, T, V_h) \times \mathcal{S}(T)$ be the solution to (1.49)-(1.51). Then (1.60) admits one unique solution

$$r \in L^2(0, T, H^2(0, 1)) \cap H^1(0, T, L^2(0, 1))$$

and there exists a constant C independent of s, s_h, u and u_h such that:

$$\|r\|_{L^2(0, T, H^2(0, 1)) \cap L^\infty(0, T, V) \cap H^1(0, T, L^2(0, 1))}^2 \leq C \|u - u_h\|_{L^2(U^T)}^2 . \quad (1.61)$$

PROOF : The problem is linear and a Faedo-Galerkin method is used for proving the existence and regularity of a solution and a variational argument for proving the uniqueness (see [29, Volume 8]). The energy inequality (1.61) is obtained with *a priori* estimates. \square

Consider (1.60) with $v = u - u_h \in V$. This means:

$$\begin{aligned} \|u - u_h\|_{L^2(0, 1)}^2 &= \int_0^1 \frac{\partial r}{\partial t} (u - u_h) dx - \frac{\varepsilon}{s^2(t)} \int_0^1 \frac{\partial r}{\partial x} \frac{\partial (u - u_h)}{\partial x} dx \\ &\quad - \frac{\alpha}{s(t)} \int_0^1 \left(ur \frac{\partial (u - u_h)}{\partial x} + \frac{\partial u_h}{\partial x} r (u - u_h) \right) dx \\ &\quad + \int_0^1 x \frac{\dot{s}(t)}{s(t)} r \frac{\partial (u - u_h)}{\partial x} dx . \end{aligned} \quad (1.62)$$

The summation of (1.52) and (1.62) gives, $\forall v_h \in V_h$:

1.5. A PRIORI AND A POSTERIORI ERROR ESTIMATES

$$\begin{aligned}
\|u - u_h\|_{L^2}^2 &= \int_0^1 \frac{\partial r}{\partial t} (u - u_h) dx - \frac{\varepsilon}{s^2(t)} \int_0^1 \frac{\partial r}{\partial x} \frac{\partial(u - u_h)}{\partial x} dx \\
&\quad - \frac{\alpha}{s(t)} \int_0^1 \left(ur \frac{\partial(u - u_h)}{\partial x} + \frac{\partial u_h}{\partial x} r (u - u_h) \right) dx + \int_0^1 x \frac{\dot{s}(t)}{s(t)} r \frac{\partial(u - u_h)}{\partial x} dx \\
&\quad + \left\{ \int_0^1 \frac{\partial(u - u_h)}{\partial t} v_h dx - \int_0^1 x \left(\frac{\dot{s}(t)}{s(t)} \frac{\partial u}{\partial x} - \frac{\dot{s}_h(t)}{s_h(t)} \frac{\partial u_h}{\partial x} \right) v_h dx \right. \\
&\quad + \varepsilon \int_0^1 \left(\frac{1}{s^2(t)} \frac{\partial u}{\partial x} - \frac{1}{s_h^2(t)} \frac{\partial u_h}{\partial x} \right) \frac{\partial v_h}{\partial x} dx \\
&\quad \left. + \alpha \int_0^1 \left(\frac{u}{s(t)} \frac{\partial u}{\partial x} - \frac{u_h}{s_h(t)} \frac{\partial u_h}{\partial x} \right) v_h dx - \int_0^1 (f - f_h) v_h dx \right\} \\
&= \left(\int_0^1 \frac{\partial r}{\partial t} (u - u_h) dx + \int_0^1 \frac{\partial(u - u_h)}{\partial t} v_h dx \right) \\
&\quad + \varepsilon \left[\int_0^1 \left(\frac{1}{s^2(t)} \frac{\partial u}{\partial x} - \frac{1}{s_h^2(t)} \frac{\partial u_h}{\partial x} \right) \frac{\partial v_h}{\partial x} dx - \int_0^1 \frac{1}{s^2(t)} \frac{\partial(u - u_h)}{\partial x} \frac{\partial r}{\partial x} dx \right] \\
&\quad + \alpha \left[\int_0^1 \left(\frac{u}{s(t)} \frac{\partial u}{\partial x} - \frac{u_h}{s_h(t)} \frac{\partial u_h}{\partial x} \right) v_h dx - \int_0^1 \frac{1}{s(t)} \left(u \frac{\partial u}{\partial x} - u_h \frac{\partial u_h}{\partial x} \right) r dx \right] \\
&\quad + \left[\int_0^1 x \frac{\dot{s}(t)}{s(t)} r \frac{\partial(u - u_h)}{\partial x} dx - \int_0^1 x \left(\frac{\dot{s}(t)}{s(t)} \frac{\partial u}{\partial x} - \frac{\dot{s}_h(t)}{s_h(t)} \frac{\partial u_h}{\partial x} \right) v_h dx \right] \\
&\quad - \int_0^1 (f - f_h) v_h dx .
\end{aligned}$$

It is possible to integrate by parts the time derivative term:

$$\int_0^1 \frac{\partial r}{\partial t} (u - u_h) dx + \int_0^1 \frac{\partial(u - u_h)}{\partial t} v_h dx = \frac{d}{dt} \int_0^1 (u - u_h) r dx - \int_0^1 \frac{\partial(u - u_h)}{\partial t} (r - v_h) dx .$$

The Cauchy-Schwarz inequality leads to the existence of constants C_i , $i = 1, \dots, 6$ independent of t and h such that:

$$\begin{aligned}
\|u - u_h\|_{L^2}^2 &\leq \frac{d}{dt} \int_0^1 (u - u_h) r dx + \left\| \frac{\partial(u - u_h)}{\partial t} \right\|_{L^2} \|r - v_h\|_{L^2} + \|f - f_h\|_{L^2} \|v_h\|_{L^2} \\
&\quad + C_1 \left\| \frac{\partial(u - u_h)}{\partial x} \right\|_{L^2} \left\| \frac{\partial(r - v_h)}{\partial x} \right\|_{L^2} + C_2 \left\| \frac{\partial v_h}{\partial x} \right\|_{L^2} \left| \frac{1}{s^2(t)} - \frac{1}{s_h^2(t)} \right| \\
&\quad + C_3 \|r - v_h\|_{L^2(0,1)} \left\| u \frac{\partial u}{\partial x} - u_h \frac{\partial u_h}{\partial x} \right\|_{L^2} + C_4 \|v_h\|_{L^2} \left| \frac{1}{s(t)} - \frac{1}{s_h(t)} \right| \\
&\quad + C_5 \left\| \frac{\partial(u - u_h)}{\partial x} \right\|_{L^2} \|r - v_h\|_{L^2} + C_6 \|v_h\|_{L^2} \left| \frac{\dot{s}(t)}{s(t)} - \frac{\dot{s}_h(t)}{s_h(t)} \right|, \forall v_h \in V_h .
\end{aligned}$$

Triangle inequalities imply that $\left\| \frac{\partial v_h}{\partial x} \right\|_{L^2} \leq \left\| \frac{\partial r}{\partial x} \right\|_{L^2} + \left\| \frac{\partial r}{\partial x} - \frac{\partial v_h}{\partial x} \right\|_{L^2}$ and $\|v_h\|_{L^2} \leq \|r\|_{L^2} + \|r - v_h\|_{L^2}$. Hence previous expression leads to:

$$\begin{aligned}
 \|u - u_h\|_{L^2}^2 &\leq \frac{d}{dt} \int_0^1 (u - u_h) r dx + \left\| \frac{\partial(u - u_h)}{\partial t} \right\|_{L^2} \|r - v_h\|_{L^2} \\
 &+ \|f - f_h\|_{L^2} \|r\|_{L^2} + \|f - f_h\|_{L^2} \|r - v_h\|_{L^2} \\
 &+ D_1 \left\| \frac{\partial(u - u_h)}{\partial x} \right\|_{L^2} \left\| \frac{\partial(r - v_h)}{\partial x} \right\|_{L^2} \\
 &+ D_2 \left\| \frac{\partial r}{\partial x} \right\|_{L^2} \left| \frac{1}{s^2(t)} - \frac{1}{s_h^2(t)} \right| + D_3 \left\| \frac{\partial(r - v_h)}{\partial x} \right\|_{L^2} \left| \frac{1}{s^2(t)} - \frac{1}{s_h^2(t)} \right| \\
 &+ D_4 \|r - v_h\|_{L^2(0,1)} \left\| u \frac{\partial u}{\partial x} - u_h \frac{\partial u_h}{\partial x} \right\|_{L^2} \\
 &+ D_5 \|r\|_{L^2} \left| \frac{1}{s(t)} - \frac{1}{s_h(t)} \right| + D_6 \|r - v_h\|_{L^2} \left| \frac{1}{s(t)} - \frac{1}{s_h(t)} \right| \\
 &+ D_7 \left\| \frac{\partial(u - u_h)}{\partial x} \right\|_{L^2} \|r - v_h\|_{L^2} \\
 &+ D_8 \|r\|_{L^2} \left| \frac{\dot{s}(t)}{s(t)} - \frac{\dot{s}_h(t)}{s_h(t)} \right| + D_9 \|r - v_h\|_{L^2} \left| \frac{\dot{s}(t)}{s(t)} - \frac{\dot{s}_h(t)}{s_h(t)} \right|, \forall v_h \in V_h .
 \end{aligned}$$

Here D_1, \dots, D_9 are constants independent of h . The Lagrange interpolant of $r \in V$ is considered as the test function $v_h = R_h r$. Recall that $\|r - R_h r\|_{L^2} + h \|r - R_h r\|_{H^1} \leq Ch^2 |r|_{H^2}$ and $\|f - f_h\|_{L^2} \leq C |s - s_h|$. Interpolation result 1.2 leads to:

$$\begin{aligned}
 \|u - u_h\|_{L^2}^2 &\leq \frac{d}{dt} \int_0^1 (u - u_h) r dx + \left\| \frac{\partial(u - u_h)}{\partial t} \right\|_{L^2} h^2 \left\| \frac{\partial^2 r}{\partial x^2} \right\|_{L^2} \\
 &+ E_1 |s(t) - s_h(t)| \|r\|_{L^2} + E_2 |s(t) - s_h(t)| h^2 \left\| \frac{\partial^2 r}{\partial x^2} \right\|_{L^2} \\
 &+ E_3 \left\| \frac{\partial(u - u_h)}{\partial x} \right\|_{L^2} h \left\| \frac{\partial^2 r}{\partial x^2} \right\|_{L^2} \\
 &+ E_4 \left\| \frac{\partial r}{\partial x} \right\|_{L^2} |s(t) - s_h(t)| + E_5 |s(t) - s_h(t)| h \left\| \frac{\partial^2 r}{\partial x^2} \right\|_{L^2} \\
 &+ E_6 \left\| u \frac{\partial u}{\partial x} - u_h \frac{\partial u_h}{\partial x} \right\|_{L^2} h^2 \left\| \frac{\partial^2 r}{\partial x^2} \right\|_{L^2} \\
 &+ E_7 \|r\|_{L^2} |s(t) - s_h(t)| + E_8 h^2 \left\| \frac{\partial^2 r}{\partial x^2} \right\|_{L^2} |s(t) - s_h(t)| \\
 &+ E_9 \left\| \frac{\partial(u - u_h)}{\partial x} \right\|_{L^2} h^2 \left\| \frac{\partial^2 r}{\partial x^2} \right\|_{L^2} \\
 &+ E_{10} \|r\|_{L^2} |s(t) - s_h(t)| + E_{11} \|r\|_{L^2} |\dot{s}(t) - \dot{s}_h(t)| \\
 &+ E_{12} h^2 \left\| \frac{\partial^2 r}{\partial x^2} \right\|_{L^2} |s(t) - s_h(t)| + E_{13} h^2 \left\| \frac{\partial^2 r}{\partial x^2} \right\|_{L^2} |\dot{s}(t) - \dot{s}_h(t)| ,
 \end{aligned}$$

where E_1, \dots, E_{13} are constants depending on D_1, \dots, D_9 and γ_1 and γ_2 introduced in Lemma 1.2. The inequality is integrated on $(0, T)$ and the *a priori* estimate (1.61) is used

1.5. A PRIORI AND A POSTERIORI ERROR ESTIMATES

($\|r\|_{L^2(H^2)} \leq C \|u - u_h\|_{L^2(U^T)}$). Several Young inequalities imply that there exist new constants C_1, \dots, C_7 such that:

$$\begin{aligned} \frac{1}{2} \int_0^T \|u - u_h\|_{L^2(0,1)}^2 dt &\leq -((u - u_h)(0), r(0)) + C_1 h^4 \\ &+ C_2 h^2 \int_0^T \left\| \frac{\partial(u - u_h)}{\partial x} \right\|_{L^2(0,1)}^2 dt \\ &+ C_3 T \|s - s_h\|_{L^\infty(0,T)}^2 + C_4 T h^2 \|s - s_h\|_{L^\infty(0,T)}^2 \\ &+ C_5 \|\dot{s} - \dot{s}_h\|_{L^2(0,T)}^2 + C_6 h^4 \|\dot{s} - \dot{s}_h\|_{L^2(0,T)}^2 \\ &+ C_7 T h^4 \|s - s_h\|_{L^\infty(0,T)}^2 . \end{aligned} \quad (1.63)$$

The initial condition leads to:

$$\begin{aligned} |((u - u_h)(0), r(0))| &\leq \|u_0 - u_{0,h}\|_{L^2(0,1)} \|r(0)\|_{L^2(0,1)} \leq \bar{C} h^2 \|u_0\|_{H^2(0,1)} \|r(0)\|_{L^2(0,1)} \\ &\leq \tilde{C} h^2 \|r\|_{L^\infty(L^2)} \leq C h^2 \left(\int_0^T \|u - u_h\|_{L^2(0,1)}^2 dt \right)^{1/2} . \end{aligned} \quad (1.64)$$

From (1.63) and (1.64), the conclusion is that there exist two constants K_1 and K_2 such that:

$$\int_0^T \|u - u_h\|_{L^2(0,1)}^2 dt \leq K_1 h^4 + K_2 \left(\|s - s_h\|_{L^\infty(0,T)}^2 + \|\dot{s} - \dot{s}_h\|_{L^2(0,T)}^2 \right) .$$

This ends the proof of Thm 1.6 □

There exists one unique solution to the continuous problem. For all $h > 0$ the semi-discretized problem also admits one unique solution. *A priori* error estimates imply convergence of (a subsequence of) the solutions to the discretized problem toward the solution to the continuous problem when h tends to zero.

The second part of this section is concerned with *a posteriori* error estimates.

Theorem 1.7 (A posteriori error estimate)

Let $f \in L^2(0, T, H^1(0, \beta_1))$ and $u_0 \in H^2(0, 1) \cap V$ be given functions and set $h_i = |x_{i+1} - x_i|$ and $J_i = (x_i, x_{i+1})$, $i = 0, \dots, N$. There exists $0 < \tilde{T} \leq T$, $\delta > 0$ independent of $h > 0$ and a constant C independent of $h > 0$ such that the following estimate holds:

$$\begin{aligned} \|u - u_h(t)\|_{L^2(0,1)}^2 + \delta |s(t) - s_h(t)|^2 + \frac{\varepsilon}{4\beta_1^2} \int_0^t \left\| \frac{\partial(u - u_h)}{\partial x} \right\|_{L^2(0,1)}^2 ds \\ \leq C \left\{ \sum_{i=0}^N \|F(u_h)\|_{L^2(J_i)} h_i^2 + h^4 \right\}, \quad 0 \leq t \leq \tilde{T} , \end{aligned}$$

where

$$F(u_h) = f_h - \frac{\partial u_h}{\partial t} - \frac{\alpha}{s_h(t)} u_h \frac{\partial u_h}{\partial x} + \frac{\dot{s}_h(t)}{s_h(t)} x \frac{\partial u_h}{\partial x} .$$

PROOF : Define the error $e = u - u_h$ and

$$I(v) = \int_0^1 \frac{\partial e}{\partial t} v dx + \frac{\varepsilon}{s(t)^2} \int_0^1 \frac{\partial e}{\partial x} \frac{\partial v}{\partial x} dx, \quad \forall v \in V .$$

Equations (1.46) and (1.49) lead to the following relation for all v in V :

$$\begin{aligned} I(v) &= \int_0^1 \frac{\partial e}{\partial t} v dx + \frac{\varepsilon}{s(t)^2} \int_0^1 \frac{\partial e}{\partial x} \frac{\partial v}{\partial x} dx \\ &= \int_0^1 f v dx + \frac{\dot{s}(t)}{s(t)} \int_0^1 x \frac{\partial u}{\partial x} v dx - \frac{\alpha}{s(t)} \int_0^1 u \frac{\partial u}{\partial x} v dx - \int_0^1 \frac{\partial u_h}{\partial t} v dx \\ &\quad - \frac{\varepsilon}{s^2(t)} \int_0^1 \frac{\partial u_h}{\partial x} \frac{\partial v}{\partial x} dx + \left[\int_0^1 f_h v dx - \frac{\alpha}{s_h(t)} \int_0^1 u_h \frac{\partial u_h}{\partial x} v dx + \int_0^1 \frac{\dot{s}_h(t)}{s_h(t)} x \frac{\partial u_h}{\partial x} v dx \right. \\ &\quad \left. - \frac{\varepsilon}{s_h^2(t)} \int_0^1 \frac{\partial u_h}{\partial x} \frac{\partial v}{\partial x} dx - \int_0^1 f_h v dx + \frac{\alpha}{s_h(t)} \int_0^1 u_h \frac{\partial u_h}{\partial x} v dx - \int_0^1 \frac{\dot{s}_h(t)}{s_h(t)} x \frac{\partial u_h}{\partial x} v dx \right. \\ &\quad \left. + \frac{\varepsilon}{s_h^2(t)} \int_0^1 \frac{\partial u_h}{\partial x} \frac{\partial v}{\partial x} dx \right] \\ &= \int_0^1 (f - f_h) v dx + \frac{\dot{s}(t)}{s(t)} \int_0^1 x \frac{\partial u}{\partial x} v dx - \frac{\alpha}{s(t)} \int_0^1 u \frac{\partial u}{\partial x} v dx - \frac{\varepsilon}{s^2(t)} \int_0^1 \frac{\partial u_h}{\partial x} \frac{\partial v}{\partial x} dx \\ &\quad - \frac{\dot{s}_h(t)}{s_h(t)} \int_0^1 x \frac{\partial u_h}{\partial x} v dx + \frac{\alpha}{s_h(t)} \int_0^1 u_h \frac{\partial u_h}{\partial x} v dx + \frac{\varepsilon}{s_h^2(t)} \int_0^1 \frac{\partial u_h}{\partial x} \frac{\partial v}{\partial x} dx \quad (1.65) \\ &\quad + \left[\int_0^1 \left(f_h - \frac{\partial u_h}{\partial t} - \frac{\alpha}{s_h(t)} u_h \frac{\partial u_h}{\partial x} + \frac{\dot{s}_h(t)}{s_h(t)} x \frac{\partial u_h}{\partial x} \right) v dx - \frac{\varepsilon}{s_h^2(t)} \int_0^1 \frac{\partial u_h}{\partial x} \frac{\partial v}{\partial x} dx \right] . \end{aligned}$$

After integration by parts, the last term of (1.65) between brackets becomes:

$$\begin{aligned} &\left\{ \int_0^1 \left(f_h - \frac{\partial u_h}{\partial t} - \frac{\alpha}{s_h(t)} u_h \frac{\partial u_h}{\partial x} + \frac{\dot{s}_h(t)}{s_h(t)} x \frac{\partial u_h}{\partial x} \right) v - \frac{\varepsilon}{s_h^2(t)} \frac{\partial u_h}{\partial x} \frac{\partial v}{\partial x} dx \right\} = \\ &\sum_{i=0}^N \left\{ \int_{x_i}^{x_{i+1}} \left(f_h - \frac{\partial u_h}{\partial t} - \frac{\alpha}{s_h(t)} u_h \frac{\partial u_h}{\partial x} + \frac{\dot{s}_h(t)}{s_h(t)} x \frac{\partial u_h}{\partial x} + \frac{\varepsilon}{s_h^2(t)} \frac{\partial^2 u_h}{\partial x^2} \right) v dx \right. \\ &\quad \left. - \left[\frac{\partial u_h}{\partial x} v \right]_{x_i}^{x_{i+1}} \right\} . \end{aligned}$$

Notice that $\frac{\partial^2 u_h}{\partial x^2} = 0$, a.e. $x \in (0, 1)$. Let the *residual* quantity be denoted by $F(u_h)$ and defined by:

$$F(u_h) = f_h - \frac{\partial u_h}{\partial t} - \frac{\alpha}{s_h(t)} u_h \frac{\partial u_h}{\partial x} + \frac{\dot{s}_h(t)}{s_h(t)} x \frac{\partial u_h}{\partial x} . \quad (1.66)$$

The solution u_h to (1.36)-(1.39) satisfies:

1.5. A PRIORI AND A POSTERIORI ERROR ESTIMATES

$$\sum_{i=0}^N \left\{ \int_{x_i}^{x_{i+1}} F(u_h) v_h dx - \left[\frac{\partial u_h}{\partial x} v_h \right]_{x_i}^{x_{i+1}} \right\} = 0, \quad \forall v_h \in V_h. \quad (1.67)$$

Equation (1.67) is added to relationship (1.65) with $v = e \in V$; this leads to:

$$\begin{aligned} I(e) &= \sum_{i=0}^N \left\{ \int_{x_i}^{x_{i+1}} F(u_h)(e - v_h) dx - \left[\frac{\partial u_h}{\partial x} (e - v_h) \right]_{x_i}^{x_{i+1}} \right\} + \int_0^1 (f - f_h) e dx \\ &+ \int_0^1 x \left(\frac{\dot{s}(t)}{s(t)} \frac{\partial u}{\partial x} - \frac{\dot{s}_h(t)}{s_h(t)} \frac{\partial u_h}{\partial x} \right) e dx + \alpha \int_0^1 \left(\frac{u_h}{s_h(t)} \frac{\partial u_h}{\partial x} - \frac{u}{s(t)} \frac{\partial u}{\partial x} \right) e dx \\ &+ \varepsilon \left(\frac{1}{s_h^2(t)} - \frac{1}{s^2(t)} \right) \int_0^1 \frac{\partial u_h}{\partial x} \frac{\partial e}{\partial x} dx, \quad \forall v_h \in V_h. \end{aligned} \quad (1.68)$$

Let $v_h = R_h e$ be the Lagrange interpolant of $e \in V$ which satisfies $e(x_i) = v_h(x_i)$, $i = 0, \dots, N+1$. Then there exist constants C_1, C_2, C_3 , depending on $f, u_0, T, \varepsilon, \beta_1, \beta_2$ and K such that:

$$\begin{aligned} I(e) &\leq \sum_{i=0}^N \int_{x_i}^{x_{i+1}} F(u_h)(e - v_h) dx + \|f - f_h\|_{L^2(0,1)} \|e\|_{L^2(0,1)} \\ &+ C_1 \|e\|_{L^2(0,1)} \left(\left\| \frac{\partial e}{\partial x} \right\|_{L^2(0,1)} + \left| \frac{\dot{s}(t)}{s(t)} - \frac{\dot{s}_h(t)}{s_h(t)} \right| \right) \\ &+ C_2 \|e\|_{L^2(0,1)} \left(\|e\|_{L^2(0,1)} + \left\| \frac{\partial e}{\partial x} \right\|_{L^2(0,1)} + |s(t) - s_h(t)| \right) \\ &+ C_3 \left\| \frac{\partial e}{\partial x} \right\|_{L^2(0,1)} |s(t) - s_h(t)|. \end{aligned} \quad (1.69)$$

By using Young inequalities, for all $\theta_1, \theta_2 > 0$, there exist C_1, C_2 and C_3 such that:

$$\begin{aligned} \frac{1}{2} \frac{d}{dt} \|e\|_{L^2(0,1)}^2 + \frac{\varepsilon}{\beta_1^2} \left\| \frac{\partial e}{\partial x} \right\|_{L^2(0,1)}^2 &\leq \sum_{i=0}^N \|F(u_h)\|_{L^2(J_i)} \|e - v_h\|_{L^2(J_i)} \\ &+ C_1 \|f - f_h\|_{L^2(0,1)}^2 + C_2 \|e\|_{L^2(0,1)}^2 + \theta_1 \left\| \frac{\partial e}{\partial x} \right\|_{L^2(0,1)}^2 + \theta_2 |\dot{s} - \dot{s}_h|^2 + C_3 |s - s_h|^2, \end{aligned}$$

where $J_i = (x_i, x_{i+1})$.

Recall that $\|f - f_h\|_{L^2(0,1)} \leq C |s - s_h|$ (see (1.57)) and $|\dot{s} - \dot{s}_h|^2 \leq C \left\| \frac{\partial e}{\partial x} \right\|_{L^2(0,1)}^2$ (see (1.56a)). Finally, by using these two relations and lemma 1.2, there exist constants K_1, K_2 and K_3 such that:

$$\begin{aligned} \frac{1}{2} \frac{d}{dt} \|e\|_{L^2(0,1)}^2 + \frac{\varepsilon}{2\beta_1^2} \left\| \frac{\partial e}{\partial x} \right\|_{L^2(0,1)}^2 &\leq K_1 \sum_{i=0}^N \|F(u_h)\|_{L^2(J_i)} h_i^2 |e|_{H^2(J_i)} \\ &\quad + K_2 \|e\|_{L^2(0,1)}^2 + K_3 |s - s_h|^2 . \end{aligned}$$

Let $\delta > 0$ be a real given number. The term $\frac{\delta}{2} \frac{d}{dt} |s - s_h|^2$ is added to the inequality. Equation (1.56b) leads to:

$$\begin{aligned} \frac{1}{2} \frac{d}{dt} \|e\|_{L^2(0,1)}^2 + \frac{\delta}{2} \frac{d}{dt} |s - s_h|^2 + \frac{\varepsilon}{2\beta_1^2} \left\| \frac{\partial e}{\partial x} \right\|_{L^2(0,1)}^2 &\leq K_1 \sum_{i=0}^N \|F(u_h)\|_{L^2(J_i)} h_i^2 |e|_{H^2(J_i)} \\ &\quad + K_2 \|e\|_{L^2(0,1)}^2 + K_3 |s - s_h|^2 \\ &\quad + \frac{\delta}{2} \left\| \frac{\partial e}{\partial x} \right\|_{L^2(0,1)}^2 + \frac{\delta}{2} |s - s_h|^2 . \end{aligned}$$

Finally, set $\delta = \frac{\varepsilon}{2\beta_1^2}$ and notice that $|e|_{H^2(J_i)} = |u|_{H^2(J_i)}$. There exists two constants K_1 and K_2 such that:

$$\begin{aligned} &\frac{1}{2} \frac{d}{dt} \left(\|e\|_{L^2(0,1)}^2 + \delta |s - s_h|^2 \right) + \frac{\varepsilon}{4\beta_1^2} \left\| \frac{\partial e}{\partial x} \right\|_{L^2(0,1)}^2 \\ &\leq K_1 \sum_{i=0}^N \|F(u_h)\|_{L^2(J_i)} h_i^2 |u|_{H^2(J_i)} + K_2 \left(\|e\|_{L^2(0,1)}^2 + \delta |s - s_h|^2 \right) . \end{aligned}$$

The conclusion is obtained with Gronwall's lemma and by noticing that $|s(0) - s_h(0)| = 0$ and $\|e(0)\|_{L^2(0,1)} \leq Ch^2 \|u_0\|_{H^2(0,1)}$. \square

Thus the model problem (1.2)-(1.7) admits a local solution in time in some well-chosen function spaces. The approximation for a semi-discretization in space by finite elements converges when the spatial step tends to zero and *a priori* and *a posteriori* error estimates are obtained. The next step is to consider a time splitting scheme inspired by the one presented in [73] for the two- and three-dimensional cases.

1.6 A Time Splitting Scheme

In [74, 75], a numerical algorithm was introduced to solve free surface flows in two and three space dimensions (see also Chap. 3). This Eulerian scheme consists in using a fixed triangulation but adding an unknown function φ which is the characteristic function of the domain Q_T . This function satisfies an advection equation $\frac{\partial \varphi}{\partial t} + \mathbf{v} \cdot \nabla \varphi = 0$ in Q_T , where \mathbf{v} is the velocity field. This model is the so-called volume-of-fluid (VOF) method (see [53] for instance). The incompressible Navier-Stokes equations are solved in the domain Q_T . A

1.6. A TIME SPLITTING SCHEME

splitting algorithm is used to decouple the advection and diffusion phenomena. Advection phenomena (including the advection of the characteristic function φ and the advection part of the Navier-Stokes equations in the liquid) are solved using a forward Characteristics method on a grid of small cells, while the diffusion part of the Navier-Stokes equations is solved using finite element techniques on a fixed, unstructured mesh. Post-processing techniques are added in order to avoid numerical diffusion and artificial compression.

In this section, an Eulerian time splitting scheme for solving (1.2)-(1.7) is discussed in an heuristic way. It is a one-dimensional version of the scheme described just before and used in [74, 75]. Advection and diffusion parts of our model are decoupled. A special attention is paid to the advection part.

Let $M > 0$ be a positive integer which represents the total number of time steps to reach final time T and let $0 = t^0 < t^1 < \dots < t^M = T$ be the sequence of discrete times with time steps $\tau^n = t^{n+1} - t^n$. It will be assumed, without loss of generality, that $\tau^n = \tau = \text{constant}$.

Let $u^0 = u_0$ and $s^0 = s_0$ be the initial conditions. The initial velocity u_0 is assumed to be a positive and increasing function. Furthermore, it is assumed to be sufficiently regular so that u is remaining sufficiently regular for all times (see for instance [64]).

At each time step, we are looking for $u^n(x)$ and s^n which are approximations of $u(x, t^n)$ and $s(t^n)$. The following splitting algorithm is suggested at each time step:

(1) Compute the approximation of the boundary at time t^{n+1} :

$$s^{n+1} \simeq s(t^{n+1})$$

by discretizing (1.6) with an explicit Euler scheme:

$$\frac{s^{n+1} - s^n}{\tau^n} = u^n(s^n) . \quad (1.70)$$

(2) Solve the advection step related to (1.2)-(1.5), namely:

$$\begin{cases} \frac{\partial u}{\partial t}(x, t) + u(x, t) \frac{\partial u}{\partial x}(x, t) = 0, & x \in (0, s^n), \quad t \in (t^n, t^{n+1}) , \\ u(0, t) = 0, & t \in (t^n, t^{n+1}) , \\ u(x, t^n) = u^n(x), & x \in (0, s^n) . \end{cases} \quad (1.71)$$

Since the initial velocity u_0 is assumed to be positive and increasing, boundary conditions have to be enforced at the left end of the interval and shocks do not appear. The characteristics method (see for instance [91, 96]) is used and leads to a prediction of velocity:

$$u^{n+1/2}(x + \tau^n u^n(x)) = u^n(x), \quad x \in (0, s^n) .$$

This step is treated in Sect. 1.6.1. Notice that $x + \tau^n u^n(x) = s^{n+1}$ if $x = s^n$, which is (1.70).

(3) Solve the diffusion step related to (1.2)-(1.5), namely:

$$\begin{cases} \frac{\partial u}{\partial t}(x, t) - \varepsilon \frac{\partial^2 u}{\partial x^2}(x, t) = f(x, t), & x \in (0, s^{n+1}), \quad t \in (t^n, t^{n+1}) , \\ u(0, t) = \frac{\partial u}{\partial x}(s^{n+1}, t) = 0, & t \in (t^n, t^{n+1}) , \\ u(x, t^n) = u^{n+1/2}(x) & x \in (0, s^{n+1}) . \end{cases} \quad (1.72)$$

Here $u^{n+1/2}(x)$ is the prediction of velocity obtained by solving (1.71). In Sect. 1.6.2, an implicit finite differences scheme is used to solve this problem.

About the Splitting Method. Whatever methods are used to solve (1)-(3), an error is introduced by the splitting algorithm (see for instance [72, page 146ff]). Let us assume that the time step $\tau > 0$ is constant and consider the following model problem: find \vec{u} such that:

$$\vec{u}_t + (A + B)\vec{u} = 0 .$$

Here A and B are two positive definite matrices. This problem results for instance from the discretization of a partial differential equation. Once the splitting algorithm is introduced, the two problems $\vec{u}_t + A\vec{u} = 0$ followed by $\vec{u}_t + B\vec{u} = 0$ are solved successively.

Between two time steps t^n and t^{n+1} , the solution to the original equation is $\vec{u}(t^{n+1}) = e^{-(A+B)\tau}\vec{u}(t^n)$, while $\vec{u}_{\text{split}}(t^{n+1}) = e^{-A\tau}e^{-B\tau}\vec{u}(t^n)$ is the solution obtained with the splitting method. By using the Taylor expansion of the exponential function, the difference between these two solutions can be expressed by:

$$(\vec{u}(t^{n+1}) - \vec{u}_{\text{split}}(t^{n+1})) = \left[\frac{\tau^2}{2} (AB - BA) + \mathcal{O}(\tau^3) \right] \vec{u}(t^n) .$$

The conclusion is that, if $[A, B] = AB - BA \neq 0$ (the matrices do not commute), an additional error of order $\mathcal{O}(\tau^2)$ is added at each time step.

In the light of this remark, each of the steps of the algorithm can be studied separately. Let $N > 0$ be a positive integer and $h = \frac{\beta_1}{N+1}$, where β_1 is the upper bound for s introduced in the definition (1.8). We set $x_i = ih$, $i = 0, \dots, N+1$ and $x_{i-1/2} = \frac{x_{i-1} + x_i}{2}$, $i = 1, \dots, N+1$. The space of continuous functions on $(0, \beta_1)$ which are vanishing into $x = 0$ and whose restriction on $[x_i, x_{i+1}]$ belongs to \mathbb{P}_r is denoted by $X_h^r(0, \beta_1)$.

Recall that the positive integer $M > 0$ is the total number of time steps to reach final time T and $0 = t^0 < t^1 < \dots < t^M = T$. We are looking for $s^n \simeq s(t^n)$ and $u_h^n \in X_h^1(0, s^n) \simeq u(x, t^n)$, $x \in (0, s(t^n))$, $n = 0, 1, \dots, M$. The initialization at time $t^0 = 0$ is made by setting $s^0 = s_0$ and by defining u^0 as the interpolant of u_0 in $X_h^1(0, s_0)$. We also define $k^0 = \max \{k \in [0, N+1] : x_k < s^0\}$ and $u_j^0 = u_0(x_j)$, $j = 1, \dots, k^0 + 1$.

1.6.1 Advection Step

In two and three space dimensions (see [74, 75]), the advection step consists in solving two advection equations for the prediction of the velocity and the characteristic function,

1.6. A TIME SPLITTING SCHEME

namely $\frac{\partial \mathbf{v}}{\partial t} + \mathbf{v} \cdot \nabla \mathbf{v} = 0$ and $\frac{\partial \varphi}{\partial t} + \mathbf{v} \cdot \nabla \varphi = 0$. First equation is the advection part of the Navier-Stokes equations while the second is the advection equation appearing in the volume-of-fluid method. Both equations are solved with the characteristics method, the incompressibility condition $\text{div} \mathbf{v} = 0$ implying that the characteristic curves do not intersect. The advection step is solved on a regular grid of small cells and the functions \mathbf{v}^n and φ^n at time t^n are assumed to be constant in each cell. The advection step on each cell consists in advecting these quantities \mathbf{v}^n and φ^n with velocity \mathbf{v}^n on each cell and then projecting the values on the grid (see also Sect. 3.3).

The characteristics method with projection is investigated here in the one-dimensional case. Paradoxically, there is no incompressibility condition in the one-dimensional case (since divergence-free corresponds to $\frac{\partial u}{\partial x} = 0$ in one space dimension and would imply $u = 0$ because of the boundary condition). However the absence of shocks implies that the characteristic curves do not intersect.

Consider the n -th time step. Approximations of the velocity and the boundary function are known at time t^n and have to be computed at time t^{n+1} . Let k^n be the integer given by:

$$k^n = \max \{k \in [0, N + 1] : x_k < s^n\} . \quad (1.73)$$

The computation of an approximation $s^{n+1} \simeq s(t^{n+1})$ of the boundary at time t^{n+1} is given by:

$$s^{n+1} = s^n + \tau^n u^n(s^n) .$$

When s^n does not correspond to a grid node, $u^n(s^n)$ is the value obtained by interpolation between the two nodes of the discretization which are the neighbours of s^n at time t^n :

$$u^n(s^n) = \left(\frac{(k^n + 1)h - s^n}{h} \right) u_{k^n}^n + \left(\frac{s^n - k^n h}{h} \right) u_{k^n+1}^n .$$

This step determines the new domain $(0, s^{n+1})$ and k^{n+1} is defined with (1.73). Then, problem (1.71) is solved with method of characteristics [90, 91]. Let u_i^n be an approximation of $u^n(x_i)$ at point x_i . The initial function at time step t^n is piecewise constant and its value on each cell centred in x_i , $i = 0, \dots, N$ is u_i^n . The prediction $u^{n+1/2}$ in the time splitting algorithm is denoted by u^{n+1} in this subsection.

The advection step on each cell i consists in advecting the quantity u_i^n by τu_i^n and then projecting the value on the grid. Figure 1.2 illustrates the case of the advection of the cell number i ; the value u_i^n is constant on the cell $[x_{i-1/2}, x_{i+1/2}]$. It is advected with velocity u_i^n and contributes to both cells i and $i + 1$ at time t^{n+1} , that is the quantity $\frac{1}{3}u_i^n$ contributes to u_i^{n+1} while the quantity $\frac{2}{3}u_i^n$ contributes to u_{i+1}^{n+1} . The prediction of the velocity after advection step is thus piecewise constant and is denoted by u^{n+1} .

Let us assume that the Courant-Friedrichs-Lewy condition holds:

$$\tau \leq \frac{h}{\max_{i=0, \dots, k^n} |u_i^n|}, \quad \forall n = 0, 1, \dots, M . \quad (1.74)$$

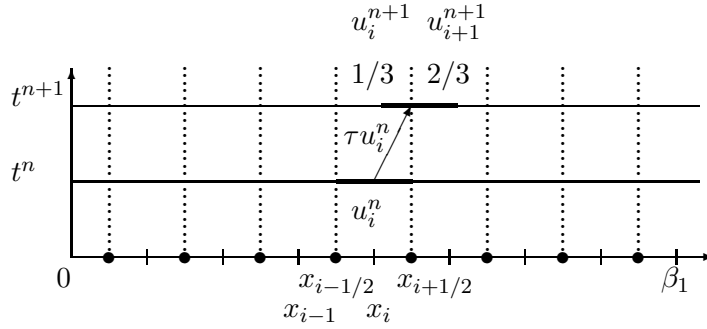


Figure 1.2: Forward characteristics method for the transport of the cells. The quantity in each cell is advected with constant velocity and its value is projected on the grid at time t^{n+1} .

The velocity is assumed to be such that $u_i^n \geq 0$ and $u_i^n \leq u_{i+1}^n$, for all $i = 1, \dots, k^n$ (this being in agreement at time $t = 0$ with the assumptions $u^0 \geq 0$ and u^0 is an increasing function).

Under the condition (1.74), the value of each field in cell number i has thus only two contributions: one from the cell number i and one from the cell number $i - 1$. This is the case of Fig. 1.2. The characteristic method can be written by summing these two contributions and gives: $hu_i^{n+1} = \tau u_{i-1}^n u_{i-1}^n + (h - \tau u_i^n) u_i^n$. Therefore it corresponds to an explicit finite differences scheme:

$$\frac{u_i^{n+1} - u_i^n}{\tau} + \frac{(u_i^n)^2 - (u_{i-1}^n)^2}{h} = 0, \quad i = 1, \dots, k^n. \quad (1.75)$$

This scheme is not consistent for the approximation of the equation $\frac{\partial u}{\partial t} + u \frac{\partial u}{\partial x} = 0$ since a factor one-half is missing.

In order to understand what happens in this situation and how does this method work, we consider a given positive continuous function $a : (0, \beta_1) \times (0, T) \rightarrow \mathbb{R}$ and the generic problem: find $u : (0, \beta_1) \times (0, T) \rightarrow \mathbb{R}$ such that:

$$\frac{\partial u}{\partial t}(x, t) + a(x, t) \frac{\partial u}{\partial x}(x, t) = 0, \quad (x, t) \in (0, \beta_1) \times (0, T). \quad (1.76)$$

with boundary condition $u(0, t) = 0$ and initial condition $u(x, 0) = u_0(x)$, where u_0 is a positive increasing regular function. We assume that condition (1.74) holds. The method of characteristics with projection described before can be written again by $hu_i^{n+1} = \tau a_{i-1}^n u_{i-1}^n + (h - \tau a_i^n) u_i^n$ and, therefore consists to write the following finite differences scheme:

$$\frac{u_j^{n+1} - u_j^n}{\tau} + a_j^n \frac{u_j^n - u_{j-1}^n}{h} + u_{j-1}^n \frac{a_j^n - a_{j-1}^n}{h} = 0. \quad (1.77)$$

If the velocity a is constant, the scheme (1.77) is clearly consistent (see for instance [64]). In the opposite, if a is not a constant function, (1.77) is not consistent for the

1.6. A TIME SPLITTING SCHEME

advection equation (1.76) under non-conservative form. In particular, if $a = u$, (1.77) leads to (1.75).

In order to avoid this lack of consistency, the characteristic function φ of the domain $Q_T = \{(x, t) : 0 < x < s(t), t \in (0, T)\}$ is introduced. This function is defined on $(0, \beta_1) \times (0, T)$ and has value one in Q_T and zero elsewhere. Let φ_i^n be an approximation of $\varphi(x_i, t^n)$, this approximation being constant in the cell centred in x_i . Instead of the velocity u , the function φ and the product $\varphi \cdot u$ are transported with velocity u , so that $\frac{\partial \varphi}{\partial t} + u \frac{\partial \varphi}{\partial x} = 0$ and $\frac{\partial(\varphi \cdot u)}{\partial t} + u \frac{\partial(\varphi \cdot u)}{\partial x} = 0$ (this model is in agreement with the method described in [73]). Thus, under assumption (1.74), when $u_j^n \geq 0$ we have the following two equations, corresponding to the transport of functions φ and $\varphi \cdot u$:

$$h\varphi_j^{n+1}u_j^{n+1} = \tau u_{j-1}^n \varphi_{j-1}^n u_{j-1}^n + (h - \tau u_j^n) \varphi_j^n u_j^n, \quad (1.78)$$

$$h\varphi_j^{n+1} = \tau u_{j-1}^n \varphi_{j-1}^n + (h - \tau u_j^n) \varphi_j^n, \quad (1.79)$$

for $j = 1, \dots, k^n$. Equations (1.78) (1.79) can be written:

$$\frac{\varphi_j^{n+1}u_j^{n+1} - \varphi_j^n u_j^n}{\tau} + \frac{\varphi_j^n (u_j^n)^2 - \varphi_{j-1}^n (u_{j-1}^n)^2}{h} = 0, \quad (1.80)$$

$$\frac{\varphi_j^{n+1} - \varphi_j^n}{\tau} + \frac{\varphi_j^n u_j^n - \varphi_{j-1}^n u_{j-1}^n}{h} = 0. \quad (1.81)$$

Let us consider the n -th time step and assume that $\varphi_j^n = 1$ if $j = 0, \dots, k^n$ and zero elsewhere. Hence, (1.80) leads to:

$$\frac{\varphi_j^{n+1}u_j^{n+1} - u_j^n}{\tau} + \frac{(u_j^n)^2 - (u_{j-1}^n)^2}{h} = 0. \quad (1.82)$$

Inserting relationship (1.81) (with $\varphi_j^n = \varphi_{j-1}^n = 1$) into (1.82) yields:

$$\frac{u_j^{n+1} - u_j^n}{\tau} - \frac{1}{h} (u_j^n - u_{j-1}^n) u_j^{n+1} + \frac{(u_j^n)^2 - (u_{j-1}^n)^2}{h} = 0, \quad (1.83)$$

for $j = 1, \dots, k^n$. In conclusion, the characteristics method with projection for the advection of the velocity times the characteristic function of the domain Q_T corresponds to a semi-implicit upwind finite differences scheme for the equation:

$$\frac{\partial u}{\partial t} - u \frac{\partial u}{\partial x} + \frac{\partial}{\partial x} (u^2) = 0. \quad (1.84)$$

Equation (1.84) is equivalent to the initial advection equation $\frac{\partial u}{\partial t} + u \frac{\partial u}{\partial x} = 0$ when u is sufficiently regular. The scheme is thus consistent.

The numerical properties of the scheme (1.83) are investigated now. Recall that u_0 is a positive increasing regular function, implying that the function u remains sufficiently regular. Let us assume that there exists a constant $\gamma > 0$ such that the following condition holds:

$$\frac{\tau}{h} \max_{i=0, \dots, k^n} u_i^n \leq \gamma < 1, \quad \forall n = 0, 1, \dots, M, \quad (1.85)$$

The assumption (1.85) corresponds to a *strict CFL* condition.

Consistency Error. The scheme (1.83) was proven to be consistent. The consistency error is defined by:

$$\mathcal{E}^c = \left| \frac{u(x_j, t^{n+1}) - u(x_j, t^n)}{\tau} + \frac{(u(x_j, t^n))^2 - (u(x_{j-1}, t^n))^2}{h} - u(x_j, t^{n+1}) \frac{u(x_j, t^n) - u(x_{j-1}, t^n)}{h} \right| \quad (1.86)$$

By developing in Taylor expansion, (1.86) leads to:

$$\begin{aligned} \mathcal{E}^c = & \left| \frac{\partial u}{\partial t}(x_j, t^n) + \frac{\tau}{2} \frac{\partial^2 u}{\partial t^2}(x_j, t^n) + \frac{\partial}{\partial x}(u^2(x_j, t^n)) + \frac{h}{2} \frac{\partial^2}{\partial x^2}(u^2(x_j, t^n)) \right. \\ & - u(x_j, t^n) \frac{\partial u}{\partial x}(x_j, t^n) + u(x_j, t^n) \frac{h}{2} \frac{\partial^2 u}{\partial x^2}(x_j, t^n) \\ & \left. + \tau \frac{\partial u}{\partial t}(x_j, t^n) \frac{\partial u}{\partial x}(x_j, t^n) + \mathcal{O}(\tau^2) + \mathcal{O}(h^2) \right|. \end{aligned}$$

We use the fact that $\frac{\partial u}{\partial t}(x_j, t^n) + \frac{\partial}{\partial x}(u^2(x_j, t^n)) - u(x_j, t^n) \frac{\partial u}{\partial x}(x_j, t^n) = 0$. Hence there exists a constant K independent of h and τ such that the consistency error \mathcal{E}^c satisfies $\mathcal{E}^c \leq K(\tau + h)$.

Stability Analysis. We first prove that the scheme is positive. More precisely, if $u_j^n \geq 0$, $\forall j = 1, \dots, k^n$, then $u_j^{n+1} \geq 0$, $\forall j = 1, \dots, k^{n+1}$. Relationship (1.83) leads to:

$$\begin{aligned} u_j^{n+1} \underbrace{\left(1 - \frac{\tau}{h} (u_j^n - u_{j-1}^n)\right)}_{>0 \text{ under (1.85)}} &= u_j^n + \frac{\tau}{h} ((u_{j-1}^n)^2 - (u_j^n)^2) \\ &= u_j^n \left(1 - \frac{\tau}{h} (u_j^n + u_{j-1}^n)\right) + u_{j-1}^n \frac{\tau}{h} (u_j^n + u_{j-1}^n) \\ &= u_j^n \underbrace{\left(1 - \frac{\tau}{h} u_j^n\right)}_{\geq 0 \text{ under (1.74)}} + u_{j-1}^n \underbrace{\frac{\tau}{h} u_{j-1}^n}_{\geq 0}. \end{aligned}$$

The right-hand side member is positive if $u_j^n \geq 0$, $\forall j = 1, \dots, k^n$. The conclusion $u_j^{n+1} \geq 0$, $\forall j = 1, \dots, k^{n+1}$ is straightforward. Moreover, this same relation yields:

1.6. A TIME SPLITTING SCHEME

$$\begin{aligned} u_j^{n+1} \left(1 - \frac{\tau}{h} (u_j^n - u_{j-1}^n)\right) &= u_j^n \left(1 - \frac{\tau}{h} u_j^n\right) + u_{j-1}^n \left(\frac{\tau}{h} + u_{j-1}^n\right) \\ &\leq \max_{k=1, \dots, k^n} u_k^n \left(1 - \frac{\tau}{h} (u_j^n - u_{j-1}^n)\right) . \end{aligned}$$

Again the conclusion is straightforward and leads to:

$$\max_{j=1, \dots, k^{n+1}} u_j^{n+1} \leq \max_{j=1, \dots, k^n} u_j^n .$$

This scheme is finally proved to be monotonous. More precisely, we prove that, if $u_j^n \leq u_{j+1}^n, \forall j$, then $u_j^{n+1} \leq u_{j+1}^{n+1}, \forall j$. In order to prove this property, set $\lambda = \frac{\tau}{h}$ and define $v_i = \lambda u_i^n, \forall i$. We multiply (1.83) by τ and then by λ and obtain the following relation:

$$\lambda u_i^{n+1} = \frac{v_i + (v_{i-1}^2 - v_i^2)}{1 - (v_i - v_{i-1})} = v_i + \frac{v_{i-1}(v_{i-1} - v_i)}{1 - (v_i - v_{i-1})} .$$

According to (1.74), $0 \leq v_{i-1} \leq v_i \leq v_{i+1} \leq 1$, for all i by monotonicity assumption. Our goal is to prove that $u_{i+1}^{n+1} - u_i^{n+1}$ is positive. Set $a = v_{i+1} - v_i$ and $b = v_i - v_{i-1}$ and notice that $0 \leq a, b \leq 1$. We develop then the difference $\lambda u_{i+1}^{n+1} - \lambda u_i^{n+1}$:

$$\begin{aligned} \lambda(u_{i+1}^{n+1} - u_i^{n+1}) &= v_{i+1} + \frac{v_i(v_i - v_{i+1})}{1 - (v_{i+1} - v_i)} - v_i - \frac{v_{i-1}(v_{i-1} - v_i)}{1 - (v_i - v_{i-1})} \\ &= a - v_i \frac{a}{1 - a} + v_{i-1} \frac{b}{1 - b} \\ &= \frac{1}{(1 - a)(1 - b)} (a - a^2 - ab + a^2b - v_i a + v_i ab + v_{i-1} b - v_{i-1} ab) . \end{aligned}$$

By ordering these terms, we obtain:

$$\begin{aligned} \lambda(u_{i+1}^{n+1} - u_i^{n+1}) &= \frac{1}{(1 - a)(1 - b)} [(a - a^2 - v_i a) + (a^2 b + v_i ab - v_{i-1} ab) + (v_{i-1} b - ab)] \\ &= \frac{1}{(1 - a)(1 - b)} [a(1 - v_{i+1}) + ab(v_{i+1} - v_{i-1}) + b(v_{i-1} - a)] \\ &= \frac{1}{(1 - a)(1 - b)} [a(1 - b)(1 - v_{i+1}) + b v_{i-1} (1 - a)] \geq 0 , \end{aligned}$$

since $0 \leq a, b \leq 1$. The conclusion is that if the initial condition u_0 is a positive increasing function, the solution u is also positive increasing and this scheme provides a stable positive increasing approximation of the solution u^n at each time step under the condition (1.85).

Convergence Order. The difference between the numerical scheme (1.83) and the equation (1.84) is estimated. Recall that:

$$\begin{aligned} \frac{\partial u}{\partial t}(x_j, t^n) - u(x_j, t^n) \frac{\partial u}{\partial x}(x_j, t^n) + \frac{\partial}{\partial x}(u^2(x_j, t^n)) &= 0 ; \\ \frac{u_j^{n+1} - u_j^n}{\tau} - u_j^{n+1} \frac{u_j^n - u_{j-1}^n}{h} + \frac{(u_j^n)^2 - (u_{j-1}^n)^2}{h} &= 0 . \end{aligned}$$

Let $e_j^n = u_j^n - u(x_j, t^n)$ be the pointwise error at time t^n and at grid point x_j . The error satisfies the equation:

$$\begin{aligned} \frac{e_j^{n+1} - e_j^n}{\tau} + \frac{(u_j^n)^2 - (u_{j-1}^n)^2 - (u^2(x_j, t^n) - u^2(x_{j-1}, t^n))}{h} \\ - \left(u_j^{n+1} \frac{u_j^n - u_{j-1}^n}{h} - u(x_j, t^n) \frac{\partial u}{\partial x}(x_j, t^n) \right) \\ + \frac{\tau}{2} \frac{\partial^2 u}{\partial t^2}(x_j, \theta^n) + \frac{h}{2} \frac{\partial^2}{\partial x^2} u^2(\eta_j, t^n) + u(x_j, t^n) \frac{h}{2} \frac{\partial^2 u}{\partial x^2}(\xi_j, t^n) = 0 , \end{aligned}$$

where $\xi_j, \eta_j \in [x_{j-1}, x_j]$ and $\theta^n \in [t^n, t^{n+1}]$. By ordering some terms, this relation leads to:

$$\begin{aligned} \frac{e_j^{n+1} - e_j^n}{\tau} + \frac{1}{h} [e_j^n (u_j^n + u(x_j, t^n)) - e_{j-1}^n (u_{j-1}^n + u(x_{j-1}, t^n))] \\ - \left(e_j^{n+1} \frac{u_j^n - u_{j-1}^n}{h} + u(x_j, t^{n+1}) \frac{e_j^n - e_{j-1}^n}{h} \right) \\ + \left(\frac{1}{2} \frac{\partial^2 u}{\partial t^2}(x_j, \theta^n) \right) \tau + \frac{1}{2} \left(\frac{\partial^2}{\partial x^2} u^2(\eta_j, t^n) + u(x_j, t^n) \frac{\partial^2 u}{\partial x^2}(\xi_j, t^n) \right) h = 0 . \end{aligned} \quad (1.87)$$

Thanks to the regularity of u , the derivatives of u appearing in (1.87) are bounded and there exist two generic constants K_1 and K_2 such that (1.87) yields:

$$\begin{aligned} \left| e_j^{n+1} \left(1 - \frac{\tau}{h} (u_j^n - u_{j-1}^n) \right) \right| &\leq |e_j^n| \left| 1 - \frac{\tau}{h} (u_j^n + u(x_j, t^n) - u(x_j, t^{n+1})) \right| \\ &\quad + |e_{j-1}^n| \left| \frac{\tau}{h} (u_{j-1}^n + u(x_{j-1}, t^n) - u(x_j, t^{n+1})) \right| \\ &\quad + K_1 \tau^2 + K_2 \tau h \\ &\leq |e_j^n| \left| 1 - \frac{\tau}{h} u_j^n \right| + |e_j^n| \frac{\tau}{h} |u(x_j, t^n) - u(x_j, t^{n+1})| \\ &\quad + |e_{j-1}^n| \left| \frac{\tau}{h} u_{j-1}^n \right| + |e_{j-1}^n| \frac{\tau}{h} |u(x_{j-1}, t^n) - u(x_j, t^{n+1})| \\ &\quad + K_1 \tau^2 + K_2 \tau h . \end{aligned} \quad (1.88)$$

Both quantities $|e_j^n|$ and $|e_{j-1}^n|$ are bounded by $\max_{l=0, \dots, k^n} |e_l^n|$ and the coefficients $1 - \frac{\tau}{h} u_j^n$ and $\frac{\tau}{h} u_{j-1}^n$ are positive under assumption (1.74). Relationship (1.88) becomes:

1.6. A TIME SPLITTING SCHEME

$$\begin{aligned}
\left|e_j^{n+1}\right| \left(1 - \frac{\tau}{h}(u_j^n - u_{j-1}^n)\right) &\leq \max_{l=0,\dots,k^n} |e_l^n| \left[\left(1 - \frac{\tau}{h}(u_j^n - u_{j-1}^n)\right) \right. \\
&\quad \left. + \frac{\tau}{h} |u(x_j, t^n) - u(x_j, t^{n+1})| \right. \\
&\quad \left. + \frac{\tau}{h} |u(x_{j-1}, t^n) - u(x_j, t^{n+1})| \right] \\
&\quad + K_1 \tau^2 + K_2 \tau h .
\end{aligned} \tag{1.89}$$

The two terms appearing in absolute values in (1.89) can be estimated:

$$\begin{aligned}
|u(x_j, t^n) - u(x_j, t^{n+1})| &= \tau \left| \frac{\partial u}{\partial t}(x_j, \theta^n) \right| , \\
|u(x_{j-1}, t^n) - u(x_j, t^{n+1})| &= |u(x_{j-1}, t^n) - u(x_j, t^n)| + |u(x_j, t^n) - u(x_j, t^{n+1})| \\
&= h \left| \frac{\partial u}{\partial x}(\eta_j, t^n) \right| + \tau \left| \frac{\partial u}{\partial t}(x_j, \theta^n) \right| .
\end{aligned}$$

Here $\theta^n \in [t^n, t^{n+1}]$ and $\eta_j \in [x_{j-1}, x_j]$. Thanks to the regularity of u , both derivatives can be bounded independently of the indices n and j . There exist then two constants C_1 and C_2 independent of the indices n and j and independent of h and τ such that relationship (1.89) leads to:

$$\begin{aligned}
\left|e_j^{n+1}\right| \left(1 - \frac{\tau}{h}(u_j^n - u_{j-1}^n)\right) &\leq \max_{l=0,\dots,k^n} |e_l^n| \left[\left(1 - \frac{\tau}{h}(u_j^n - u_{j-1}^n)\right) + C_1 \tau + C_2 \frac{\tau^2}{h} \right] \\
&\quad + K_1 \tau^2 + K_2 \tau h .
\end{aligned}$$

Under assumption (1.74), there exists another constant C independent of τ and h such that:

$$\left|e_j^{n+1}\right| \left(1 - \frac{\tau}{h}(u_j^n - u_{j-1}^n)\right) \leq \max_{l=0,\dots,k^n} |e_l^n| \left[\left(1 - \frac{\tau}{h}(u_j^n - u_{j-1}^n)\right) + C \tau \right] + K_1 \tau^2 + K_2 \tau h . \tag{1.90}$$

By using (1.85) again, the term $1 - \frac{\tau}{h}(u_j^n - u_{j-1}^n)$ is greater than $1 - \gamma$ and strictly positive. Relation (1.90) can be divided by $1 - \frac{\tau}{h}(u_j^n - u_{j-1}^n)$ and there exists new constants, also denoted by C , K_1 and K_2 , independent of τ and h , such that:

$$\left|e_j^{n+1}\right| \leq (1 + C \tau) \max_{l=0,\dots,k^n} |e_l^n| + K_1 \tau^2 + K_2 \tau h ,$$

and the same relation is true for the maximum. By summation on the index n , this leads to:

$$\max_{j=0,\dots,k^{n+1}} \left|e_j^{n+1}\right| \leq C \sum_{i=0}^n \tau \max_{j=0,\dots,k^i} |e_j^i| + (n+1) \tau (K_1 \tau + K_2 h) .$$

Let $T > 0$ denote the final time of simulation. Discrete Gronwall's lemma (see for instance [96, page 14]) leads to conclusion:

$$\max_{j=0,\dots,k^{n+1}} |e_j^{n+1}| \leq e^{CT} T (K_1 \tau + K_2 h) . \quad (1.91)$$

In conclusion, the method of characteristics with projection for the transport of the quantity $\varphi \cdot u$ is stable and convergent under condition (1.85), assuming that no shocks are appearing. It gives a prediction of velocity $u_j^{n+1/2}$, $j = 1, \dots, k^{n+1} + 1$ which is used as the initial condition of the diffusion step.

1.6.2 Diffusion Step

The diffusion step at time step n consists in finding $u : (0, s^{n+1}) \times (t^n, t^{n+1}) \rightarrow \mathbb{R}$ such that:

$$\frac{\partial u}{\partial t}(x, t) - \varepsilon \frac{\partial^2 u}{\partial x^2}(x, t) = f(x, t), \quad x \in (0, s^{n+1}), \quad t \in (t^n, t^{n+1}) \quad (1.92)$$

$$u(0, t) = 0 = \frac{\partial u}{\partial x}(s^{n+1}, t), \quad t \in (t^n, t^{n+1}) \quad (1.93)$$

$$u(x, t^n) = u^{n+1/2}(x), \quad x \in (0, s^{n+1}) . \quad (1.94)$$

where s^{n+1} is the right end of the new domain of the computation. This problem is well-posed and admits one unique solution (see for instance [97]). A \mathbb{P}_1 finite element method is considered together with an implicit Euler scheme to solve (1.92)-(1.94). If the exact solution to (1.92)-(1.94) is sufficiently smooth, there exists a constant K such that the error introduced at each time step is given by (see for instance [81, page 102]):

$$\|u(t^{n+1}) - u^{n+1}\|_{\Delta_{n+1}} \leq \|u(t^n) - u^{n+1/2}\|_{\Delta_n} + \tau K (h^2 + \tau) ,$$

where $\|v\|_{\Delta_n} = \max_{1 \leq j \leq k^n} |v_j|$.

An additional error is introduced since (1.92)-(1.94) is solved on the space interval $(0, s^{n+1})$ instead of $(0, s(t^{n+1}))$. Consider now the solution u to the problem (1.92)-(1.94) and let v denote the solution to the same problem on the space interval $(0, s(t^{n+1}))$. Both problems can be transformed onto the space interval $(0, 1)$. By making the difference between the two problems and using a priori estimates for the heat equation (see [29, volume 8] for instance), there exists a constant K such that

$$\|u - v\|_{L^2(0,1,H^2(0,1)) \cap H^1(0,T,L^2(0,1))} \leq K \left[\|f^{n+1} - f(t^{n+1})\|_{L^2(U^T)} + |s^{n+1} - s(t^{n+1})| \right] ,$$

where f^{n+1} (respectively $f(t^{n+1})$) is the image of f under the linear application which transforms $(0, s^{n+1})$ (respectively $(0, s(t^{n+1}))$) onto $(0, 1)$. By using an estimate similar to (1.57), there exists another constant \tilde{K} such that this estimate becomes:

$$\|u - v\|_{L^2(0,1,H^2(0,1)) \cap H^1(0,T,L^2(0,1))} \leq \tilde{K} |s^{n+1} - s(t^{n+1})| . \quad (1.95)$$

1.7. NUMERICAL RESULTS

In order to conclude, notice that an explicit Euler scheme (1.70) is used to solve (1.6). Thus, at each time step, the error on the approximation of the boundary is given by:

$$|s^{n+1} - s(t^{n+1})| \leq C\tau^2 ,$$

see [49] for instance.

Convergence Summary Several errors come from the splitting algorithm, the advection and diffusion steps. The addition of these errors at each time step leads to:

$$\begin{aligned} \|u(t^{n+1}) - u^{n+1}\|_{\Delta_{n+1}} &\leq C \left(\underbrace{\tau^2}_{\text{error splitting}} + \underbrace{\tau^2}_{\text{error on the boundary}} \right. \\ &\quad \left. + \underbrace{\tau(\tau + h)}_{\text{advection error}} + \underbrace{\tau(\tau + h^2)}_{\text{diffusion error}} \right) \\ &\leq C\tau(\tau + h) . \end{aligned}$$

We conclude then that our splitting algorithm is an order one algorithm. Numerical experiments in the next section confirm this result. For these reasons, we believe that the time splitting scheme introduced in [74, 75] in two and three space dimensions is also an order one algorithm.

1.7 Numerical Results

Numerical experiments are made and numerical results are compared with theoretical results. Numerical implementation is made with MATLABTM. The error is computed in various norms, namely $\|s - s_h\|_{L^\infty(0,T)}$ and $\|s - s_h\|_{W^{1,\infty}(0,T)}$ for the boundary function and $\|u - u_h\|_{L^2(Q_T)}$ and $\left\| \frac{\partial(u - u_h)}{\partial x} \right\|_{L^2(Q_T)}$ for the velocity.

No Moving Boundary. The situation with $s(t) = 1$, $t \in (0, T)$ and $u(x, t) = (1 + t)(1 - \cos(2\pi x))$, $(x, t) \in Q_T$ is considered. Compatibility conditions between initial velocity and boundary conditions are satisfied. The values of parameters are $\beta_1 = 2$, $\beta_2 = 0.01$, $T = 0.1$, $s_0 = 1$, $\alpha = 1$ and $\varepsilon = 1$. The time interval $(0, T)$ is divided into M time steps and the interval $(0, \beta_1)$ is divided into $N + 1$ intervals. Sequences of spatial steps h and time steps τ are chosen such that the CFL condition (1.85) is satisfied. The spatial step h is divided by two while τ is divided by two. Figure 1.3 illustrates convergence order of the errors for velocity and boundary functions.

Figure 1.3 shows that the convergence order for the approximation of the boundary is in this case:

$$\|s - s_h\|_{L^\infty(0,T)} \leq C(h^2 + \tau^2) , \quad (1.96a)$$

$$\|\dot{s} - \dot{s}_h\|_{L^\infty(0,T)} \leq C(h^{7/5} + \tau^{7/5}) , \quad (1.96b)$$

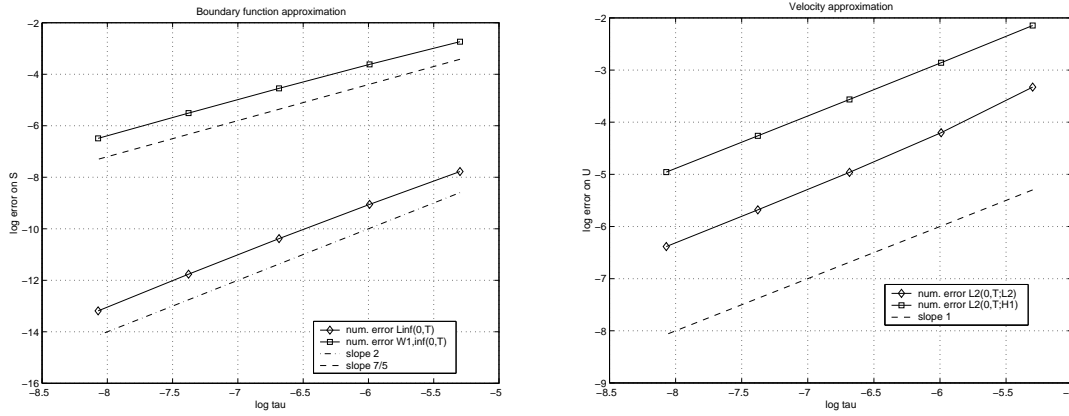


Figure 1.3: Convergence orders for test without moving boundary. Left: Log log scale plot of error on the boundary $\|s - s_h\|$ vs τ (blue and light blue: numerical results, red: line of slope 2). Right: Log log scale plot of error on the velocity $\|u - u_h\|$ vs τ (blue and light blue: numerical results, red: line of slope 1, magenta: line of slope 7/5).

while the convergence order for the approximation of the velocity is:

$$\|u - u_h\|_{L^2(Q_T)} + \left\| \frac{\partial(u - u_h)}{\partial x} \right\|_{L^2(Q_T)} \leq C(h + \tau) . \quad (1.97)$$

Relationships (1.96a-b) and (1.97) are not in disagreement with theoretical results obtained in Sect. 1.7. They also illustrate that the convergence order for the approximation of the boundary function is better than one in the particular case of a constant boundary.

A Linear Free Boundary Function. The situation with $s(t) = 1 + t$, $t \in (0, T)$ and $u(x, t) = \frac{2x}{1+t} - \frac{x^2}{(1+t)^2}$, $(x, t) \in Q_T$ is investigated. Compatibility conditions between initial velocity and boundary conditions are satisfied. The values of parameters are similar to the ones of the first test case. A sequence of spatial steps h and time steps τ which satisfy CFL condition (1.85) is chosen and h is assumed to be divided by two while τ is divided by two. Results are presented in Fig. 1.4.

The convergence order for boundary approximation is $\|s - s_h\|_{W^{1,\infty}(0,T)} \leq C(h + \tau)$ and is in agreement with the results obtained in Sect. 1.6, while the convergence order for the approximation of velocity in both norms $\|u\|_{L^2(U_T)}$ and $\left\| \frac{\partial u}{\partial t} \right\|_{L^2(U_T)}$ are of order one.

A Free Boundary Example Finally the situation with $s(t) = e^{\frac{t}{2} + \frac{t^2}{4}}$, $t \in (0, T)$ and $u(x, t) = \dot{s}(t) \sin\left(\frac{\pi x}{2s(t)}\right)$, $(x, t) \in Q_T$ is considered. Compatibility conditions between initial velocity and boundary conditions are satisfied. The values of parameters are similar to the ones of precedent test cases. Figure 1.5 illustrates the convergence of the approximations of the boundary function and velocity in the various norms. The convergence orders are similar to the ones of the previous case.

1.7. NUMERICAL RESULTS

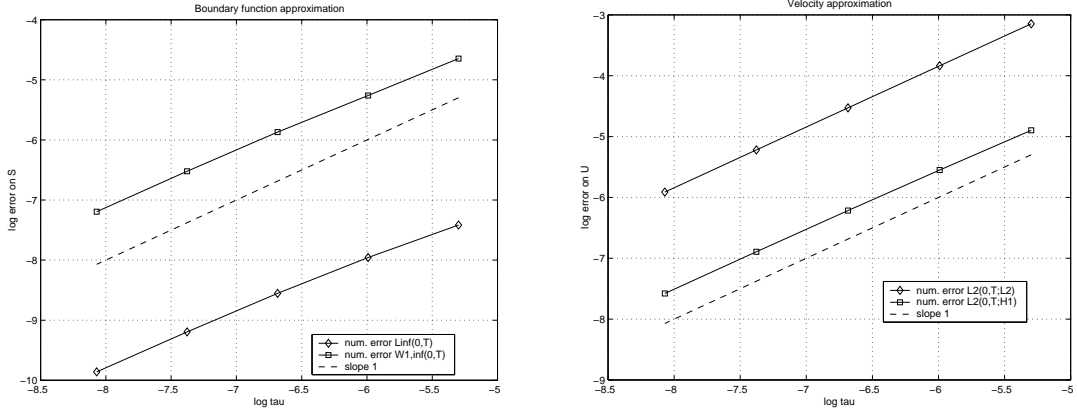


Figure 1.4: Convergence orders for test case of a linear free boundary function. Left: Log log scale plot of error on the boundary $\|s - s_h\|$ vs τ (blue and light blue: numerical results, red: line of slope 1). Right: Log log scale plot of error on the velocity $\|u - u_h\|$ vs τ (blue and light blue: numerical results, red: line of slope 1, magenta: line of slope 3/2).

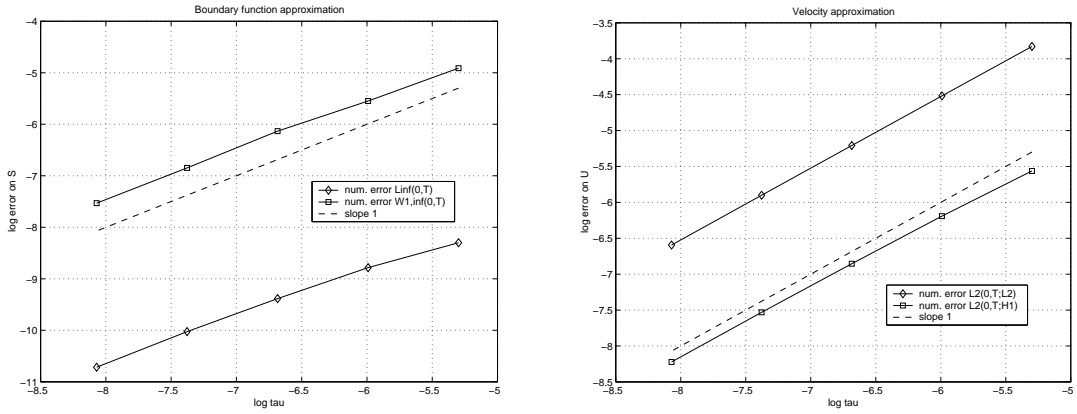


Figure 1.5: Convergence orders for free boundary test case. Left: Log log scale plot of error on the boundary $\|s - s_h\|$ vs τ (blue and light blue: numerical results, red: line of slope 1). Right: Log log scale plot of error on the velocity $\|u - u_h\|$ vs τ (blue and light blue: numerical results, red: line of slope 1).

Figure 1.6 on page 48 shows the importance of CFL stability criterion. In the first simulation (in magenta), the CFL condition is satisfied and the algorithm is stable. In the other hand, if the CFL condition is not satisfied (in red), some instabilities appear and give rise to oscillations. Parameters are $T = 2$, $\beta_1 = 20$, $\varepsilon = 0.01$ and $(N, M) = (199, 200)$ in the first case and $(N, M) = (199, 100)$ in the second. The oscillations are propagating from the free right end point of the interval.

Numerical results are in agreement with the theoretical results. For the approximation of the boundary function, we generally obtain $\|s - s_h\|_{W^{1,\infty}(0,T)} \leq C(h + \tau)$, except if the boundary function is constant. On the other hand, the numerical error for the approximation of the velocity in both norms $\|u - u_h\|_{L^2(Q_T)}$ and $\left\| \frac{\partial(u - u_h)}{\partial x} \right\|_{L^2(Q_T)}$ is also of order one. This confirms partially the results obtained in Sect. 1.5 and 1.6. These results are

CHAPTER 1. ANALYSIS OF 1D FREE SURFACE PROBLEM

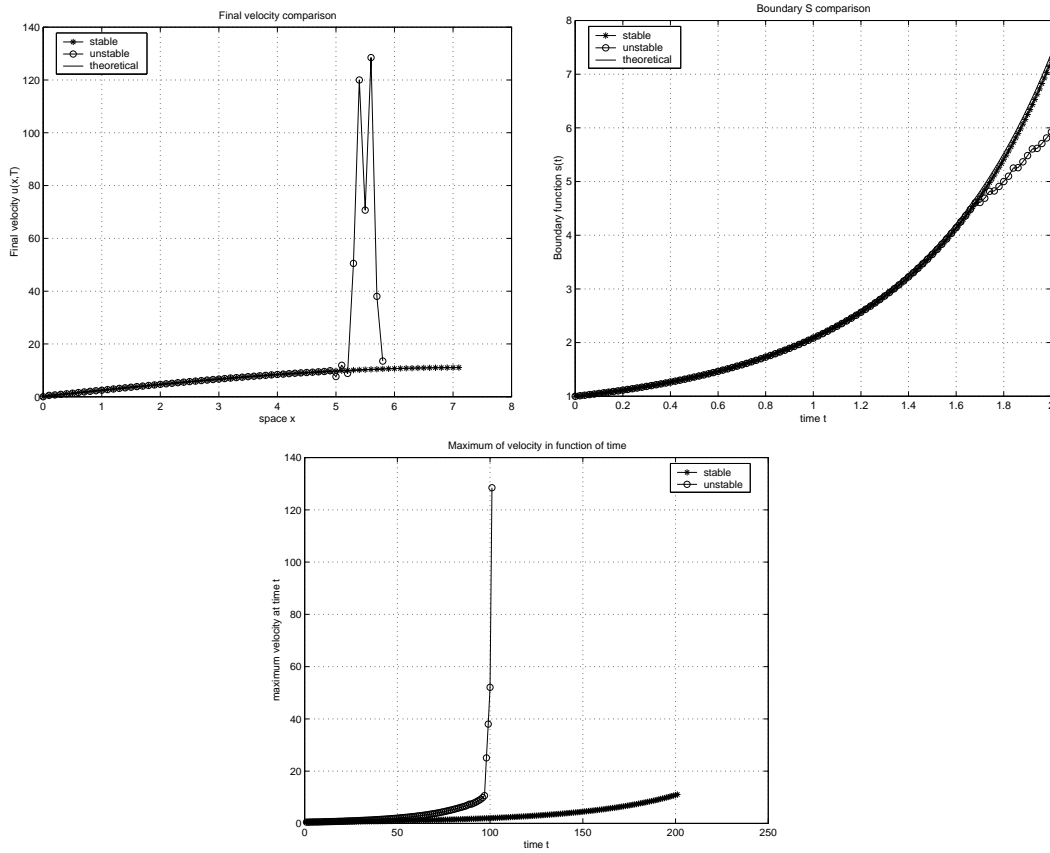


Figure 1.6: Stability for free boundary test case. In red, non-stable situation, in magenta, stable simulation and in blue theoretical functions. First row: velocity at time T , second row: evolution of boundary function s and third row: maximum of velocity function of time.

local in time and the simulation blows up if the time simulation is too large.

We have investigated this one-dimensional free surface flow problem and compared the theoretical results with simulations. We turn us now to the two-dimensional Navier-Stokes equations which is the subject of the next chapter.

Chapter 2

A Two-Dimensional Free Surface Problem

This chapter is concerned with a two-dimensional free surface problem, for instance the modelling of the motion of a droplet of water in the presence of a gravity field. Governing equations in the liquid are the Navier-Stokes equations. A zero force boundary condition is applied on the boundary of the liquid domain since the surrounding gas and the surface tension effects are not taken into account. The whole boundary is assumed to be the free surface. Existence and uniqueness of a solution are investigated in this chapter. We are interested in applying the same methodology we used in Chap. 1.

A similar problem has already been considered in the literature. Local in time existence of a solution has been proved in [108] in Sobolev spaces $W^{m,p}$ for $p > 3$. In [111] (and references therein), local in time results have been presented in Hölder spaces. In [107, 110], similar results as the ones presented in this chapter have been obtained. The approach was different. The problem has been expressed in Lagrangian coordinates and a fixed point theorem for the velocity has been used. In [45], the problem with Dirichlet boundary conditions has been considered. In [2, 6, 7] (and references therein), the problem of an infinite horizontal layer of fluid has been treated (with or without surface tension) with mixed boundary conditions on the upper and lower parts of the horizontal layer.

The procedure used for treating the one-dimensional problem is adapted to the two-dimensional case we consider here. This methodology has been suggested by [6] and some results from this work are used here. However the problem here is not expressed in Lagrangian coordinates.

In Sect. 2.1, the model and the method are presented. Existence results for the Stokes problem are recalled in Sect. 2.2. Given the shape of the domain, a modified Stokes problem is then considered in Sect. 2.3. The nonlinear advective term is added in Sect. 2.4 to study the problem with given moving domain. Section 2.5 deals with the free boundary problem.

2.1 Mathematical Model

The two-dimensional case is considered. Let $T > 0$ be a finite horizon of time. Consider a bounded moving domain $\Omega_t \subset \mathbb{R}^2$, $t \in (0, T)$ with boundary $\partial\Omega_t$. Note Q_T the space-time

domain $Q_T = \{(x, t) \in \mathbb{R}^2 \times (0, T) : x \in \Omega_t, t \in (0, T)\}$; its space-time free boundary is denoted by $\Sigma_T = \{(x, t) \in \mathbb{R}^2 \times (0, T) : x \in \partial\Omega_t, t \in (0, T)\}$. The whole boundary is assumed to be the free surface. Let $\eta : \Omega_0 \times (0, T) \rightarrow \mathbb{R}^2$ be the mapping (*a priori* unknown) that transforms Ω_0 into Ω_t for all times $t \in (0, T)$.

The velocity and the pressure in the fluid are denoted by \mathbf{u} and p . The problem reads: find $\mathbf{u} : Q_T \rightarrow \mathbb{R}^2$, $p : Q_T \rightarrow \mathbb{R}$ and $\eta : \Omega_0 \times (0, T) \rightarrow \mathbb{R}^2$ such that:

$$\left\{ \begin{array}{ll} \frac{\partial \mathbf{u}}{\partial t} - 2\mu \nabla \cdot D(\mathbf{u}) + (\mathbf{u} \cdot \nabla) \mathbf{u} + \nabla p = \mathbf{f}, & \text{in } Q_T, \quad (2.1) \\ \nabla \cdot \mathbf{u} = 0, & \text{in } Q_T, \quad (2.2) \\ -p\mathbf{n} + 2\mu D(\mathbf{u})\mathbf{n} = 0, & \text{on } \Sigma_T, \quad (2.3) \\ \mathbf{u}(0) = \mathbf{u}_0, & \text{in } \Omega_0, \quad (2.4) \\ \frac{\partial \eta}{\partial t} = \mathbf{u} \circ \eta, & \text{in } \Omega_0 \times (0, T), \quad (2.5) \\ \eta(0) = Id, & \text{in } \Omega_0. \quad (2.6) \end{array} \right.$$

Here $\mu > 0$ is a given positive constant, $\nabla \cdot \mathbf{u}$ denotes the divergence operator of \mathbf{u} and $D(\mathbf{u})$ denotes the rate of deformation tensor $D(\mathbf{u}) = \frac{1}{2}(\nabla \mathbf{u} + \nabla \mathbf{u}^T)$. The spatial unit normal vector is denoted by \mathbf{n} and Id denotes the identity operator $Id : \xi \in \Omega_0 \rightarrow \xi \in \Omega_0$. The bounded domain Ω_0 is given and is assumed to be convex. The boundary $\partial\Omega_0$ is assumed to be sufficiently regular (say C^∞) in the whole chapter, even if this assumption could be relaxed. Finally, the functions \mathbf{f} and \mathbf{u}_0 are given, respectively on $\mathbb{R}^2 \times (0, T)$ and Ω_0 .

Here the mapping η permits to determine the domain Ω_t for all times $t \in (0, T)$. The domain Ω_t is given by

$$\Omega_t = \{x \in \mathbb{R}^2 : x = \eta(\xi, t), \xi \in \Omega_0\} .$$

The surrounding gas and surface tension effects are not taken into account; this implies a zero force boundary condition (2.3) on the boundary. The described situation is illustrated in Fig. 2.1 and we are interested in finding a solution to (2.1)-(2.6) for small times.

Remark 2.1 *The free boundary problem (2.1)-(2.6) is a problem extracted from [74]. However the shape of the liquid domain is described here by the mapping η instead of the characteristic function φ of the domain Ω_t (see Chap. 3 for the formulation of the free surface problem with characteristic function φ).*

The principle of the proof is the following. Let us first assume that the domain Ω_t is known for all times $t \in (0, T)$. The mapping η is thus assumed to be given is a well-chosen space that will be described later and the equations (2.5)-(2.6) are disregarded for the moment. The problem (2.1)-(2.4) is transformed in order to consider a cylindrical space-time domain. Let η be a sufficiently regular application that maps Ω_0 into Ω_t for all $t \in (0, T)$:

2.1. MATHEMATICAL MODEL

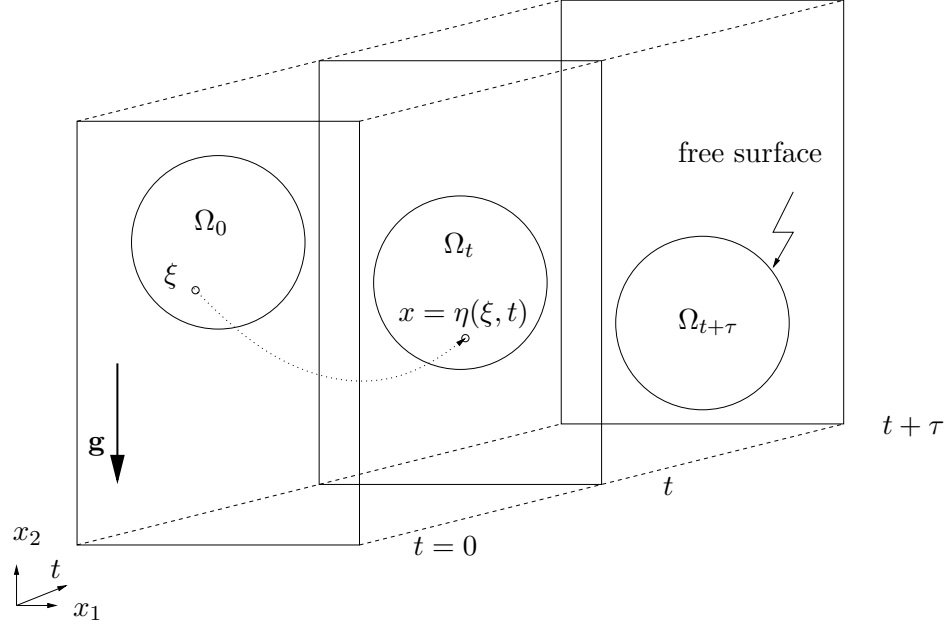


Figure 2.1: Example of a free surface problem in two space dimensions: water droplet in a gravity field with zero force boundary conditions on the whole free surface.

$$\begin{aligned} \eta_t : \quad \Omega_0 &\rightarrow \Omega_t , \\ \xi &\rightarrow x = \eta_t(\xi) . \end{aligned} \quad (2.7)$$

Here the notation $\eta_t(\xi)$ is equivalent to $\eta(\xi, t)$. The mapping η_0 at time $t = 0$ is assumed to be the identity operator and is denoted by Id . Let us assume that the inverse transformation of η_t exists and is also sufficiently regular. It is defined $\forall t \in (0, T)$ by:

$$\begin{aligned} \xi_t : \quad \Omega_t &\rightarrow \Omega_0 , \\ x &\rightarrow \xi = \xi_t(x) . \end{aligned} \quad (2.8)$$

The functions $\mathbf{v} : \Omega_0 \times (0, T) \rightarrow \mathbb{R}^2$ and $q : \Omega_0 \times (0, T) \rightarrow \mathbb{R}$ are respectively defined by $\mathbf{v}(\xi, t) = \mathbf{u}(\eta(\xi, t), t) = \mathbf{u}(x, t)$ and $q(\xi, t) = p(\eta(\xi, t), t) = p(x)$ when $x = \eta(\xi, t)$. Let the matrix $A = A(x, t)$ be the Jacobian matrix given by

$$(A)_{i,j} = \frac{\partial(\xi_t)_i}{\partial x_j}, \quad 1 \leq i, j \leq 2 , \quad (2.9)$$

so that $\nabla_x = A^T \nabla_\xi$ and $\nabla_x \mathbf{u} = (\nabla_\xi \mathbf{v})A$, where ∇_x is the gradient with respect to the variable x (respectively ∇_ξ is the gradient with respect to ξ). The inverse matrix $A^{-1} = A^{-1}(\xi, t)$ is defined by $(A^{-1})_{i,j} = \frac{\partial(\eta_t)_i}{\partial \xi_j}$, $1 \leq i, j \leq 2$. Let ∇_ξ be denoted by ∇

for the sake of simplicity. The problem (2.1)-(2.4) is transformed into a problem in the cylindrical space-time domain $\Omega_0 \times (0, T)$: find $\mathbf{v} : \Omega_0 \times (0, T) \rightarrow \mathbb{R}^2$ and $q : \Omega_0 \times (0, T) \rightarrow \mathbb{R}$ such that:

$$\left\{ \begin{array}{ll} \frac{\partial \mathbf{v}}{\partial t} - \mu(A^T \nabla) \cdot (\nabla \mathbf{v} A + (\nabla \mathbf{v} A)^T) + \frac{\partial \xi}{\partial t} \nabla \mathbf{v} \\ \quad + (\mathbf{v} \cdot A^T \nabla) \mathbf{v} + A^T \nabla q = \mathbf{f} \circ \eta, & \text{in } \Omega_0 \times (0, T) , \quad (2.10) \\ (A^T \nabla) \cdot \mathbf{v} = 0, & \text{in } \Omega_0 \times (0, T) , \quad (2.11) \\ -q A^T \mathbf{N} + \mu (\nabla \mathbf{v} A + (\nabla \mathbf{v} A)^T) A^T \mathbf{N} = 0, & \text{on } \partial \Omega_0 \times (0, T) , \quad (2.12) \\ \mathbf{v}(0) = \mathbf{u}_0 \circ \eta_0 = \mathbf{u}_0, & \text{in } \Omega_0 , \quad (2.13) \end{array} \right.$$

where \mathbf{N} is the external normal vector to Ω_0 and η_0 is assumed to satisfy $\eta_0 = Id$. The functions \mathbf{f} and \mathbf{u}_0 are given respectively on $\mathbb{R}^2 \times (0, T)$ and Ω_0 and are sufficiently regular. The function $\mathbf{F} = \mathbf{f} \circ \eta$ is defined in order to simplify the notations.

Remark 2.2 *The Neumann boundary condition (2.3) is translated on the initial domain Ω_0 . Without loss of generality, the boundary $\partial \Omega_t$ is assumed to be the zero level line of a smooth function $\tilde{\varphi}_t : \mathbb{R}^2 \rightarrow \mathbb{R}$ which is positive in the fluid part and negative outside. The normal vector oriented outside the liquid is then given by $\mathbf{n}(x, t) = -\frac{\nabla_x \tilde{\varphi}_t(x)}{\|\nabla_x \tilde{\varphi}_t(x)\|}$ (see [103] for instance). The change of variables (2.7)-(2.8) leads to the boundary equation (2.12) (see also [108]).*

The function η , as well as the coefficients of A and $\frac{\partial \xi}{\partial t}$ are assumed to be known for the moment. Regularity of η will be precised later. The existence of the problem with given mapping η is obtained in three steps that are detailed hereafter. The first step is to consider a classical Stokes problem in the cylindrical space-time domain $\Omega_0 \times (0, T)$. Then (2.10)-(2.13) without the nonlinear term $(\mathbf{v} \cdot A^T \nabla) \mathbf{v}$ is considered. Finally (2.10)-(2.13) is investigated by adding the nonlinear advection term.

The following Stokes problem is first obtained when we replace A by the identity matrix in (2.10)-(2.13) and by disregarding the nonlinear term $(\mathbf{v} \cdot A^T \nabla) \mathbf{v}$ and the advection term $\frac{\partial \xi}{\partial t} \nabla \mathbf{v}$: find $\mathbf{v} : \Omega_0 \times (0, T) \rightarrow \mathbb{R}^2$ and $q : \Omega_0 \times (0, T) \rightarrow \mathbb{R}$ such that:

$$\left\{ \begin{array}{ll} \frac{\partial \mathbf{v}}{\partial t} - \mu \nabla \cdot (\nabla \mathbf{v} + (\nabla \mathbf{v})^T) + \nabla q = \mathbf{F}, & \text{in } \Omega_0 \times (0, T) , \quad (2.14) \\ \nabla \cdot \mathbf{v} = 0, & \text{in } \Omega_0 \times (0, T) , \quad (2.15) \\ -q \mathbf{N} + \mu (\nabla \mathbf{v} + (\nabla \mathbf{v})^T) \mathbf{N} = 0, & \text{on } \partial \Omega_0 \times (0, T) , \quad (2.16) \\ \mathbf{v}(0) = \mathbf{u}_0, & \text{in } \Omega_0 . \quad (2.17) \end{array} \right.$$

This problem is a Stokes problem with Neumann boundary conditions. In Sect. 2.2, the existence of the velocity and pressure satisfying (2.14)-(2.17) is investigated and previous

with initial condition $\mathbf{v}(0) = \mathbf{u}_0$. The following result holds:

Theorem 2.1

Let $\mathbf{F} \in L^2(0, T, W')$, $\mathbf{u}_0 \in L^2(\Omega_0)^2$ be given functions. There exists one unique function $\mathbf{v} \in L^2(0, T, V) \cap H^1(0, T, W')$, which is solution to (2.23). Furthermore, there exists a constant C depending on T such that \mathbf{v} satisfies the following *a priori* estimate:

$$\|\mathbf{v}\|_{L^\infty(0, T, L^2(\Omega_0)^2) \cap L^2(0, T, V) \cap H^1(0, T, W')}^2 \leq C \left[\|\mathbf{u}_0\|_{L^2(\Omega_0)^2}^2 + \|\mathbf{F}\|_{L^2(0, T, W')}^2 \right] . \quad (2.24)$$

PROOF : This result is known (see [118] for instance when Dirichlet boundary conditions are taken into account or [35, page 156ff] for instance when Neumann boundary conditions are considered). However a sketch of the proof is given here for obtaining *a priori* estimates. Since V is a separable Hilbert space, an Hilbert basis of V can be considered. The existence is obtained with a Faedo-Galerkin method (see [118] or [29, Volume 8, page 620ff]). *A priori* estimates (2.24) are obtained by using the *Korn inequality*, see for instance [35], that is there exists a constant $K = K(\Omega_0)$ such that $\forall \mathbf{w} \in W$:

$$\sum_{i,j=1}^2 \|D_{ij}(\mathbf{w})\|_{L^2(\Omega_0)}^2 + \|\mathbf{w}\|_{L^2(\Omega_0)^2}^2 \geq K(\Omega_0) \|\mathbf{w}\|_{H^1(\Omega_0)^2}^2 . \quad (2.25)$$

Formally, an energy inequality is obtained by taking $\boldsymbol{\psi} = \mathbf{v}$ in (2.23) and by using a Young inequality. This leads to:

$$\frac{1}{2} \frac{d}{dt} \|\mathbf{v}\|_{L^2(\Omega_0)^2}^2 + 2\mu \sum_{i,j} \|D(\mathbf{v})_{ij}\|_{L^2(\Omega_0)}^2 \leq \frac{1}{2\varepsilon} \|\mathbf{F}\|_{W'}^2 + \frac{\varepsilon}{2} \|\mathbf{v}\|_{H^1(\Omega_0)^2}^2 ,$$

for all $\varepsilon > 0$. Korn inequality (2.25) and Gronwall's lemma permits to obtain the first estimate:

$$\|\mathbf{v}\|_{L^\infty(0, T, L^2(\Omega_0)^2)}^2 \leq C \left(\|\mathbf{F}\|_{L^2(0, T, W')}^2 + \|\mathbf{u}_0\|_{L^2(\Omega_0)^2}^2 \right) . \quad (2.26)$$

The other estimates in $L^2(0, T, V)$ and $H^1(0, T, W')$ norms are obtained by using (2.25) the same way as in Prop. 1.1. The uniqueness comes from a variational principle. \square

About the Existence of the Pressure. The existence of the pressure q is deduced from the projection result (see [118]). Problem (2.23) implies:

$$\left\langle \frac{\partial \mathbf{v}}{\partial t} - \mathcal{A}\mathbf{v} - \mathbf{F}, \boldsymbol{\psi} \right\rangle_{W', W} = 0, \quad \forall \boldsymbol{\psi} \in V .$$

Here the operator $\mathcal{A} = \mathcal{A}(t) : W \rightarrow W'$ is such that $\langle \mathcal{A}\mathbf{v}, \boldsymbol{\psi} \rangle_{W', W} = 2\mu \int_{\Omega_0} D(\mathbf{v}) : D(\boldsymbol{\psi}) dx$, $\forall \boldsymbol{\psi}, \mathbf{v} \in W$. Let us define the space $H^{1/2}(\partial\Omega_0)$ by

$$H^{1/2}(\partial\Omega_0) = \{ \mathbf{v} \in H^1(\Omega_0) : -\Delta \mathbf{v} + \mathbf{v} = 0 \text{ in } \Omega_0 \} .$$

Let $H^{-1/2}(\partial\Omega_0)$ denote the dual space of $H^{1/2}(\partial\Omega_0)$. The space $H^1(\Omega_0)^2$ can be decomposed into

2.2. STOKES PROBLEM

$$H^1(\Omega_0)^2 = H_0^1(\Omega_0)^2 \oplus H^{1/2}(\partial\Omega_0)^2 ,$$

see [29, Volume 3, page 911ff] for instance. Thus if $\boldsymbol{\psi} \in H^1(\Omega_0)^2$ then $\boldsymbol{\psi} = \boldsymbol{\psi}_1 + \boldsymbol{\psi}_2$ with $\boldsymbol{\psi}_1 \in H_0^1(\Omega_0)^2$ and $\boldsymbol{\psi}_2 \in H^{1/2}(\partial\Omega_0)^2$. The dual space W' satisfies

$$W' = H^{-1}(\Omega_0)^2 \oplus H^{-1/2}(\partial\Omega_0)^2 .$$

If $\mathbf{g} \in (H^1(\Omega_0)^2)'$, it can also be decomposed in $\mathbf{g} = \mathbf{g}_1 + \mathbf{g}_2$ with $\mathbf{g}_1 \in H^{-1}(\Omega_0)^2$ and $\mathbf{g}_2 \in H^{-1/2}(\partial\Omega_0)^2$.

Define $\mathbf{G} = \frac{\partial \mathbf{v}}{\partial t} - A\mathbf{v} - \mathbf{F} \in W'$. This operator can be decomposed into $\mathbf{G} = \mathbf{G}_1 + \mathbf{G}_2$ with $\mathbf{G}_1 \in H^{-1}(\Omega_0)^2$ and $\mathbf{G}_2 \in H^{-1/2}(\partial\Omega_0)^2$. Thus, if $\mathbf{G} \in W'$ and $\boldsymbol{\psi} \in W$:

$$\langle \mathbf{G}, \boldsymbol{\psi} \rangle_{W',W} = \langle \mathbf{G}_1, \boldsymbol{\psi}_1 \rangle_{H^{-1},H_0^1} + \langle \mathbf{G}_2, \boldsymbol{\psi}_2 \rangle_{H^{-1/2},H^{1/2}} .$$

Finally notice that if $\boldsymbol{\psi} \in H_0^1(\Omega_0)$, then $\boldsymbol{\psi}_2 = 0$ and $\langle \mathbf{G}, \boldsymbol{\psi} \rangle_{W',W} = \langle \mathbf{G}_1, \boldsymbol{\psi}_1 \rangle_{H^{-1},H_0^1}$.

In our case $\langle \mathbf{G}, \boldsymbol{\psi} \rangle_{W',W} = 0$, $\forall \boldsymbol{\psi} \in V$. *A fortiori* this relation is also satisfied for $\boldsymbol{\psi} \in C_c^\infty(\Omega_0)^2$ such that $\nabla \cdot \boldsymbol{\psi} = 0$, where $C_c^\infty(\Omega_0)$ is the space of functions infinitely differentiable with compact support in Ω_0 . Notice that $\boldsymbol{\psi} \in C_c^\infty(\Omega_0)^2$ satisfy $\boldsymbol{\psi}|_{\partial\Omega_0} = 0$. For such test functions, $\langle \mathbf{G}, \boldsymbol{\psi} \rangle_{W',W} = \langle \mathbf{G}_1, \boldsymbol{\psi}_1 \rangle_{H^{-1},H_0^1}$. Hence, for fixed $t \in (0, T)$, there exists $q(t)$ in the dual space of $C_c^\infty(\Omega_0)$ such that the H^{-1} -part of \mathbf{G} is equal to $-\nabla q$ in the sense of distributions (see [118, page 14]), *i.e.* $\mathbf{G}_1 = -\nabla q$ in the sense of distributions. The existence of the pressure is extracted from this relation.

In order to apply fixed point theorems, the solution has to be more regular. The following notation is introduced (see also [6, 71]):

$$K_T^r(\Omega) = H^{r, \frac{r}{2}}(\Omega \times (0, T)) = L^2(0, T, H^r(\Omega)) \cap H^{\frac{r}{2}}(0, T, L^2(\Omega)) . \quad (2.27)$$

The same notation is used for vector-valued functions. Useful results about embeddings are recalled in the next result (see [58, theorem 3.8, page 1.88] for instance).

Result 2.1 (Some embeddings)

Let Ω be a bounded open set of \mathbb{R}^d and $Q_T = \Omega \times (0, T)$. Let r, s be two real positive numbers and

$$H^{r,s}(Q_T) = L^2(0, T, H^r(\Omega)) \cap H^s(0, T, L^2(\Omega)) .$$

Then the following properties hold:

- (i) If $r, s \geq 0$ and $0 \leq \theta \leq 1$, then $H^{r,s}(Q_T) \hookrightarrow H^{\theta s}(0, T, H^{(1-\theta)r}(\Omega))$ with continuous embedding;
- (ii) If $r, s > 0$ and $\frac{d}{r} + \frac{1}{s} < 2$, then $H^{r,s}(Q_T) \overset{c}{\hookrightarrow} C^0(\overline{Q_T})$ with compact embedding.

A theorem concerning a generalized Stokes problem is recalled here. Consider the functions $\tilde{\mathbf{f}} \in K_T^r(\Omega_0)$, $\tilde{\mathbf{u}}_0 \in H^{r+1}(\Omega_0)^2$, $\tilde{\sigma} \in L^2(0, T, H^{r+1}(\Omega_0)) \cap H^{1+\frac{r}{2}}(0, T, W')$ and $\tilde{\mathbf{g}} \in K_T^{r+\frac{1}{2}}(\partial\Omega_0)$. The inhomogeneous Stokes problem reads: find $\mathbf{v} : \Omega_0 \times (0, T) \rightarrow \mathbb{R}^2$ and $q : \Omega_0 \times (0, T) \rightarrow \mathbb{R}$ such that:

$$\begin{cases} \frac{\partial \mathbf{v}}{\partial t} - \mu \nabla \cdot (\nabla \mathbf{v} + (\nabla \mathbf{v})^T) + \nabla q = \tilde{\mathbf{f}}, & \text{in } \Omega_0 \times (0, T) , \\ \nabla \cdot \mathbf{v} = \tilde{\sigma}, & \text{in } \Omega_0 \times (0, T) , \\ -q \mathbf{N} + \mu (\nabla \mathbf{v} + (\nabla \mathbf{v})^T) \mathbf{N} = \tilde{\mathbf{g}}, & \text{on } \partial\Omega_0 \times (0, T) , \\ \mathbf{v}(0) = \tilde{\mathbf{u}}_0, & \text{in } \Omega_0 . \end{cases} \quad (2.28)$$

The given functions are assumed to satisfy the compatibility conditions:

$$\nabla \cdot \tilde{\mathbf{u}}_0 = \tilde{\sigma}(0) \text{ in } \Omega_0, \quad \mu (\nabla \tilde{\mathbf{u}}_0 + (\nabla \tilde{\mathbf{u}}_0)^T) \mathbf{N} \cdot \mathbf{T} = \tilde{\mathbf{g}}(0) \cdot \mathbf{T} \text{ on } \partial\Omega_0 , \quad (2.29)$$

where \mathbf{T} is the tangent vector on the boundary. The following theorem is concerned with existence and regularity results for the generalized Stokes problem (2.28).

Theorem 2.2 (Inhomogeneous Stokes problem)

Set $1 < r < 3/2$. Let $\tilde{\mathbf{f}} \in K_T^r(\Omega_0)$, $\tilde{\mathbf{u}}_0 \in H^{r+1}(\Omega_0)^2$, $\tilde{\mathbf{g}} \in K_T^{r+\frac{1}{2}}(\partial\Omega_0)$ and $\tilde{\sigma} \in L^2(0, T, H^{r+1}(\Omega_0)) \cap H^{1+\frac{r}{2}}(0, T, W')$ be given functions which satisfy compatibility conditions (2.29). Then there exists one unique solution (\mathbf{v}, q) to (2.28) and $\mathbf{v} \in K_T^{r+2}(\Omega_0)$, $\nabla q \in K_T^r(\Omega_0)$ and $q|_{\partial\Omega_0} \in K_T^{r+\frac{1}{2}}(\partial\Omega_0)$. Furthermore, there exists a constant C_I such that

$$\begin{aligned} \|\mathbf{v}\|_{K_T^{r+2}(\Omega_0)} + \|\nabla q\|_{K_T^r(\Omega_0)} + \|q\|_{K_T^{r+\frac{1}{2}}(\partial\Omega_0)} &\leq C_I \left[\|\tilde{\mathbf{f}}\|_{K_T^r(\Omega_0)} + \|\tilde{\mathbf{u}}_0\|_{H^{r+1}(\Omega_0)^2} \right. \\ &\quad \left. + \|\tilde{\mathbf{g}}\|_{K_T^{r+\frac{1}{2}}(\partial\Omega_0)} \right. \\ &\quad \left. + \|\tilde{\sigma}\|_{L^2(0, T, H^{r+1}(\Omega_0)) \cap H^{1+\frac{r}{2}}(0, T, W')} \right] . \end{aligned}$$

This theorem is a particular case of the theorem 4.1 of Beale [6] and ensures the existence of a unique solution to (2.28). This result can also be found in Solonnikov [109]. The homogeneous problem (2.14)-(2.17) is a particular case of (2.28). The existence of a solution to (2.14)-(2.17) can then be obtained by using this result.

The results of this section for the Stokes problem are used in the following sections for studying the existence of solutions to the problem (2.10)-(2.13). In the following, we will assume that $1 < r < 3/2$ in order to use Thm 2.2.

2.3 Modified Stokes Problem

In this section the problem (2.18)-(2.21) is investigated for given function η . The mapping η is given in a well-chosen set that is now described. Set $1 < r < 3/2$. Consider the operator $I_0 : (\xi, t) \in \Omega_0 \times (0, T) \rightarrow \xi \in \mathbb{R}^2$. This operator is constant in time. Define

$$C(\Omega_0) = \|I_0\|_{H^1(0, T, H^{r+2}(\Omega_0)^2) \cap H^{2+\frac{r}{2}}(0, T, L^2(\Omega_0)^2)} .$$

$$\left\{ \begin{array}{ll} \frac{\partial \mathbf{v}}{\partial t} - \mu \nabla \cdot (\nabla \mathbf{v} + (\nabla \mathbf{v})^T) + \nabla q = \mu (A^T \nabla) \cdot (\nabla \mathbf{v} A + (\nabla \mathbf{v} A)^T) \\ \quad - \frac{\partial \xi}{\partial t} \nabla \mathbf{v} - A^T \nabla q - \mu \nabla \cdot (\nabla \mathbf{v} + (\nabla \mathbf{v})^T) + \nabla q + \mathbf{F}, & \text{in } \Omega_0 \times (0, T) , \\ \nabla \cdot \mathbf{v} = \nabla \cdot \mathbf{v} - (A^T \nabla) \cdot \mathbf{v}, & \text{in } \Omega_0 \times (0, T) , \\ -q \mathbf{N} + \mu (\nabla \mathbf{v} + (\nabla \mathbf{v})^T) \mathbf{N} = q A^T \mathbf{N} - \mu (\nabla \mathbf{v} A + (\nabla \mathbf{v} A)^T) A^T \mathbf{N} \\ \quad - q \mathbf{N} + \mu (\nabla \mathbf{v} + (\nabla \mathbf{v})^T) \mathbf{N}, & \text{on } \partial \Omega_0 \times (0, T), \\ \mathbf{v}(0) = \mathbf{u}_0, & \text{in } \Omega_0 . \end{array} \right.$$

In order to determine a solution to this problem, a fixed point theorem is used. Let W^T be the function space defined by

$$W^T = \left\{ (\mathbf{v}, q) \in K_T^{r+2}(\Omega_0) \times \left[L^2(0, T, H^{r+1}(\Omega_0)) \cap H^{\frac{r}{2}}(0, T, H^1(\Omega_0)) \right] : \right. \\ \left. q|_{\partial \Omega_0} \in K_T^{r+\frac{1}{2}}(\partial \Omega_0) \right\} . \quad (2.32)$$

Let L be the real positive number given by $C_I \left\{ \|\mathbf{F}\|_{K_T^r} + \|\mathbf{u}_0\|_{H^{r+1}} \right\} = \frac{L}{2}$, where C_I is the constant appearing in Thm 2.2. The following subset of W^T is defined:

$$W_L^T = \left\{ (\mathbf{v}, q) \in W^T : \|\mathbf{v}\|_{K_T^{r+2}(\Omega_0)} + \|\nabla q\|_{K_T^r(\Omega_0)} + \|q\|_{K_T^{r+\frac{1}{2}}(\partial \Omega_0)} \leq L \right\} . \quad (2.33)$$

The norm $\|\mathbf{v}\|_{K_T^{r+2}(\Omega_0)} + \|\nabla q\|_{K_T^r(\Omega_0)} + \|q\|_{K_T^{r+\frac{1}{2}}(\partial \Omega_0)}$ in W^T will also be noted $\|(\mathbf{v}, q)\|_{W^T}$. Define also:

$$X_T = \left\{ (\tilde{\mathbf{f}}, \tilde{\sigma}, \tilde{\mathbf{g}}, \tilde{\mathbf{u}}_0) : \tilde{\mathbf{f}} \in K_T^r(\Omega_0), \tilde{\sigma} \in L^2(0, T, H^{r+1}(\Omega_0)^2) \cap H^{1+\frac{r}{2}}(0, T, W'), \right. \\ \left. \tilde{\mathbf{g}} \in K^{r+1/2}(\partial \Omega_0) \text{ and } \tilde{\mathbf{u}}_0 \in H^{r+1}(\Omega_0)^2 \text{ such that (2.29) are satisfied} \right\} . \quad (2.34)$$

Let τ_1 be the application:

$$\tau_1 : \begin{array}{ll} W_L^T & \rightarrow X_T \\ (\mathbf{v}, q) & \rightarrow (\mathbf{f}, \sigma, \mathbf{g}, \mathbf{u}_0) \end{array} ,$$

defined by

$$\begin{aligned} \mathbf{f} &= \mathbf{F} + \mu A^T \nabla \cdot (\nabla \mathbf{v} A + (\nabla \mathbf{v} A)^T) - A^T \nabla q - \mu \nabla \cdot (\nabla \mathbf{v} + (\nabla \mathbf{v})^T) \\ &\quad - \frac{\partial \xi}{\partial t} \nabla \mathbf{v} + \nabla q , \\ \sigma &= \nabla \cdot \mathbf{v} - A^T \nabla \cdot \mathbf{v} , \\ \mathbf{g} &= q A^T \mathbf{N} - \mu (\nabla \mathbf{v} A + (\nabla \mathbf{v} A)^T) A^T \mathbf{N} - q \mathbf{N} + \mu (\nabla \mathbf{v} + (\nabla \mathbf{v})^T) \mathbf{N} , \\ \mathbf{u}_0 &= \mathbf{u}_0 . \end{aligned}$$

2.3. MODIFIED STOKES PROBLEM

Lemma 2.1

Let $1 < r < 3/2$ and $\eta \in \mathcal{S}(T)$ given by (2.31). Let W_L^T and X_T be defined respectively by (2.33) and (2.34). Assume that $\mathbf{F} \in K_T^r(\Omega_0)$ and $\mathbf{u}_0 \in H^{r+1}(\Omega_0)^2$. Then τ_1 is a continuous operator from W_L^T onto X_T .

PROOF : The continuity of τ_1 comes from the definition. The compatibility conditions (2.29) are also guaranteed. The regularity of $(\mathbf{f}, \sigma, \mathbf{g}, \mathbf{u}_0)$ is checked formally in the following.

The coefficients of $A^{-1} = \nabla \eta_t$ belong to $H^1(0, T, H^{r+1}(\Omega_0)) \cap H^{\frac{r}{2}+2}(0, T, W')$ (since $\eta \in \mathcal{S}(T)$). The Jacobian of the transformation η_t is uniformly equal to one by definition of $\mathcal{S}(T)$. Then the coefficients of $A(\eta_t(\xi)) = [\nabla \eta_t(\xi)]^{-1}$ have the same regularity.

Consider the function \mathbf{f} . We have to check that $\mathbf{f} \in K_T^r(\Omega_0)$. By assumption $\mathbf{F}, \nabla q$ and $\mu \nabla \cdot (\nabla \mathbf{v} + (\nabla \mathbf{v})^T)$ belong to $K_T^r(\Omega_0)$. The term $A^T \nabla q$ belongs to $L^2(0, T, H^r(\Omega_0))$ (since $\nabla q \in L^2(0, T, H^r(\Omega_0))$ and $A \in H^1(0, T, H^{r+1}(\Omega_0))$) and $A^T \nabla q \in H^{r/2}(0, T, L^2(\Omega_0))$ (since $\nabla q \in H^{r/2}(0, T, L^2(\Omega_0))$ and $A \in H^{3/2}(0, T, H^r(\Omega_0))$). Hence $A^T \nabla q \in K_T^r(\Omega_0)$.

Let us turn to the second term of \mathbf{f} . The term $\nabla \mathbf{v} A \in L^2(0, T, H^{r+1}(\Omega_0))$ (since $\nabla \mathbf{v} \in L^2(0, T, H^{r+1}(\Omega_0))$ and $A \in H^1(0, T, H^{r+1}(\Omega_0))$) and $\nabla \mathbf{v} A \in H^{r/2}(0, T, H^1(\Omega_0))$ (since $\nabla \mathbf{v} \in H^{r/2}(0, T, H^1(\Omega_0))$ and $A \in H^1(0, T, H^{r+1}(\Omega_0))$). Hence the arguments used for the term $A^T \nabla q$ lead to

$$\mu(A^T \nabla) \cdot (\nabla \mathbf{v} A + (\nabla \mathbf{v} A)^T) \in K_T^r(\Omega_0) .$$

Concerning the advection term $\frac{\partial \xi}{\partial t} \nabla \mathbf{v}$, note that the relation $\xi_t \circ \eta_t = Id$ implies $\frac{\partial}{\partial t} (\xi_t \circ \eta_t)(\xi) = 0$. This implies that

$$\frac{\partial \xi_t}{\partial t}(\eta_t(\xi)) \nabla \mathbf{v}(\xi) = -A(\eta_t(\xi)) \frac{\partial \eta_t}{\partial t}(\xi) \nabla \mathbf{v}(\xi) .$$

The regularity of this term is thus treated with the same arguments: the term $A \nabla \mathbf{v}$ belongs to $L^2(0, T, H^{r+1}(\Omega_0)) \cap H^{r/2}(0, T, H^1(\Omega_0))$; then $A \nabla \mathbf{v} \frac{\partial \eta}{\partial t} \in K_T^r(\Omega_0)$ (since $\frac{\partial \eta}{\partial t} \in H^1(0, T, H^r(\Omega_0)) \cap H^{\frac{r+2}{2}}(0, T, L^2(\Omega_0))$).

The regularity of σ and \mathbf{g} is also obtained with similar arguments. \square

Let τ_2 be the application defined by:

$$\begin{aligned} \tau_2 : \quad X_T &\rightarrow W^T \\ (\mathbf{f}, \sigma, \mathbf{g}, \mathbf{u}_0) &\rightarrow (\tilde{\mathbf{v}}, \tilde{q}) \end{aligned} \quad , \quad (2.35)$$

where $(\tilde{\mathbf{v}}, \tilde{q})$ is the unique solution to the inhomogeneous Stokes problem (2.28) with right-hand sides given by $(\mathbf{f}, \sigma, \mathbf{g}, \mathbf{u}_0)$. This application is linear and bounded and therefore continuous.

The composed continuous application $\tau = \tau_2 \circ \tau_1$ is considered now. It is an operator depending on the final time T and therefore τ is denoted in the following by τ_T . Let T_a be any time in $(0, T)$. The operator τ_{T_a} can be defined for each time T_a , $\tau_{T_a} : W_L^{T_a} \rightarrow W^{T_a}$. In the following lemma, we prove that there exists a particular time denoted by \tilde{T} such that, if $(\mathbf{v}, q) \in W_L^{\tilde{T}}$, $(\tilde{\mathbf{v}}, \tilde{q}) = \tau_{\tilde{T}}((\mathbf{v}, q))$ belongs to $W_L^{\tilde{T}}$, $\forall (\mathbf{v}, q) \in W_L^{\tilde{T}}$.

Lemma 2.2

Let T_a be any time in $(0, T]$ and $\tau_{T_a} : W_L^{T_a} \rightarrow W^{T_a}$ be the operator defined by $\tau_2 \circ \tau_1$. Then there exists a time $\tilde{T} \in (0, T]$ such that the range of $\tau_{\tilde{T}} : W_L^{\tilde{T}} \rightarrow W^{\tilde{T}}$ is included in $W_L^{\tilde{T}}$ and $\tau_{\tilde{T}}$ is a contraction from $W_L^{\tilde{T}}$ into $W_L^{\tilde{T}}$.

PROOF : Let (\mathbf{v}, q) be an element of $W_L^{T_a}$ and $(\tilde{\mathbf{v}}, \tilde{q})$ its image in W^{T_a} under application τ_{T_a} . First we prove that $\|(\tilde{\mathbf{v}}, \tilde{q})\|_{W^{T_a}} \leq \frac{L}{2} + f(T_a) \|(\mathbf{v}, q)\|_{W^{T_a}}$ where f is a function that tends to zero when T_a tends to zero. For all $T_a \in (0, T]$, Thm 2.2 permits to write:

$$\begin{aligned}
 & \| \tilde{\mathbf{v}} \|_{K_{T_a}^{r+2}(\Omega_0)} + \| \nabla \tilde{q} \|_{K_{T_a}^r(\Omega_0)} + \| \tilde{q} \|_{K_{T_a}^{r+\frac{1}{2}}(\partial\Omega_0)} \\
 & \leq C_I \left[\| \mathbf{f} \|_{K_{T_a}^r(\Omega_0)} + \| \mathbf{u}_0 \|_{H^{r+1}(\Omega_0)^2} \right. \\
 & \quad \left. + \| \mathbf{g} \|_{K_{T_a}^{r+\frac{1}{2}}(\partial\Omega_0)} + \| \sigma \|_{L^2(H^{r+1}) \cap H^{1+\frac{r}{2}}(W')} \right] \\
 & \leq C_I \left[\| \mathbf{F} \|_{K_{T_a}^r(\Omega_0)} + \| \mathbf{u}_0 \|_{H^{r+1}(\Omega_0)^2} + \left\| \frac{\partial \xi}{\partial t} \nabla \mathbf{v} \right\|_{K_{T_a}^r(\Omega_0)} \right. \\
 & \quad + \| (I - A^T) \nabla \cdot \mathbf{v} \|_{L^2(H^{r+1}) \cap H^{1+\frac{r}{2}}(W')} \\
 & \quad + \mu \| (A^T \nabla) \cdot (\nabla \mathbf{v} A + (\nabla \mathbf{v} A)^T) - \nabla \cdot (\nabla \mathbf{v} + (\nabla \mathbf{v})^T) \|_{K_{T_a}^r(\Omega_0)} \\
 & \quad + \| q(A^T - I) \mathbf{N} \|_{K_{T_a}^{r+1/2}(\partial\Omega_0)} + \| (A^T - I) \nabla q \|_{K_{T_a}^r(\Omega_0)} \\
 & \quad \left. + \mu \| (\nabla \mathbf{v} A + (\nabla \mathbf{v} A)^T) A^T \mathbf{N} - (\nabla \mathbf{v} + \nabla \mathbf{v}^T) \mathbf{N} \|_{K_{T_a}^{r+1/2}(\partial\Omega_0)} \right] \\
 & \leq \frac{L}{2} + C_I \left[\| (I - A^T) \nabla \cdot \mathbf{v} \|_{L^2(H^{r+1}) \cap H^{1+\frac{r}{2}}(W')} + \left\| \frac{\partial \xi}{\partial t} \nabla \mathbf{v} \right\|_{K_{T_a}^r(\Omega_0)} \right. \\
 & \quad + \mu \| (A^T \nabla) \cdot (\nabla \mathbf{v} A + (\nabla \mathbf{v} A)^T) - \nabla \cdot (\nabla \mathbf{v} + (\nabla \mathbf{v})^T) \|_{K_{T_a}^r(\Omega_0)} \\
 & \quad + \| q(A^T - I) \mathbf{N} \|_{K_{T_a}^{r+1/2}(\partial\Omega_0)} + \| (A^T - I) \nabla q \|_{K_{T_a}^r(\Omega_0)} \\
 & \quad \left. + \mu \| (\nabla \mathbf{v} A + (\nabla \mathbf{v} A)^T) A^T \mathbf{N} - (\nabla \mathbf{v} + \nabla \mathbf{v}^T) \mathbf{N} \|_{K_{T_a}^{r+1/2}(\partial\Omega_0)} \right], \quad (2.36)
 \end{aligned}$$

by using the definition of L . According to [6, Theorem 1], the development of the terms in (2.36) involving the difference between I and A leads to the existence of two strictly positive constants D and δ independent of η and T_a such that (2.36) gives:

$$\begin{aligned}
 \|(\tilde{\mathbf{v}}, \tilde{q})\|_{W^{T_a}} & \leq \frac{L}{2} + D(T_a)^\delta \|(\mathbf{v}, q)\|_{W^{T_a}} + \left\| \frac{\partial \xi}{\partial t} \right\|_{K_{T_a}^r(\Omega_0)} \|(\mathbf{v}, q)\|_{W^{T_a}} \quad (2.37) \\
 & \leq \frac{L}{2} + D(T_a)^\delta L + \left\| \frac{\partial \xi}{\partial t} \right\|_{K_{T_a}^r(\Omega_0)} L.
 \end{aligned}$$

Since $\eta \in \mathcal{S}(T)$, it implies $A \frac{\partial \eta}{\partial t} \Big|_{t=0} = \mathbf{u}_0$. The term $\left\| \frac{\partial \xi}{\partial t} \right\|_{K_{T_a}^r(\Omega_0)}$ gives:

2.3. MODIFIED STOKES PROBLEM

$$\left\| A \frac{\partial \eta}{\partial t} \right\|_{K_{T_a}^r} \leq \left\| A \frac{\partial \eta}{\partial t} - \mathbf{u}_0 \right\|_{K_{T_a}^r} + \|\mathbf{u}_0\|_{K_{T_a}^r} \leq \left\| A \frac{\partial \eta}{\partial t} - \mathbf{u}_0 \right\|_{K_{T_a}^r} + \sqrt{T_a} \|\mathbf{u}_0\|_{H^{r+1}(\Omega_0)^2} .$$

The first term of the right-hand side can be expressed by

$$A \frac{\partial \eta}{\partial t} - A \frac{\partial \eta}{\partial t} \Big|_{t=0} = \int_0^t \left(\frac{\partial A}{\partial t} \frac{\partial \eta}{\partial t} + A \frac{\partial^2 \eta}{\partial t^2} \right) ds ,$$

where the integrand belongs to $K_{T_a}^r(\Omega_0)$. The Jensen inequality in a domain with finite measure may be used and leads to:

$$\begin{aligned} \left\| A \frac{\partial \eta}{\partial t} \right\|_{K_{T_a}^r} &\leq \sqrt{T_a} \left\| \frac{\partial A}{\partial t} \frac{\partial \eta}{\partial t} + A \frac{\partial^2 \eta}{\partial t^2} \right\|_{K_{T_a}^r} + \sqrt{T_a} \|\mathbf{u}_0\|_{H^{r+1}(\Omega_0)^2} \\ &\leq \left(2S_1^2 + \|\mathbf{u}_0\|_{H^{r+1}(\Omega_0)^2} \right) \sqrt{T_a} . \end{aligned}$$

Hence there exists two strictly positive constants E and $\beta = 1/2$ independent of η and T_a such that

$$\left\| \frac{\partial \xi}{\partial t} \right\|_{K_{T_a}^r(\Omega_0)} \leq E(T_a)^\beta .$$

This relationship permits to conclude that there exists a time $\tilde{T} \in (0, T)$ such that the right-hand side of (2.37) is smaller than L if $T_a = \tilde{T}$, *i.e.*

$$\|(\tilde{\mathbf{v}}, \tilde{q})\|_{W^{\tilde{T}}} \leq L .$$

Furthermore the time \tilde{T} is given by $D(\tilde{T})^\delta + E(\tilde{T})^\beta = \frac{1}{2}$ and is independent of η . Moreover let (\mathbf{v}_1, q_1) and (\mathbf{v}_2, q_2) be two elements of $W_L^{\tilde{T}}$ and $(\tilde{\mathbf{v}}_1, \tilde{q}_1)$ and $(\tilde{\mathbf{v}}_2, \tilde{q}_2)$ their images under $\tau_{\tilde{T}}$. The operator $\tau_{\tilde{T}}$ being affine, the following relation holds:

$$\begin{aligned} \|(\tilde{\mathbf{v}}_1 - \tilde{\mathbf{v}}_2, \tilde{q}_1 - \tilde{q}_2)\|_{W^{\tilde{T}}} &\leq \left(D(\tilde{T})^\delta + E(\tilde{T})^\beta \right) \|(\mathbf{v}_1 - \mathbf{v}_2, q_1 - q_2)\|_{W^{\tilde{T}}} \\ &\leq \frac{1}{2} \|(\mathbf{v}_1 - \mathbf{v}_2, q_1 - q_2)\|_{W^{\tilde{T}}} . \end{aligned}$$

The application $\tau_{\tilde{T}}$ is then a contraction from $W_L^{\tilde{T}}$ onto $W_L^{\tilde{T}}$. □

The conclusion of this section is the following. Let $T > 0$, $1 < r < 3/2$ and $\eta \in \mathcal{S}(T)$. If $\mathbf{F} \in K_T^r(\Omega_0)$ and $\mathbf{u}_0 \in H^{r+1}(\Omega_0)^2$ satisfy compatibility conditions (2.29), we define $L = 2C_I \left\{ \|\mathbf{F}\|_{K_T^r} + \|\mathbf{u}_0\|_{H^{r+1}} \right\}$. Then, for all times $T_a \in (0, T)$, the image of $W_L^{T_a}$ under τ_{T_a} is included in W^{T_a} . Furthermore there exists a time \tilde{T} such that

$$\tau_{\tilde{T}} : W_L^{\tilde{T}} \rightarrow W_L^{\tilde{T}}$$

is a continuous contraction. The time \tilde{T} does not depend on the given mapping η .

Hence application $\tau_{\tilde{T}}$ admits one unique fixed point (\mathbf{v}, q) in $W_L^{\tilde{T}}$. This fixed point is the solution to the problem (2.18)-(2.21) for $T = \tilde{T}$ with given function $\eta \in \mathcal{S}(\tilde{T})$ and satisfies

$$\|\mathbf{v}\|_{K_{\tilde{T}}^{r+2}(\Omega_0)} + \|\nabla q\|_{K_{\tilde{T}}^r(\Omega_0)} + \|q\|_{K_{\tilde{T}}^{r+\frac{1}{2}}(\partial\Omega_0)} \leq 2C_I \left\{ \|\mathbf{F}\|_{K_{\tilde{T}}^r(\Omega_0)} + \|\mathbf{u}_0\|_{H^{r+1}(\Omega_0)^2} \right\}. \quad (2.38)$$

Remark 2.3 *The same result can be obtained for the inhomogeneous problem, that is (2.18)-(2.21) with inhomogeneous right-hand sides $(\tilde{\mathbf{f}}, \tilde{\sigma}, \tilde{\mathbf{g}}, \tilde{\mathbf{u}}_0)$ defined as in (2.28). In this case the parameter L is defined by*

$$L = 2C_I \left\{ \left\| \tilde{\mathbf{f}} \right\|_{K_{\tilde{T}}^r(\Omega_0)} + \|\tilde{\mathbf{u}}_0\|_{H^{r+1}(\Omega_0)^2} + \|\tilde{\sigma}\|_{L^2(H^{r+1}) \cap H^{1+r/2}(W')} + \|\tilde{\mathbf{g}}\|_{K_{\tilde{T}}^{r+1/2}(\Omega_0)} \right\}. \quad (2.39)$$

The conclusion is the same, i.e. there exists a time $\tilde{T} \in (0, T]$ such that $\tau_{\tilde{T}} : W_L^{\tilde{T}} \rightarrow W_L^{\tilde{T}}$ is a continuous contraction. The unique fixed point of $\tau_{\tilde{T}}$ satisfies an inequality like (2.38) involving the value of L given by (2.39).

Let us now treat the nonlinear term appearing in (2.10)-(2.13) in the next section.

2.4 Given Boundary Problem

In this section, the problem (2.10)-(2.13) is studied. First the problem is rescaled. Let λ be a real positive number. Define the functions \mathbf{w} and p by $\mathbf{v} = \lambda\mathbf{w}$ and $q = \lambda p$. The problem (2.10)-(2.13) is equivalent to finding $\mathbf{w} : \Omega_0 \times (0, \tilde{T}) \rightarrow \mathbb{R}^2$ and $p : \Omega_0 \times (0, \tilde{T}) \rightarrow \mathbb{R}$ such that:

$$\left\{ \begin{array}{ll} \frac{\partial \mathbf{w}}{\partial t} - \mu(A^T \nabla) \cdot (\nabla \mathbf{w} A + (\nabla \mathbf{w} A)^T) + \frac{\partial \xi}{\partial t} \nabla \mathbf{w} \\ \quad + \lambda(\mathbf{w} \cdot A^T \nabla) \mathbf{w} + A^T \nabla p = \frac{\mathbf{F}}{\lambda}, & \text{in } \Omega_0 \times (0, \tilde{T}) , \\ (A^T \nabla) \cdot \mathbf{w} = 0, & \text{in } \Omega_0 \times (0, \tilde{T}) , \\ -p A^T \mathbf{N} + \mu(\nabla \mathbf{w} A + (\nabla \mathbf{w} A)^T) A^T \mathbf{N} = 0, & \text{on } \partial\Omega_0 \times (0, \tilde{T}) , \\ \mathbf{w}(0) = \frac{\mathbf{u}_0}{\lambda}, & \text{in } \Omega_0 , \end{array} \right. \quad (2.40)$$

The existence and uniqueness of a solution to this problem are the subject of the following theorem.

Theorem 2.3

Set $1 < r < 3/2$. Assume that $\mathbf{F} \in K_{\tilde{T}}^r(\Omega_0)$ and $\mathbf{u}_0 \in H^{r+1}(\Omega_0)^2 \cap V$ which satisfies the compatibility condition $\mu(\nabla \mathbf{u}_0 + (\nabla \mathbf{u}_0)^T) \mathbf{N} \cdot \mathbf{T} = 0$ on $\partial\Omega_0$, where \mathbf{T} is a tangent vector on the boundary. Assume that

2.4. GIVEN BOUNDARY PROBLEM

$$\|\mathbf{F}\|_{K_{\tilde{T}}^r(\Omega_0)} + \|\mathbf{u}_0\|_{H^{r+1}(\Omega_0)^2} < \frac{3}{4} \cdot \frac{1}{4C_I^2 S_1}, \quad (2.41)$$

where C_I is the constant defined in Thm 2.2 and S_1 is the constant defined in (2.30)-(2.31). Then there exists $\lambda_0 > 0$ such that (2.40) admits one unique solution $(\mathbf{w}, p) \in W_L^{\tilde{T}}$ for $\lambda = \lambda_0$.

PROOF : Recall that the set $W_L^{\tilde{T}}$ is defined by:

$$W_L^{\tilde{T}} = \left\{ (\mathbf{v}, q) \in K_{\tilde{T}}^{r+2}(\Omega_0) \times \left[L^2(0, \tilde{T}, H^{r+1}(\Omega_0)) \cap H^{\frac{r}{2}}(0, \tilde{T}, H^1(\Omega_0)) \right] : \right. \\ \left. q|_{\partial\Omega_0} \in K_{\tilde{T}}^{r+\frac{1}{2}}(\partial\Omega_0) \text{ and } \|\mathbf{v}\|_{K_{\tilde{T}}^{r+2}(\Omega_0)} + \|\nabla q\|_{K_{\tilde{T}}^r(\Omega_0)} + \|q\|_{K_{\tilde{T}}^{r+\frac{1}{2}}(\partial\Omega_0)} \leq L \right\}.$$

The norm $\|\mathbf{v}\|_{K_{\tilde{T}}^{r+2}(\Omega_0)} + \|\nabla q\|_{K_{\tilde{T}}^r(\Omega_0)} + \|q\|_{K_{\tilde{T}}^{r+\frac{1}{2}}(\partial\Omega_0)}$ is also noted $\|(\mathbf{v}, q)\|_{W^{\tilde{T}}}$. The following application is considered:

$$\chi : \quad W_L^{\tilde{T}} \quad \rightarrow \quad K_{\tilde{T}}^r(\Omega_0) \times H^{r+1}(\Omega_0)^2 \quad \rightarrow \quad W_L^{\tilde{T}} \\ (\mathbf{w}, p) \quad \rightarrow \quad \left(\frac{\mathbf{F}}{\lambda} - \lambda(\mathbf{w} \cdot A^T \nabla) \mathbf{w}, \frac{\mathbf{u}_0}{\lambda} \right) \quad \rightarrow \quad (\tilde{\mathbf{w}}, \tilde{p}),$$

where $(\tilde{\mathbf{w}}, \tilde{p})$ is the solution to the modified Stokes problem (2.18)-(2.21) associated with right-hand side $\frac{\mathbf{F}}{\lambda} - \lambda(\mathbf{w} \cdot A^T \nabla) \mathbf{w}$ and initial velocity $\frac{\mathbf{u}_0}{\lambda}$. We want to prove that operator χ is a continuous contraction from $W_L^{\tilde{T}}$ into $W_L^{\tilde{T}}$.

We have to check first that $(\tilde{\mathbf{w}}, \tilde{p}) \in W_L^{\tilde{T}}$. Theorem 2.2 implies:

$$\|(\tilde{\mathbf{w}}, \tilde{p})\|_{W^{\tilde{T}}} \leq \frac{C_I}{\lambda} \left[\|\mathbf{F}\|_{K_{\tilde{T}}^r(\Omega_0)} + \|\mathbf{u}_0\|_{H^{r+1}(\Omega_0)^2} \right] + \lambda C_I \|(\mathbf{w} \cdot A^T \nabla) \mathbf{w}\|_{K_{\tilde{T}}^r(\Omega_0)} \\ \leq \frac{C_I}{\lambda} \left[\|\mathbf{F}\|_{K_{\tilde{T}}^r(\Omega_0)} + \|\mathbf{u}_0\|_{H^{r+1}(\Omega_0)^2} \right] + \lambda C_I S_1 L^2.$$

This last term is smaller than L when

$$\lambda \in \left[\frac{1 - \sqrt{1 - 4C_I^2 S_1 (\|\mathbf{F}\|_{K_{\tilde{T}}^r} + \|\mathbf{u}_0\|_{H^{r+1}})}}{2LC_I S_1}, \frac{1 + \sqrt{1 - 4C_I^2 S_1 (\|\mathbf{F}\|_{K_{\tilde{T}}^r} + \|\mathbf{u}_0\|_{H^{r+1}})}}{2LC_I S_1} \right]. \quad (2.42)$$

The extremities of this interval are real numbers thanks to assumption (2.41). Furthermore this interval is strictly contained in \mathbb{R}_+ .

The operator χ is now proved to be a contraction. Consider (\mathbf{w}_1, p_1) and (\mathbf{w}_2, p_2) two elements of $W_L^{\tilde{T}}$ and $(\tilde{\mathbf{w}}_i, \tilde{p}_i) = \chi((\mathbf{w}_i, p_i))$, $i = 1, 2$. The difference is denoted again by $(\tilde{\mathbf{w}}_1, \tilde{p}_1) - (\tilde{\mathbf{w}}_2, \tilde{p}_2) = (\mathbf{w}, p)$ and satisfies:

$$\left\{ \begin{array}{ll} \frac{\partial \mathbf{w}}{\partial t} - \mu(A^T \nabla) \cdot (\nabla \mathbf{w} A + (\nabla \mathbf{w} A)^T) + A^T \nabla p + \frac{\partial \xi}{\partial t} \nabla \mathbf{w} \\ \qquad \qquad \qquad = -\lambda [(\mathbf{w}_1 \cdot A^T \nabla) \mathbf{w}_1 - (\mathbf{w}_2 \cdot A^T \nabla) \mathbf{w}_2], & \text{in } \Omega_0 \times (0, \tilde{T}) , \\ (A^T \nabla) \cdot \mathbf{w} = 0, & \text{in } \Omega_0 \times (0, \tilde{T}) , \\ -p A^T \mathbf{N} + \mu (\nabla \mathbf{w} A + (\nabla \mathbf{w} A)^T) A^T \mathbf{N} = 0, & \text{on } \partial \Omega_0 \times (0, \tilde{T}) , \\ \mathbf{w}(0) = 0, & \text{in } \Omega_0 , \end{array} \right.$$

This problem is similar to (2.18)-(2.21) when \mathbf{F} and \mathbf{u}_0 are replaced respectively by $-\lambda [(\mathbf{w}_1 \cdot A^T \nabla) \mathbf{w}_1 - (\mathbf{w}_2 \cdot A^T \nabla) \mathbf{w}_2]$ and 0. By using the results obtained in Sect. 2.3, this problem admits a solution and this solution satisfies (2.38), that is

$$\begin{aligned} \|(\tilde{\mathbf{w}}_1, \tilde{p}_1) - (\tilde{\mathbf{w}}_2, \tilde{p}_2)\|_{W_L^{\tilde{T}}} &\leq 2C_I \lambda \|(\mathbf{w}_1 \cdot A^T \nabla) \mathbf{w}_1 - (\mathbf{w}_2 \cdot A^T \nabla) \mathbf{w}_2\|_{K_T^r(\Omega_0)} \\ &\leq 4C_I S_1 \lambda L \|(\mathbf{w}_1, p_1) - (\mathbf{w}_2, p_2)\|_{W^{\tilde{T}}} . \end{aligned}$$

This implies that χ is a continuous application and that χ is a contraction if λ is smaller than $\frac{1}{4LS_1C_I}$. Conclusion is obtained by choosing λ_0 in the interval (2.42) such that $\lambda_0 < \frac{1}{4LS_1C_I}$ (which is possible under assumption (2.41)). \square

Hence, there exists one unique solution $(\mathbf{w}, p) \in W_L^{\tilde{T}}$ to (2.40). Relationship (2.41) implies a restriction on the initial velocity \mathbf{u}_0 and on the final time \tilde{T} . This restriction is independent of η and the final time is still denoted by \tilde{T} . The unique solution to (2.10)-(2.13) can be deduced directly from (\mathbf{w}, p) with $\lambda = \lambda_0$ (*i.e.* $\mathbf{v} = \lambda_0 \mathbf{w}$ and $q = \lambda_0 p$). This solution $(\mathbf{v}, q) \in W_{\lambda_0 L}^{\tilde{T}}$ is thus defined on a time interval $(0, \tilde{T})$ independent of η .

Let us now deal with the free boundary problem in the last section.

2.5 Free Surface Problem

In previous sections we proved that, for each function η which belongs to the set $\mathcal{S}(T)$, there exists a time $\tilde{T} \in (0, T)$ independent of η and one unique solution to the problem (2.10)-(2.13) in $(0, \tilde{T})$ with given η . Recall that the set $\mathcal{S}(T)$ defined by (2.31) is:

$$\mathcal{S}(T) = \left\{ \eta : \Omega_0 \times (0, T) \rightarrow \mathbb{R}^2 : \eta \in H^1(0, T, H^{r+2}(\Omega_0)^2) \cap H^{2+\frac{\epsilon}{2}}(0, T, L^2(\Omega_0)^2), \right. \\ \left. \|\eta\|_{H^1(H^{r+2}) \cap H^{2+\frac{\epsilon}{2}}(L^2)} \leq S_1, \eta_0 = Id, \det(\nabla \eta_t) = 1, \forall t \in (0, T), \right. \\ \left. \frac{\partial \eta_0}{\partial t} = \mathbf{u}_0, \eta_t \text{ invertible and } \xi_t = \eta_t^{-1} \in C^1(\Omega_t), \forall t \in (0, T) \right\} .$$

Let the following application be defined:

2.5. FREE SURFACE PROBLEM

$$\begin{aligned} \gamma_1 : \mathcal{S}(\tilde{T}) &\rightarrow W_{\lambda_0 L}^{\tilde{T}} \\ \eta &\rightarrow (\mathbf{v}, q) \end{aligned} ,$$

where the image of η is the solution (\mathbf{v}, q) to the problem (2.10)-(2.13) for given function η . Since there exists one unique solution (\mathbf{v}, q) in $W_{\lambda_0 L}^{\tilde{T}}$, γ_1 is well-defined. Continuity of γ_1 is the object of next lemma.

Lemma 2.3

With the notations introduced before, the application $\gamma_1 : \mathcal{S}(\tilde{T}) \rightarrow W_{\lambda_0 L}^{\tilde{T}}$ is continuous.

PROOF : Let η_1, η_2 be two elements of $\mathcal{S}(\tilde{T})$ and $(\mathbf{v}_1, q_1), (\mathbf{v}_2, q_2)$ the respective solution to:

$$\left\{ \begin{array}{ll} \frac{\partial \mathbf{v}_i}{\partial t} - \mu A_i^T \nabla \cdot (\nabla \mathbf{v}_i A_i + (\nabla \mathbf{v}_i A_i)^T) + \frac{\partial \xi_i}{\partial t} \nabla \mathbf{v}_i \\ \quad + (\mathbf{v}_i \cdot A_i^T \nabla) \mathbf{v}_i + A_i^T \nabla q_i = \mathbf{F}, & \text{in } \Omega_0 \times (0, \tilde{T}) , \\ A_i^T \nabla \cdot \mathbf{v}_i = 0, & \text{in } \Omega_0 \times (0, \tilde{T}) , \\ -q_i A_i^T \mathbf{N} + \mu (\nabla \mathbf{v}_i A_i + (\nabla \mathbf{v}_i A_i)^T) A_i^T \mathbf{N} = 0, & \text{on } \partial \Omega_0 \times (0, \tilde{T}), \\ \mathbf{v}_i(0) = \mathbf{u}_0, & \text{in } \Omega_0 , \end{array} \right.$$

associated with η_i , for $i = 1, 2$. The solution (\mathbf{v}_i, q_i) is defined on $(0, \tilde{T})$, $i = 1, 2$. A rescaling procedure is used here again. Let \mathbf{w}_i and p_i be defined by $\mathbf{v}_i = \lambda \mathbf{w}_i$ and $q_i = \lambda p_i$, $i = 1, 2$. The new variables (\mathbf{w}_i, p_i) are solutions to the following problem:

$$\left\{ \begin{array}{ll} \frac{\partial \mathbf{w}_i}{\partial t} - \mu A_i^T \nabla \cdot (\nabla \mathbf{w}_i A_i + (\nabla \mathbf{w}_i A_i)^T) + \frac{\partial \xi_i}{\partial t} \nabla \mathbf{w}_i \\ \quad + \lambda (\mathbf{w}_i \cdot A_i^T \nabla) \mathbf{w}_i + A_i^T \nabla p_i = \frac{\mathbf{F}}{\lambda}, & \text{in } \Omega_0 \times (0, \tilde{T}) , \\ A_i^T \nabla \cdot \mathbf{w}_i = 0, & \text{in } \Omega_0 \times (0, \tilde{T}) , \\ -p_i A_i^T \mathbf{N} + \mu (\nabla \mathbf{w}_i A_i + (\nabla \mathbf{w}_i A_i)^T) A_i^T \mathbf{N} = 0, & \text{on } \partial \Omega_0 \times (0, \tilde{T}) , \\ \mathbf{w}_i(0) = \frac{\mathbf{u}_0}{\lambda}, & \text{in } \Omega_0 . \end{array} \right.$$

By taking the difference between the two problems, the difference $(\mathbf{w}_1, p_1) - (\mathbf{w}_2, p_2)$ is denoted by (\mathbf{w}, p) and satisfies:

$$\left\{ \begin{array}{ll} \frac{\partial \mathbf{w}}{\partial t} - \mu (A_1^T \nabla) \cdot (\nabla \mathbf{w} A_1^T + (\nabla \mathbf{w} A_1^T)^T) + A_1^T \nabla p + \frac{\partial \xi_1}{\partial t} \nabla \mathbf{w} \\ \quad = \hat{\mathbf{F}} - \lambda [(\mathbf{v}_1 \cdot A_1^T \nabla) \mathbf{v}_1 - (\mathbf{v}_2 \cdot A_2^T \nabla) \mathbf{v}_2], & \text{in } \Omega_0 \times (0, \tilde{T}) , \\ (A_1^T \nabla) \cdot \mathbf{w} = \hat{\sigma}, & \text{in } \Omega_0 \times (0, \tilde{T}) , \\ -p A_1^T \mathbf{N} + \mu (\nabla \mathbf{w} A_1^T + (\nabla \mathbf{w})^T A_1^T) A_1^T \mathbf{N} = \hat{\mathbf{g}}, & \text{on } \partial \Omega_0 \times (0, \tilde{T}), \\ \mathbf{w}(0) = 0, & \text{in } \Omega_0 , \end{array} \right. \quad (2.43)$$

where

$$\begin{aligned}
 \hat{\mathbf{F}} &= \mu A_1^T \nabla \cdot (\nabla \mathbf{w}_2 A_1 + (\nabla \mathbf{w}_2 A_1)^T) - \mu A_2^T \nabla \cdot (\nabla \mathbf{w}_2 A_2 + (\nabla \mathbf{w}_2 A_2)^T) \\
 &\quad - (A_1^T - A_2^T) \nabla p_2 - \left(\frac{\partial \xi_1}{\partial t} - \frac{\partial \xi_2}{\partial t} \right) \nabla \mathbf{w}_2, \\
 \hat{\sigma} &= -(A_1^T - A_2^T) \nabla \cdot \mathbf{w}_2, \\
 \hat{\mathbf{g}} &= p_2 (A_1^T - A_2^T) \mathbf{N} - \mu (\nabla \mathbf{w}_2 A_1 + (\nabla \mathbf{w}_2 A_1)^T) A_1^T \mathbf{N} \\
 &\quad + \mu (\nabla \mathbf{w}_2 A_2 + (\nabla \mathbf{w}_2 A_2)^T) A_2^T \mathbf{N}.
 \end{aligned}$$

Compatibility conditions (2.29) are satisfied for problem (2.43). The remark 2.3 made at the end of Sect. 2.3 can be applied for the problem (2.43) and implies:

$$\begin{aligned}
 \|(\mathbf{w}, p)\|_{W^{\tilde{T}}} &\leq 2C_I \left(\left\| \hat{\mathbf{F}} \right\|_{K_{\tilde{T}}^r} + \|\hat{\sigma}\|_{L^2(H^{r+1}) \cap H^{1+r/2}(W')} + \|\hat{\mathbf{g}}\|_{K_{\tilde{T}}^{r+1/2}} \right. \\
 &\quad \left. + \lambda \|(\mathbf{v}_1 \cdot A_1^T \nabla) \mathbf{v}_1 - (\mathbf{v}_2 \cdot A_2^T \nabla) \mathbf{v}_2\|_{K_{\tilde{T}}^r} \right) \\
 &\leq 2C_I \left(\left\| \hat{\mathbf{F}} \right\|_{K_{\tilde{T}}^r} + \|\hat{\sigma}\|_{L^2(H^{r+1}) \cap H^{1+r/2}(W')} + \|\hat{\mathbf{g}}\|_{K_{\tilde{T}}^{r+1/2}} \right) \\
 &\quad + 2C_I \lambda \|(\mathbf{v}_1 \cdot A_1^T \nabla) \mathbf{v}_1 - (\mathbf{v}_2 \cdot A_2^T \nabla) \mathbf{v}_2\|_{K_{\tilde{T}}^r}. \tag{2.44}
 \end{aligned}$$

The last term of the right-hand side of (2.44) can be bounded by:

$$\begin{aligned}
 2C_I \lambda \|(\mathbf{v}_1 \cdot A_1^T \nabla) \mathbf{v}_1 - (\mathbf{v}_2 \cdot A_2^T \nabla) \mathbf{v}_2\|_{K_{\tilde{T}}^r} &\leq 2C_I \lambda \|(\mathbf{v}_1 \cdot (A_1^T - A_2^T) \nabla) \mathbf{v}_1\|_{K_{\tilde{T}}^r} \\
 &\quad + \lambda 4LS_1 C_I \|(\mathbf{w}, p)\|_{W^{\tilde{T}}}.
 \end{aligned}$$

For $\lambda = \lambda_1$ sufficiently small ($\lambda_1 < \frac{1}{8S_1 C_I L}$) the term $\lambda 4LC_I S_1 \|(\mathbf{w}, p)\|_{W^{\tilde{T}}}$ is smaller than $\frac{1}{2} \|(\mathbf{w}, p)\|_{W^{\tilde{T}}}$ and can be shifted into the left-hand side of (2.44). This gives:

$$\begin{aligned}
 \|(\mathbf{w}, p)\|_{W^{\tilde{T}}} &\leq 4C_I \left(\left\| \hat{\mathbf{F}} \right\|_{K_{\tilde{T}}^r} + \|\hat{\sigma}\|_{L^2(H^{r+1}) \cap H^{1+r/2}(W')} + \|\hat{\mathbf{g}}\|_{K_{\tilde{T}}^{r+1/2}} \right. \\
 &\quad \left. + \lambda_1 \|(\mathbf{v}_1 \cdot (A_1^T - A_2^T) \nabla) \mathbf{v}_1\|_{K_{\tilde{T}}^r} \right).
 \end{aligned}$$

The term on the right-hand side is small when the difference between η_1 and η_2 is small. That is for each $\eta_1 \in \mathcal{S}(\tilde{T})$ and for all $\varepsilon > 0$, there exists $\delta > 0$ such that $\|(\mathbf{w}, p)\|_{W^{\tilde{T}}} < \varepsilon$ as soon as $\|\eta_1 - \eta_2\|_{\mathcal{S}(\tilde{T})} < \delta$. Moreover the application that maps (\mathbf{v}_i, q_i) with (\mathbf{w}_i, p_i) is clearly continuous and conclusion follows. \square

Finally the application γ_2 is defined by:

$$\begin{aligned}
 \gamma_2 : W_{\lambda_0 L}^{\tilde{T}} &\rightarrow H^1(0, \tilde{T}, H^{r+2}(\Omega_0)^2) \cap H^{\frac{r}{2}+2}(0, \tilde{T}, L^2(\Omega_0)^2), \\
 (\mathbf{v}, q) &\rightarrow \tilde{\eta}
 \end{aligned}$$

2.5. FREE SURFACE PROBLEM

where the function $\tilde{\eta}$ is expressed for $\xi \in \Omega_0$ and $t \in (0, \tilde{T})$ by:

$$\tilde{\eta}(\xi, t) = \xi + \int_0^t \mathbf{v}(\xi, s) ds . \quad (2.45)$$

The application γ_2 depends on the final time \tilde{T} and therefore is denoted by $\gamma_{2\tilde{T}}$. The application γ_{2T_a} is well-defined for all times T_a in the interval $(0, \tilde{T}]$ since $\mathbf{v} \in K_{\tilde{T}}^{r+2}(\Omega_0)$.

Recall that $I_0 : (\xi, t) \in \Omega_0 \times (0, T) \rightarrow \xi \in \Omega_0$ is an operator with norm $\|I_0\|_{\mathfrak{S}(\tilde{T})}$ denoted by $C(\Omega_0)$. In the following lemma, we prove that there exists a time $\hat{T} \in (0, \tilde{T}]$, such that the range of $\gamma_{2\hat{T}}$ is included in the set $\mathfrak{S}(\hat{T})$ and $\gamma_{2\hat{T}}$ is a continuous operator from $W_{\lambda_0 L}^{\hat{T}}$ into $\mathfrak{S}(\hat{T})$.

Lemma 2.4

Assume that $\frac{S_1}{2} > 2\lambda_0 C_I \|\mathbf{u}_0\|_{H^{r+1}} + C(\Omega_0)$. There exists a time $\hat{T} \in (0, \tilde{T}]$ such that the range of $\gamma_{2\hat{T}}$ is included in $\mathfrak{S}(\hat{T})$ and the operator $\gamma_{2\hat{T}} : W_{\lambda_0 L}^{\hat{T}} \rightarrow \mathfrak{S}(\hat{T})$ is continuous.

PROOF : Recall that $\tilde{\eta} \in H^1(0, \tilde{T}, H^{r+2}(\Omega_0)^2) \cap H^{\frac{r}{2}+2}(0, \tilde{T}, L^2(\Omega_0)^2)$ since $\mathbf{v} \in K_{\tilde{T}}^{r+2}(\Omega_0)$. Then:

$$\begin{aligned} \|\tilde{\eta}\|_{\mathfrak{S}(\tilde{T})} &\leq \|I_0\|_{\mathfrak{S}(\tilde{T})} + \left\| \int_0^t \mathbf{v}(s) ds \right\|_{\mathfrak{S}(\tilde{T})} \\ &\leq C(\Omega_0) + \left\| \int_0^t \mathbf{v}(s) ds \right\|_{H^1(H^{r+2})} + \left\| \int_0^t \mathbf{v}(s) ds \right\|_{H^{2+r/2}(L^2)} \\ &\leq C(\Omega_0) + \left\| \int_0^t \mathbf{v}(s) ds \right\|_{L^2(H^{r+2})} + \|\mathbf{v}\|_{L^2(H^{r+2})} \\ &\quad + \left\| \int_0^t \mathbf{v}(s) ds \right\|_{L^2(L^2)} + \|\mathbf{v}\|_{H^{1+r/2}(L^2)} \\ &\leq C(\Omega_0) + \left\| \int_0^t \mathbf{v}(s) ds \right\|_{L^2(H^{r+2})} + \left\| \int_0^t \mathbf{v}(s) ds \right\|_{L^2(L^2)} + \|\mathbf{v}\|_{K_{\tilde{T}}^{r+2}} . \end{aligned}$$

Notice that the norm is a convex function and that the domain $\Omega_0 \times (0, \tilde{T})$ is bounded. The Jensen inequality in a domain with finite measure leads to:

$$\left\| \int_0^t \mathbf{v}(s) ds \right\|_{H^k} \leq \int_0^t \|\mathbf{v}(s)\|_{H^k} ds, \quad \forall k \geq 0 .$$

Hence

$$\|\tilde{\eta}\|_{\mathfrak{S}(\tilde{T})} \leq C(\Omega_0) + \|\mathbf{v}\|_{K_{\tilde{T}}^{r+2}} + 2\sqrt{\tilde{T}} \|\mathbf{v}\|_{L^2(H^{r+2})} .$$

By using Thm 2.3, the velocity \mathbf{v} satisfies $\|\mathbf{v}\|_{K_{\tilde{T}}^{r+2}} \leq \lambda_0 L$. The definition of L and the assumption for S_1 imply

$$\begin{aligned} \|\tilde{\eta}\|_{\mathcal{S}(\hat{T})} &\leq C(\Omega_0) + 2C_I\lambda_0 \|\mathbf{u}_0\|_{H^{r+1}} + 2C_I\lambda_0 \|\mathbf{F}\|_{K_{\hat{T}}^r} + 2\sqrt{\hat{T}}\lambda_0 L \\ &\leq \frac{S_1}{2} + 2C_I\lambda_0 \|\mathbf{F}\|_{K_{\hat{T}}^r} + 2\sqrt{\hat{T}}\lambda_0 L . \end{aligned}$$

Thus there exists a time $\hat{T} \in (0, \tilde{T}]$ such that $\|\tilde{\eta}\|_{\mathcal{S}(\hat{T})} \leq S_1$.

According to the local inversion theorem (see for instance [19, 22]), the function $\tilde{\eta}_t$ is invertible if, $\forall \bar{\xi} \in \Omega_0$, $\nabla \tilde{\eta}(\bar{\xi}, t)$ is invertible for $t \in (0, \hat{T})$ (at least from a neighbourhood of $\bar{\xi}$ onto a neighbourhood of $\tilde{\eta}(\bar{\xi}, t)$). But

$$\det \nabla \tilde{\eta}_t = 1, \quad \forall t \in (0, \hat{T}) ,$$

since the flow (solution to (2.1)-(2.6)) is incompressible (see [95, 108] for instance). Then $\nabla \tilde{\eta}(\bar{\xi}, t)$ is invertible $\forall t \in (0, \hat{T})$ and $\tilde{\eta}_t$ is a (local) C^1 -diffeomorphism. Thus the inverse $\tilde{\xi}_t = \tilde{\eta}_t^{-1}$ exists and belongs to $C^1(\Omega_t)$ for $t \in (0, \hat{T})$. Furthermore the relations $\eta_0 = Id$ and $\frac{\partial \eta_0}{\partial t} = \mathbf{u}_0$ are satisfied.

Finally, notice that $\gamma_{2\hat{T}}$ is linear and bounded. Therefore it is clearly continuous. \square

At this point, the application $\gamma_{\hat{T}} = \gamma_{2\hat{T}} \circ \gamma_1$ from $\mathcal{S}(\hat{T})$ to $\mathcal{S}(\hat{T})$ is considered. For each function $\eta \in \mathcal{S}(\hat{T})$, the image $\tilde{\eta} = \gamma_{\hat{T}}\eta$ belongs to $\mathcal{S}(\hat{T})$. This application is continuous.

We still have to prove that the application $\gamma_{\hat{T}}$ is a contraction from $\mathcal{S}(\hat{T})$ into $\mathcal{S}(\hat{T})$. A sketch of the proof is described hereafter. Let $\eta_1, \eta_2 \in \mathcal{S}(\hat{T})$ and let $\tilde{\eta}_1, \tilde{\eta}_2 \in \mathcal{S}(\hat{T})$ be given by $\tilde{\eta}_i = \gamma_{\hat{T}}\eta_i$, $i = 1, 2$. Starting like in lemma 2.4, we can write:

$$\begin{aligned} \|\tilde{\eta}_1 - \tilde{\eta}_2\|_{\mathcal{S}(\hat{T})} &\leq \|\mathbf{v}_1 - \mathbf{v}_2\|_{K_{\hat{T}}^{r+2}} + 2\sqrt{\hat{T}} \|\mathbf{v}_1 - \mathbf{v}_2\|_{L^2(H^{r+2})} \\ &\leq (1 + 2\sqrt{\hat{T}}) \|\mathbf{v}_1 - \mathbf{v}_2\|_{K_{\hat{T}}^{r+2}} . \end{aligned}$$

By using lemmas 2.2 and 2.3, it is possible to show that there exists $\delta < 1$ such that the norm $\|\mathbf{v}_1 - \mathbf{v}_2\|_{K_{\hat{T}}^{r+2}}$ is smaller than $\delta \|\eta_1 - \eta_2\|_{\mathcal{S}(\hat{T})}$ if \hat{T} is sufficiently small. Hence $\gamma_{\hat{T}} : \mathcal{S}(\hat{T}) \rightarrow \mathcal{S}(\hat{T})$ is a contraction for \hat{T} sufficiently small.

The application $\gamma_{\hat{T}}$ is a continuous contraction. Then it admits one unique fixed point in $\mathcal{S}(\hat{T})$ via the contraction fixed point theorem (see [42]). This fixed point η associated to the solution (\mathbf{v}, q) to the given domain problem (2.10)-(2.13) corresponding to the mapping η , is a local in time solution to the free surface problem (2.1)-(2.6).

The theoretical part of this work ends with this chapter. Numerical investigations for this two-dimensional problem are still missing, in particular a theoretical justification of the algorithm used in [73]. In the next chapters, numerical methods in relation with free surface flows are investigated.

Chapter 3

Numerical Simulation of Free Surface Flows with Bubbles of Gas

This chapter is mainly extracted from [16, 17] and is dedicated to the simulation of free surface flows. The interaction between an incompressible liquid and a compressible gas is considered, specially in the frame of mould filling. In this framework, not only the free surface flow is simulated, but also the behaviour of the surrounding gas and, particularly, the influence of the compressibility effect of the bubbles of trapped gas on the liquid evolution.

In [74, 75], the simulation of free surface flows without taking into account the surrounding gas has been presented. Some features are recalled in this chapter. The complete mathematical model in the liquid and gas domains is described in Sect. 3.1. Then the time splitting scheme introduced in [74, 75] is completed in order to take into account the surrounding gas, see Sect. 3.2. Spatial discretization is explained in Sect. 3.3. Numerical results are given in Sect. 3.4.

3.1 Mathematical Model

Let Λ be a cavity of \mathbb{R}^d , $d = 2, 3$, in which the liquid and gas must be confined and let $T > 0$ be the final time of simulation. For any given time t , let Ω_t be the domain occupied by the liquid with boundary $\partial\Omega_t$ and let Γ_t be the free surface defined by $\partial\Omega_t \setminus \partial\Lambda$. The notations are reported in Fig. 3.1 in the frame of a two-dimensional situation, namely the filling of an S-shaped channel. This situation (see also Sect. 3.4 for a description) corresponds to water entering a thin S-shaped channel lying between two horizontal planes. Gravity effects are neglected. A valve is located at the end of the channel to let the gas escape.

3.1.1 Volume-of-Fluid method

Let Q_T be the space-time domain containing the liquid and Σ_T the space-time free surface between liquid and gas. Let $\varphi : \Lambda \times (0, T) \rightarrow \mathbb{R}$ be the characteristic function of the liquid domain Q_T . The function φ equals one if liquid is present, zero if it is not. Thus $\varphi(x, t)$ represents the volume fraction of liquid at point x and time t . In order to describe the kinematics of the free surface Σ_T , φ must satisfy (in a weak sense):

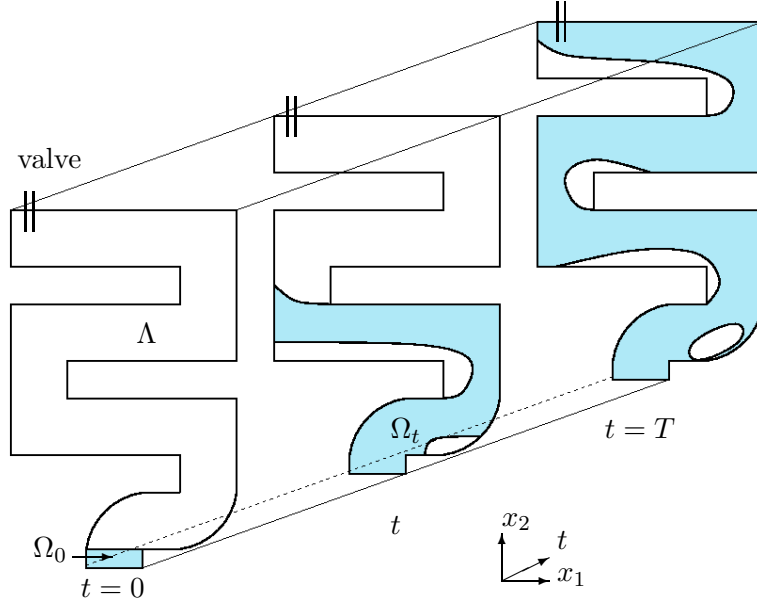


Figure 3.1: Computational domain for the filling of an S-shaped channel. At initial time, the cavity Λ is empty. Then water enters from the bottom of the channel and fills the entire cavity.

$$\frac{\partial \varphi}{\partial t} + \mathbf{v} \cdot \nabla \varphi = 0 \quad \text{in } Q_T, \quad (3.1)$$

where \mathbf{v} is the liquid velocity in Q_T . Therefore the function φ is constant along the trajectories of the liquid particles, *i.e.* $\varphi(X(t), t) = \varphi(X(0), 0)$, where $X(t)$ is the trajectory of a liquid particle, thus $X'(t) = \mathbf{v}(X(t), t)$.

3.1.2 Governing Equations in the Liquid

The liquid flow is assumed to be Newtonian, viscous and incompressible. The unknowns in the liquid domain are the velocity field $\mathbf{v} : Q_T \rightarrow \mathbb{R}^2$ and the pressure field $p : Q_T \rightarrow \mathbb{R}$. They are assumed to satisfy the time-dependent, incompressible Navier-Stokes equations in the presence of an external force \mathbf{f} , that is

$$\begin{cases} \rho \frac{\partial \mathbf{v}}{\partial t} + \rho(\mathbf{v} \cdot \nabla) \mathbf{v} - 2 \operatorname{div}(\mu D(\mathbf{v})) + \nabla p = \mathbf{f} & \text{in } Q_T, \\ \operatorname{div} \mathbf{v} = 0 & \text{in } Q_T. \end{cases} \quad (3.2)$$

Here $D(\mathbf{v}) = \frac{1}{2}(\nabla \mathbf{v} + \nabla \mathbf{v}^T)$ is the rate of deformation tensor, ρ the density of the liquid and μ the viscosity of the liquid.

Turbulence Effects. The turbulence effects are taken into account by using a simple algebraic model. The viscosity μ is assumed to depend on the velocity gradient, see [112]

3.1. MATHEMATICAL MODEL

or for instance [30] for a complete review. It is then defined by $\mu = \mu_L + \mu_T$, where μ_L is the laminar constant viscosity and $\mu_T = \mu_T(\mathbf{v})$ is the additional turbulent viscosity, defined by $\mu_T(\mathbf{v}) = \beta_T \rho \sqrt{2D(\mathbf{v}) : D(\mathbf{v})}$, where β_T is a parameter to be chosen.

Initial and Boundary Conditions. The initial conditions are the following. At initial time, the volume fraction of liquid φ is given and defines the liquid region at time $t = 0$:

$$\Omega_0 = \{x \in \Lambda : \varphi(x, 0) = 1\} .$$

The initial velocity field \mathbf{v} is then prescribed in Ω_0 . Let us now turn to the boundary conditions for the velocity field. On the boundary of the liquid region being in contact with the walls (that is to say the boundary of Λ , see Fig. 3.1), slip, Dirichlet or Signorini boundary conditions can be enforced. Details are given in [74, 75]. On the free surface Γ_t , the only forces are the normal forces due to the pressure of the surrounding gas. Capillary forces or surface tension effects are neglected in this chapter (surface tension is introduced in Chap. 4), so that the boundary condition then is,

$$-p\mathbf{n} + 2\mu D(\mathbf{v})\mathbf{n} = -P\mathbf{n} \quad \text{on } \Gamma_t, \quad t \in (0, T) , \quad (3.4)$$

where \mathbf{n} is the unit normal vector of the liquid-gas free surface Γ_t at time $t \in (0, T)$ oriented toward the gas. Here P denotes the pressure in the gas.

For example, consider the situation of Fig. 3.2, namely the filling of a two-dimensional S-shaped cavity (the numerical experiment is described in Sect. 3.4).

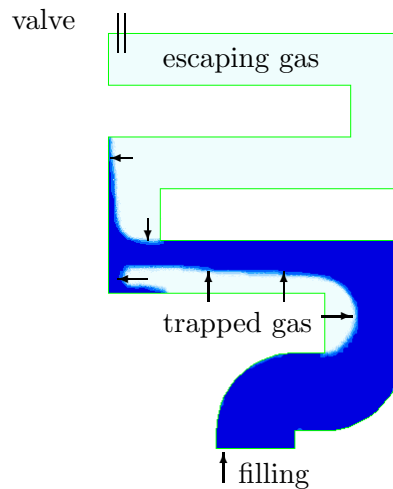


Figure 3.2: Filling of an S-shaped cavity. The gas in the upper part of the cavity is free to escape through the valve. The gas trapped by the liquid is compressed. Both bubbles of gas may exert a force on the liquid.

When the cavity is filled with liquid, the gas between the valve and the liquid can escape, thus the pressure in the gas remains the atmospheric pressure ($P = P_{\text{atmo}}$) on the upper part of the liquid-gas interface. However, a fraction of gas is trapped by the liquid and cannot escape. Each bubble of gas corresponds to a connected component of the gas

domain. A resulting force acts on the liquid-gas interface which prevents the bubbles from vanishing during experiment.

3.1.3 Governing Equations in the Gas

Consider again the case of Fig. 3.2. Some gas is trapped by the liquid and is compressed. In our model, the velocity in the gas is disregarded since modelling the gas velocity would require solving the Euler compressible equations in the gas domain and the computational cost of this procedure would be high. Furthermore, our interest is the influence of the gas on the liquid domain, but not the gas itself. The only unknown in the gas is then its pressure.

At time t , the bubbles of gas correspond to the connected components of the gas domain. Let $k(t)$ be the number of bubbles of gas at time t and let $B_i(t)$ denote the bubble number i . The pressure P in the gas is assumed to be constant inside each bubble of gas, but varying in time. Let $P_i(t)$ be the pressure in $B_i(t)$. The pressure in the gas $P : \Lambda \setminus \Omega_t \rightarrow \mathbb{R}$ is then defined by:

$$P(x, t) = P_i(t), \quad \text{if } x \in B_i(t), \quad t \in (0, T) .$$

Moreover, the gas is assumed to be an ideal gas. Let $V_i(t)$ and $n_i(t)$ be the volume and the fraction number of molecules in $B_i(t)$, at time t . At initial time, all the gas bubbles have atmospheric pressure P_{atmo} . At time t , the pressure in each bubble is computed using the ideal gas law:

$$P_i(t)V_i(t) = n_i(t)R\theta \quad i = 1, \dots, k(t) , \tag{3.5}$$

where R is the constant of ideal gases and θ the absolute temperature, assumed to be constant.

Remark 3.1 *The gas is assumed to be an ideal gas. Once it is assumed that the pressure is constant in each bubble, it is not physically realistic to introduce a more complicated model (adiabatic gas for instance), since the temperature is assumed to be constant.*

The case of a single bubble is first discussed. The situation of Fig. 3.3 is considered. Assume that the pressure $P(t)$ in the bubble at time t and the volumes $V(t)$ and $V(t + \tau)$ are known. The fraction number of molecules inside the bubble is conserved, so that the gas pressure at time $t + \tau$ is computed from the relation

$$P(t + \tau)V(t + \tau) = P(t)V(t) .$$

The case when bubbles of gas are created is now discussed. The situations of Fig. 3.4 and 3.5 are considered. In Fig. 3.4, the broken dam problem in a confined domain is described. A water column is kept in the left side of a cavity by a fictitious dam. The dam

3.1. MATHEMATICAL MODEL

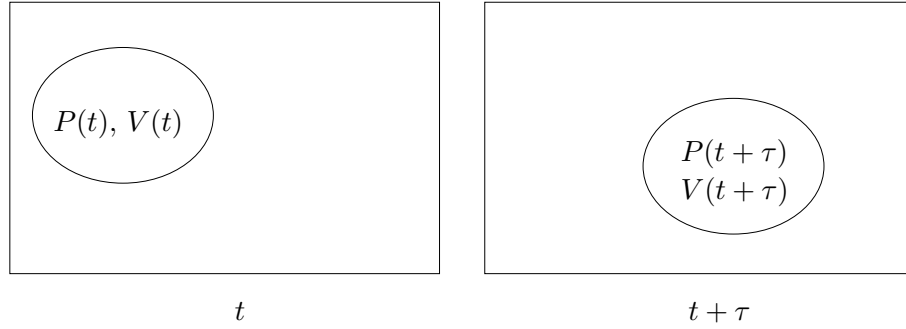


Figure 3.3: One single bubble is floating in the liquid. The product PV remains constant gas between time t and time $t + \tau$, *i.e.* $P(t + \tau)V(t + \tau) = P(t)V(t)$.

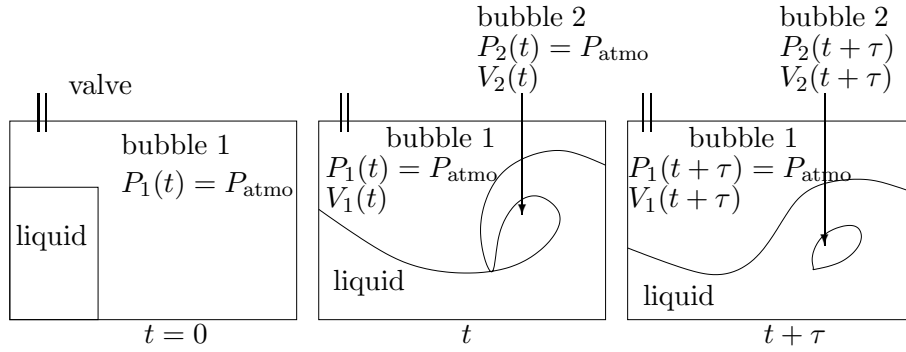


Figure 3.4: Broken dam in a confined domain. At time t , gas is trapped by the liquid and the pressure equals atmospheric pressure $P_1(t) = P_{\text{atmo}}$, $P_2(t) = P_{\text{atmo}}$. At time $t + \tau$, the pressure in bubble 2 is computed from the relation $P_2(t + \tau)V_2(t + \tau) = P_2(t)V_2(t) = P_{\text{atmo}}V_2(t)$.

is removed at time $t = 0$. At time t , the bubble number 2 is created and the gas pressure at time $t + \tau$ is computed from the relation:

$$P_2(t + \tau)V_2(t + \tau) = P_2(t)V_2(t) = P_{\text{atmo}}V_2(t) .$$

The situation of Fig. 3.5 corresponds to the merging of two bubbles. The pressure at time $t + \tau$ is computed by taking into account the conservation of the number of molecules in the bubbles which yields $n_1(t + \tau) = n_1(t) + n_2(t)$. Thus (3.5) leads to

$$P_1(t + \tau)V_1(t + \tau) = P_1(t)V_1(t) + P_2(t)V_2(t) .$$

The mathematical description of our model is now completed. The model unknowns are φ in the whole cavity and \mathbf{v} and p in the liquid domain. Additional unknowns are the position and number of connected components of gas in the cavity and the pressure P_i in each bubble of gas i . They satisfy equations (3.1), (3.2), (3.3) and (3.5) with the boundary condition (3.4) on the interface between the liquid and the gas.

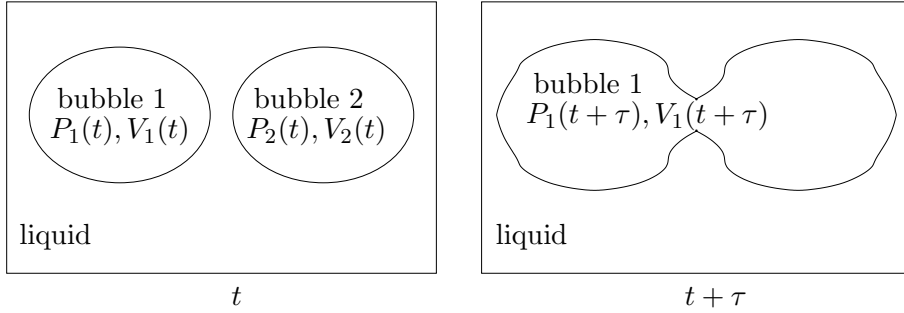


Figure 3.5: Merging of two bubbles between time t and time $t + \tau$. The pressure in bubble 1 at time $t + \tau$ is computed from the relation $P_1(t + \tau)V_1(t + \tau) = P_1(t)V_1(t) + P_2(t)V_2(t)$.

3.2 Time Discretization

A splitting algorithm is used to solve the problem (3.1)-(3.5) by decoupling all the physical phenomena.

Let $0 = t^0 < t^1 < t^2 < \dots < t^N = T$ be a subdivision of the time interval $[0, T]$, define $\tau^n = t^{n+1} - t^n$ the n -th time step, $n = 1, 2, \dots, N$, τ the largest time step.

Let $\varphi^n, \mathbf{v}^n, \Omega^n, k^n, B_i^n, P_i^n, i = 1, 2, \dots, k^n$ be approximations of $\varphi, \mathbf{v}, \Omega, k$ and $B_i, P_i, i = 1, 2, \dots, k(t)$ respectively at time t^n . Then the approximations $\varphi^{n+1}, \mathbf{v}^{n+1}, \Omega^{n+1}, k^{n+1}$ and $B_i^{n+1}, P_i^{n+1}, i = 1, 2, \dots, k^{n+1}$ at time t^{n+1} are computed by means of a splitting algorithm, as illustrated in Fig. 3.6.

First, two advection problems are solved, leading to a prediction of the new velocity $\mathbf{v}^{n+1/2}$ together with the new volume fraction of liquid φ^{n+1} which allows to determine the new liquid domain Ω^{n+1} and gas domain $\Lambda \setminus \Omega^{n+1}$. Then the bubbles of gas (the connected components of $\Lambda \setminus \Omega^{n+1}$) B_i^{n+1} and k^{n+1} are computed with a procedure we explain in the following and the pressure P_i^{n+1} inside each bubble is computed. Finally, a generalized Stokes problem is solved on Ω^{n+1} and the velocity \mathbf{v}^{n+1} and pressure p^{n+1} in the liquid are obtained.

3.2.1 Advection Step

Solve between the times t^n and t^{n+1} the two advection problems:

$$\frac{\partial \mathbf{w}}{\partial t} + (\mathbf{w} \cdot \nabla) \mathbf{w} = 0, \quad (3.6)$$

$$\frac{\partial \psi}{\partial t} + \mathbf{w} \cdot \nabla \psi = 0, \quad (3.7)$$

with initial conditions $\mathbf{w}(t^n) = \mathbf{v}^n$ and $\psi(t^n) = \varphi^n$. This step is solved exactly by the method of characteristics [90, 91, 96, 127] and yields a prediction of the velocity $\mathbf{v}^{n+1/2}$ and the new value of volume fraction of liquid φ^{n+1} . The solutions $\mathbf{v}^{n+1/2}$ and φ^{n+1} are given explicitly by:

$$\begin{aligned} \mathbf{v}^{n+1/2}(x + \tau^n \mathbf{v}^n(x)) &= \mathbf{v}^n(x), & x \in \Omega^n, \\ \varphi^{n+1}(x + \tau^n \mathbf{v}^n(x)) &= \varphi^n(x), & x \in \Omega^n. \end{aligned}$$

3.2. TIME DISCRETIZATION

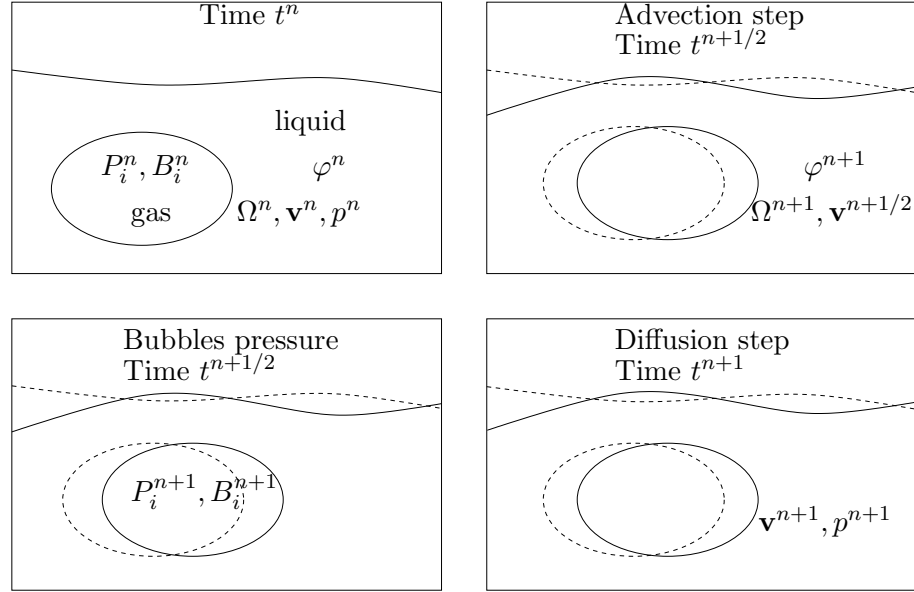


Figure 3.6: The splitting algorithm (from left to right and top to bottom). Two advection problems are solved to determine the new volume fraction of liquid φ^{n+1} , the new liquid domain Ω^{n+1} and the predicted velocity $\mathbf{v}^{n+1/2}$. Then a constant pressure P_i^{n+1} is computed in each connected component of gas. Finally, a generalized Stokes problem is solved to obtain the velocity \mathbf{v}^{n+1} and the pressure p^{n+1} in the new liquid domain Ω^{n+1} by using the boundary condition (3.4) on the surface of bubbles.

The liquid domain Ω^{n+1} is defined by $\Omega^{n+1} = \{x \in \Lambda : \varphi^{n+1}(x) = 1\}$, the gas domain is given by $\Lambda \setminus \Omega^{n+1}$ and the free surface is $\Gamma^{n+1} = \partial\Omega^{n+1} \setminus \partial\Lambda$.

3.2.2 Numbering of the Bubbles of Gas

Given the new liquid domain, the first task consists in finding the gas bubbles B_i^{n+1} , $i = 1, \dots, k^{n+1}$. Then the pressure inside each bubble has to be computed.

The principle for detecting a connected component of the gas domain is the following. The problem $-\Delta u = \delta_P$ is solved at time t in $\Lambda \setminus \Omega_t$, with $u = 0$ on Ω_t and u continuous, and P is a point outside the liquid domain $\overline{\Omega}_t$. Then the solution u will be strictly positive in all the connected component containing P and is vanishing outside.

This procedure permits to obtain each connected component of gas from the original *numbering algorithm* described hereafter. Let $k(t)$ be the number of connected components of the gas domain at time t and $B_i(t)$ the i -th connected component (*i.e.* bubble number i). Let ξ be the *bubble numbering function* defined on $\Lambda \times (0, T)$, which is negative in the liquid region Ω_t and equal to i in bubble $B_i(t)$. At each time step we compute B_i^{n+1} , ξ^{n+1} and k^{n+1} , the approximations of $B_i(t^{n+1})$, $\xi(t^{n+1})$ and $k(t^{n+1})$, as follows.

At each time step, the algorithm is initialized by setting the function ξ^{n+1} to 0 on the whole gas region $\Lambda \setminus \Omega^{n+1}$ and to -1 in Ω^{n+1} and k^{n+1} to 0. The goal is to assign to each point x in the gas an integer value $\xi^{n+1}(x) \neq 0$, the so-called *bubble number*. The algorithm is illustrated in Fig. 3.7 and is the following.

First the domain Θ^{n+1} is initialized: $\Theta^{n+1} = \{x \in \Lambda : \xi^{n+1}(x) = 0\}$. Then:

While $\Theta^{n+1} \neq \emptyset$, do:

1. Choose a point P in Θ^{n+1} ;
2. Solve the following problem: find $u : \Theta^{n+1} \rightarrow \mathbb{R}$ such that:

$$\begin{cases} -\Delta u = \delta_P, & \text{in } \Theta^{n+1} , \\ u = 0, & \text{on } \Lambda \setminus \Theta^{n+1} , \\ [u] = 0, & \text{on } \partial\Theta^{n+1} , \end{cases} \quad (3.8)$$

where δ_P is the Dirac delta function at point P ;

3. Increase the number of bubbles k^{n+1} at time t^{n+1} , $k^{n+1} = k^{n+1} + 1$;
4. Define the bubble of gas number k^{n+1} : $B_{k^{n+1}}^{n+1} = \{x \in \Theta^{n+1} : u(x) \neq 0\}$;
5. Update the bubble numbering function $\xi^{n+1}(x) = k^{n+1}$, $\forall x \in B_{k^{n+1}}^{n+1}$;
6. Update Θ^{n+1} for the next iteration

$$\Theta^{n+1} = \{x \in \Lambda \setminus \Omega^{n+1} : \xi^{n+1}(x) = 0\} .$$

End While

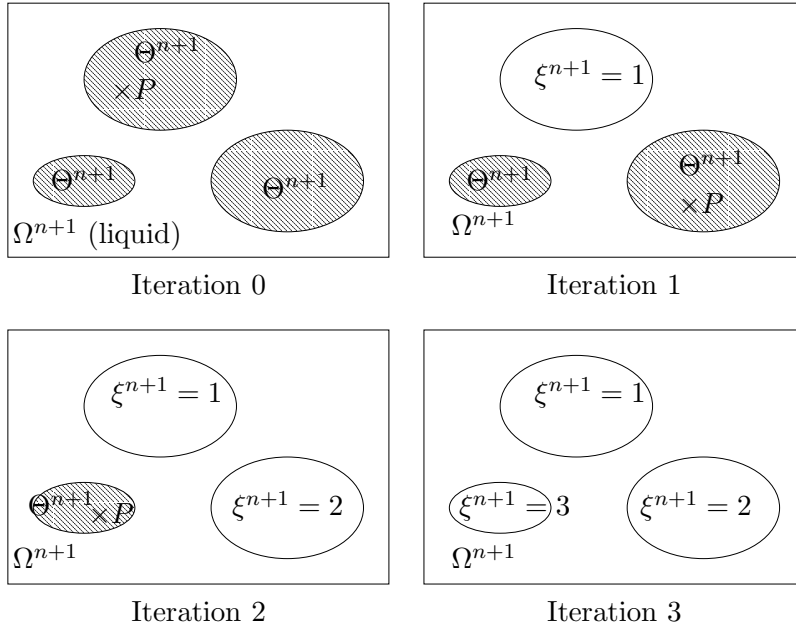


Figure 3.7: Numbering algorithm of the gas bubbles. Initially the function ξ^{n+1} equals zero everywhere in the gas domain. The domain Θ^{n+1} corresponds to the set of points in the gas region that have no bubble number ($\xi^{n+1}(x) = 0$, shaded region). At each iteration of the algorithm a point P is chosen in Θ^{n+1} . Problem (3.8) is solved and a new bubble is numbered. Then the domain Θ^{n+1} is updated and another point $P \in \Theta^{n+1}$ is chosen. The algorithm stops when $\Theta^{n+1} = \emptyset$.

The cost of this original numbering algorithm is bounded by the cost of solving k^{n+1} times a Poisson problem in the gas domain. In the numerical experiments detailed hereafter the corresponding CPU time was always less than 10 percent of the total CPU time.

3.2. TIME DISCRETIZATION

3.2.3 Computation of the Pressure in the Gas

Once the connected components of gas are numbered, an approximation P_i^{n+1} of the pressure in bubble i at time t^{n+1} is computed following the description of Section 3.1.3. The pressure is constant inside each bubble of gas and is computed with the ideal gas law (3.5), except for bubbles in contact with a valve which have atmospheric pressure, see Fig. 3.2.

In the case of Fig. 3.3, the discretization of the ideal gas law gives:

$$P^{n+1}V^{n+1} = P^nV^n ,$$

which expresses the conservation of the fraction number of molecules inside the bubble. In the situation of Fig. 3.5 (merging of two bubbles), this relation becomes:

$$P_1^{n+1}V_1^{n+1} = P_1^nV_1^n + P_2^nV_2^n ,$$

which expresses the conservation of the fraction number of molecules between t^n and t^{n+1} . These are the two simplest situations and more complex pictures can be seen in the frame of free surface flows in complex geometries, for example in mould filling, since bubbles may merge and divide at the same time and the topology of the gas domain may change.

Splitting and merging of bubbles are described in the following. Let $B_i^n, P_i^n, V_i^n, i = 0, \dots, k^n$ be the connected components of gas and their related pressure and volume at time t^n and $B_i^{n+1}, P_i^{n+1}, V_i^{n+1} i = 0, \dots, k^{n+1}$ the same variables at time t^{n+1} .

The bubble B_i^n may split in different parts between time t^n and time t^{n+1} . Each of these parts contributes to a bubble B_j^{n+1} at time t^{n+1} . This volume fraction of bubble B_i^n which contributes to bubble B_j^{n+1} is denoted by $V_{i,j}^{n+1/2}$. The computation of the pressure is then decomposed in two steps, as illustrated in Fig. 3.8.

First the volume fraction contributions $V_{i,j}^{n+1/2}$ are computed. The volume $V_{i,j}^{n+1/2}$ is constituted by the particles of gas that are in B_i^n at time t^n and in B_j^{n+1} at time t^{n+1} . That is $V_{i,j}^{n+1/2}$ is the volume of the set

$$\left\{ x \in B_i^{n+1} : x + \tau^n \mathbf{v}^n(x) \in B_j^{n+1} \right\} .$$

Once the volume fraction contributions $V_{i,j}^{n+1/2}$ are computed, the pressure in the bubble B_j^{n+1} is computed by addition of the contributions of the different bubbles at time t^n :

$$P_j^{n+1} = \frac{1}{V_j^{n+1}} \sum_{i=0}^{k^n} P_i^n V_{i,j}^{n+1/2} . \quad (3.9)$$

3.2.4 Diffusion Step

The diffusion step consists in solving a generalized Stokes problem on the new domain defined by the computed characteristic function φ^{n+1} . The velocity obtained in the advection step is used as initial velocity for the diffusion part. So the following implicit scheme is used:

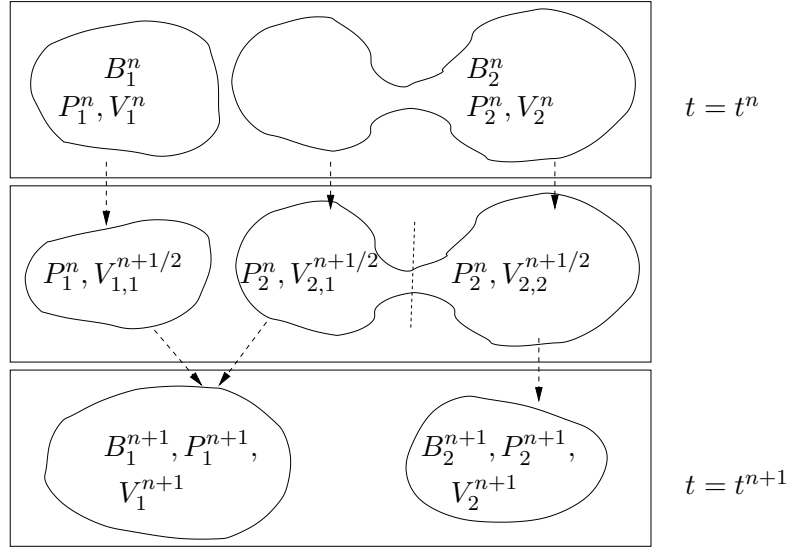


Figure 3.8: At each time step, the merging/division of bubbles is split in two parts. First $V_{i,j}^{n+1/2}$ the volume fraction of bubble B_i^n that contributes to bubble B_j^{n+1} is computed. Secondly, the pressure P_i^{n+1} is computed from conservation of the fraction number of molecules.

$$\left\{ \begin{array}{l} \rho \frac{\mathbf{v}^{n+1} - \mathbf{v}^{n+1/2}}{\tau^n} - 2\operatorname{div}(\mu D(\mathbf{v}^{n+1})) + \nabla p^{n+1} = \mathbf{f}^{n+1} \\ \operatorname{div} \mathbf{v}^{n+1} = 0 \end{array} \right. \quad \begin{array}{l} \text{in } \Omega^{n+1}, \\ \text{in } \Omega^{n+1}, \end{array} \quad \begin{array}{l} (3.10) \\ (3.11) \end{array}$$

The boundary condition on the free surface Γ^{n+1} depend on the gas pressure and is given by:

$$-p^{n+1} \mathbf{n} + 2\mu D(\mathbf{v}^{n+1}) \mathbf{n} = -P_i^{n+1} \mathbf{n}, \quad \text{on } \Gamma^{n+1} \cap \partial B_i^{n+1}, \quad i = 1, \dots, k^{n+1}.$$

Here $\Gamma^{n+1} \cap \partial B_i^{n+1}$ denotes the boundary of the liquid domain which is in contact with bubble number i .

3.3 Space Discretization

Gas treatment and advection and diffusion phenomena are now decoupled. Concerning the liquid flow, advection and diffusion phenomena are decoupled and their numerical treatment is directly extracted from [73] but recalled hereafter for the convenience of the reader. Details are given in [73, 74, 75]. Concerning the gas treatment, space discretization of the bubbles numbering algorithm and computation of the pressure in each bubble are outlined in the sequel.

3.3. SPACE DISCRETIZATION

Equations (3.6) (3.7) are solved using the method of characteristics on a structured mesh of small cells in order to reduce numerical diffusion and have an accurate approximation of the liquid region, see [74]. Finite element techniques are then used for solving (3.8) on an unstructured mesh, see Fig. 3.9. Hence the numbering of the bubbles and the computation of pressure inside the bubbles are carried out on the unstructured mesh. Furthermore, finite element techniques are also well suited for solving (3.10)-(3.11).

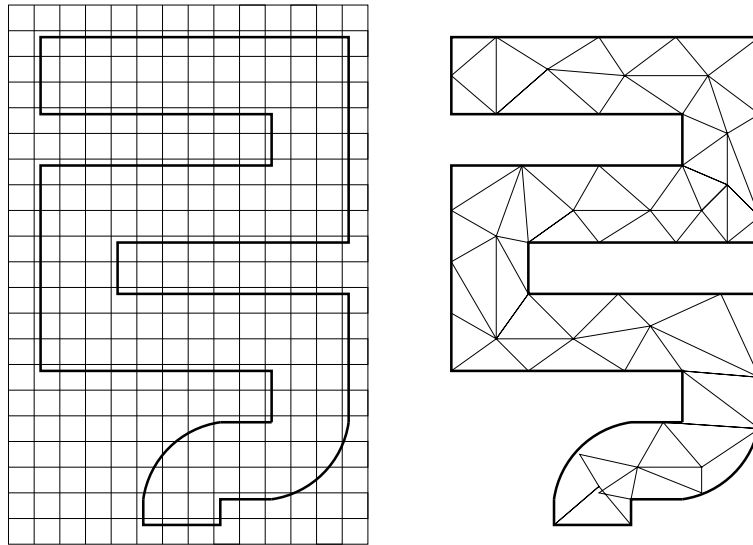


Figure 3.9: Two-dimensional representation of the two-grid method. A grid of small cells is used for advection step (left), while an unstructured finite element mesh is used for bubbles computations and diffusion step (right).

Advection Step. Assume that the grid in three space dimensions is made out of cubic cells of size h , each cell being labelled by indices (ijk) (in two space dimensions, the cells are labelled by (ij)). Let φ_{ijk}^n and \mathbf{v}_{ijk}^n be the approximate value of φ and \mathbf{v} at the centre of cell number (ijk) at time t^n . The advection step on cell number (ijk) consists in advecting φ_{ijk}^n and \mathbf{v}_{ijk}^n by $\tau^n \mathbf{v}_{ijk}^n$ and then projecting the values on the structured grid. An example of cell advection and projection is presented in Fig. 3.10 in two space dimensions.

This method can be interpreted as a forward characteristics method with projection and therefore is unconditionally stable (no Courant-Friedrichs-Lewy (CFL) condition) and convergent (Characteristics-Galerkin method, see [90, 91, 96]). Since the volume fraction of liquid φ is a step function, numerical diffusion is introduced when the values contained in the advected cells are projected on the grid. This diffusion is reduced with a simplified implementation of the SLIC (Simple Linear Interface Calculation) algorithm [24, 82]. Moreover a post-processing procedure avoids numerical (artificial) compression induced by two cells arriving at the same place or loss of liquid mass due to cells transported outside the cavity Λ . The complete algorithm is described in [73].

In order to treat (3.8) and (3.10)-(3.11) a finite element triangulation \mathcal{T}_h of the cavity Λ is introduced and the values of velocity \mathbf{v}^{n+1} and volume fraction of liquid φ^{n+1} are needed at the nodes of the triangulation \mathcal{T}_h . Let φ_{ijk}^{n+1} (respectively \mathbf{v}_{ijk}^{n+1}) denote the

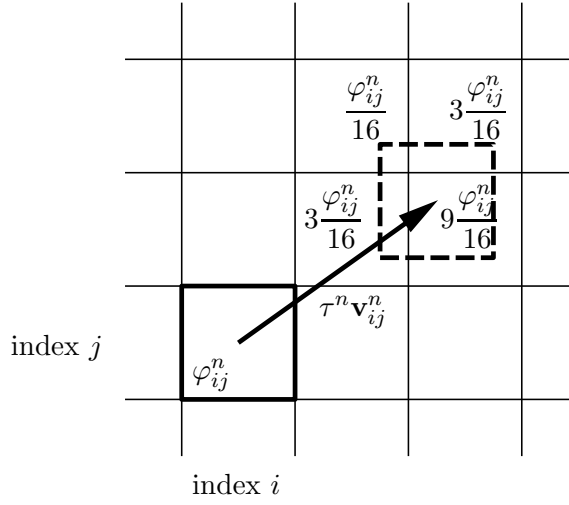


Figure 3.10: An example of two-dimensional advection of φ_{ij}^n by $\tau^n \mathbf{v}_{ij}^n$, and projection on the grid. The advected cell is represented by the dashed lines. The four cells containing the advected cell receive a fraction of φ_{ij}^n , according to the position of the advected cell.

approximated constant value of φ^{n+1} (respectively \mathbf{v}^{n+1}) on the cell ijk of the grid. After the advection step, the values φ_{ijk}^{n+1} and \mathbf{v}_{ijk}^{n+1} are known on the cells grid. The values of the fraction of liquid φ_P^{n+1} and of the velocity field $\mathbf{v}_P^{n+\frac{1}{2}}$ are then computed at the nodes P of the finite element mesh by interpolation techniques, see [47]. The approximation Ω_h^{n+1} of the liquid region Ω^{n+1} is then defined as the union of all elements which contain (at least) one vertex P with value $\varphi_P^{n+1} > 0.5$.

Numbering of the Bubbles of Gas. At each time step, the number of bubbles and the bubbles positions are computed. Numbering of the bubbles requires the resolution of several Poisson problems. Such a problem (3.8) is solved with piecewise linear finite elements on the finite element unstructured mesh.

The gas domain is initially defined as the union of the gas elements, *i.e.* the elements which contain (at least) one vertex P with value $\varphi_P^{n+1} \leq 0.5$. At each iteration of the numbering algorithm, the domain Θ_h^{n+1} is defined by the union of elements which contain (at least) one vertex P with number $\xi_P^{n+1} = 0$, where ξ^{n+1} is the bubble numbering function at time t^{n+1} . The right-hand side of (3.8) is defined by a continuous piecewise linear function with value $C > 0$ at one grid node P which belongs to the domain Θ_h^{n+1} and 0 for every other grid node of Θ_h^{n+1} .

The solution u to (3.8) is continuous piecewise linear on Θ_h^{n+1} . The triangulation \mathcal{T}_h is assumed to satisfy some topological properties (see [26, Volume II, page 144ff] or [62] for instance). In the two-dimensional case, the required topological properties are satisfied if the triangulation is *weakly acute* (*i.e.* for any pairs of adjacent triangles, the sum of opposite angles relative to a common side does not exceed π). This is the case for a Delaunay triangulation. In this case, the discrete maximum principle holds and implies that the scheme is *positive*. Thus the discrete approximation of the solution of (3.8) is

3.3. SPACE DISCRETIZATION

strictly positive in the connected component where the right-hand side is positive.

At iteration k of the algorithm, the vertices Q inside Θ_h^{n+1} such that $u_Q \neq 0$ are numbered with number k . Each time that a connected component is numbered, the size of the Poisson problem (3.8) decreases as the number of grid points in Θ_h^{n+1} decreases. Linear systems are solved using conjugate gradient algorithm with an algebraic incomplete LU preconditioner.

Computation of the Pressure in the Gas. The pressure inside each bubble of gas is computed with (3.9). Let the volume V_K^n be the geometrical volume of element K weighted by the mean volume fraction of liquid φ^n in K at time t^n . The approximations of the fractions of volumes $V_{i,j}^{n+1/2}$ are computed on the finite element mesh. The fraction of volume $V_{i,j}^{n+1/2}$ is the volume V_i^n multiplied by the relative fraction of volume of bubble i at time t^n which is in bubble j at time t^{n+1} .

This relative fraction is computed by the ratio between the sum of the volumes at time t^n of elements K containing one node in bubble i at time t^n and in bubble j at time t^{n+1} divided by the sum of the volumes at time t^n of elements K containing one node in the bubble i at time t^n and at least one node in the gas domain at time t^{n+1} . That means:

$$V_{i,j}^{n+1/2} = \frac{\sum_{K \in J_{i,j}^n} V_K^n}{\sum_{K \in J_i^n} V_K^n} \cdot V_i^n ,$$

where $J_{i,j}^n = \left\{ K \in \mathcal{T}_h : \exists P_l \in K \text{ s.t. } P_l \in B_i^n \text{ and } P_l \in B_j^{n+1} \right\}$ and $J_i^n = \left\{ K \in \mathcal{T}_h : \exists P_l \in K \text{ s.t. } P_l \in B_i^n \text{ and } P_l \notin \Omega^{n+1} \right\}$.

In order to detail the computation of the pressure, consider the two situations illustrated in Fig. 3.11. First situation (left) is when B_1^n and B_1^{n+1} intersect each other ($V_{1,1}^{n+1/2} = 1$). The particles of gas in B_1^{n+1} are thus coming from the bubble B_1^n and the pressure is computed with (3.9). If the time step is too large, the second situation (right) appears. The bubble B_1^{n+1} does not intersect any bubble at time t^n ($V_{1,1}^{n+1/2} = 0$). If many bubbles are trapped in the flow, the origin of the particles of gas in B_1^{n+1} is unknown.

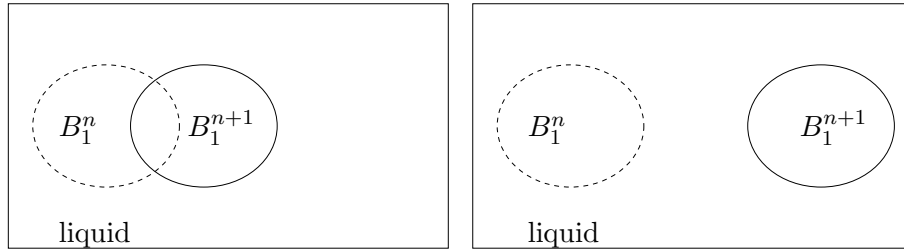


Figure 3.11: Computation of the pressure. Two cases can occur. Left: the bubble at time t^{n+1} intersects one of the previous bubbles at time t^n , the pressure can be computed with (3.9). Right: the bubble at time t^{n+1} does not intersect any bubble at previous time and the pressure is computed by a mean pressure (3.12).

In the first case when bubble B_j^{n+1} intersects at least one bubble of time t^n (there exists at least one index i such that $V_{i,j}^{n+1/2} \neq 0$), the pressure P_j^{n+1} is computed with (3.9). In the second case ($V_{i,j}^{n+1/2} = 0$, for all $i = 0, \dots, k^n$), B_j^{n+1} does not intersect any bubble of time t^n . Relation (3.9) is useless and then the pressure P_j^{n+1} is computed by dividing the remaining molecules at time t^n by the remaining volume at time t^{n+1} :

$$P_j^{n+1} = \frac{(P^n V^{n+1/2})_r}{(V^{n+1})_r} ; \quad (3.12)$$

where

$$\begin{aligned} (P^n V^{n+1/2})_r &= \sum_{i=0}^{k^n} P_i^n \left(V_i^n - \sum_{j=0}^{k^{n+1}} V_{i,j}^{n+1/2} \right) ; \\ (V^{n+1})_r &= \sum_{j=0}^{k^{n+1}} \left(V_j^{n+1} - \sum_{i=0}^{k^n} V_{i,j}^{n+1/2} \right) . \end{aligned}$$

This last situation appears generally when the time step τ is too large.

In the numerical experiment detailed in Sect. 3.4, the CPU time due to bubbles computations, *i.e.* numbering and pressure computations, is always less than 10% of total CPU time.

Diffusion Step. Finite element techniques are used for solving (3.10) (3.11) with boundary conditions given in Sect. 3.1.2. The approximations of the velocity and pressure are taken continuous, piecewise linear and a Galerkin Least-Squares stabilization is used (see [38, 39]). The velocity \mathbf{v}^{n+1} and the pressure p^{n+1} satisfy, for all test functions \mathbf{w} and q of same type:

$$\begin{aligned} &\int_{\Omega^{n+1}} \frac{\mathbf{v}^{n+1} - \mathbf{v}^{n+1/2}}{\tau^n} \mathbf{w} dx + 2\mu \int_{\Omega^{n+1}} D(\mathbf{v}^{n+1}) : D(\mathbf{w}) dx - \int_{\Omega^{n+1}} p^{n+1} \operatorname{div} \mathbf{w} dx \\ &- \int_{\Omega^{n+1}} \mathbf{f} \mathbf{w} dx + \sum_{i=1}^{k^{n+1}} \int_{\partial\Omega^{n+1} \cap \partial B_i^{n+1}} P_i^{n+1} \mathbf{n} \mathbf{w} dS - \int_{\Omega^{n+1}} \operatorname{div} \mathbf{v}^{n+1} q dx \\ &- \sum_{K \subset \Omega^{n+1}} \alpha_K \int_K \left(\frac{\mathbf{v}^{n+1} - \mathbf{v}^{n+1/2}}{\tau^n} + \nabla p^{n+1} - \mathbf{f} \right) \cdot \nabla q dx = 0 . \end{aligned} \quad (3.13)$$

Here \mathbf{w} and q are the velocity and pressure test functions, compatible with the boundary conditions on the boundary of the cavity Λ . In [74, 75], the stability coefficient α_K should be defined on each element K as a function of the local Reynolds number

$Re_K = \frac{\rho |\mathbf{v}^{n+1/2}|_\infty h_K}{2\mu}$ (see [38] for the justification) such that:

3.4. NUMERICAL RESULTS

$$\alpha_K = \begin{cases} \frac{1}{12} \frac{h_K^2}{\mu} & \text{if } Re_K \leq 3 , \\ \frac{1}{4Re_K} \frac{h_K^2}{\mu} & \text{if } Re_K > 3 . \end{cases}$$

The degrees of freedom are the (two or three) velocity components and pressure at each vertex of the finite element mesh. At the moment, all the degrees of freedom are stored in a big matrix and the linear system is solved using a BICGSTAB algorithm and a classical incomplete LU preconditioner. Therefore, the memory cost of this method is high and splitting algorithms for the resolution of the linear system should be investigated in the future, see for instance [88, 126].

Once the new velocity field \mathbf{v}^{n+1} is computed at the vertices of the finite element mesh, values are interpolated at the centre of the cells. The CPU time spent for interpolation is negligible.

The size of the cells should be as small as possible, in order to avoid numerical diffusion when advecting the volume fraction of liquid, whereas the size of the finite element mesh can be larger. Numerical experiments reported in [73, 74, 75] have shown that choosing the size of the cells three to five times smaller than the size of the finite element mesh is a good compromise between accuracy and memory requirements. Furthermore, since the characteristics method is used, the time step is not restricted by the CFL number (which is the ratio between the time step times the maximal velocity divided by the mesh size). Nevertheless numerical results in [74, 75] have shown that a good choice generally consists in choosing CFL numbers ranging from 1 to 5.

Data Structures for Bubbles Treatment. In addition to the data structures used for the treatment of liquid domain and free surface (see [73]), one degree of freedom is added at each vertex of the finite element mesh in order to describe the bubble number. Furthermore, two additional arrays contain the pressure and volume of each bubble of gas. Naturally, one degree of freedom is also added to implement (3.8).

Implementation of the Force. The force (3.4) on the free surface induces a boundary integral in the weak formulation (3.13). In order to avoid computing an external normal vector to the liquid domain, this term is transformed by using Stokes theorem (see for instance [22]): if ϕ_j is a vectorial basis function of \mathbb{P}_1 finite element function space,

$$\int_{\partial\Omega_h^{n+1}} -P_i^{n+1} \mathbf{n} \phi_j dS = -P_i^{n+1} \int_{\Omega_h^{n+1} \cap \text{supp}\phi_j} \text{div}\phi_j d\mathbf{x} ,$$

if P_j is on the boundary of B_i^{n+1} . Here Ω_h^{n+1} is the approximation of the liquid domain on the finite element mesh, B_i^{n+1} is the bubble number i , or better say its approximation on the finite element mesh and $\text{supp}\phi_j = \text{closure of } \{x \in \Lambda : \phi_j(x) \neq 0\}$.

3.4 Numerical Results

Numerical results in two and three space dimensions are presented to validate our model and to compare with previous results [73, 74, 75]. All the computations were performed on

a computer with single processor Pentium Xeon 2.8GHz CPU, 3 Gb Memory and running under Linux operating system. The results are post-processed with CalcoSOFT™ or Enight™ softwares.

Linear Filling. Water enters a rectilinear three-dimensional channel and compresses the gas contained inside the channel. Dimensions of the channel are $0.08 \text{ m} \times 0.1 \text{ m} \times 0.5 \text{ m}$ and water is injected at horizontal speed 4.2 m/s . Figure 3.12 shows a two-dimensional cut of the channel. Density and viscosity are taken to be respectively $\rho = 1000 \text{ kg/m}^3$ and $\mu = 0.01 \text{ kg/(ms)}$ and initial pressure in the gas is $P_{\text{atmo}} = 101300.0 \text{ Pa}$. At time $T = \frac{0.5}{4.2} \text{ s}$, the channel is filled. Slip boundary conditions are enforced on the lateral sides of the cavity. Turbulence effects are not taken into account. The mesh is a regular grid made out of 9449 nodes and 48000 tetrahedrons. The grid of small cells is made out of 4'000'000 cells and the time step is $\tau = 0.001 \text{ s}$. From Tab. 3.1, it can be seen that the product pressure times volume (and therefore the number of molecules of gas) is conserved.

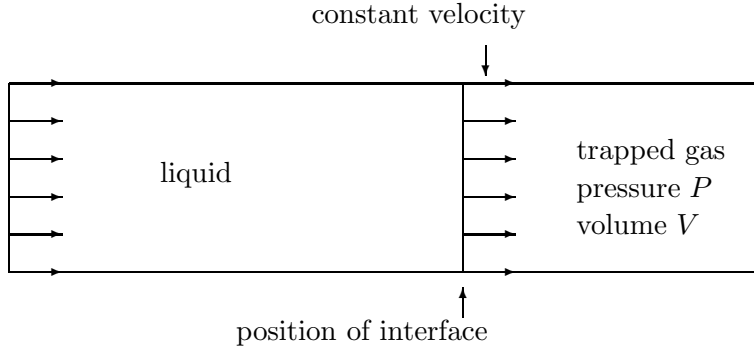


Figure 3.12: Linear filling of a 3D channel: 2D cut. The interface moves with constant velocity $\vec{v} \text{ m/s}$; the position of interface is given by $x(t) = |\vec{v}| \cdot t \text{ m}$.

Time [s]	Computed Pressure [Pa]	Computed Volume [m^3]	PV
0.0	101300.0	0.00386999	392.03093
0.03	134854.3	0.00290706	392.03093
0.06	207512.3	0.00188919	392.03093
0.09	441426.3	0.00088810	392.03093
0.115	9323641.5	0.00004204	392.03093

Table 3.1: Filling of a rectilinear channel with compression of the gas. Pressure P , volume V and product PV function of time for a coarse mesh.

For this simple test case, the exact volume and pressure can be computed with the ideal gas law. The volume of gas is function of time t and given by $V(t) = 0.08 \text{ m} \times 0.1 \text{ m} \times (0.5 - 4.2 \times t) \text{ m}$ for $t \in (0, 0.5/4.2)$ and then the pressure in the gas domain is $P(t) = P_{\text{atmo}} \frac{V(0)}{V(t)}$. Figure 3.13 shows that the computation of the pressure and volume is accurate.

Three different regular meshes are then considered, a coarse mesh with 1380 nodes and 6000 elements, a middle mesh with 9449 nodes and 48000 elements and a finer mesh with

3.4. NUMERICAL RESULTS

69657 nodes and 384000 elements. Final time is $T = 0.120$ s. Figure 3.14 shows that the computation of the pressure converges when the mesh size h tends to zero, the rate of convergence being approximately $\mathcal{O}(h^{1/4})$. The error on the approximation of the pressure in the gas is independent of the Reynolds number of the fluid.

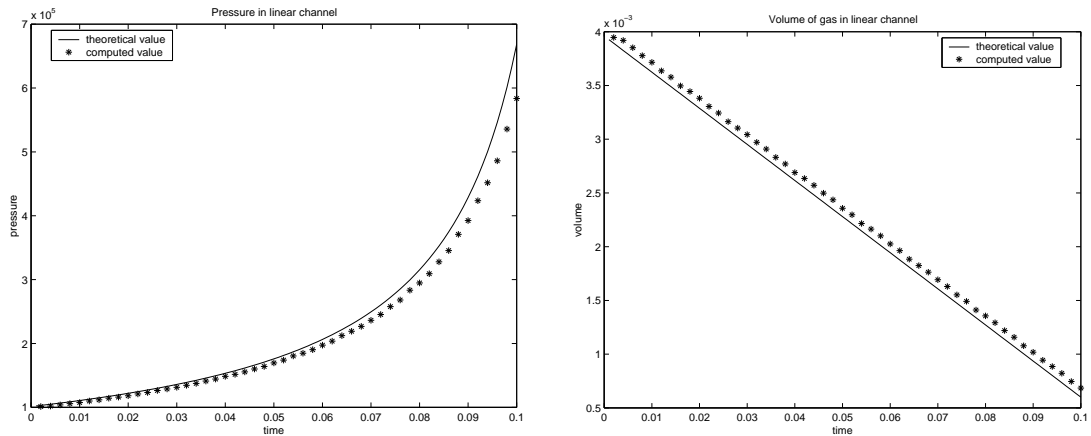


Figure 3.13: Filling of a rectilinear channel with compression of gas. Comparisons between computations and theoretical values for the coarse mesh. Left: pressure in the gas function of time, right: volume of the gas domain function of time.

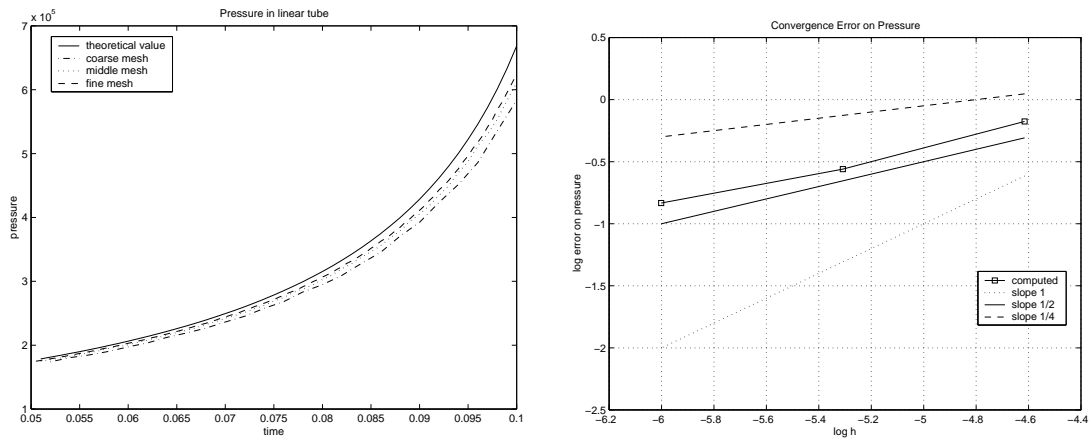


Figure 3.14: Filling of a rectilinear channel with compression of gas. Comparisons between three different mesh sizes. Left: pressure in the gas function of time, right: convergence error of the computation of the pressure in the gas function of mesh size.

The total CPU time is respectively 5 mn, 92 mn and 25 hours and is multiplied approximately by $2^4 = 16$ each time that the mesh size and time step are divided by 2. The number of operations is thus of order $\mathcal{O}(N^4)$, where N is the number of discretization points along each axis. This corresponds to the computational cost required to solving a Laplace problem with conjugate gradient algorithm without preconditioning (see for instance [3]). CPU time used for bubbles computations is less than 10% of total CPU time.

S-shaped Channel. An S-shaped channel lying between two horizontal plates is filled. Two- and three-dimensional results are compared with experiments [102]. In the two-dimensional case, the channel is contained in a $0.17\text{ m} \times 0.24\text{ m}$ rectangle. In the three-dimensional case, the distance between the two horizontal plates is 0.008 m . Water is injected with velocity 8.7 m/s . Density and viscosity are taken to be respectively $\rho = 1000\text{ kg/m}^3$ and $\mu = 0.01\text{ kg/(ms)}$ and initial pressure in the gas is $P_{\text{atmo}} = 101300.0\text{ Pa}$. Gravity has no effect and no forces are applied at the right-hand side of (3.10). A valve is located at the top of the channel, as in Fig. 3.2, allowing gas to escape. Several meshes are considered, see Fig. 3.15.



Figure 3.15: Meshes used for the computations of the S-shaped channel: left: 2D coarse mesh, middle: 2D middle mesh, right: 2D fine mesh. Second row: 3D mesh extracted with five layers of 2D coarse mesh.

In two space dimensions, the coarser mesh has 3483 nodes and 6418 elements; the middle mesh has 8249 nodes and 15654 elements while the fine mesh is made out of 14550 nodes and 27972 elements. The three-dimensional meshes are constructed using 5, respectively 8 and 10 layers of the 2D mesh.

Numerical results are first presented with the coarser mesh and $\beta_T = 0$ (no turbulence

3.4. NUMERICAL RESULTS

modelling, see Sect. 3.1). The final time is $T = 0.00532$ s and the time step is $\tau = 0.0001$ s. Since the Reynolds number is large ($Re \simeq 10^6$), the mesh does not allow the wall boundary layers to be captured. Therefore slip boundary conditions are imposed on the boundary of the channel. Since the ratio between Capillary number and Reynolds number is very small ($Ca \simeq 1.5$), the surface tension effects can be neglected.

In Fig. 3.16 on page 88, the experiment is compared to 2D and 3D computations when the influence of the surrounding gas is taken into account and to 2D computations without influence of gas. When the gas is not taken into account, numerical results show that the bubbles of trapped gas are vanishing rapidly, specially at the enter of the channel. On the other side, when the effects of the surrounding gas onto the liquid are taken into account, numerical results are much closer to experiment. The CPU time for the simulations in two space dimensions is approximately 14 mn without the bubbles computations and 15 mn with the bubbles computations. In three space dimensions, these CPU times become 319 mn without taking into account the gas effect and 344 mn with the bubbles computations. Most of the CPU time is spent in solving the Stokes problem.

The influence of the mesh size is reported in Figs 3.17 and 3.18 on page 89 in two and three space dimensions. The time steps are $\tau = 0.0001$ s for the coarse mesh, $\tau = 0.00008$ s for the middle mesh and $\tau = 0.00005$ s for the fine mesh. The size of the cells of the structured mesh used for advection step is approximately 5 to 10 times smaller than the size of the finite elements, see Sect. 3.3. The numerical results on the coarse mesh are in better agreement with experiment than the results on the fine mesh. This effect is due to the numerical diffusion on the finite element mesh which is larger in the case of a coarse mesh. It has a great impact on the simulation, especially on the front of the liquid region.

Numerical results show that the behaviour of bubbles is well simulated but that the liquid flow goes a little bit too fast. In Fig. 3.19 on page 90, results are presented when the turbulent viscosity is used with β_T proportional to h^2 , see [112]. Clearly the liquid velocity decreases and the numerical results are in better agreement with experimental ones. The total CPU time for 3D computations to reach final time is approximately 29 hours for the middle mesh and 110 hours for the finer mesh.

3D Mould Filling of a Fork. A mould with four arms is considered. Water enters from the top of the mould with velocity 4.2 m/s. Two arms are closed, while there is a valve at the end of the other arms so that gas can escape. Viscosity is $\mu = 0.01$ kg/(ms), while density is $\rho = 1000$ kg/m³. Initial pressure in the gas is $P_{\text{atmo}} = 101300.0$ Pa and turbulence effects are not taken into account. External forces \mathbf{f} in (3.10) are zero (in particular gravity effects). The mesh has 31961 vertices and 168000 elements, see Fig. 3.20 on page 91, and the cells grid contains approximately 50'000'000 cells. The final time of simulation is 0.5 s with time step $\tau = 0.001$ s. The CPU time is approximately 24 hours. For this test case, the goal is to see the influence of gas on the filling of each arm. Figures 3.21 and 3.22 show that if a valve is located at the end of an arm, the arm is filled faster.

2D and 3D Rising Bubble under a Free Surface. The case of a bubble of gas rising under gravity effects in a water cylinder is considered. The cylinder is not filled entirely with water. In this situation, the compressibility effect of the gas cannot be neglected and

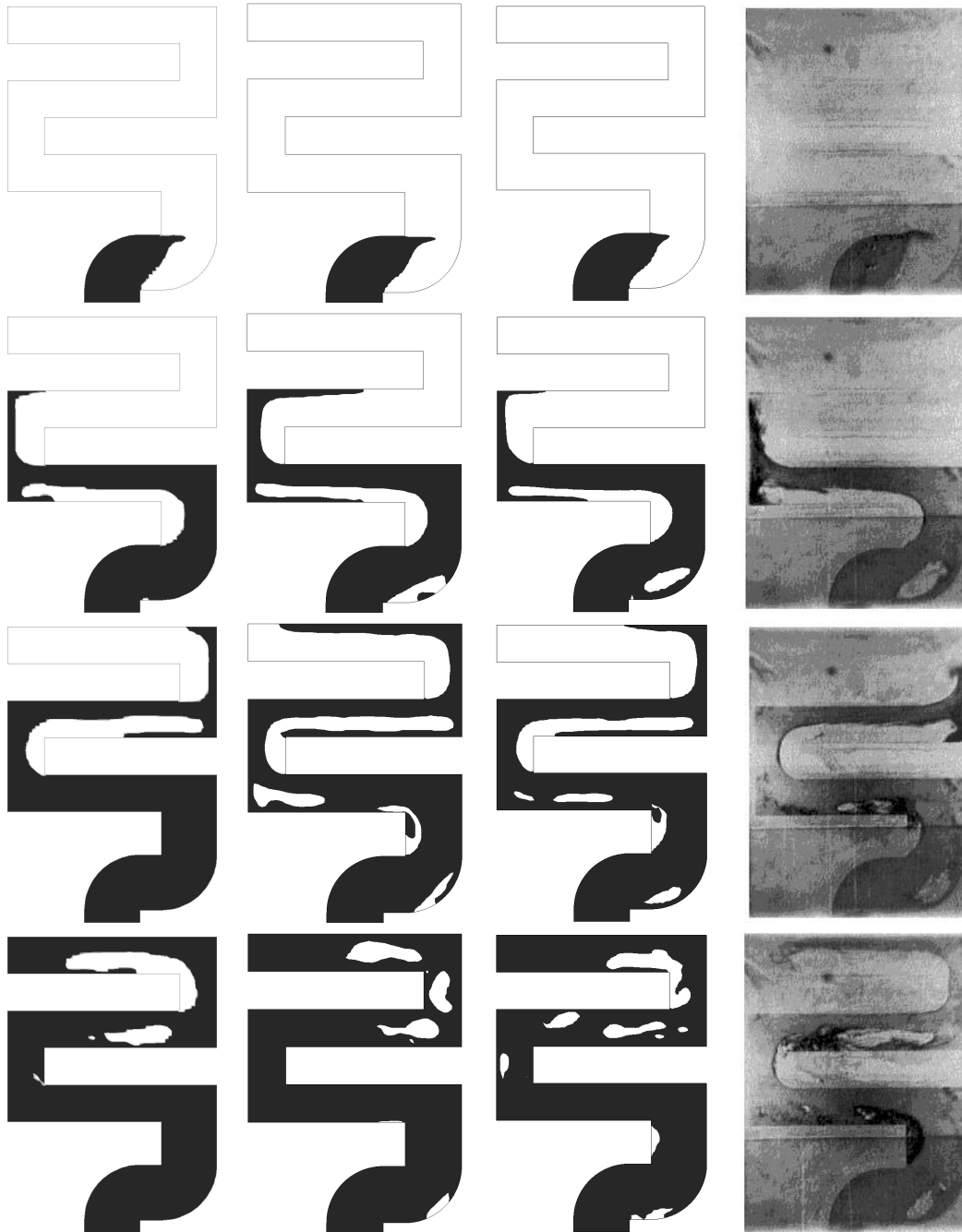


Figure 3.16: S-shaped channel with and without influence of gas. Computations with coarser mesh and $\beta_T = 0$ (no turbulence modelling): column one: 2D results without bubbles, column two: 2D results with bubbles, column three: 3D results with bubbles in a middle cut, and column four: experimental results [102]. First row: time equals 7.15 ms, second row: 25.3 ms, third row: 39.3 ms and fourth row: 53.6 ms.

3.4. NUMERICAL RESULTS

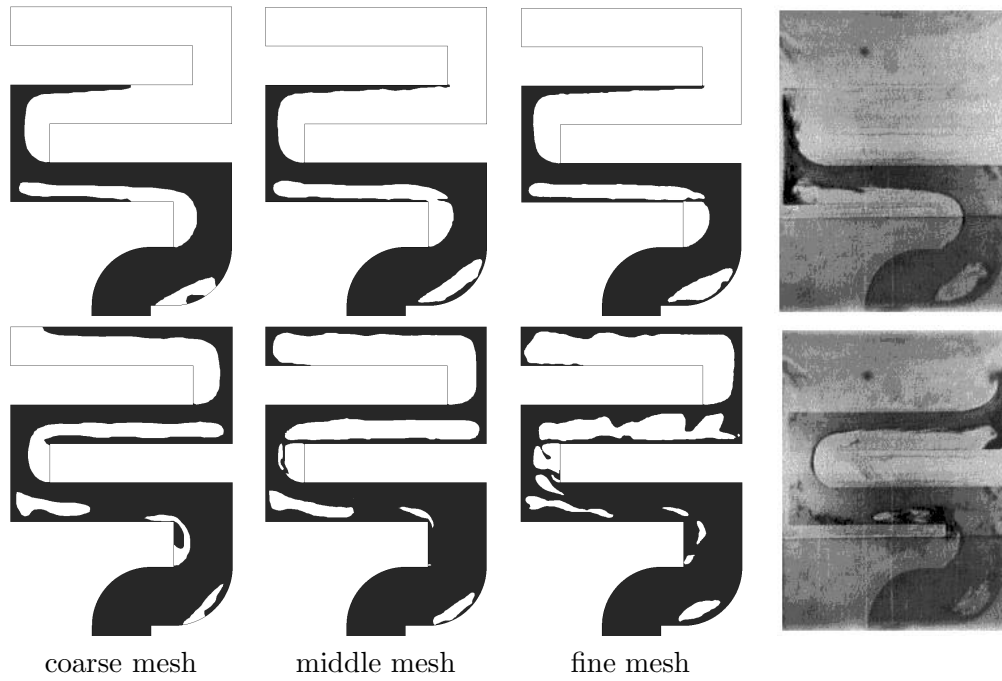


Figure 3.17: S-shaped channel with influence of gas and $\beta_T = 0$ (no turbulence modelling), 2D results: left: coarse mesh, middle: middle mesh, right: fine mesh and extreme right: experimental results [102]. First row: time equals 25.3 ms and second row: 39.3 ms.

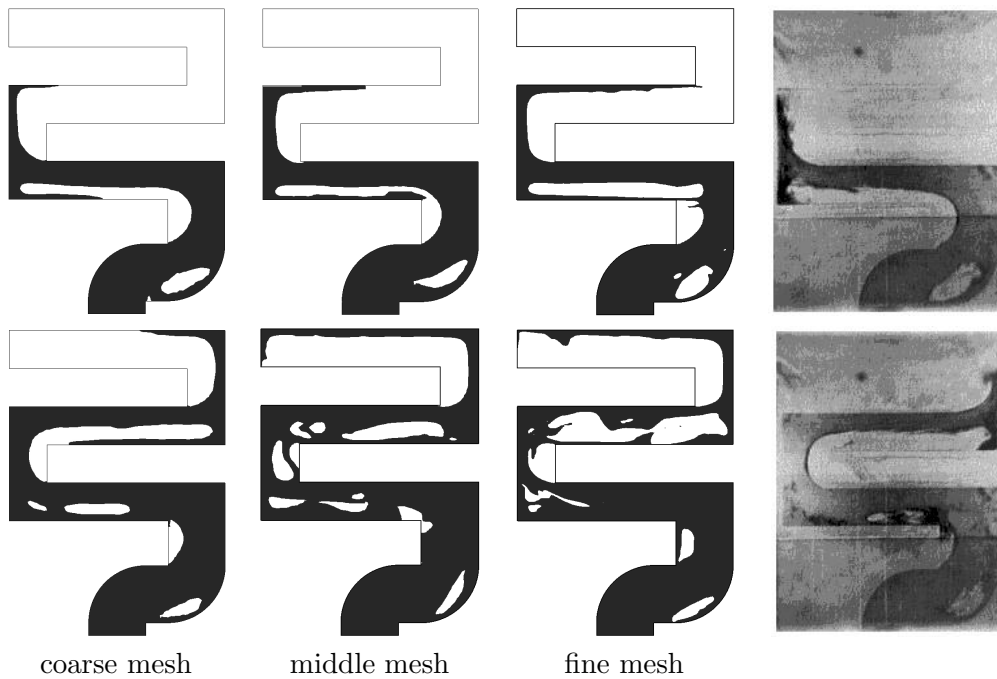
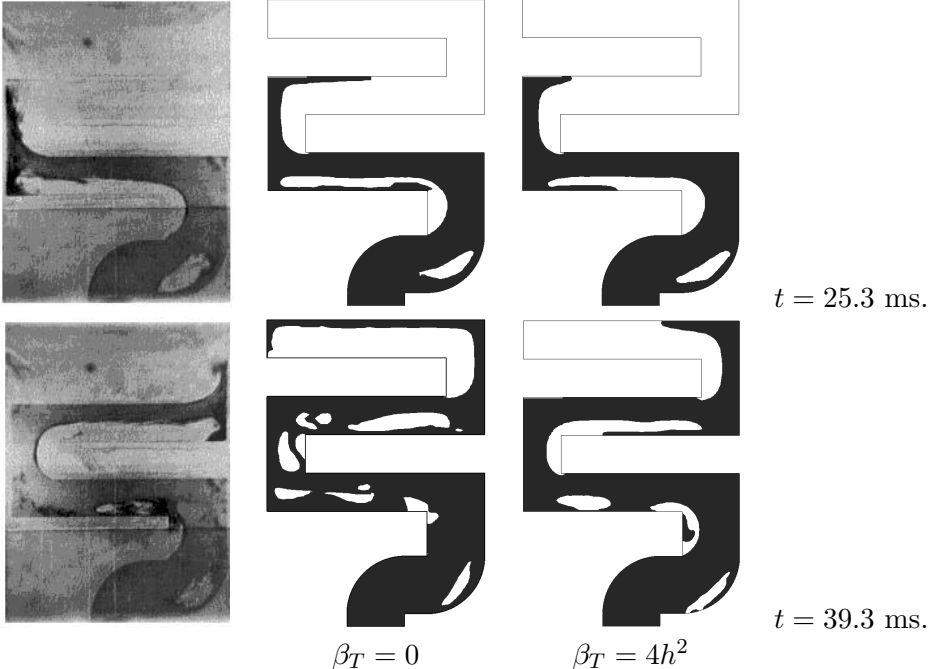


Figure 3.18: S-shaped channel with influence of gas and $\beta_T = 0$ (no turbulence modelling), 3D results, cut in 2D: left: coarse mesh, middle: middle mesh, right: fine mesh and extreme right: experimental results [102]. First row: time equals 25.3 ms and second row: 39.3 ms.

Middle Mesh



Finer Mesh

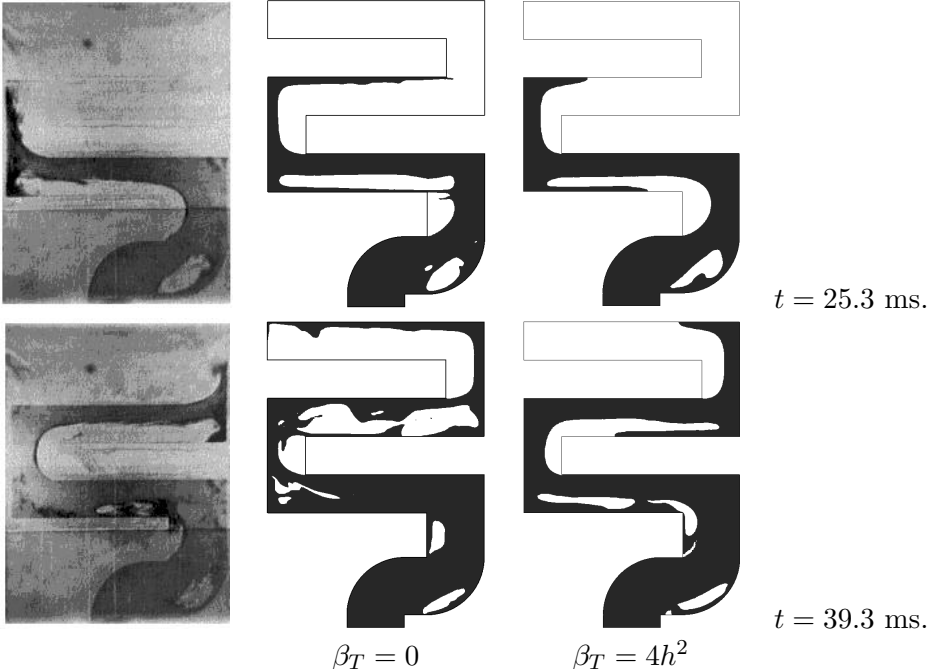


Figure 3.19: S-shaped channel with influence of gas, 3D results, cut in 2D. Influence of turbulence modelling: left: without turbulence ($\beta_T = 0$), right: with turbulence ($\beta_T = 4h^2$). First two rows: middle mesh, last two rows: fine mesh.

3.4. NUMERICAL RESULTS

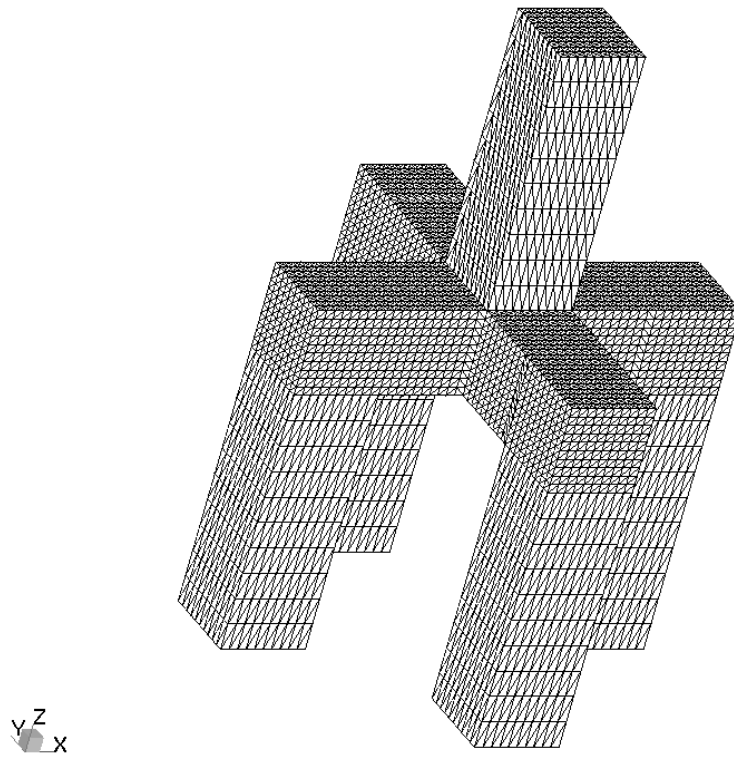


Figure 3.20: 3D mould filling: Finite element mesh.

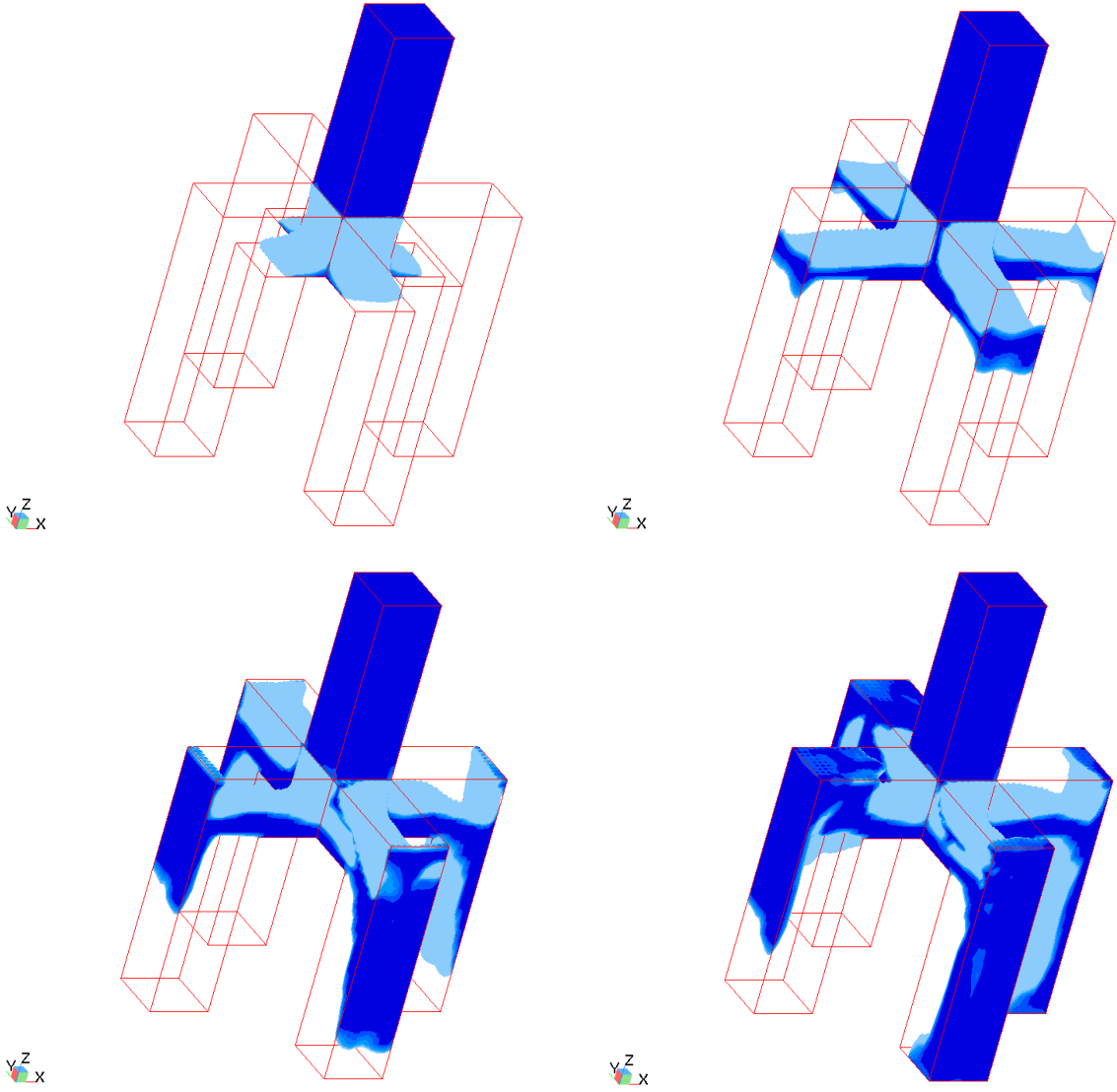


Figure 3.21: 3D mould filling. Liquid region: from top to bottom, left to right at times 0.05, 0.10, 0.15 and 0.20 s.

3.4. NUMERICAL RESULTS

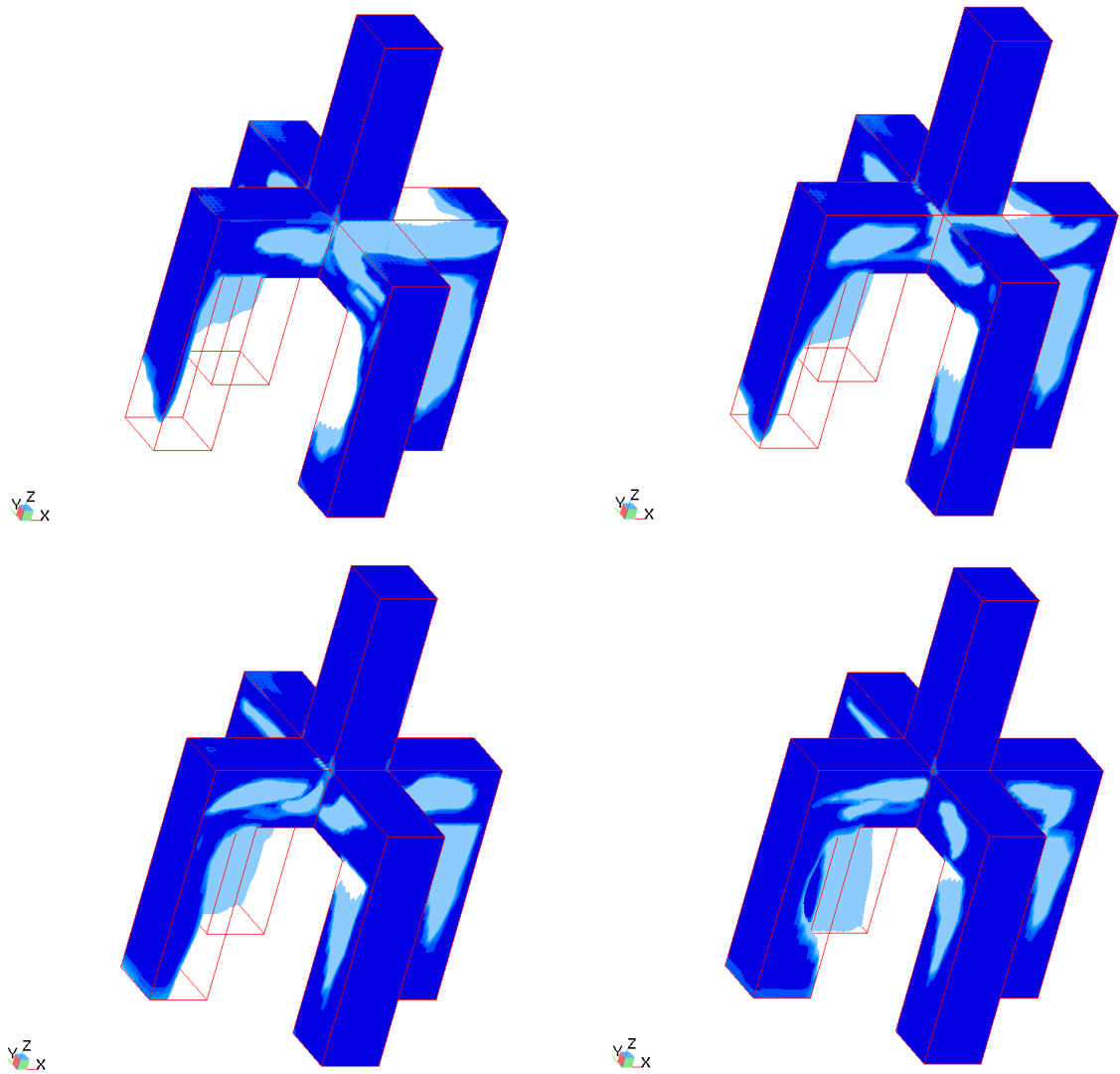


Figure 3.22: 3D mould filling (continued). Volume fraction of liquid: from top to bottom, left to right at times 0.25, 0.30, 0.35 and 0.40 s.

CHAPTER 3. SIMULATION OF FREE SURFACE FLOWS WITH BUBBLES

numerical results are compared with the ones obtained without taking into account the gas pressure. Surface tension effects have not yet been taken into account (see Chap. 4).

A circular bubble of air is initially at the bottom of a water cylinder and free to move up under the effect of the gravity field. The top of the cylinder is filled with escaping gas (*i.e.* there is a valve at the top of the cylinder). Viscosity is $\mu = 0.01$ kg/(ms), while density is $\rho = 1000$ kg/m³. Initial pressure in the gas is $P_{\text{atmo}} = 101300.0$ Pa and turbulence effects are not taken into account. The only force \mathbf{f} in (3.10) is due to the gravity effects ($\mathbf{f} = \rho\mathbf{g}$). In the two-dimensional case, dimensions of the cylinder are 0.054 m \times 0.102 m. The initial radius of the bubble is 0.01 m and the height of the free surface is 0.08 m. A symmetrical structured mesh, made out of 10151 nodes and 20000 elements, is considered. The time step is set to $\tau = 0.0005$ s and the structured grid is made out of 720'000 cells. The CPU time used for achieving 800 time steps is approximately 3 hours. Figures 3.23 and 3.24 illustrate the influence of the compressibility effect of the gas. When the compressibility effect of the gas is not taken into account, the bubble vanishes rapidly under the water pressure and the water level goes down (see Fig. 3.23). When the compressible gas fills the bubble, the bubble rises and the fraction number of molecules of gas inside the bubble is conserved (see Fig. 3.24).

In the three-dimensional case, dimensions of the cavity are 0.045 m \times 0.045 m \times 0.09 m. The initial radius of the bubble is 0.014 m and the height of the free surface is 0.07 m. A structured mesh, made out of 31096 nodes and 168750 elements, is considered. The time step is set to $\tau = 0.001$ s and the structured grid is made out of about 2'800'000 cells. The CPU time for the simulation is approximately 24 hours.

Numerical results are similar to the ones obtained in Figs 3.23 and 3.24. When the compressibility effect of gas is not taken into account, the bubbles of gas disappear rapidly as in the two-dimensional case. This situation is not illustrated here. In the opposite, when the gas pressure is applied on the interface, Fig. 3.25 on page 96 shows in a two-dimensional middle cut that the bubble rises and a hollow is appearing under the bubble.

Conclusions. A numerical method for the simulation of incompressible liquid free surface flows with surrounding compressible gas has been presented. Numerical results, in particular in the frame of mould filling, show that the influence of gas cannot be neglected and that the computational cost of this method is not very high. In the next chapter, a numerical model for taking into account the surface tension effects at the interface between liquid and gas is presented.

3.4. NUMERICAL RESULTS

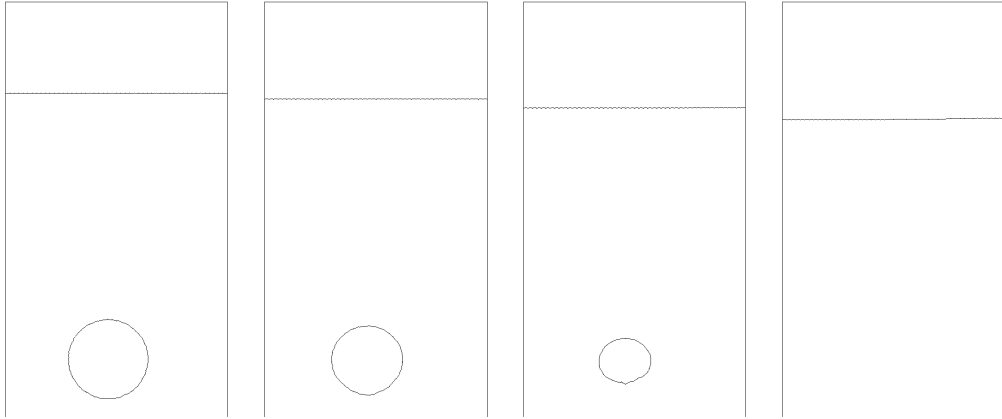


Figure 3.23: Rising bubble under a free surface, two-dimensional case. Position of the bubble, without taking into account the gas compressibility, at times $t = 0.01$, $t = 0.02$, $t = 0.03$ and $t = 0.04$ s.

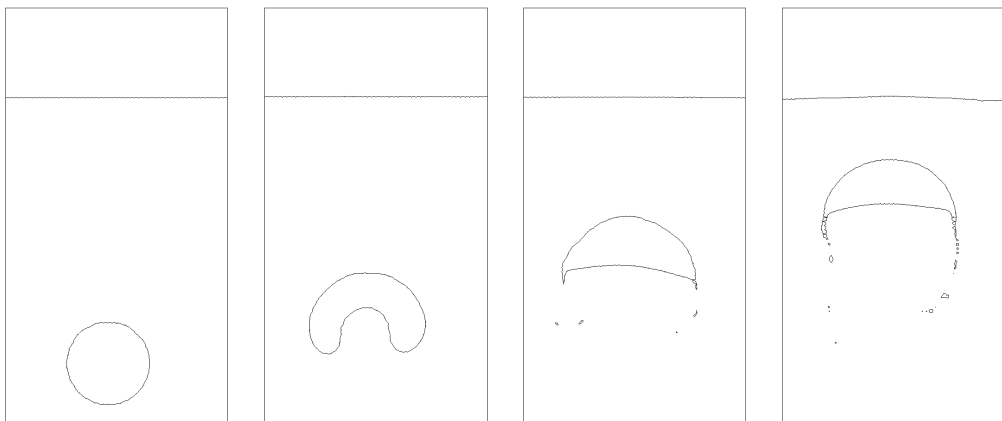


Figure 3.24: Rising bubble under a free surface, two-dimensional case. Position of the bubble, with taking into account the gas compressibility at times $t = 0.01$, $t = 0.10$, $t = 0.20$ and $t = 0.30$ s.

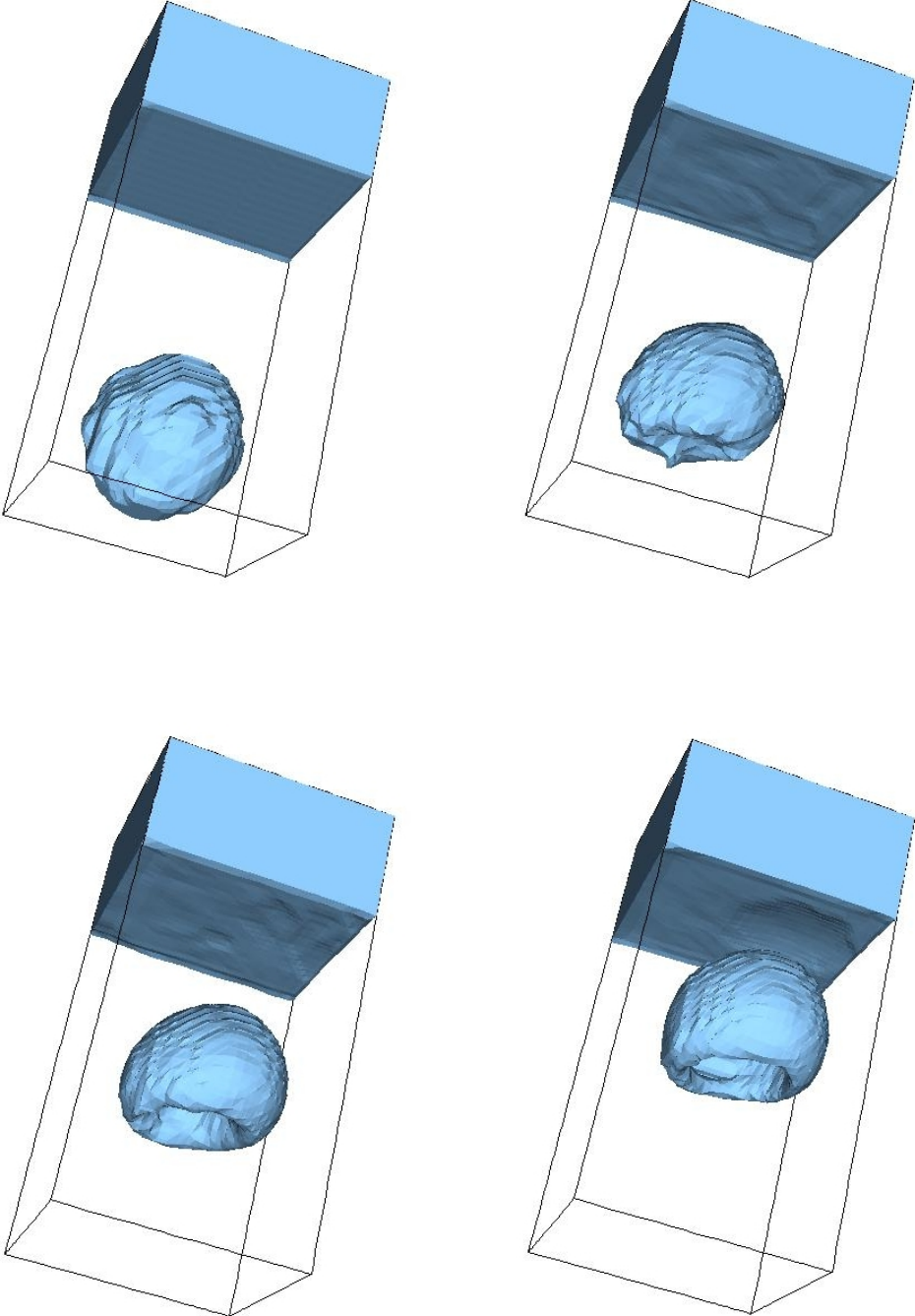


Figure 3.25: Rising bubble under a free surface, three-dimensional case, bottom view. Left to right, top to bottom: gas region at times $t = 0$, $t = 0.06$, $t = 0.12$ and $t = 0.18$ s with compressibility effect of the gas.

Chapter 4

Numerical Approximation of Surface Tension Effects and Curvature

Small bubbles of gas or droplets of water may appear in various physical situations. The motion and the shape of bubbles and drops depend mainly on the surface tension effects, especially when the ratio between the Capillary number Ca and the Reynolds number Re is large, see for instance [94, 99].

The surface tension effects are expressed by an additional force on the free surface between liquid and gas. The approximation of this force involves the computation of the curvature of the interface, which is difficult to approximate numerically for volume-of-fluid methods because of the discontinuity of the volume fraction of liquid.

In this chapter, the numerical approximation of surface tension effects is discussed mainly in the two-dimensional case, even if most of the techniques can be easily implemented in three space dimensions. Wall effects are neglected and contact angles with the walls are not modelled. In Sect. 4.1, modelling of surface tension effects is presented and some comments on the approximation of the external normal vector are made. In Sect. 4.2, emphasis is laid on the computation of the curvature and two methods of approximation are highlighted. Then two smoothing procedures are detailed in Sects 4.3 and 4.4. Finally, in Sects 4.6 and 4.7, numerical results are presented to study the convergence and the accuracy of the approximation of the curvature and to validate our model.

4.1 Modelling

Let Λ be a cavity of \mathbb{R}^2 in which the fluid is confined and let $T > 0$ be the final time of simulation. For any time $t \in (0, T)$, let Ω_t be the domain occupied by the liquid and $\partial\Omega_t$ its boundary. Let $\Gamma_t \subset \partial\Omega_t$ be the liquid free surface. Finally, let Q_T be the space-time domain containing the liquid and Σ_T the space-time free surface between liquid and gas.

The time-dependent, incompressible Navier-Stokes equations in the presence of an external force \mathbf{f} are assumed to hold in the liquid domain. That is

$$\begin{cases} \rho \frac{\partial \mathbf{v}}{\partial t} + \rho(\mathbf{v} \cdot \nabla)\mathbf{v} - 2\operatorname{div}(\mu D(\mathbf{v})) + \nabla p = \mathbf{f} & \text{in } Q_T, \\ \operatorname{div} \mathbf{v} = 0 & \text{in } Q_T. \end{cases}$$

Here $D(\mathbf{v}) = \frac{1}{2}(\nabla \mathbf{v} + \nabla \mathbf{v}^T)$ is the rate of deformation tensor, ρ the density of the liquid and μ its viscosity. Initial conditions and boundary conditions enforced on the boundary in contact with the wall of the cavity are prescribed as in Chap. 3. Let us turn to the boundary conditions prescribed on the free surface Σ_T . The *continuum surface force* (CSF) model (see [11, 12, 33, 100, 128] for various examples) is considered for the modelling of surface tension effects. The force acting on the free surface is then the sum of the normal forces due to the pressure of the surrounding gas (3.4) and the normal forces due to surface tension effects, denoted by \mathbf{F}_{ST} . Capillary forces and tangential forces are neglected, so that the boundary condition is,

$$-p\mathbf{n} + 2\mu D(\mathbf{v})\mathbf{n} = -P\mathbf{n} + \mathbf{F}_{ST} \quad \text{on } \Gamma_t, \quad t \in (0, T). \quad (4.1)$$

where \mathbf{n} is the external normal vector of the liquid domain. At given time t , let $\kappa(x, t)$ be the curvature of the interface Γ_t at point x . The curvature $\kappa(x, t)$ is supposed to be negative if the centre of the osculating circle at point x is on the liquid side of the interface (see [25] for a similar definition). Once the external normal vector is assumed to be oriented outside the liquid domain, this sign convention is in agreement with the geometric definition of the curvature using arc-length parametrization of the interface (see for instance [93]).

Let $x \in \Gamma_t$ be a point on the free surface at time t . The additional force due to surface tension effects is given by:

$$\mathbf{F}_{ST}(x, t) = \sigma \kappa(x, t) \mathbf{n}(x, t), \quad x \in \Gamma_t, \quad t \in (0, T), \quad (4.2)$$

where σ is the surface tension coefficient which depends on both media on each side of the interface (namely the liquid and the gas). Surface tension coefficient is assumed to be constant and, in the case of an interface between water and air, its value is approximately $\sigma = 0.0738 \text{ Nm}^{-1}$.

Time Discretization. The computation of curvature is included in the time splitting scheme described in Sect. 3.2. Let $0 = t^0 < t^1 < t^2 < \dots < t^N = T$ be a subdivision of the time interval $[0, T]$ and define $\tau^n = t^{n+1} - t^n$ the n -th time step, $n = 0, 2, \dots, N - 1$. In addition to the unknowns described in Chap. 3, let κ^n and \mathbf{n}^n be approximations of κ and \mathbf{n} at time t^n , defined on the free surface. Then the approximations κ^{n+1} and \mathbf{n}^{n+1} are computed by means of an additional step in the splitting algorithm.

The two advection problems (3.6) (3.7) are solved first, leading in particular to the new volume fraction of liquid φ^{n+1} . The function φ^{n+1} allows the new liquid domain Ω^{n+1} and boundary $\partial\Omega^{n+1}$ to be defined, see Subsect. 3.2.1. Then the values of curvature κ^{n+1} and \mathbf{n}^{n+1} are computed with a procedure given in the following. Then the treatment

4.1. MODELLING

of the gas domain is made according to Chap. 3 (see Subsects 3.2.2 and 3.2.3). Finally, the generalized Stokes problem (3.10) (3.11) with boundary condition (4.1) is solved, see Subsect. 3.2.4.

Approximations of the curvature and normal vector are obtained by a method independent of time, that is κ^{n+1} and \mathbf{n}^{n+1} depend only on φ^{n+1} and Ω^{n+1} at each time step t^{n+1} . The algorithms used to estimate κ^{n+1} and \mathbf{n}^{n+1} on the finite element mesh are described later in this chapter.

Space Discretization. Let \mathcal{T}_h be the finite element triangulation of Λ , P_j , $j = 1, \dots, N$ the nodes of the triangulation and φ_j , $j = 1, \dots, N$ the basis functions of the \mathbb{P}_1 finite element space constructed on \mathcal{T}_h . Let $X_h^r(\Lambda)$ be the function space of continuous functions on Λ , whose restrictions on each element $K \in \mathcal{T}_h$ belong to \mathbb{P}_r . Finally, let Ω_h^{n+1} be the approximation of domain Ω^{n+1} . The nodes lying on the interface $\partial\Omega_h^{n+1}$ are known (as well as the liquid domain Ω_h^{n+1}), thanks to the values of the volume fraction of liquid φ^{n+1} in the neighbourhood of each node. Recall that φ^{n+1} is determined after advection step, see Sect. 3.2. An approximation of the normal vector will be computed at each grid point of the finite element mesh, according to the comments made hereafter, then an approximation of the curvature will be computed by using the methods described in Sect. 4.2.

Some Considerations on the Approximation of the Normal Vector. Several approximations of the normal vector (4.2) are possible. The external normal vector to the cavity Λ is computed in [73] with mass-conservative definition, extracted from [34], and is used to enforce slip boundary conditions on the walls of the cavity. The external normal of the liquid domain Ω_h^{n+1} is then defined at point P_i by:

$$\mathbf{n}_h^{n+1}(P_i) = \frac{1}{\alpha_i} \begin{pmatrix} \int_{\Omega_h^{n+1}} \frac{\partial \varphi_i}{\partial x_1}(x) dx \\ \int_{\Omega_h^{n+1}} \frac{\partial \varphi_i}{\partial x_2}(x) dx \end{pmatrix}, \quad (4.3)$$

where α_i is a normalization coefficient in order to have $\|\mathbf{n}_h^{n+1}(P_i)\|_2 = 1$, where $\|\cdot\|_2$ is the Euclidean norm in \mathbb{R}^2 . Definition (4.3) is easily generalized in three space dimensions but can be very mesh-dependent on the free surface boundary.

Another approach for the computation of the external normal vector to the liquid domain is based on the level set theory, see [84, 103]. Let Φ^{n+1} be the approximation at time t^{n+1} of a smooth *level set* function Φ , such that the liquid domain is defined by $\Omega^{n+1} = \{x \in \Lambda : \Phi^{n+1}(x) > 1/2\}$ and such that the gas domain is defined by $\Lambda \setminus \Omega^{n+1} = \{x \in \Lambda : \Phi^{n+1}(x) < 1/2\}$. The interface between liquid and gas is then given by the level line $\partial\Omega^{n+1} = \{x \in \Lambda : \Phi^{n+1}(x) = 1/2\}$. The external normal vector is then defined by:

$$\mathbf{n}^{n+1}(x) = -\frac{\nabla \Phi^{n+1}(x)}{\|\nabla \Phi^{n+1}(x)\|_2}. \quad (4.4)$$

Expression (4.4) is consistent in some sense when Φ is sufficiently regular (see [84, 103] and references therein).

In our framework, no smooth function is available, since the volume fraction of liquid φ^{n+1} is discontinuous across the interface, see Chap. 3. In order to obtain such a smooth function Φ^{n+1} , the volume fraction of liquid will be regularized at each time step, see Sect. 4.3.

Let Φ_h^{n+1} be the approximation of Φ^{n+1} in $X_h^1(\Lambda)$ such that $\Phi_h^{n+1}(P_i) = \Phi^{n+1}(P_i)$, for all nodes P_i of the triangulation. The approximation of (4.4) is given by:

$$\tilde{\mathbf{n}}_h^{n+1}(x) = -\frac{\nabla\Phi_h^{n+1}(x)}{\|\nabla\Phi_h^{n+1}(x)\|_2}, \quad (4.5)$$

and belongs to $X_h^0(\Lambda)$, the space of functions constant on each element of the triangulation. The L^2 -projection of $\tilde{\mathbf{n}}_h^{n+1}$ on $X_h^1(\Lambda)$ (with mass lumping) is computed in order to obtain values of the normal vector at each grid node of \mathcal{T}_h . This projection is denoted by \mathbf{n}_h^{n+1} , belongs to $X_h^1(\Lambda)$ and is computed by:

$$\int_{\Lambda} \tilde{\mathbf{n}}_h^{n+1} \varphi_j dx = \int_{\Lambda} R_h(\mathbf{n}_h^{n+1} \varphi_j) dx, \quad j = 1, \dots, N, \quad (4.6)$$

where R_h is the Lagrange interpolant on $X_h^1(\Lambda)$ (see for instance [97]). The function \mathbf{n}_h^{n+1} is normalized afterwards. This implementation (4.4)-(4.6) of the normal vector is chosen in our algorithm.

Implementation of the Boundary Term. Boundary condition (4.2) leads to the introduction of an additional boundary integral in the variational form (3.13) of the generalized Stokes problem due to surface tension effects. Let $\Gamma_h^{n+1} \subset \partial\Omega_h^{n+1}$ be the approximation of the free surface at time t^{n+1} . Assume that an approximation κ_h^{n+1} of the curvature κ^{n+1} has been obtained on each grid node P_j of the interface and let \mathbf{F}_{ST}^{n+1} be the approximation of (4.2) at time t^{n+1} . The approximation of the additional boundary integral is given by:

$$\begin{aligned} \int_{\Gamma_h^{n+1}} \mathbf{F}_{ST}^{n+1} \varphi_j dS &= \sum_{\partial K \subset \Gamma_h^{n+1}} \int_{\partial K} \sigma \kappa^{n+1} \mathbf{n}^{n+1} \varphi_j dS \\ &\simeq \sum_{\partial K \subset \Gamma_h^{n+1}} \int_{\partial K} \sigma \kappa_h^{n+1} \mathbf{n}_h^{n+1} \varphi_j dS \\ &\simeq \sum_{\substack{\partial K \subset \Gamma_h^{n+1}, \\ P_j \in \partial K}} \frac{1}{2} |\partial K| \sigma \kappa_h^{n+1}(P_j) \mathbf{n}_h^{n+1}(P_j), \end{aligned} \quad (4.7)$$

where $|\partial K|$ is the length of the edge of the triangle K and φ_j are the \mathbb{P}_1 finite element basis functions. Numerical integration introduces an additional error of order $\mathcal{O}(h^2)$ (see for instance [97]). The approximation κ_h^{n+1} of the curvature is the subject of the next section.

4.2 Computation of the Curvature in two dimensions

Two kinds of methods may be distinguished for the computation of the curvature. The first class of methods (see [14] for an example) tracks the numerical approximation of the interface between both media and computes one value of the curvature only at the grid nodes on this interface. On the other hand, a value of an artificial curvature can be computed on every grid point of the cavity Λ and the real geometrical curvature on the interface is obtained by restriction on the interface (see for instance [20, 33]).

Two methods are presented hereafter to compute an approximation of the curvature κ_h^{n+1} . Both are implemented on an unstructured finite element mesh and are assuming that the volume fraction of liquid φ^{n+1} and liquid domain Ω^{n+1} are known. Numerical error for the interface approximation on the finite element mesh has been detailed in [73].

4.2.1 A Geometrical Method

In order to compute geometrically the curvature on the interface, this interface is reconstructed locally by a smooth function, see also for instance [92, 99]. The radius of the osculating circle of the interface is approximated on each grid point of the interface and the value of the curvature is given by its signed inverse.

Let x be a grid point located on Γ_h^{n+1} . The two grid points, neighbours of x on the interface, are known and denoted by x^+ and x^- , see Fig. 4.1. The osculating circle is approximated by the circle circumscribed to these three points. Its radius is given by:

$$r(x) = \frac{\|xx^+\|_2 \|xx^-\|_2 \|x^+x^-\|_2}{4\sqrt{p(p - \|xx^+\|_2)(p - \|x^+x^-\|_2)(p - \|xx^-\|_2)}} , \quad (4.8)$$

where $\|xx^+\|_2$ is the Euclidean distance between the points x and x^+ and p is the semi-perimeter $\frac{1}{2}(\|xx^+\|_2 + \|x^+x^-\|_2 + \|xx^-\|_2)$. The unsigned approximation of curvature at time t^{n+1} is then given by $|\kappa_h^{n+1}(x)| = \frac{1}{r(x)}$. We still have to determine the sign of the curvature, which is done by the following procedure.

Let us denote by $[\vec{a}, \vec{b}, \vec{c}]$ the mixed product between vectors \vec{a}, \vec{b} and \vec{c} . The sign of the curvature and the local convexity of the interface are determined at point x by using mixed products between the external normal vector and the vectors $\overrightarrow{xx^+}$, $\overrightarrow{xx^-}$ and $\overrightarrow{x^+x^-}$.

Consider the notations in Fig. 4.1 and let the Cartesian basis be denoted by $\vec{e}_1, \vec{e}_2, \vec{e}_3$ (\vec{e}_3 comes toward the reader). Define the two mixed products:

$$p_1 = [\mathbf{n}_h^{n+1}, \overrightarrow{x^+x^-}, \vec{e}_3] \quad \text{and} \quad p_2 = [\overrightarrow{x^+x}, \overrightarrow{x^+x^-}, \vec{e}_3] .$$

If $p_1 > 0$, the liquid is staying on the left side of the vector $\overrightarrow{x^+x^-}$ (this is the case of both situations illustrated in Fig. 4.1) and then the interface is oriented in some sense. In this case, if $p_2 > 0$, the point x is staying on the right side of the vector $\overrightarrow{x^+x^-}$ and the liquid domain is locally convex (Fig. 4.1, left). In the opposite if $p_2 < 0$, the point x is staying on the left side of the vector $\overrightarrow{x^+x^-}$ and the liquid domain is locally concave (Fig. 4.1, right). Notice that if $p_2 = 0$, the points x, x^+ and x^- are in a straight line and the curvature is zero ($r(x) = +\infty$).

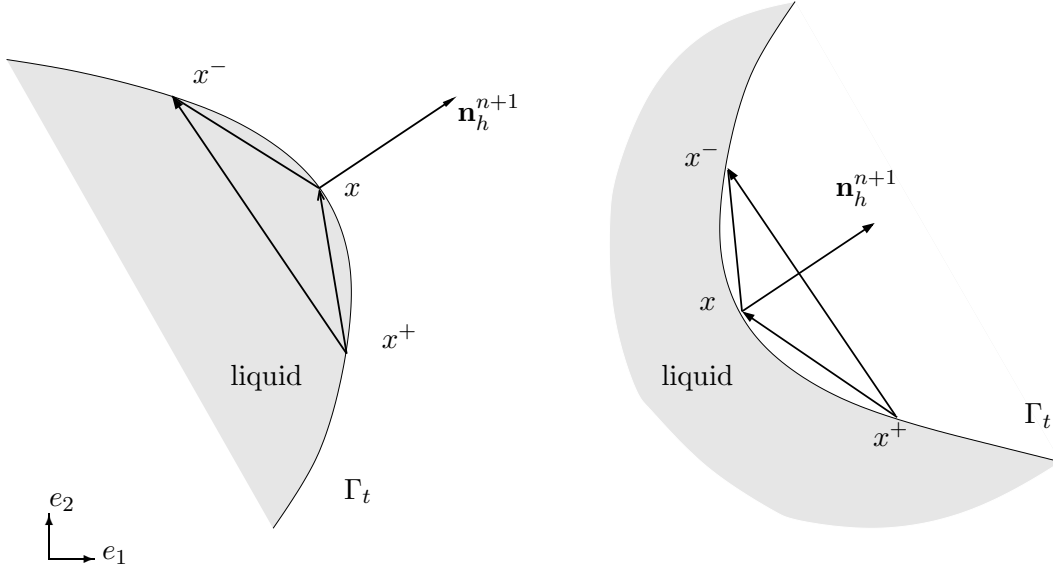


Figure 4.1: Geometric computation of the curvature of the interface: computation of an approximation of the radius of the osculating circle and determination of the local convexity of the interface. Left: convex situation, right: concave situation

If $p_1 < 0$, let us change x^+ and x^- and apply the same procedure. Note that, if $p_1 = 0$, the vectors $\overrightarrow{x^+x^-}$ and \mathbf{n}_h^{n+1} are in a straight line, this being a requirement for refining the mesh. In summary:

$$\text{sign}(\kappa_h^{n+1})(x) = \begin{cases} -1 & \text{if } p_1 > 0 \text{ and } p_2 \geq 0 , \\ +1 & \text{if } p_1 > 0 \text{ and } p_2 < 0 , \\ -1 & \text{if } p_1 < 0 \text{ and } p_2 < 0 , \\ +1 & \text{if } p_1 < 0 \text{ and } p_2 \geq 0 . \end{cases}$$

Finally let P_j denote a grid point of the finite element mesh lying on the interface; the value of the curvature at this point is given by:

$$\kappa_h^{n+1} = \text{sign}(\kappa_h^{n+1})(P_j) \frac{1}{r(P_j)} . \quad (4.9)$$

If the interface is assumed to be sufficiently regular, the circle circumscribed to x , x^+ and x^- converges, when $x^+ \rightarrow x$ and $x^- \rightarrow x$, to the osculating circle of Γ_t at point x .

The value of the curvature on the interface depends on the size and the topology of the mesh. However, it induces a regularizing effect on the interface and can be smoothed along the interface to avoid the mesh dependence, see Sect. 4.4. Although this method converges, it is not very accurate, see Sect. 4.6, and difficult to generalize in three space dimensions. Furthermore, for small Reynolds numbers, it requires small time steps in order to guarantee stability.

4.2. COMPUTATION OF THE CURVATURE IN 2D

4.2.2 A Projection Method

A second method is proposed. One value of an artificial curvature is computed at each point of the cavity Λ and the restriction on the free surface is then used to compute (4.2). The following method is based on a weak formulation in the framework of \mathbb{P}_1 finite elements. Recall that \mathcal{T}_h is the triangulation of the cavity Λ , φ_j are the basis functions associated to node P_j , $j = 1, \dots, N$ and $\mathbf{n}^{n+1}(x)$ is the external normal vector to the domain Ω^{n+1} at point x and time t^{n+1} .

Let Φ^{n+1} be an approximation of a level set function such that

$$\begin{aligned} \Omega^{n+1} &= \left\{ x \in \Lambda : \Phi^{n+1}(x) > \frac{1}{2} \right\}, & \Lambda \setminus \Omega^{n+1} &= \left\{ x \in \Lambda : \Phi^{n+1}(x) < \frac{1}{2} \right\} \\ \text{and } \partial\Omega^{n+1} &= \left\{ x \in \Lambda : \Phi^{n+1}(x) = \frac{1}{2} \right\} . \end{aligned}$$

The curvature is then given by:

$$\bar{\kappa}^{n+1}(x) = \text{div} \mathbf{n}^{n+1}(x) = -\text{div} \left(\frac{\nabla \Phi^{n+1}(x)}{\|\nabla \Phi^{n+1}(x)\|_2} \right), \quad (4.10)$$

(see for instance [84]). The curvature (4.10) is then approximated by the L^2 -projection with mass lumping on the \mathbb{P}_1 finite element space, denoted by $\kappa^{n+1} \in X_h^1(\Lambda)$, so that:

$$\int_{\Lambda} R_h(\kappa^{n+1} \varphi_j) dx = \int_{\Lambda} \bar{\kappa}^{n+1} \varphi_j dx, \quad \forall j = 1, \dots, N, \quad (4.11)$$

where R_h is the interpolation operator on $X_h^1(\Lambda)$. The left-hand side of (4.11) gives:

$$\begin{aligned} \int_{\Lambda} R_h(\kappa^{n+1} \varphi_j) dx &= \sum_{K \in \mathcal{T}_h} \int_K R_h(\kappa^{n+1} \varphi_j) dx = \sum_{K \in \mathcal{T}_h} \sum_{P_i \in K} |K| \frac{1}{3} \kappa^{n+1}(P_i) \varphi_j(P_i) \\ &= \kappa^{n+1}(P_j) \frac{1}{3} |\Omega_j|, \end{aligned} \quad (4.12)$$

where $|K|$ denotes the surface of element K and $|\Omega_j| = \sum_{K, P_j \in K} |K|$. Let \mathbf{n}_{Λ} denote the external normal vector to the cavity Λ . The right-hand side of (4.11) is integrated by parts and yields:

$$\begin{aligned}
 \int_{\Lambda} \bar{\kappa}^{n+1} \varphi_j dx &= \int_{\Lambda} \operatorname{div} \mathbf{n}^{n+1} \varphi_j dx \\
 &= \int_{\Lambda} -\operatorname{div} \frac{\nabla \Phi^{n+1}}{\|\nabla \Phi^{n+1}\|_2} \varphi_j dx \\
 &= \sum_{K \in \mathcal{T}_h} \int_K \frac{\nabla \Phi^{n+1}}{\|\nabla \Phi^{n+1}\|_2} \nabla \varphi_j dx - \sum_{\partial K \subset \partial \Lambda} \int_{\partial K} \frac{\nabla \Phi^{n+1}}{\|\nabla \Phi^{n+1}\|_2} \varphi_j \mathbf{n}_{\Lambda} dS \\
 &\simeq \sum_{K \in \mathcal{T}_h} |K| \left(\frac{1}{3} \sum_{P_i \in K} \frac{\nabla \Phi^{n+1}(P_i)}{\|\nabla \Phi^{n+1}\|_2} \right) \nabla \varphi_j|_K \\
 &\quad - \sum_{\substack{\partial K \subset \partial \Lambda \\ P_j \in K}} \frac{1}{2} \frac{\nabla \Phi^{n+1}(P_j)}{\|\nabla \Phi^{n+1}\|_2} \mathbf{n}_{\Lambda}(P_j) |\partial K|
 \end{aligned} \tag{4.13}$$

Mixing (4.12) and (4.13) leads to:

$$\begin{aligned}
 \kappa^{n+1}(P_j) &\simeq \frac{3}{|\Omega_j|} \left[\sum_{K \in \mathcal{T}_h} |K| \left(\frac{1}{3} \sum_{P_i \in K} \frac{\nabla \Phi^{n+1}(P_i)}{\|\nabla \Phi^{n+1}\|_2} \right) \nabla \varphi_j|_K \right. \\
 &\quad \left. - \sum_{\substack{\partial K \subset \partial \Lambda \\ P_j \in K}} \frac{1}{2} \frac{\nabla \Phi^{n+1}(P_j)}{\|\nabla \Phi^{n+1}\|_2} \mathbf{n}_{\Lambda}(P_j) |\partial K| \right].
 \end{aligned} \tag{4.14}$$

The values of the normal vector \mathbf{n}_{Λ} and the level set function Φ^{n+1} are replaced respectively by their approximations $\mathbf{n}_{\Lambda,h}$ and Φ_h^{n+1} in (4.14) and the estimate of curvature is:

$$\begin{aligned}
 \kappa_h^{n+1}(P_j) &= \frac{3}{|\Omega_j|} \left[\sum_{K \in \mathcal{T}_h} |K| \left(\frac{1}{3} \sum_{P_i \in K} \frac{\nabla \Phi_h^{n+1}(P_i)}{\|\nabla \Phi_h^{n+1}\|_2} \right) \nabla \varphi_j|_K \right. \\
 &\quad \left. - \sum_{\substack{\partial K \subset \partial \Lambda \\ P_j \in K}} \frac{1}{2} \frac{\nabla \Phi_h^{n+1}(P_j)}{\|\nabla \Phi_h^{n+1}\|_2} \mathbf{n}_{\Lambda,h}(P_j) |\partial K| \right].
 \end{aligned} \tag{4.15}$$

The curvature (4.15) is defined for each node P_j of the triangulation \mathcal{T}_h , an artificial value of the curvature being obtained for each level set of the function Φ^{n+1} . However (4.7) is applied only on the nodes of the interface. It suffices now to obtain an approximation of the function Φ^{n+1} . Starting from the volume fraction of liquid φ^{n+1} , the function Φ^{n+1} is obtained by smoothing the characteristic function of the liquid, see Sect. 4.3.

4.3. SMOOTHING THE VOLUME FRACTION OF LIQUID

4.3 Smoothing the Volume Fraction of Liquid

Since the curvature is given by (4.15), approximations of the derivatives of a level set function are needed. The volume fraction of liquid is not a smooth function (which is a very well-known drawback of the volume-of-fluid method) and the discontinuity across the interface implies a lack of accuracy in the approximation of the derivatives. A procedure for regularizing the volume fraction of liquid is presented in this section.

A kernel function $K(x)$ is defined by a smooth function with compact support. It must be radially-symmetric, monotonically decreasing with respect to $r = \|x\|_2$ and with normalized integral. The kernel approaches the delta Dirac function when its support tends to the empty set. The convolution of φ^{n+1} with a smooth *kernel* function leads to a smoothed volume fraction of liquid whose derivatives can be approximated numerically with accuracy, see [128]. The kernel proposed in [128] is given by:

$$K_8(x) = \begin{cases} C \left(1 - \left(\frac{\|x\|_2}{\varepsilon} \right)^2 \right)^4, & \text{if } \|x\|_2 \leq \varepsilon, \\ 0, & \text{else} \end{cases} \quad (4.16)$$

where C is a normalization coefficient ($C = \int_{\|x\|_2 \leq \varepsilon} K_8(x) dx = \frac{\pi \varepsilon^2}{5}$ in two space dimensions when $\text{supp}\{K_8\} \subset \Lambda$). The convolution of the original volume fraction of liquid with (4.16) leads to a smoothed volume fraction of liquid $\tilde{\varphi}^{n+1}$:

$$\tilde{\varphi}^{n+1}(x) = \int_{\Lambda} \varphi^{n+1}(y) K_8(x-y) dy. \quad (4.17)$$

The function $\tilde{\varphi}^{n+1}$ is k times differentiable as soon as K_8 is k times differentiable, see for instance [13]. Smoothing a step function by convolution with K_8 is illustrated in Fig. 4.2, for a two-dimensional case, namely the circular droplet described in Sect. 4.6.

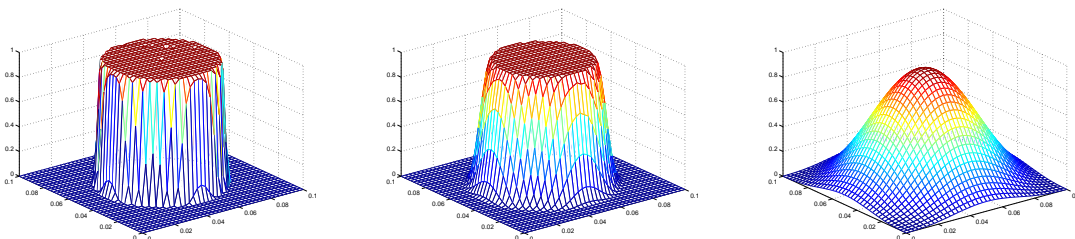


Figure 4.2: Smoothing of the volume fraction of liquid. The original volume fraction of liquid φ^{n+1} for the case of a circular droplet with radius 0.03 (left) and the smoothed volume fraction of liquid $\tilde{\varphi}^{n+1}$ with $\varepsilon = 0.01$ (middle) and $\varepsilon = 0.05$ (right).

Remark 4.1 *When the distance between the point x and the boundary of the cavity $\partial\Lambda$ is smaller than ε , the support of the kernel function is truncated by the boundary of Λ .*

In order to take this effect into account, the coefficient C in (4.16) is adapted such that $\int_{\Lambda} K_8(x-y)dy = 1$.

The curvature and normal vector are then given by:

$$\mathbf{n}^{n+1} = -\frac{\nabla\tilde{\varphi}^{n+1}}{\|\nabla\tilde{\varphi}^{n+1}\|}, \quad \kappa^{n+1} = -\operatorname{div}\frac{\nabla\tilde{\varphi}^{n+1}}{\|\nabla\tilde{\varphi}^{n+1}\|}. \quad (4.18)$$

Furthermore, an exact formulation for the first derivatives of $\tilde{\varphi}^{n+1}$ is obtained:

$$\frac{\partial\tilde{\varphi}^{n+1}}{\partial x_i}(x) = \int_{\Lambda} \varphi^{n+1}(y) \frac{\partial K_8}{\partial x_i}(x-y)dy, \quad i = 1, 2, \quad (4.19)$$

and the normal vector can also be computed using (4.19). Although it is also possible to compute an approximation of a smooth volume fraction of liquid by numerical integration on the regular grid of cells, numerical integration of (4.17) is made on the finite element mesh. The approximation of (4.17) is then given by:

$$\tilde{\varphi}^{n+1}(P_i) = \sum_{K \in \mathcal{T}_h} \frac{1}{3} |K| \sum_{P_j \in K} \varphi^{n+1}(P_j) K_8(P_j - P_i). \quad (4.20)$$

The approximation (4.15) in Sect. 4.2 is based on the smoothed function $\tilde{\varphi}^{n+1}$ in order to approximate derivatives. Let $\varphi_h^{n+1} \in X_h^1(\Lambda)$ be the approximation of φ^{n+1} . The approximation $\tilde{\varphi}_h^{n+1} \in X_h^1(\Lambda)$ of $\tilde{\varphi}^{n+1}$ is then given at the grid points P_i by:

$$\tilde{\varphi}_h^{n+1}(P_i) = \sum_{K \in \mathcal{T}_h} \frac{1}{3} |K| \sum_{P_j \in K} \varphi_h^{n+1}(P_j) K_8(P_j - P_i).$$

In the next section, another smoothing procedure is described. It is used to avoid that the curvature depends locally on the mesh topology or the mesh size.

4.4 Smoothing the Curvature along the Interface

The estimations (4.9) and (4.15) of the curvature presented in Sect. 4.2 may depend on the size and topology of the chosen mesh. In particular in the geometric approach (4.9) involves only the geometrical properties of the finite element mesh. A smoothing procedure along the interface is thus used and described hereafter, so that the final estimation of curvature does not depend on the finite element mesh, but only on a *smoothing parameter*.

Denote P_j , $j \in \{1, \dots, N_I\}$ the vertices of the free surface $\Gamma_h^{n+1} \subset \partial\Omega_h^{n+1}$. Let us assume that a non-smoothed value κ_h^{n+1} of the curvature is given either by (4.9) or by (4.15) at the grid points lying on the free surface Γ_h^{n+1} . The smoothed curvature along the interface will be denoted by $\hat{\kappa}_h^{n+1}$. The value $\hat{\kappa}_h^{n+1}(P_j)$ at the grid point P_j is computed by a mean weighted value:

4.4. SMOOTHING ALONG THE INTERFACE

$$\hat{\kappa}_h^{n+1}(P_j) = \frac{1}{N_I} \sum_{i=1}^{N_I} W_i(P_j) \kappa_h^{n+1}(P_i) , \quad (4.21)$$

where $W_i(P_j)$ are selected weights. A standard and effective method for choosing weights is *kernel smoothing* [48, 87], as in Sect. 4.3. The weights are based on a kernel function K . This function is assumed to be continuous, positive, bounded, symmetric and to satisfy $\int_{\mathbb{R}} K(u) du = 1$. The Epanechnikov function $K(u) = \frac{3}{4} (1 - u^2) I_{\{|u| \leq 1\}}$ is chosen for instance.

We assume that the grid points on the interface P_i , $i = 1, \dots, N_I$ are arranged in ascending order on each component of Γ_h^{n+1} . That means the two neighbours of P_i on the interface are P_{i-1} and P_{i+1} . Exceptions appear for example when $P_i \in \partial\Omega$ or if Γ_h^{n+1} is a closed loop (in this case the two neighbours of P_i on the interface are P_{i-1} and P_{i+1} modulo the number of nodes in the loop). The distance on the interface between two grid points P_i and P_{i+1} is defined by $d_{i,i+1} = \|P_{i+1} - P_i\|_2$. Then the distance between two grid points on the free surface, say P_j and P_k , $k > j$ is defined by $d_{j,k} = \sum_{i=j}^{k-1} d_{i,i+1}$ (with the convention $d_{k,j} = d_{j,k}$). This length $d_{j,k}$ denotes the length of the shortest path connecting P_j and P_k which is formed by grid points on the free surface, as illustrated in Fig. 4.3. Let $H > 0$ be a smoothing parameter. The weights are then defined by:

$$W_i(P_j) = \frac{K\left(\frac{d_{i,j}}{H}\right)}{\frac{1}{N_I} \sum_{l=1}^{N_I} K\left(\frac{d_{j,l}}{H}\right)} . \quad (4.22)$$

The nodes P_i such that $W_i(P_j) \neq 0$ are located in a neighbourhood around P_j , whose size is given by the smoothing parameter H , independent of the mesh size. By convention, $H = 0$ means $\hat{\kappa}_h^{n+1} = \kappa_h^{n+1}$ (no smoothing procedure).

Remark 4.2 *If the node P_j is at one end of the free surface line, for example when the free surface joins the boundary of the cavity Ω (triple point contact), the neighbourhood of P_j defined by the kernel function is asymmetric and the smoothing procedure is skewed (see for instance [48]).*

This smoothing procedure is mainly used for the geometrical method for the computation of the curvature (4.8), see Subsect. 4.2.1. Its influence is less important for the projection method with smoothing of the volume fraction of liquid. The main drawback of smoothing appears generally in high curvature regions where the smoothing must be weak to keep the local aspect of the large surface tension forces (see for instance an example in Sect. 4.7).

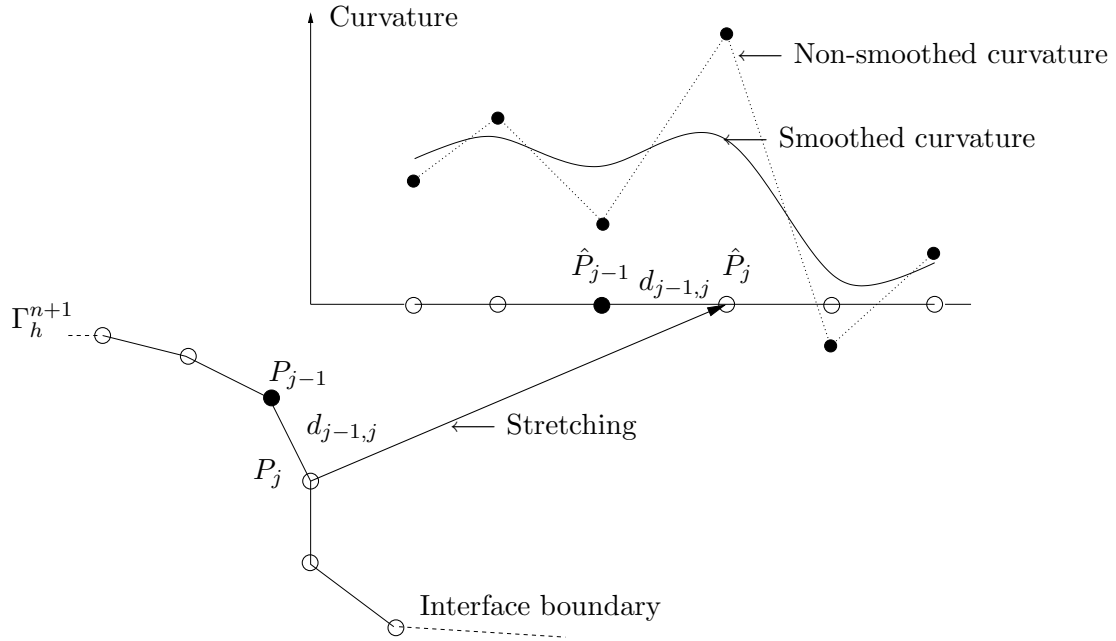


Figure 4.3: Smoothing of curvature along the interface: the free surface Γ_h^{n+1} is stretched into a rectilinear interval of \mathbb{R} , the grid points P_j being transformed into \hat{P}_j . The smoothed value of curvature is obtained by kernel smoothing on \mathbb{R} .

4.5 The Three-Dimensional case

In the three-dimensional case, the curvature κ appearing in (4.2) is also given by (4.10) (see [103]). Some computations described in the previous sections for the two-dimensional case are the same in three space dimensions.

Concerning the computation of the normal vector, (4.4) and (4.5) can be computed the same way as in the two-dimensional case. The implementation of the boundary term is identical, except that the integration is made on each face $|\partial K|$ of the tetrahedron belonging to the free surface. Relation (4.7) becomes:

$$\int_{\Gamma_h^{n+1}} \mathbf{F}_{ST}^{n+1} \varphi_j dS \simeq \sum_{\substack{\partial K \subset \Gamma_h^{n+1}, \\ P_j \in \partial K}} \frac{1}{3} |\partial K| \sigma \kappa_h^{n+1}(P_j) \mathbf{n}_h^{n+1}(P_j) ,$$

Concerning the computation of an approximation of the curvature at each grid point P_i of the free surface, the geometrical method cannot be extended easily in three space dimensions. The radius of the osculating sphere is difficult to determine unequivocally, as well as the convexity of the liquid domain, so that the other approach will be preferred. Relation (4.15) can be computed the same way as in the two-dimensional case and gives:

4.6. CONVERGENCE AND ACCURACY

$$\bar{\kappa}_h^{n+1}(P_j) = \frac{4}{|\Omega_j|} \left[\sum_{K \in \mathcal{T}_h} |K| \left(\frac{1}{4} \sum_{P_i \in K} \frac{\nabla \Phi_h^{n+1}(P_i)}{\|\nabla \Phi_h^{n+1}\|_2} \right) \nabla \varphi_j|_K - \sum_{\substack{\partial K \subset \partial \Omega \\ P_j \in K}} \frac{1}{3} \frac{\nabla \Phi_h^{n+1}(P_j)}{\|\nabla \Phi_h^{n+1}\|_2} \mathbf{n}_{\Lambda, h}(P_j) |\partial K| \right].$$

The smoothing of the volume fraction of liquid (see Sect. 4.3) is also similar, except that the value of the normalization coefficient C appearing in (4.16) is different.

On the other hand, in three space dimensions, the surface $\Gamma_h^{n+1} \subset \partial \Omega_h^{n+1}$ cannot be stretched into a plane, thus the smoothing procedure along the interface cannot be implemented the same way. Then the distance $d_{i,j}$ between two nodes P_i and P_j on the free surface is simply defined by the Euclidean norm $\|P_i - P_j\|_2$ in \mathbb{R}^3 . Relations (4.21) and (4.22) are identical.

In conclusion, the computation of (4.2) simply extends in three space dimensions. The normal vector is given by (4.4)-(4.6), while the approximation of curvature is given by the projection method (4.15) and is conjugated with a smoothing procedure of the volume fraction of liquid which is independent of the space dimension. Preliminary numerical results are given in Sect. 4.7.

4.6 Convergence and Accuracy

Test cases in two space dimensions are considered. Convergence results are obtained for the approximation of curvature.

One degree of freedom is added at each vertex of the finite element mesh in order to contain the value of the curvature. Furthermore two (respectively three in three space dimensions) degrees of freedom are defined at each vertex to contain the external normal vector to the liquid domain and one additional degree of freedom is considered for the smoothed volume fraction of liquid, according to the method described in Sect. 4.3.

The time step and the number of cells contained in the structured grid are not discussed in this chapter. The size of the cubic cells is chosen three to five times smaller than the size of the finite element mesh. The time step is set such that the CFL number does not exceed 5 (see Chap. 3).

All the computations were performed on a computer with single processor Pentium Xeon 2.8GHz CPU, 3 Gb Memory and running under Linux operating system. The results are post-processed with CalcoSOFTTM and EnightTM softwares.

4.6.1 A Geometrical Method

The geometrical method is mixed with a smoothing of the curvature along the interface. The radius of circumscribed circle is computed with (4.8) and smoothed with (4.21). The

size of the smoothing neighbourhood is denoted by H . The test case of a stationary circular water droplet lying in a square in the absence of gravity field is considered. The radius of the droplet is $\sqrt{0.001}$ and the size of the square is 0.1×0.1 . Theoretical signed curvature is constant and equal to -31.62 on the boundary of the circle (recall that the curvature is negative in this case since the liquid domain is convex, see Fig. 4.1). Several meshes are considered, namely regular structured grids of squares divided in four triangles and unstructured (isotropic) meshes, as illustrated in Fig. 4.4.

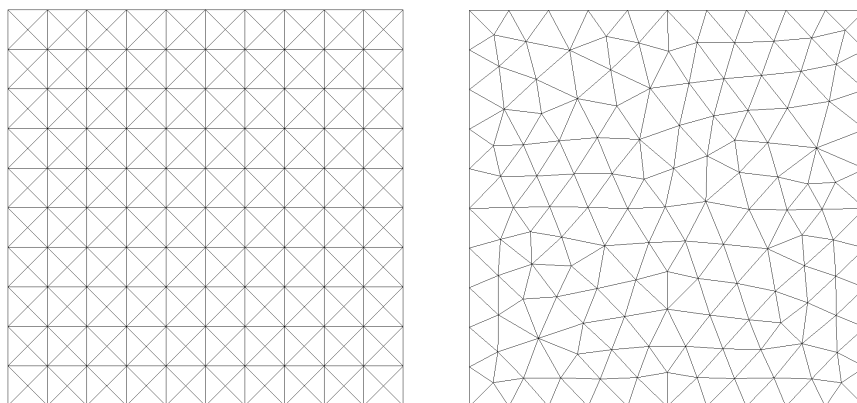


Figure 4.4: Coarse examples of the meshes used for the computations of curvature in two dimensions. Left: structured grid of quadrangles, each separated in four triangles, right: unstructured mesh.

Smoothing parameter H appearing in (4.21) is discussed first and numerical results are presented for structured meshes. Table 4.1 illustrates the value of the curvature function of the mesh size h and the smoothing parameter H .

H	Min	Mean	Max	H	Min	Mean	Max
1.	-26.7500	-23.7532	-20.9300	1.	-27.7700	-25.0170	-22.3500
0.1	-24.0400	-23.7544	-23.4400	0.1	-25.1700	-25.0198	-24.8500
0.01	-48.3800	-24.6036	-2.7100	0.01	-41.8000	-25.1562	-4.8900
0.001	-800.0000	-50.8929	800.0000	0.001	-1147.800	-31.3941	1147.700

Table 4.1: Smoothing along the interface for the stationary circular droplet. Minimum, maximum and mean values of curvatures obtained with geometrical method in function of smoothing parameter along the interface. Left: $h = 0.0025$, right: $h = 0.00125$

For small values of H , strong oscillations appear for the curvature values. Smoothing allows to obtain an almost constant value. Table 4.1 shows that the smoothing parameter should be set approximately to 0.1 which is the size of the half-perimeter of the droplet. Generally, the value of the smoothing coefficient H should be set to the size of the half-perimeter of the smallest droplets/bubbles that appear in the physical phenomenon. The parameter H is chosen independently of the mesh size and shape.

Convergence is then treated. Structured meshes are considered from 40×40 squares to 200×200 squares, each divided in four triangles. The smoothing parameter H is set to 0.1. Figure 4.5 shows that the method for the computation of curvature is convergent when

4.6. CONVERGENCE AND ACCURACY

the mesh size tends to zero, the rate of convergence being approximately $\mathcal{O}(h^{1/5})$ (with constant H). However, the method is suffering from a big lack of accuracy (see Tab. 4.2), so that it requires very fine meshes and is difficult to use for industrial computations.

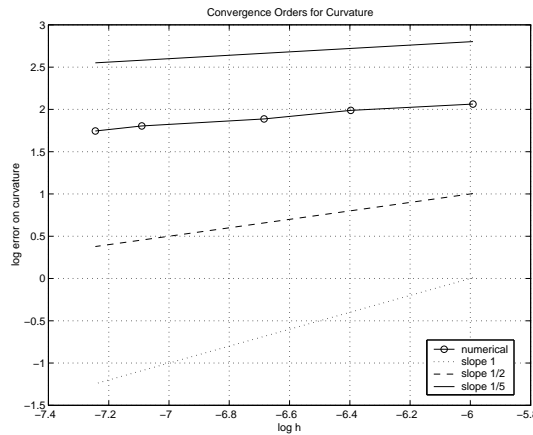


Figure 4.5: A geometric method with smoothing along the interface. Convergence order for the approximation of the curvature function of mesh size for the stationary circular droplet test case for $H = 0.1$.

h	Mean Curvature	Error	Relative Error
0.0025	-23.7544	7.8684	0.2488
0.0017	-24.3225	7.3003	0.2309
0.0013	-25.0198	6.6030	0.2088
0.0008	-25.5507	6.0721	0.1920
0.0007	-25.9000	5.7228	0.1810

Table 4.2: A geometric method with smoothing along the interface. Convergence of the approximation of the curvature for the stationary circular droplet test case for $H = 0.1$: table of mean values of curvature and errors for several mesh sizes.

4.6.2 A Projection Method

The projection method with smoothing of the volume fraction of liquid is considered (see Sects 4.2 and 4.3). The additional smoothing along the interface (see Sect. 4.4) is not always necessary.

The stationary circular droplet test case, described in the previous subsection, is considered first and $H = 0.1$. The value of smoothing parameter ε appearing in (4.16) is still to determine. Table 4.3 shows the value of curvature for several mesh sizes h and smoothing parameters ε .

If $\varepsilon \rightarrow 0$, the derivatives are difficult to approximate since the volume fraction of liquid is discontinuous. On the other hand, taking a large value of ε leads to an inaccurate approximation of the curvature (numerical diffusion). Table 4.3 shows that $\varepsilon = 0.05$ is an optimal choice and ε is chosen independently of the mesh size. Notice that the choice of the kernel or the numerical integration of (4.17) are not discussed here.

$\varepsilon \backslash h$	0.0025	0.0016	0.00125	0.001	0.0008
0.5	-30.84	-31.14	-31.16	-31.27	-31.35
0.1	-30.84	-31.17	-31.15	-31.27	-31.35
0.05	-30.85	-31.22	-31.16	-31.25	-31.35
0.01	-30.74	-31.15	-31.17	-31.27	-31.34
0.005	-29.08	-31.09	-31.15	-31.27	-31.29

Table 4.3: Circular droplet case with $H = 0.1$: smoothing of volume fraction of liquid for projection method. Values of the mean curvature of the circular droplet function of parameter ε and of mesh size h .

Remark 4.3 According to the numerical experiments, a constant value for the smoothing parameter ε has been chosen, independent of the mesh size. This method permits to obtain an order one algorithm for the computation of the curvature, However the parameter ε could be dependent of h (see e.g. [128]) in order to obtain perhaps a better convergence order.

Convergence of the approximation of the curvature is then treated. Structured meshes of squares are considered first from 40×40 squares to 400×400 squares, each square being divided in four triangles (see Fig. 4.4). Table 4.4 and Fig. 4.6 illustrate the convergence of the approximation of the curvature when the mesh size tends to zero for $H = 0.1$ and $\varepsilon = 0.05$. The convergence order is approximately $\mathcal{O}(h)$.

Mesh	h	Mean Curvature	Error	Relative Error
40x40	0.002500	-30.8450	0.7828	0.0248
80x80	0.001300	-31.1646	0.4728	0.0150
100x100	0.001000	-31.2371	0.4028	0.0127
160x160	0.000625	-31.3941	0.2528	0.0080
200x200	0.000500	-31.4253	0.2028	0.0064
300x300	0.000333	-31.5000	0.1228	0.0039
400x400	0.000250	-31.5377	0.1128	0.0036

Table 4.4: Circular droplet test case: projection method with smoothing procedures ($H = 0.1$ and $\varepsilon = 0.05$). Convergence of the approximation of the curvature for structured meshes.

Numerical results for unstructured meshes with $H = 0.1$ and $\varepsilon = 0.05$ are illustrated in Tab. 4.5 and Fig. 4.7 and show similar results. The projection method is thus accurate, independent of the mesh topology and convergent when the mesh size h tends to zero. Since the accuracy is much better for this method than for the previous geometrical method, fine meshes are not really required to obtain a satisfactory approximation of the curvature. The order of convergence is $\mathcal{O}(h)$. This order is satisfactory since the time splitting algorithm presented in Chap. 3 is an order one algorithm (see also [73] and Chap. 1 in the one-dimensional case). From an implementation point of view, the computation of the curvature by using (4.15) consists of a loop on the finite elements and therefore the computational cost is not very high. In the opposite, smoothing the volume fraction of liquid by using (4.20) requires more CPU time.

4.6. CONVERGENCE AND ACCURACY

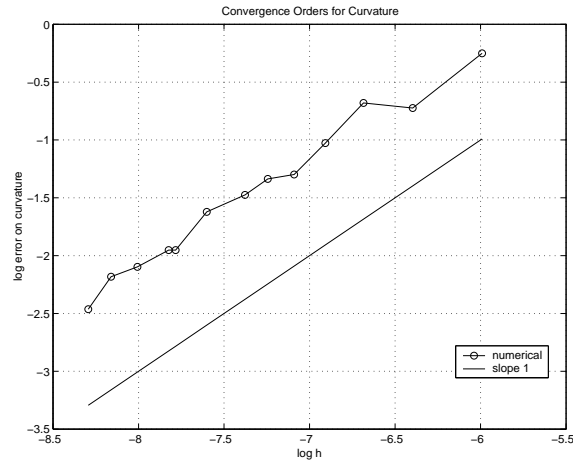


Figure 4.6: Circular droplet test case: projection method with smoothing procedures. Convergence error for the approximation of the curvature.

h	Mean Curvature	Error	Relative Error
0.0008018	-30.85	0.8328	0.0263
0.0006043	-30.98	0.6628	0.0210
0.0004663	-31.21	0.4328	0.0137
0.0004030	-31.31	0.3328	0.0105
0.0002958	-31.46	0.1728	0.0055

Table 4.5: Circular droplet test case: projection method with smoothing procedures ($H = 0.1$ and $\varepsilon = 0.05$). Convergence of the approximation of the curvature for unstructured meshes.

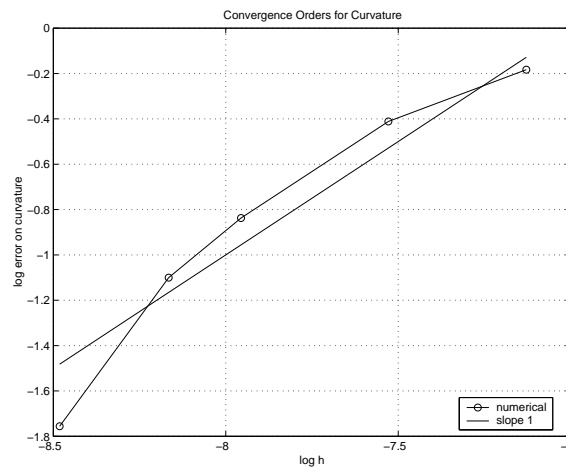


Figure 4.7: Circular droplet test case: projection method with smoothing procedures. Convergence orders for unstructured meshes, $H = 0.1$ and $\varepsilon = 0.05$. Convergence error for the approximation of the curvature.

Consider the stationary circular droplet case. The Navier-Stokes equations are solved in the liquid domain and surface tension effects are taken into account. The liquid domain is the circle described previously. In the absence of gravity forces and with zero initial velocity, the exact velocity is zero for all times. Since a normal force (4.1) is imposed on the free boundary, the numerical approximation of the velocity is not exactly zero. This boundary force (4.2) induces spurious velocities around the free surface, usually called *spurious currents* which have to be as small as possible in magnitude. Spurious currents are observed with many surface tension models and depend mainly on the ratio between $\sigma\kappa$ and the viscosity μ (see [101]) since $\sigma\kappa$ represents the force acting on the interface and counteracts viscosity effects. Numerical results are given in Fig. 4.8 on page 115 when the pressure in the surrounding gas is not taken into account. Results compare well with those of the CSF model [12, 128] or with interface reconstruction [99] in the respective range of parameters (in our case ($\sigma = 0.0738$, $\kappa = 31.6$ and $\mu = 0.01$), the order of magnitude of the spurious velocities is slightly smaller than the one of the CSF model described in [12, 128] ($\kappa = 0.5$, $\sigma = 73.0$ and $\mu = 0.01$) but bigger than the one in [99] ($\kappa \simeq 9$, $\sigma = 0.357$ and $\mu = 1$)).

Let us turn now to the second test case, namely the sinusoidal interface. For this second test case, in the square domain of size 0.1×0.1 , the liquid domain is given by:

$$\Omega_t = \{(x, y) \in [0, 0.1] \times [0, 0.1] : y \leq 0.02 \sin(16\pi x) + 0.05\}, \quad t \in (0, T) .$$

Gravity effect is not taken into account (*i.e.* external forces are $\mathbf{f} = 0$). The interface is in contact with the boundary of the cavity and an additional smoothing error near the boundary is introduced in the computation of the curvature. The value of the curvature at point (x, y) on the interface curve (given by $y = 0.02 \sin(16\pi x) + 0.05$) is

$$\kappa(x, t) = \frac{-0.02(16\pi)^2 \sin(16\pi x)}{\sqrt{1 + (0.02 \cdot 16\pi)^2 \cos(16\pi x)^2}^3}, \quad t \in (0, T) .$$

Since there is no gravity field and the initial velocity is set to zero, the liquid domain is the same for all times and the liquid velocity is zero. The value of normalization coefficient C in (4.16) is adapted in the neighbourhood of the boundary of the cavity. The smoothing parameters H and ε are first discussed on two structured meshes, composed by 40×40 , respectively 80×80 squares, each divided in four triangles. Let H be fixed first to zero (that is there is no smoothing procedure along the interface by convention, see Sect. 4.4). Numerical results are compared with theoretical values of curvature in Fig. 4.9 on page 116 and illustrates the effect of the parameter ε .

Hence, when $H = 0$, the value of parameter ε is chosen approximately between 0.005 and 0.008, independently of the mesh size, in order to obtain some satisfactory results. If ε is larger, the error near the boundary is propagated inside the domain, while a very noisy value of curvature is obtained when ε tends to zero.

Let us turn to the influence of the parameter H . The influence of smoothing parameter H is illustrated in Fig. 4.10 when $\varepsilon = 0.005$ is fixed. For large values of the parameter H , the smoothing procedure along the interface introduces a bias in a neighbourhood of the boundary of the cavity. On the other hand, the approximation of the curvature is less

4.6. CONVERGENCE AND ACCURACY

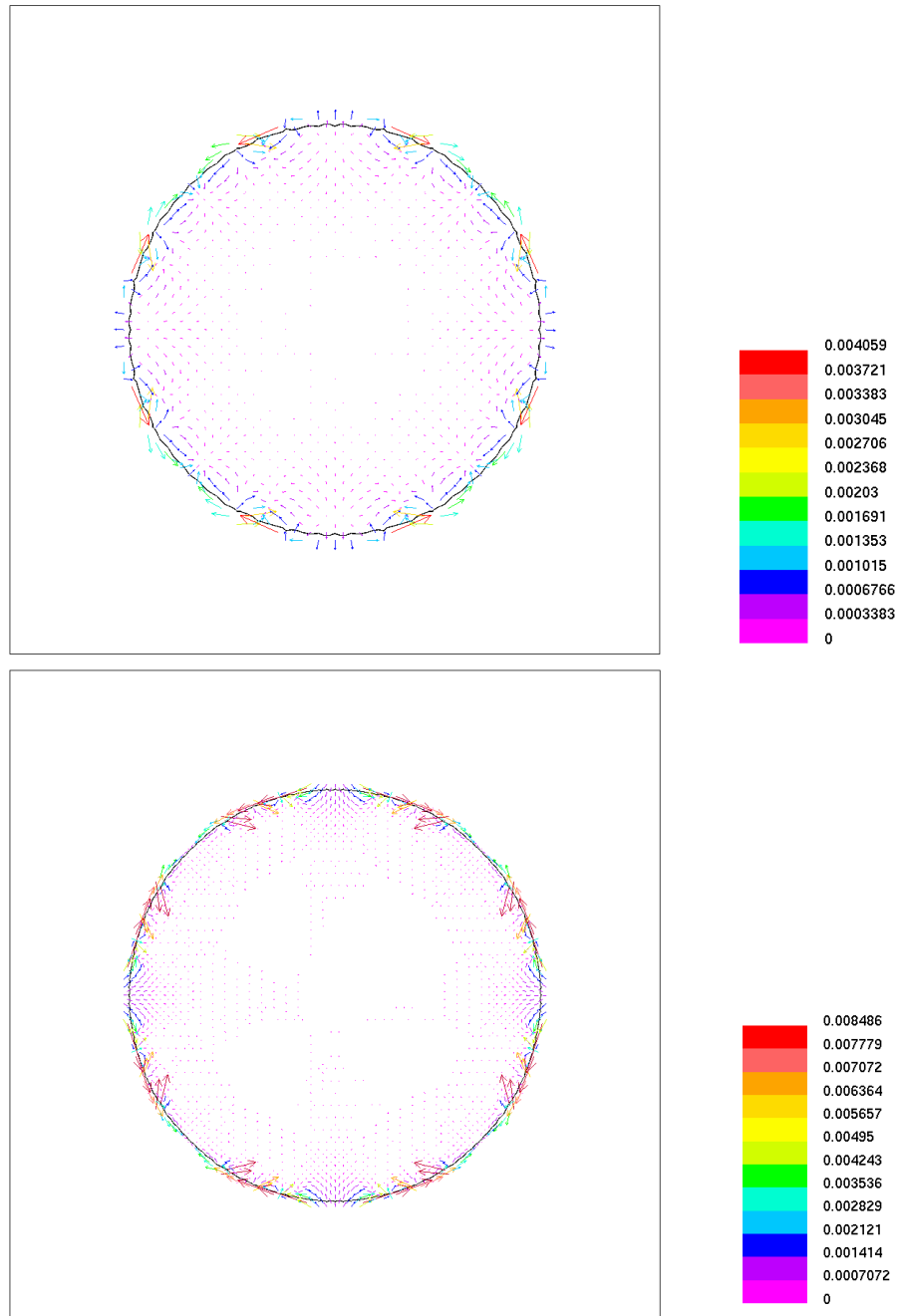


Figure 4.8: Circular droplet test case: projection method with smoothing procedures. Spurious velocities after 5 time steps and $\tau = 0.001$ ($H = 0.1$ and $\varepsilon = 0.05$). Top: Structured mesh 40×40 , bottom: mesh 80×80 .

variable and less noisy and more accurate in the interior of Λ . A trade-off is obtained for H approximately equal to 0.02.

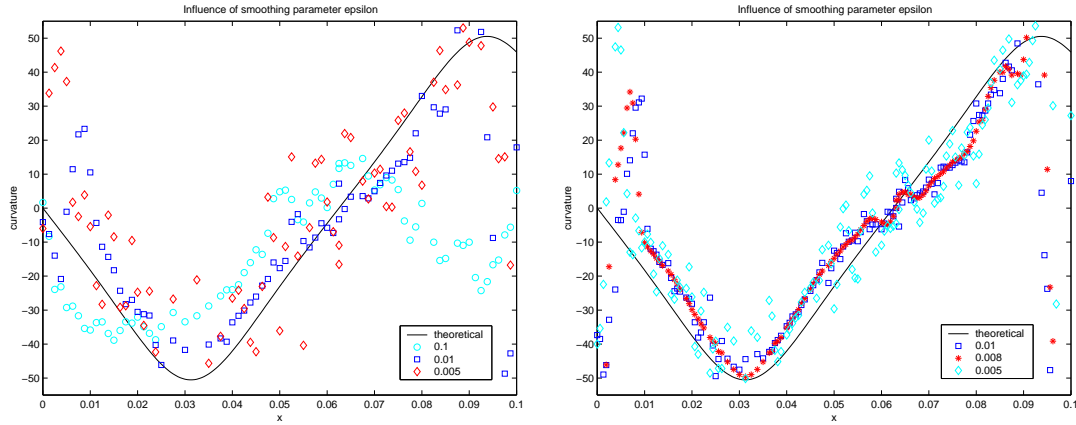


Figure 4.9: Stationary sinusoidal test case: projection method with smoothing procedures. Value of curvature function of x for several smoothing parameters ε ($H = 0$) and two mesh sizes. Left: mesh 40×40 , right: mesh 80×80 .

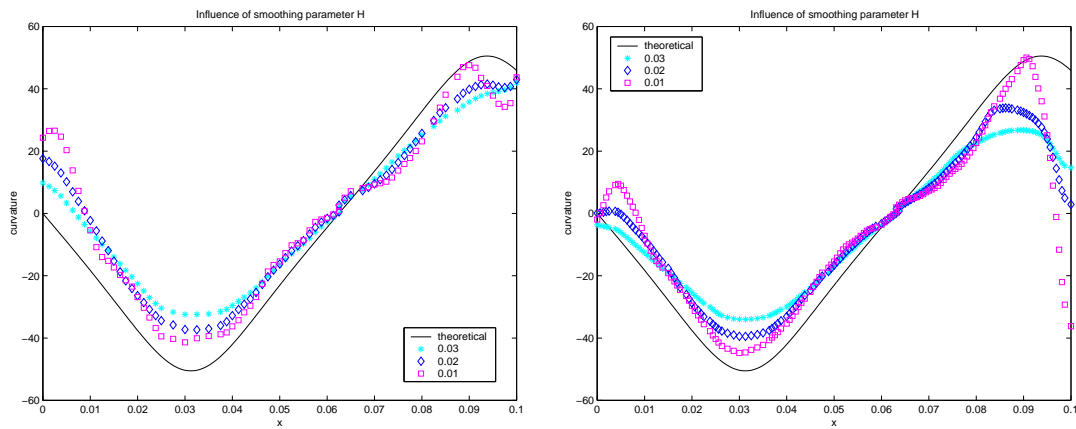


Figure 4.10: Stationary sinusoidal test case: projection method with smoothing procedures. Value of curvature function of x for several smoothing parameters H ($\varepsilon = 0.005$) and two mesh sizes. Left: mesh 40×40 , right: mesh 80×80 .

Results show that the value of the curvature in a wall boundary layer is not very accurate. Satisfactory results are obtained but the computation of the curvature in a neighbourhood of the triple point (the point where the free surface joins $\partial\Lambda$) is still an open question. However numerical simulations in Sect. 4.7 do not always suffer from this lack of accuracy. With the geometrical method presented in Subsect. 4.2.1, the conclusions about the computation of the curvature at the triple point are the same, *i.e.* the method is not accurate in the neighbourhood of this point.

4.7. NUMERICAL RESULTS

Remark 4.4 *The computation of the external normal vector is not discussed here. However, the results with the normal vector computed by convolution (4.19) or with mollified volume fraction of liquid (4.4) are not significantly different.*

4.7 Numerical Results

Numerical simulations are presented in this section, in particular for curvature driven phenomena. Wall effects are neglected and the contact angle with the walls is not modelled. Applications of simulations of droplets or bubbles flows are various, for example in image recognition, industry, natural sciences, *etc.* Since numerical results are more satisfactory and generalization in three space dimensions is possible, the curvature is computed in all these simulations with the projection method described in Subsect. 4.2.2.

Square Droplets and Bubbles. A stationary water droplet in the absence of gravity field is assumed to be initially a square. With surface tension effects, the droplet becomes circular. Physical parameters are $\mu = 1. \text{ kg}/(\text{ms})$, $\sigma = 7.038 \text{ Nm}^{-1}$ and $\rho = 1000. \text{ kg}/\text{m}^3$. External forces \mathbf{f} in (3.10) and initial velocity are zero. The cavity is the $0.1 \text{ m} \times 0.1 \text{ m}$ square and several structured meshes are considered. The coarse mesh is made out of 40×40 squares (each divided in four triangles), the middle mesh is made out of 60×60 squares while the finer mesh is made out of 80×80 squares. The time step is $\tau = 0.001 \text{ s}$. The curvature is computed with the projection method and smoothing procedures. Since the theoretical curvature at initial time is zero everywhere on the free surface except in the four corners of the domain, the numerical approximation of the curvature should not be too much diffused. For this reason no smoothing along the interface is applied. Thus smoothing parameters are $\varepsilon = 0.005 \text{ m}$ and $H = 0 \text{ m}$ for this test case. Pressure in the surrounding gas is not taken into account. Numerical simulations show that the droplet becomes a circle for every mesh size, see Fig. 4.11. Furthermore, the evolution of velocities is symmetric and magnitude decreases with time, see Fig. 4.12 on page 119. Oscillations that appear for instance in [12] are negligible and the droplet reaches its stationary circular shape. Similar results can be obtained with unstructured meshes.

The inverse situation is then considered, that is an initially square bubble of gas in water in the absence of gravity field. Numerical results in Fig. 4.13 on page 119 are illustrated for the middle structured mesh and shows that our computations are independent of the convexity of the interface.

Curvature Driven Oval. A stationary droplet with initial oval form is considered in the square domain $0.1 \text{ m} \times 0.1 \text{ m}$ in the absence of gravity field (right-hand side $\mathbf{f} = 0$ in (3.10)). Deformed droplets are omnipresent in natural process, but also in industry for ink-jet printers (see [23, 80, 116] for instance). The initial liquid domain Ω_0 is

$$\Omega_0 = \left\{ (x, y) \in [0, 1] \times [0, 1] : \left(\frac{x - 0.005}{0.1} \right)^2 + \left(\frac{y - 0.005}{0.2} \right)^2 \leq 0.02 \right\} .$$

The oval droplet becomes a circle under surface tension effects, since forces are larger in regions of high curvature. Physical parameters are $\mu = 1. \text{ kg}/(\text{ms})$, $\sigma = 0.738 \text{ Nm}^{-1}$ and

Coarse mesh:



Middle mesh:



Fine mesh:



$t = 0.001$ $t = 0.003$ $t = 0.006$ $t = 0.009$ $t = 0.012$ $t = 0.015$

Figure 4.11: An initially square droplet becomes circular under surface tension effects. Representation of liquid region at times 0.001 s, 0.003 s, 0.006 s, 0.009 s, 0.012 s and 0.015 s. First row: coarse mesh, second row: middle mesh and third row: fine mesh.

$\rho = 1000$ kg/m³. Pressure in the surrounding gas is not taken into account. Numerical results are obtained for a structured mesh of 60×60 squares and for a time step $\tau = 0.001$ s and are illustrated in Fig. 4.14 on page 120. Smoothing parameters are $\varepsilon = 0.005$ m and $H = 0.005$ m. After 0.5 s the process is stationary and oscillations are negligible. Results are identical for several mesh sizes. The value of the smoothing parameter H has not much influence on the result of the simulation.

Droplet Splashing on a Film of Water. The splashing of a droplet of water falling in the presence of gravity field onto a thin layer of water at rest is considered in two space dimensions, see also [56, 129]. Such situation appears with raindrop splashing on a pool of water for instance.

Situation is described in Fig. 4.15 on page 122. The cavity is the $0.1 \text{ m} \times 0.1 \text{ m}$ square. External forces in (3.10) are $\mathbf{f} = \rho \mathbf{g}$, where \mathbf{g} is the gravity field. The droplet has initial velocity $\mathbf{v}_0 = 2 \text{ m/s}$ and falls from $\bar{h} = 0.0625 \text{ m}$. The initial radius of the bubble is $R = 0.007 \text{ m}$ and the height of the thin layer of water is $h = 0.02 \text{ m}$. Surface tension effects and pressure in the gas are taken into account. Physical parameters are $\mu = 0.05 \text{ kg/(ms)}$, $\rho = 1000 \text{ kg/m}^3$ and $\sigma = 0.0738 \text{ Nm}^{-1}$. Numerical results are presented for a structured mesh of 80×80 squares and the time step is $\tau = 0.001 \text{ s}$. Final time is $T = 0.4 \text{ s}$. Smoothing parameters are $\varepsilon = 0.05 \text{ m}$ and $H = 0.02 \text{ m}$. Slip boundary conditions are enforced on the lateral walls, while Dirichlet boundary conditions $\mathbf{v} = 0$ are enforced at

4.7. NUMERICAL RESULTS

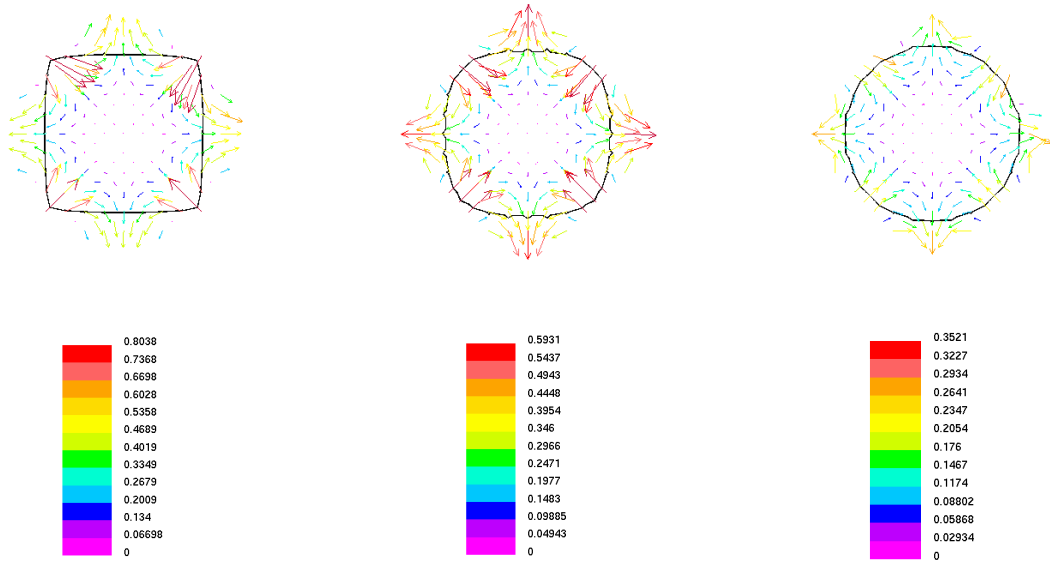


Figure 4.12: An initially square droplet becomes circular under surface tension effects. Representation of velocities and interface at times $t = 0.002$ s ($|\mathbf{v}|_{\max} = 0.80$ m/s), $t = 0.004$ s ($|\mathbf{v}|_{\max} = 0.59$ m/s) and $t = 0.006$ s ($|\mathbf{v}|_{\max} = 0.35$ m/s) for the coarse mesh,

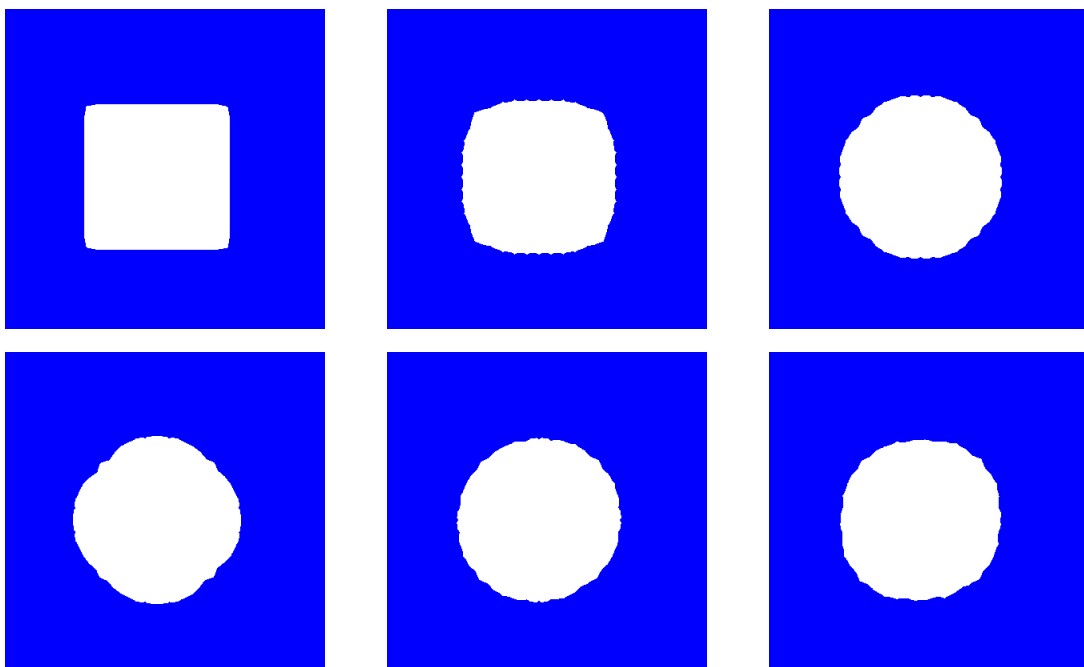


Figure 4.13: An initially square bubble becomes circular under surface tension effects. Representation of liquid region (from left to right, top to bottom), at times 0.001 s, 0.003 s, 0.005 s, 0.008 s, 0.012 s and 0.015 s.

CHAPTER 4. SURFACE TENSION AND CURVATURE

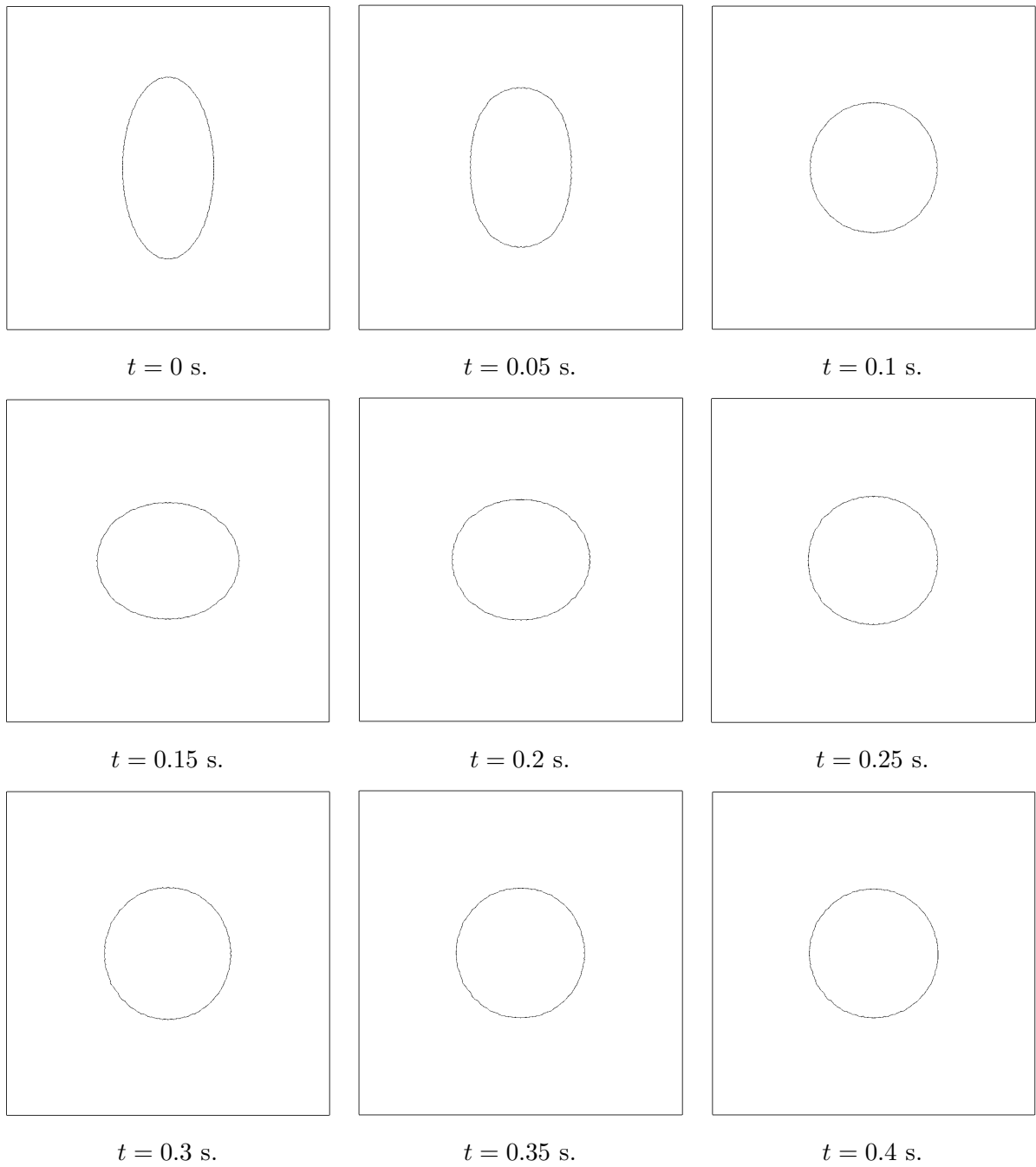


Figure 4.14: Initially oval droplet under surface tension effects. From left to right, top to bottom: interface between water and gas from $t = 0$ s to $t = 0.4$ s (by steps of 0.05 s).

4.7. NUMERICAL RESULTS

the bottom of the cavity. The position of the free boundary is illustrated in Fig. 4.15 on page 122 for various times between $t = 0.025$ s and $t = 0.1$ s. The results are in a good agreement with [56], in particular the formation of a surfacing wave.

Rising Bubble. Gas bubbles may appear in various physical phenomena, for example in the *aluminium electrolysis* process. See for instance [40, 60] for a complete description. A simple case of a gas bubble flow is presented here. A circular bubble of air is initially at the bottom of a cylinder in 2D filled with water. It is free to move up by effect of the gravity field ($\mathbf{f} = \rho\mathbf{g}$). Dimensions of the cylinder are $0.054 \text{ m} \times 0.102 \text{ m}$. The initial radius of the bubble is 0.01 m and its centre is located at height 0.015 m . Viscosity is $\mu = 0.01 \text{ kg}/(\text{ms})$, while density is $\rho = 1000 \text{ kg}/\text{m}^3$. The gas pressure is disregarded. A symmetrical structured mesh is considered. Three meshes are considered. The coarse mesh is made out of 2576 nodes and 5000 elements, the middle mesh is made out of 10151 nodes and 20000 elements and the fine mesh is made out of 22726 nodes and 45000 elements. Smoothing parameters are $\varepsilon = 0.005 \text{ m}$ and $H = 0.05 \text{ m}$.

Surface tension effects are reported in Fig. 4.16 on page 123 for the coarse mesh (see also [65]). The liquid-gas interface is illustrated. The time step is $\tau = 0.005 \text{ s}$. When surface tension effects are not taken into account, small bubbles are gathering at the extremities of the bubble. For larger values of the surface tension coefficient σ , surface tension effects stabilize (partially or not) the bubble.

The influence of the mesh size is reported in Figs 4.17 (for $\sigma = 0 \text{ Nm}^{-1}$) and 4.18 (for $\sigma = 0.0738 \text{ Nm}^{-1}$). The time steps are $\tau = 0.005 \text{ s}$ for the coarse mesh, $\tau = 0.0025 \text{ s}$ for the middle mesh and $\tau = 0.0016 \text{ s}$ for the fine mesh. The size of the cells of the structured mesh used for advection step is approximately 5 to 10 times smaller than the size of the finite elements, see Sect 3.3. Figures 4.17 and 4.18 are compared. Numerical results show that the convergence of the algorithm when the mesh size tends to zero is not guaranteed when $\sigma = 0 \text{ Nm}^{-1}$. In the opposite, numerical results converge when the mesh size tends to zero when surface tension effects are taken into account.

3D Cubic Droplet. Implementation of the projection method (see Subsect. 4.2.2) in the three-dimensional case is illustrated on an example. Preliminary results are given here with smoothing of the volume fraction of liquid (4.17) and computation of the curvature with (4.15). A cubic droplet of water in the centre of a cubic cavity is considered. This example is the three-dimensional version of the square droplet example described previously in two space dimensions.

Dimensions of the cavity are $0.1\text{m} \times 0.1\text{m} \times 0.1\text{m}$, while dimensions of the droplet are $0.5\text{m} \times 0.5\text{m} \times 0.5\text{m}$. Viscosity is $\mu = 0.01 \text{ kg}/(\text{ms})$, while density is $\rho = 1000 \text{ kg}/\text{m}^3$. The gas pressure is disregarded and no external volumic forces \mathbf{f} are applied (in particular, gravity forces are neglected). The surface tension coefficient σ is set to 7.038 Nm^{-1} . A structured mesh made out of 34481 nodes and 192000 elements is considered. The time step is set to $\tau = 0.001 \text{ s}$. Smoothing parameters are $\varepsilon = 0.01 \text{ m}$ and $H = 0 \text{ m}$ ($H = 0$ in order to keep the local effects of the surface tension forces around the corners).

Figure 4.19 on page 126 illustrates the evolution of the liquid droplet and shows that the droplet becomes spherical under surface tension forces. However a slight influence of the mesh size remains since a relatively coarse three-dimensional mesh is considered here.

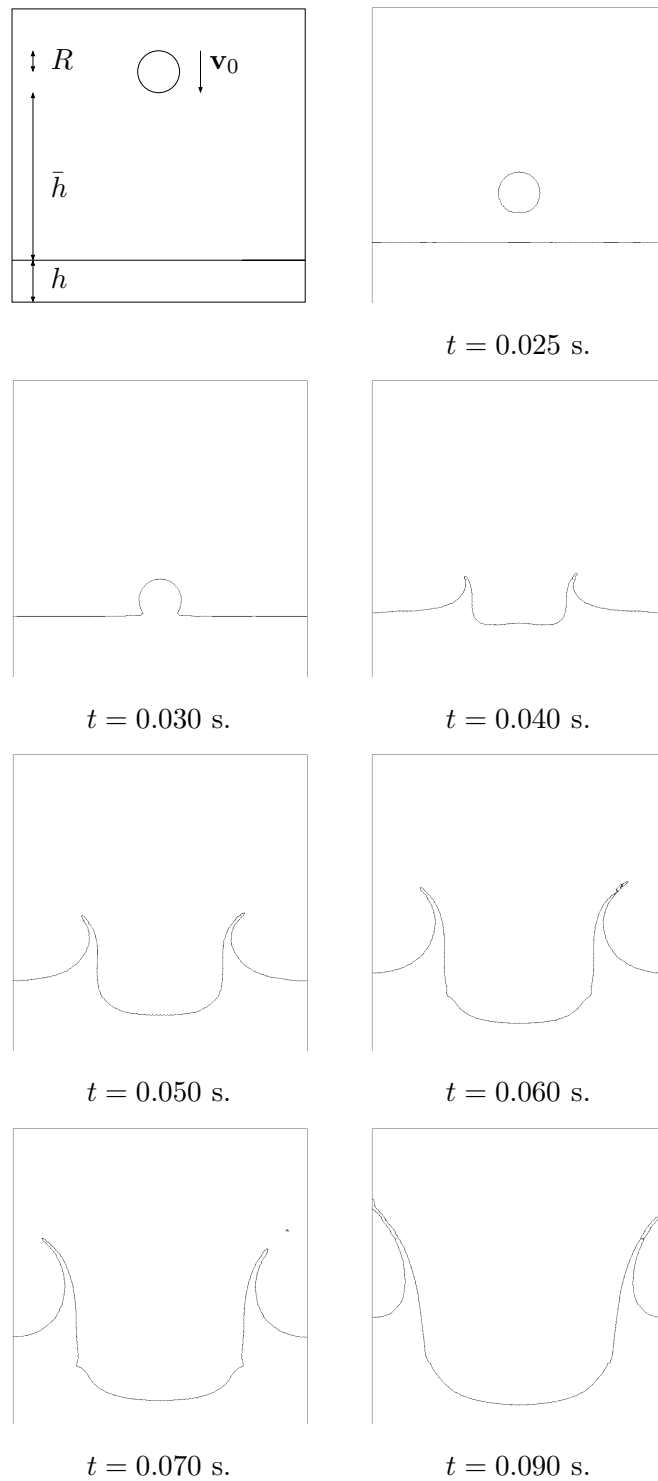


Figure 4.15: Droplet splashing on a thin layer of water. Top left: representation of the simulation setup, then, top to bottom from left to right: position of the free boundary at several times.

4.7. NUMERICAL RESULTS

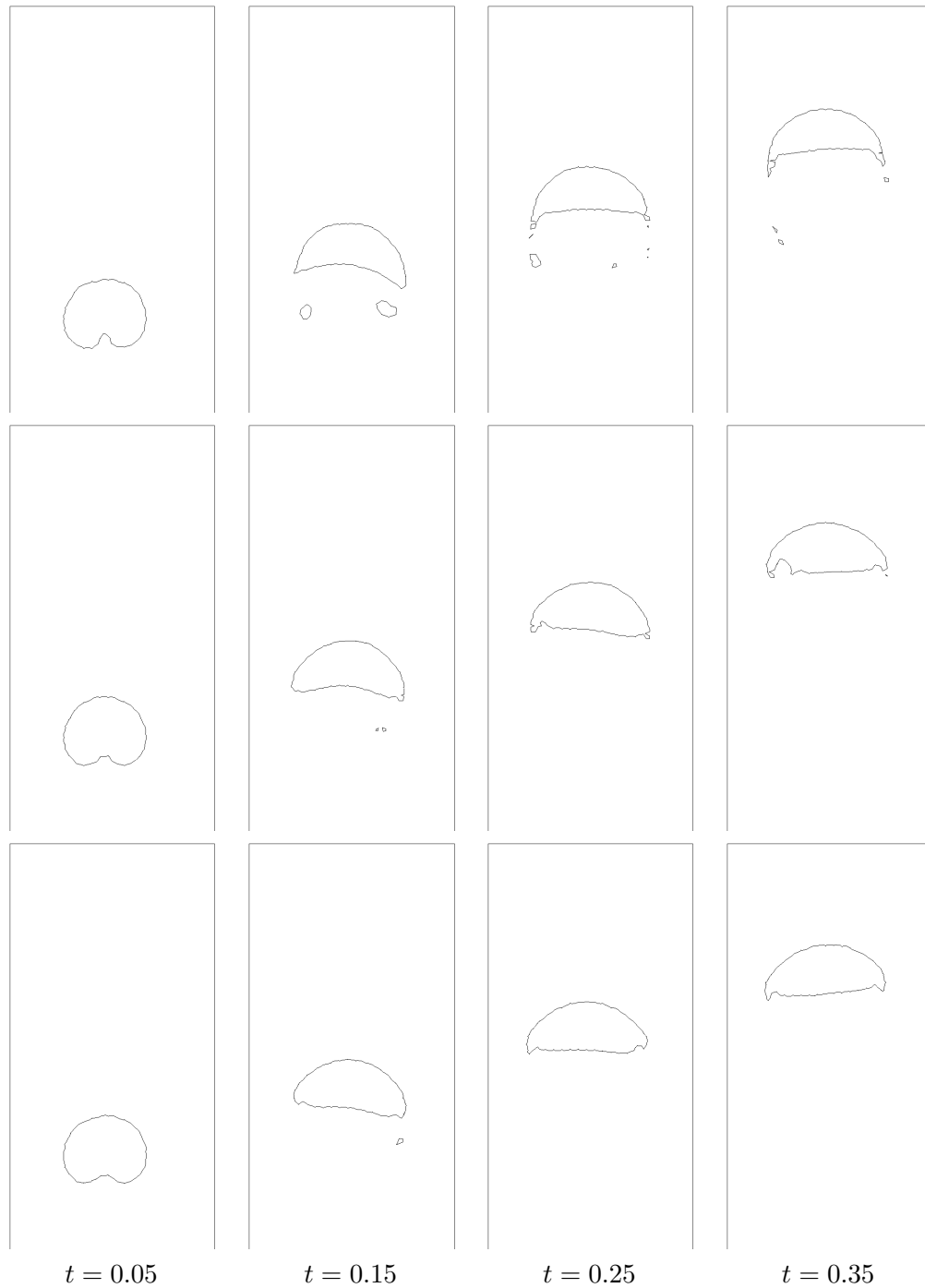


Figure 4.16: Rising Bubble: results for the coarse mesh. From left to right, position of the interface at times 0.05, 0.15, 0.25 and 0.35 s. First row: $\sigma = 0 \text{ Nm}^{-1}$, second row: $\sigma = 0.0738 \text{ Nm}^{-1}$, third row: $\sigma = 0.14 \text{ Nm}^{-1}$.

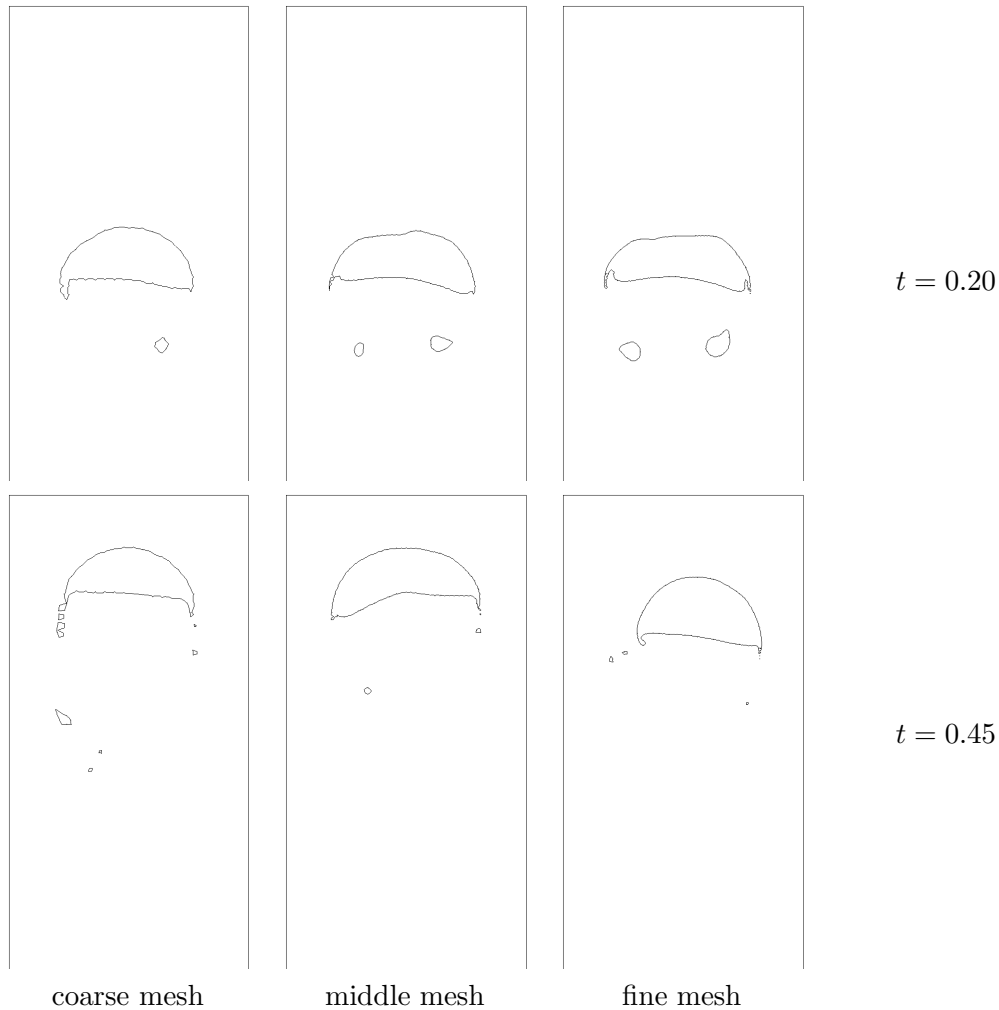


Figure 4.17: Rising Bubble: results for $\sigma = 0 \text{ Nm}^{-1}$ and several mesh sizes. Position of the free surface at times $t = 0.2 \text{ s}$ (first row) and $t = 0.45 \text{ s}$ (second row). Left: coarse mesh, middle: middle mesh and right: fine mesh.

Similar results can be obtained for unstructured meshes, even if an influence of the mesh size remains.

Conclusions. Two methods for the computation of the curvature and surface tension effects have been presented. Although it is not very accurate, the geometrical method may be used for mould filling problems. On the other hand, when the ratio between Capillary number and Reynolds number is high, the projection method guarantees accuracy and convergence of the approximation of the curvature inside the cavity. The estimation of the surface tension effects near the boundary of the cavity have been discussed but a satisfactory solution has not been obtained yet. Many numerical results for curvature-driven flows have been obtained.

4.7. NUMERICAL RESULTS

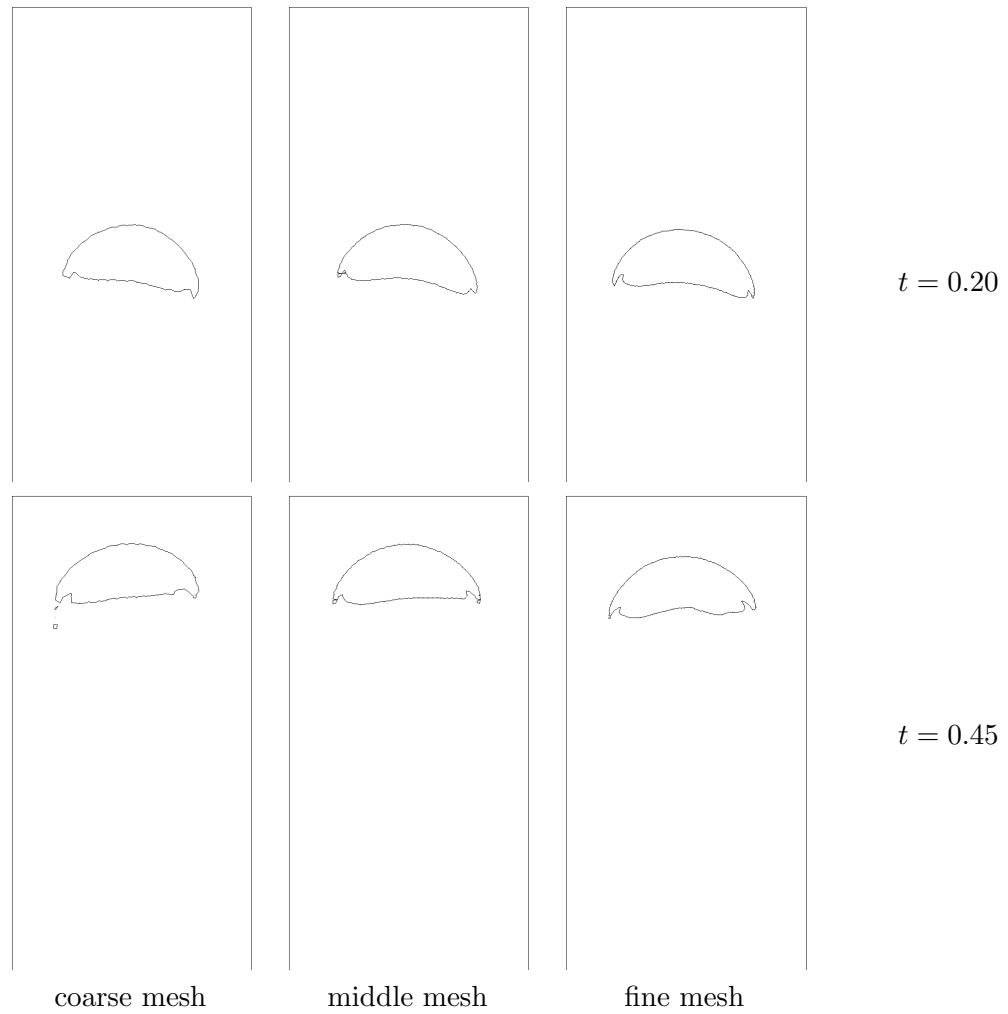


Figure 4.18: Rising Bubble: results for $\sigma = 0.0738 \text{ Nm}^{-1}$ and several mesh sizes. Position of the free surface at times $t = 0.2 \text{ s}$ (first row) and $t = 0.45 \text{ s}$ (second row). Left: coarse mesh, middle: middle mesh and right: fine mesh.

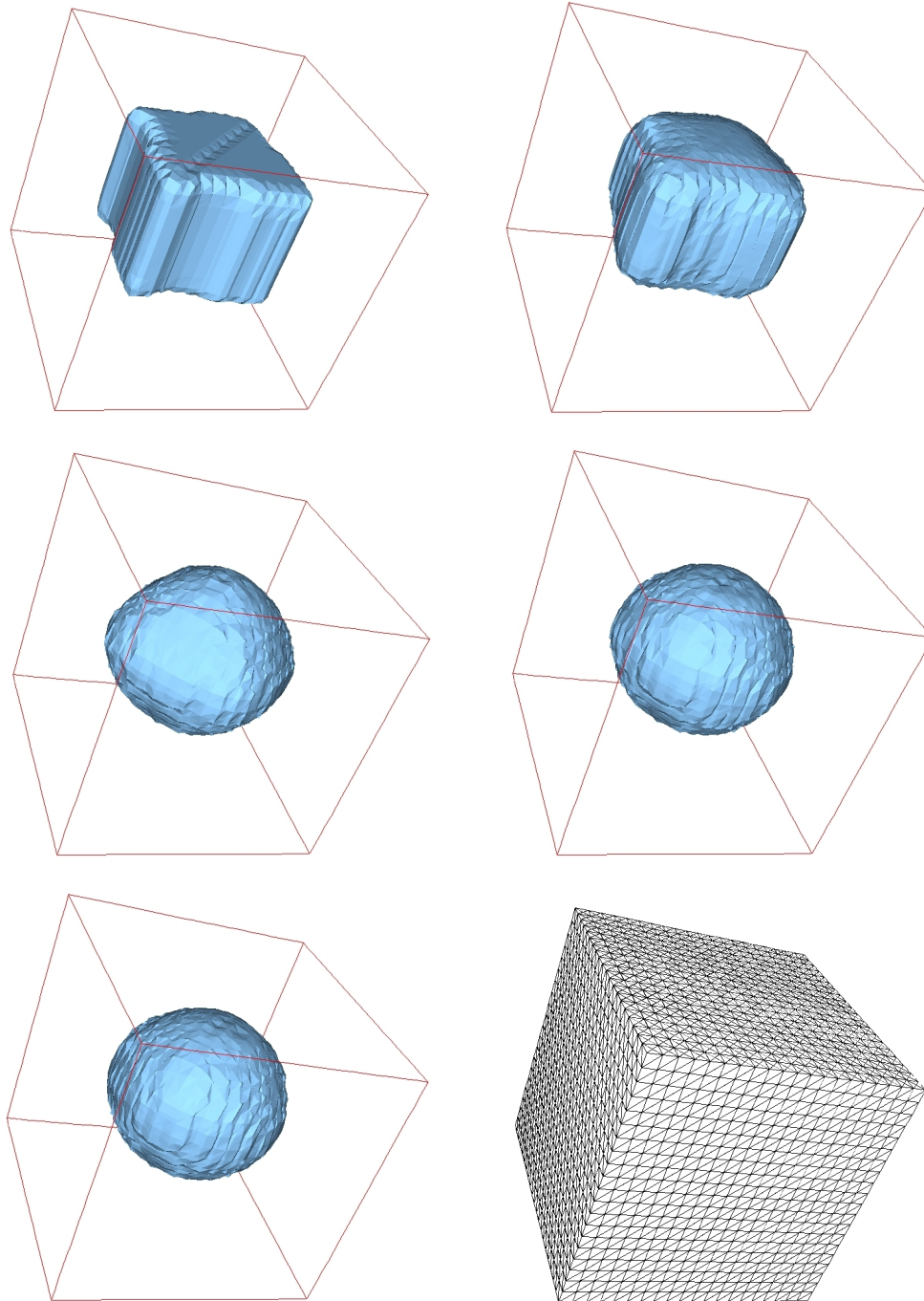


Figure 4.19: Initially cubic droplet. Liquid region at initial time at times $t = 0$ s, $t = 0.01$ s, $t = 0.035$ s, $t = 0.05$ s and $t = 0.06$ s. and structured mesh (from left to right, top to bottom)

Conclusions

Free surface flows have been investigated from both theoretical and numerical points of view.

On one hand, some theoretical questions have been discussed. A one-dimensional model problem for free surface flows has been considered. Local existence in time and uniqueness results have been obtained. Then error estimates have been derived for the semi-discretization in space. A one-dimensional version of the time splitting algorithm used in [73] has been discussed.

Next, the two-dimensional Navier-Stokes equations with a free surface have been investigated. Neumann boundary conditions have been enforced on the whole boundary of the liquid region. The whole boundary has been assumed to be the free surface. Local existence in time and uniqueness of a solution have been proved with the same methodology we used for the one-dimensional case. We are looking forward to studying theoretically the time splitting algorithm for the two-dimensional problem.

On the other hand, the time splitting scheme proposed in [73] for the simulation of free surface flows has been improved. The compressibility effects of the surrounding gas onto the liquid are considered. A numbering algorithm is used to recognize the bubbles of gas. The pressure inside each bubble is computed by using the ideal gas law. Gas pressure is imposed as a normal force on the interface between liquid and gas. Numerical results have validated our model and have shown that the influence of gas cannot be neglected, in particular in mould filling situations. Furthermore the computational cost of this method is not very high.

Finally, some algorithms to compute the interface curvature and therefore surface tension effects have been discussed. The lack of regularity of the volume fraction of liquid has been circumvented by convolution. The approximated curvature converges to the exact one when the mesh size tends to zero. Convergence does not depend on the mesh topology. Our results compare well with other methods. Surface tension effects are not relevant for mould filling problems, but have a strong impact for curvature-driven flows, such as rising bubbles or deformed droplets flows. Validation in three space dimensions is still required.

CONCLUSIONS

Bibliography

- [1] R. Abgrall and R. Saurel. Discrete Equations for Physical and Numerical Compressible Multiphase Mixtures. *J. Comp. Phys.*, 186:361–396, 2003.
- [2] G. Allain. Small-Time Existence for the Navier-Stokes Equations with a Free Surface. *Appl. Math. Optim.*, 16:37–50, 1987.
- [3] O. Axelsson and V.A. Barker. *Finite Element Solution of Boundary Value Problems*. Computer Science and Applied Mathematics. Academic Press, 1984.
- [4] J. Baranger and H. El Amri. Estimateurs a posteriori d’Erreur pour le Calcul Adaptatif d’Ecoulements Quasi-Newtoniens. *M²AN*, 25(1):31–48, 1991.
- [5] T. J. Barth and J. A. Sethian. Numerical Schemes for the Hamilton-Jacobi and Level Set Equations on Triangulated Domains. *J. Comp. Phys.*, 145(1):1–40, 1998.
- [6] J. T. Beale. The Initial Value Problem for the Navier-Stokes Equations with a Free Surface. *Comm. Pure Appl. Math.*, 34:359–392, 1981.
- [7] J. T. Beale. Large-Time Regularity of Viscous Surface Waves. *Arch Rational Mech. Anal.*, 84:307–352, 1984.
- [8] M. Bertsch, D. Hilhorst, and Cl. Schmidt-Lainé. The Well-Posedness of a Free Boundary Problem for Burgers’ Equation. *Nonlinear Analysis, Theory, Methods and Applications*, 23(9):1211–1224, 1994.
- [9] D. Boffi and L. Gastaldi. A Finite Element Approach for the Immersed Boundary Method. *Computer and Structures*, 81:491–501, 2003.
- [10] A. Bonito, M. Picasso, and M. Laso. Numerical Simulation of 3D Viscoelastic Flows with Free Surfaces. In *J. Non-Newtonian Fluid Mechanics*. XIIIth Workshop on Numerical Methods for non-Newtonian Flows, 2003, submitted.
- [11] J. U. Brackbill and D. B. Kothe. Dynamical Modelling of Surface Tension. Technical Report LANL LA-UR-96-1706, Los Alamos National Laboratory, 1996.
- [12] J. U. Brackbill, D. B. Kothe, and C. Zemach. A Continuum Method for Modeling Surface Tension. *J. Comp. Phys.*, 100:335–354, 1992.
- [13] H. Brézis. *Analyse Fonctionnelle, Théorie et Applications*. Collection Mathématiques appliquées pour la Maîtrise. Masson, 1983.

BIBLIOGRAPHY

- [14] J.W. Bullard, E.J. Garboczi, W.C. Carter, and E.R. Fuller Jr. Numerical Methods for Computing Interfacial Mean Curvature. *Computational Materials Science*, 4:103–116, 1995.
- [15] J. Burns, A. Balogh, D.S. Gilliam, and V.I. Shubov. Numerical Stationary Solutions for a Viscous Burgers' Equation. *Journal of Mathematical Systems, Estimation and Control*, 8(2):1–16, 1998.
- [16] A. Caboussat, V. Maronnier, M. Picasso, and J. Rappaz. Numerical Simulation of Three Dimensional Free Surface Flows with Bubbles. *Lecture Notes in Computational Science and Engineering, Springer-Verlag series*, 35:69–86, 2003.
- [17] A. Caboussat, M. Picasso, and J. Rappaz. Numerical Simulation of Free Surface Incompressible Liquid Flows Surrounded by Compressible Gas. *submitted to J. Comp. Phys.*, 2003.
- [18] R. Caiden, R. P. Fedkiw, and C. Anderson. A Numerical Method for Two-Phase Flow Consisting of Separate Compressible and Incompressible Regions. *J. Comp. Phys.*, 166:1–27, 2001.
- [19] G. Caloz and J. Rappaz. *Numerical Analysis for Nonlinear and Bifurcation Problems*, volume 5 of *Handbook of Numerical Analysis (P.G. Ciarlet, J.L. Lions eds)*, pages 487–637. Elsevier, 1997.
- [20] A. Celić and G. G. Ziliac. Computational Study of Surface Tension and Wall Adhesion Effects on an Oil Film Flow Underneath. Technical Report NASA/TM-1998-112230, Nasa, 1998.
- [21] Y. C. Chang, T. Y. Hou, B. Merriman, and S. Osher. A Level Set Formulation of Eulerian Interface Capturing Methods for Incompressible Fluid Flows. *J. Comp. Phys.*, 124(2):449–464, 1996.
- [22] S. D. Chatterji. *Cours d'Analyse. 1 Analyse vectorielle*. Presse Polytechnique et Universitaires Romandes, première édition, 1997.
- [23] D. L. Chopp and J. A. Sethian. Motion by Intrinsic Laplacian of Curvature. *Interfaces and Free Boundaries*, 1:107–123, 1999.
- [24] A. J. Chorin. Flame Advection and Propagation Algorithms. *J. Comp. Phys.*, 35:1–11, 1980.
- [25] A. J. Chorin. Curvature and Solidification. *J. Comp. Phys.*, 58:472–490, 1985.
- [26] P. G. Ciarlet and J.-L. Lions, editors. *Handbook of Numerical Analysis - Finite Element Methods (Part I)*. North-Holland, 1991.
- [27] R. Codina and O. Soto. A Numerical Model to Track Two-Fluid Interfaces Based on a Stabilized Finite Element Method and a Level Set Technique. *Int. J. Numer. Meth. Fluids*, 40:293–301, 2002.

BIBLIOGRAPHY

- [28] R. Codina, U. Schäfer and E. Oñate. Mould Filling Simulation using Finite Elements. *Int. J. Numer. Meth. Heat Fluid Flow*, 4:291–310, 1994.
- [29] R. Dautray and J.-L. Lions. *Analyse Mathématique et Calcul Numérique pour les Sciences et les Techniques, Volumes 1-9*. Masson, Paris, 1987.
- [30] P. Degond and M. Lemou. Turbulence Models for Incompressible Fluids Derived from Kinetic Theory. *Journal of Mathematical Fluid Mechanics*, 4:257–284, 2002.
- [31] B. Desjardins, M. J. Esteban, C. Grandmont, and P. Le Tallec. Weak Solutions for a Fluid-Elastic Structure Interaction Model. *Rev. Mat. Comput.*, 14(2):523–538, 2001.
- [32] G. Dhatt, D. M. Gao, and A. Ben Cheikh. A Finite Element Simulation of Metal Flow in Moulds. *Int. J. Numer. Meth. Eng.*, 30:821–831, 1990.
- [33] S. Dufour and D. Pelletier. Computations of Multiphase Flows with Surface Tension using Adaptive Finite Element Methods. In *Proceedings of the 37th AIAA Aerospace Sciences Meeting and Exhibit, Reno*, number 99-0544 in AIAA Paper, 1999.
- [34] M. S. Engelman, S. L. Sani, and P. M. Gresho. The Implementation of Normal and/or Tangential Boundary Conditions in Finite Element Codes for Incompressible Fluid Flow. *Int. J. Num. Meth. Fluids*, 2:225–238, 1982.
- [35] A. Ern and J.-L. Guermond. *Éléments Finis: Théorie, Applications, Mise en Oeuvre*. Mathématiques et Applications, vol 36. Springer, first edition, 2001.
- [36] D. Errate, M. J. Esteban, and Y. Maday. Couplage Fluide-Structure. Un Modèle Simplifié en Dimension 1. *C.R. Acad. Sci. Paris*, 318, Série 1:275–281, 1994.
- [37] R. P. Fedkiw, B. Merriman, and S. Osher. Numerical Methods for a One-Dimensional Interface Separating Compressible and Incompressible Flows. In V. Venkatakrishnan, M. Salas, and S. Chakravarthy, editors, *Barriers and Challenges in Computational Fluid Dynamics*, pages 155–194. Kluwer Academic Publishers, 1998.
- [38] L. P. Franca and S. L. Frey. Stabilized finite Element Method: II. The incompressible Navier-Stokes equations. *Comp. Meth. Appl. Mech. Engrg*, 99:209–233, 1992.
- [39] L. P. Franca and T. J. R. Hugues. Convergence Analyses of Galerkin Least-Squares Methods for Symmetric Advective-Diffusive Forms of the Stokes and Incompressible Navier-Stokes equations. *Comp. Meth. Appl. Mech. Engrg*, 105:285–298, 1993.
- [40] J.-F. Gerbeau, T. Lelievre, and C. Le Bris. Simulations of MHD Flows with Moving Interfaces. *J. Comp. Phys.*, 184(1):163–191, 2003.
- [41] M. Gerhardt, H. Schuster, and J. J. Tyson. A Cellular Automaton Model of Excitable Media: II Curvature, Dispersion, Rotating Waves and Meandering Waves. *Physica D*, 46:392–415, 1990.
- [42] D. Gilbarg and N. S. Trudinger. *Elliptic Partial Differential Equations of Second Order*. Springer-Verlag, second edition, 1983.

BIBLIOGRAPHY

- [43] J. Glimm, J. W. Grove, X. L. Li, K.-M. Shyue, Y. Zeng, and Q. Zhang. 3-Dimensional Front Tracking. *SIAM J. Sci. Computing*, 19:703–727, 1998.
- [44] J. Gomes and O. Faugeras. Reconciling Distance Functions and Level Sets. *Journal of Visualization Communication and Image Representation*, 11:209–223, 2000.
- [45] C. Grandmont and Y. Maday. Existence for an Unsteady Fluid-Structure Interaction Problem. *M²AN*, 34(3):609–636, 2000.
- [46] D. Gueyffier, J. Li, A. Nadim, R. Scardovelli, and S. Zaleski. Volume-of-Fluid Interface Tracking with Smoothed Surface Stress Methods for Three-Dimensional Flows. *J. Comp. Phys.*, 152:423–456, 1999.
- [47] W. Hackbusch. *Multi-Grid Methods and Applications*. Springer-Verlag, 1985.
- [48] W. Härdle. *Applied Nonparametric Regression*. Cambridge University Press, 1993.
- [49] E. Hairer, S. P. Nørsett, and G. Wanner. *Solving Ordinary Differential Equations I, Non Stiff Problems*. Springer-Verlag, Berlin, 2nd edition, 1993.
- [50] P. Hansbo. The Characteristic Streamline Diffusion Method for the Time-Dependent Incompressible Navier-Stokes Equations. *Comp. Meth. Appl. Mech. Engrg.*, 99:171–186, 1992.
- [51] P. Hansbo. A Free-Lagrange Finite Element Method using Space-Time Elements. *Comp. Meth. Appl. Mech. Engrg.*, 188:347–361, 2000.
- [52] J. G. Heywood and R. Rannacher. Finite Element Approximation of the Nonstationary Navier-Stokes Problem. Part I. Regularity of Solutions and Second-Order Error Estimates for Spatial Discretization. *SIAM J. Numerical Analysis*, 19(2):275–311, 1982.
- [53] C. W. Hirt and B. D. Nichols. Volume of Fluid (VOF) Method for the Dynamics of Free Boundaries. *J. Comp. Phys.*, 39:201–225, 1981.
- [54] A. Huerta and W. K. Liu. Viscous Flow with Large Free Surface Motion. *Comp. Meth. Appl. Mech. Engrg.*, 69:277–324, 1988.
- [55] G.-S. Jiang and D. Peng. Weighted ENO Schemes for Hamilton-Jacobi Equations. *SIAM J. Sci. Comp.*, 21:2126, 2000.
- [56] Ch. Josserand and S. Zaleski. Droplet Splashing on a Thin Liquid Film. *Phys. Fluids*, 15(6):1650–1657, 2003.
- [57] M. Kang, R. P. Fedkiw, and X.-D. Liu. A Boundary Condition Capturing Method for Multiphase Incompressible Flow. *Journal of Scientific Computing*, 15:323–360, 2000.
- [58] H.N. Kardestuncer and D. H. Norrie, editors. *Finite Element Handbook*. McGraw-Hill, New York, NY, USA, 1987.

BIBLIOGRAPHY

- [59] M. S. Kim, J. S. Park, and W. I. Lee. A New VOF-Based Numerical Scheme for the Simulation of Fluid Flow with Free Surface. Part II: Application to the Cavity Filling and Sloshing Problems. *Int. J. Num. Meth. Fluids*, 42:791–812, 2003.
- [60] P. Klouček and M. V. Romero. The Detachment of Bubbles under a Porous Rigid Surface during Aluminium Electrolysis. *Math. Mod. Meth. App. Sci.*, 12(11):1617–1652, 2002.
- [61] B. Koren, M.R. Lewis, E.H. van Brummelen, and B. van Leer. Riemann-Problem and Level-Set Approaches for Two-Fluid Flow Computations I. Linearized Godunov Scheme. Technical Report MAS-R0112, CWI, Amsterdam, 2001.
- [62] S. Korotov, M. Kříšek, and P. Neittaanmäki. Weakened Acute Type Condition for Tetrahedral Triangulations and the Discrete Maximum Principle. *Math. Comp.*, 70(233):107–119, 2001.
- [63] S. Kutluay, A.R. Bahadir, and A. Özdes. Numerical Solution of One-Dimensional Burgers' Equation: Explicit and Exact-Explicit Finite Difference Methods. *J. Comp. Appl. Math.*, 103:251–261, 1999.
- [64] R. J. LeVeque. *Numerical Methods for Conservation Laws*. Birkhauser-Verlag, first edition, 1990.
- [65] R. J. Leveque and Z. Li. Immersed Interface Methods for Stokes Flow with Elastic Boundaries or Surface Tension. *SIAM J. Sci. Comput.*, 18(3):709–735, 1997.
- [66] R. W. Lewis, S. E. Navti, and C. Taylor. A Mixed Lagrangian-Eulerian Approach to Modelling Fluid Flow During Mould Filling. *Int. J. Numer. Meth. Fluids*, 25:931–952, 1997.
- [67] R.W. Lewis, A.S. Usmani and J.T. Cross. Efficient Mould Filling Simulation in Castings by an Explicit Finite Element Method. *Int. J. Numer. Meth. Fluids*, 20:493–506, 1995.
- [68] J. Li and Y. Renardy. Numerical Study of Flows of Two Immiscible Liquids at Low Reynolds Number. *SIAM Rev.*, 42(3):417–439, 2000.
- [69] J.-L. Lions. Sur les Problèmes Mixtes pour Certains Systèmes Paraboliques dans des Ouverts Non Cylindriques. *Annales de l'Institut Fourier*, VII:143–182, 1957.
- [70] J.-L. Lions. *Quelques Méthodes de Résolution de Problèmes aux Limites Non Linéaires*. Dunod, 1969.
- [71] J.-L. Lions and E. Magenes. *Problèmes aux Limites Non Homogènes et Applications, Volumes 1-3*. Dunod, 1968.
- [72] G.I. Marchuk. *Methods of Numerical Mathematics*. Springer, Applications of Mathematics, 1975.
- [73] V. Maronnier. *Simulation Numérique d'Écoulements de Fluides Incompressibles avec Surface Libre*. PhD thesis, École Polytechnique Fédérale de Lausanne, 2000.

BIBLIOGRAPHY

- [74] V. Maronnier, M. Picasso, and J. Rappaz. Numerical Simulation of Free Surface Flows. *J. Comp. Phys.*, 155:439–455, 1999.
- [75] V. Maronnier, M. Picasso, and J. Rappaz. Numerical Simulation of Three Dimensional Free Surface Flows. *Int. J. Num. Meth. Fluids*, 42(7):697–716, 2003.
- [76] J. C. Martin and W. J. Moyce. An Experimental Study of the Collapse of Liquid Columns on a Rigid Horizontal Plate. *Philos. Trans. Roy. Soc. London Ser., A* 244:312–324, 1952.
- [77] F. Mashayek and N. Ashgriz. A Hybrid Finite-Element-Volume-Of-Fluid Method for Simulating Free Surface Flows and Interfaces. *Int. J. Num. Meth. Fluids*, 20:1367–1380, 1995.
- [78] B. Maury. Direct Simulations of 2D Fluid-Particle Flows in Biperiodic Domains. *J. Comp. Phys.*, 156:325–351, 1999.
- [79] M. Medale and M. Jaeger. Numerical Simulations of Incompressible Flows with Moving Interfaces. *Int. J. Num. Meth. Fluids*, 24:615–638, 1997.
- [80] M. Meier, G. Yadigaroglu, and B. L. Smith. A Novel Technique for Including Surface Tension in PLIC-VOF Methods. *European Journal of Mechanics B - Fluids*, 21:61–73, 2002.
- [81] M. Mori. *The Finite Element Method and Its Applications*. Collier MacMillan Publishers, New York, 1986.
- [82] W.F. Noh and P. Woodward. *SLIC (Simple Line Interface Calculation)*, volume 59 of *Lectures Notes in Physics*, pages 330–340. Springer-Verlag, 1976.
- [83] K. Ohmori. Numerical Solution of Two-Fluid Flows using Finite Element Method. *Applied Mathematics and Computation*, 92:125–133, 1998.
- [84] S. Osher and R. P. Fedkiw. Level Set Methods : An Overview and Some Recent Results. *J. Comp. Phys.*, 169:463–502, 2001.
- [85] S. Osher and R. P. Fedkiw. *Level Set Methods and Dynamic Implicit Surfaces*. Applied Mathematical Sciences. Springer-Verlag, 2003.
- [86] D. Peng, B. Merriman, S. Osher, H. Zhao, and M. Kang. A PDE-Based Fast Local Level Set Method. *J. Comp. Phys.*, 155:410–438, 1999.
- [87] C. Peskin. Numerical Analysis of Blood Flow in the Heart. *J. Comp. Phys.*, 25:220–252, 1977.
- [88] M. Picasso and J. Rappaz. Stability of Time-Splitting Schemes for the Stokes Problem with Stabilized Finite Elements. *Numerical Methods for Partial Differential Equations*, 17(6):632–656, 2001.
- [89] M. Picasso, J. Rappaz, A. Reist, M. Funk, and H. Blatter. Numerical Simulation of the Motion of a Two Dimensional Glacier. *Int. J. Num. Meth. Engrg*, submitted, 2003.

BIBLIOGRAPHY

- [90] O. Pironneau. *Finite Element Methods for Fluids*. Wiley, Chichester, 1989.
- [91] O. Pironneau, J. Liou, and T. Tezduyar. Characteristic-Galerkin and Galerkin/Least-Squares Space-Time Formulations for the Advection-Diffusion Equation with Time-Dependent Domain. *Comp. Meth. Appl. Mech. Engrg*, 100:117–141, 1992.
- [92] S. Popinet and S. Zaleski. A Front-Tracking Algorithm for Accurate Representation of Surface Tension. *Int. J. Numer. Meth. Fluids*, 30:777–793, 1999.
- [93] A. Pressley. *Elementary Differential Geometry*. Undergraduate Mathematics. Springer, 2000.
- [94] A.R.M. Primo, L.C. Wrobel, and H. Power. Low Reynolds Number Deformation of Viscous Drops in a Bounded Flow Region under Surface Tension. *Mathematical and Computer Modelling*, 31:99–118, 2000.
- [95] A. Quarteroni and L. Formaggia. *Mathematical Modelling and Numerical Simulation of the Cardiovascular System*, volume to appear of *Handbook of Numerical Analysis (P.G. Ciarlet, J.L. Lions eds)*, chapter Modelling of Living Systems. Elsevier, 2002.
- [96] A. Quarteroni and A. Valli. *Numerical Approximation of Partial Differential Equations*. Springer-Verlag Series in Computational Mathematics, n^o 23, second edition, 1994.
- [97] P.-A. Raviart and J.-M. Thomas. *Introduction à l'Analyse Numérique des Equations aux Dérivées Partielles*. Collection Mathématiques appliquées pour la Maîtrise. Masson, 1993.
- [98] M. Renardy, Y. Renardi, and J. Li. Numerical Simulation of Moving Contact Line Problems Using a Volume-of-Fluid Method. *J. Comp. Phys.*, 171:243–263, 2001.
- [99] Y. Renardy and M. Renardy. PROST : A Parabolic Reconstruction of Surface Tension for the Volume-Of-Fluid Method. *J. Comp. Phys.*, 183:400–421, 2002.
- [100] W.J. Rider and D.B. Kothe. Reconstructing Volume Tracking. *J. Comp. Phys.*, 141:112–152, 1998.
- [101] R. Scardovelli and S. Zaleski. Direct Numerical Simulation of Free Surface and Interfacial Flows. *Annual Review of Fluid Mechanics*, 31:567–603, 1999.
- [102] M. Schmid and F. Klein. Einfluß der Wandreibung auf das Füllverhalten Dünner Platten. *Preprint, Steinbeis Transferzentrum, Fachhochschule Aachen*, 1996.
- [103] J.A. Sethian. *Level Set Methods, Evolving Interfaces in Geometry, Fluid Mechanics, Computer Vision, and Material Science*. Monographs on Applied and Computational Mathematics. Cambridge University Press, 1996.
- [104] M. J. Shelley, F.-R. Tian, and K. Wlodarski. Hele-Shaw Flow and Pattern Formation in a Time-Dependent Gap. *Nonlinearity*, 10:1471–1495, 1997.

BIBLIOGRAPHY

- [105] K.-M. Shyue. A Fluid-Mixture Type Algorithm for Compressible Multicomponent Flow with van der Waals Equation of State. *J. Comp. Phys.*, 156:43–88, 1999.
- [106] K.-M. Shyue. A Volume-Of-Fluid type Algorithm for Compressible Two-Phase Flows. *Intl. Series of Numerical Mathematics*, 130:895–904, 1999.
- [107] V. A. Solonnikov. Solvability of the Problem of Evolution of an Isolated Volume of Viscous, Incompressible Capillary Fluid. *J. Soviet Math.*, 32(2):179–186, 1986.
- [108] V. A. Solonnikov. On the Transient Motion of an Isolated Volume of Viscous Incompressible Fluid. *Math. USSR Izvestiya*, 31(2):381–405, 1988.
- [109] V. A. Solonnikov. On an Initial-Boundary Value Problem for the Stokes Systems Arising in the Study of a Problem with a Free Boundary. *Proc. Steklov Inst. Math.*, 3:191–239, 1991.
- [110] V. A. Solonnikov. Solvability of the Problem of Evolution of a Viscous Incompressible Fluid Bounded by a Free Surface on a Finite Time Interval. *St Petersburg Math. J.*, 3(1):189–220, 1992.
- [111] V.A. Solonnikov. The Solvability of the Second Initial Boundary-Value Problem for the Linear, Time-dependent System of Navier-Stokes Equations. *J. Soviet Math.*, 10(1):141–155, 1978.
- [112] Ch. G. Speziale. Analytical Methods for the Development of Reynolds-Stress Closures in Turbulence. *Annual Review of Fluid Mechanics*, 23:107–157, 1991.
- [113] M. Sussman, A. S. Almgren, J. B. Bell, Ph. Colella, L. H. Howell, and M. L. Welcome. An Adaptive Level Set Approach for Incompressible Two-Phase Flows. *J. Comp. Phys.*, 148:81–124, 1999.
- [114] M. Sussman, E. Fatemi, P. Smereka, and S. Osher. An Improved Level Set Method for Incompressible Two-Phase Flows. *Computers and Fluids*, 27(5-6):663–680, 1998.
- [115] M. Sussman and E. G. Puckett. A Coupled Level Set and Volume-of-Fluid Method for Computing 3D and Axisymmetric Incompressible Two-Phase Flows. *J. Comp. Phys.*, 162:301–337, 2000.
- [116] M. Sussman and P. Smereka. Axisymmetric Free Boundary Problems. *J. Fluid Mech.*, 341:269–294, 1997.
- [117] M. Sussman, P. Smereka, and S. Osher. A Level Set Approach for Computing Solutions to Incompressible Two-Phase Flow. *J. Comp. Phys.*, 114:146–159, 1994.
- [118] R. Temam. *Navier-Stokes Equations, Theory and Numerical Analysis*. Studies in mathematics and its applications. North Holland Publishing Company, third edition, 1984.

BIBLIOGRAPHY

- [119] T.E. Tezduyar, M. Behr, S. Mittal and J. Liou. A New Strategy for Finite Element Computations Involving Boundaries and Interfaces - The Deforming-Spatial-Domain/Space-Time Procedure: II. Computations of Free Surface Flows, Two-Liquid Flows, and Flows with Drifting Cylinders. *Comp. Meth. Appl. Mech. Engrg.*, 94:353–371, 1992.
- [120] E. Thompson. Use of Pseudo-Concentrations to Follow Creeping Viscous Flows During Transient Analysis. *Int. J. Numer. Meth. Fluids*, 6:749–761, 1986.
- [121] A.-K. Tornberg and B. Engquist. Interface Tracking in Multiphase Flows. *Multifield Problems in Solid and Fluid Mechanics*, to appear, 2000.
- [122] G. Tryggvason, B. Bunner, A. Esmaeeli, D. Juric, N. Al-Rawahi, W. Tauber, J. Han, S. Nas, and Y.-J. Jan. A Front-Tracking Method for the Computations of Multiphase Flows. *J. Comp. Phys.*, 169:708–759, 2001.
- [123] S.O. Unverdi and G. Tryggvason. Computations of Multi-Fluid Flows. *Physica D*, 60:70–83, 1992.
- [124] S.P. van der Pijl, A. Segal, and C. Vuik. A Mass-Conserving Level-Set (MCLS) Method for Modeling of Multi-Phase Flows. Technical Report 03-03, Delft University of Technology, 2003.
- [125] R. Verfürth. *A Review of A Posteriori Error Estimation and Adaptive Mesh-Refinement Techniques*. Wiley-Teubner, 1996.
- [126] C. Vuik, A. Saghir, and G. P. Boerstoel. The Krylov Accelerated SIMPLE(R) Method for Flow Problems in Industrial Furnaces. *Int. J. Num. Meth. Fluids*, 33:1027–1040, 2000.
- [127] H. Wang, H.K. Dahle, R.E. Ewing, M.S. Espedal, R.C. Sharpley, and S. Man. An ELLAM Scheme for Advection-Diffusion Equations in Two Dimensions. *SIAM J. Sci. Comput.*, 20(6):2160–2194, 1999.
- [128] M. W. Williams, D. B. Kothe, and E. G. Puckett. Accuracy and Convergence of Continuum Surface Tension Models. In Cambridge Cambridge Univ. Press, editor, *Fluid Dynamics at Interfaces*, pages 294–305. Fluid Dynamics at Interfaces, Gainesville, FL, 1998, 1999.
- [129] F. Xiao and A. Ikebata. An Efficient Method for Capturing Free Boundaries in Multi-Fluid Simulations. *Int. J. Num. Meth. Fluids*, 42:187–210, 2003.
- [130] K. Yosida. *Functional Analysis*. Springer-Verlag, Berlin, 6th edition, 1980.
- [131] H. Zhao, B. Merriman, S. Osher, and L. Wang. Capturing the Behavior of Bubbles and Drops Using the Variational Level Set Approach. *J. Comp. Phys.*, 143:495–518, 1998.

BIBLIOGRAPHY

Curriculum Vitae

I was born on March 17th, 1977 in Lausanne, Switzerland. I have done all my school years in Lausanne and I obtained the *baccalauréat de type C* (scientific option) in 1995 in the *Gymnase de Chamblandes*, Pully. I was then admitted in the Swiss Federal Institute of Technology (EPFL) in Lausanne in 1995. I got the degree of mathematician engineer in 2000, after having done my M.S. work in scientific computing under the supervision of Professor Jacques Rappaz in the spin-off Calcom SA, Lausanne. The same year, I got the Master degree in mathematical engineering, given jointly by the EPFL and the *Ecole Polytechnique de Paris*, Palaiseau. Since 2001, I have been working as an assistant in the Chair of Numerical Analysis and Simulation for Professor Jacques Rappaz. My research thema is free surface flows.

